

# Non-Alternant Polycyclic Aromatic Hydrocarbons

*versus*

## Closed Carbon Surfaces

Niet-Alternerende Polycyclische Koolwaterstoffen

*versus*

Gesloten Koolstofoppervlakken

(Met een samenvatting in het Nederlands)

### Proefschrift

ter verkrijging van de graad van doctor  
aan de Universiteit van Utrecht  
op gezag van Rector Magnificus, Prof. Dr. W. H. Gispen  
ingevolge het besluit van het College van Promoties  
in het openbaar te verdedigen  
op 16 juni 2003 des middags te 12.45 uur

door

Carola Koper

geboren op 17 juni 1975 te Soest

Promotor: Prof. Dr. L. W. Jenneskens

Verbonden aan het Debye Instituut van de Universiteit Utrecht

ISBN 90-393-3394-7

*Voor mijn ouders*



## Contents

<b>1</b>	<b>General Introduction</b>	11
1.1	Introduction	
1.2	Non-Alternant PAH	
1.2.1	Aromaticity: the concept	
1.2.2	Models for aromaticity	
1.2.3	Aromaticity: the magnetic criterion	
1.2.4	Synthesis of non-alternant PAH: the FVT approach	
1.2.5	Behavior of (CP)-PAH under high temperature conditions	
1.2.6	Properties of non-alternant PAH	
1.3	Fullerenes	
1.3.1	Fullerene formation	
1.3.2	Properties of fullerenes	
1.4	Fullerenes; the Schlegel-match proposition	
1.4.1	Carbon nanotubes	
1.5	Corollary	
1.6	Outline of this Thesis	
	References	
<b>I</b>	<b>Rearrangements</b>	
<b>2</b>	<b>Unexpectedly Facile Hydrogen Migrations in Cyclopenta-Fused Polycyclic Aromatic Hydrocarbons under High Temperature Conditions</b>	37
2.1	Introduction	
2.2	Results & Discussion	
2.2.1	FVT of 9- <sup>2</sup> H-ethynylphenanthrene	
2.2.2	FVT of 1- <sup>2</sup> H-ethynyl-naphthalene	
2.2.3	FVT of 1-(1-chloroethenyl)-4- <sup>2</sup> H-naphthalene	
2.2.4	GC-cryo-FT-IR spectroscopy	
2.3	Mechanistic implications	
2.4	Conclusions	
2.5	Experimental section	
	References and notes	

**3 FVT of 1-<sup>2</sup>H-naphthalene and 2-<sup>2</sup>H-naphthalene; Hydrogen Migration along a PAH Perimeter** 61

- 3.1 Introduction
  - 3.2 Results & Discussion
    - 3.2.1 FVT of 1-<sup>2</sup>H-naphthalene
    - 3.2.2 FVT of 2-<sup>2</sup>H-naphthalene
    - 3.2.3 GC-cryo-FT-IR spectroscopy
  - 3.3 Mechanistic considerations
  - 3.4 Conclusions
  - 3.5 Experimental section
- References and notes

**II The Schlegel-Match Proposition**

**4 Benzo[1,2-*e*:3,4-*e'*:5,6-*e''*]tribenzo[*l*]acephenanthrylene (C<sub>60</sub>H<sub>30</sub>): a Progenitor of C<sub>60</sub>. Its Stepwise Conversion into C<sub>60</sub>.** 75

- 4.1 Introduction
  - 4.2 Results & Discussion
    - 4.2.1 Zipping up C<sub>60</sub>H<sub>30</sub> to C<sub>60</sub> by MALDI TOF-MS
    - 4.2.2 The effect of laser fluence
  - 4.3 Corollary
  - 4.4 The zipping-up process of C<sub>60</sub>H<sub>30</sub> to C<sub>60</sub>
  - 4.5 Conclusions
  - 4.6 Experimental section
- References and notes

**5 Identification of C<sub>70</sub> Progenitors** 93

- 5.1 Introduction
  - 5.2 Results & Discussion
    - 5.2.1 *Semi*-empirical AM1 calculations
    - 5.2.2 *Ab initio* calculations
  - 5.3 Conclusions
  - 5.4 Experimental section
- References and notes

6	Synthesis by Design of Novel Ionic Triaza-Fullerane $C_{57}H_2N_3$ by	107
---	---	-----

**'Zipping up' its Schlegel-Match Progenitor  $C_{57}H_{33}N_3$**

- 6.1 Introduction
  - 6.2 Results & Discussion
    - 6.2.1 Cyclodehydrogenations from  $C_{57}H_{33}N_3$  and  $C_{57}H_{27}^2H_6N_3$
    - 6.2.2 *Semi*-empirical and *ab initio* calculations
  - 6.3 Conclusions
  - 6.4 Experimental section
- References and notes

### III Non-Alternant PAH as Sub-Structures for Closed Carbon Surfaces

7	Redox Properties of Non-Alternant Cyclopenta-Fused Polycyclic Aromatic Hydrocarbons	125
---	---	-----

- 7.1 Introduction
  - 7.2 Results & Discussion
    - 7.2.1 Cyclic voltammetry
    - 7.2.2 Applicability of Hückel theory
    - 7.2.3 Peripheral pentagons in *mono*- and *bis*-CP-PAH act as a substituent
    - 7.2.4 Hückel Theory *versus* *mono*- and *bis*-CP-PAH
    - 7.2.5 The second half-wave reduction of *mono*- and *bis*-CP-PAH
    - 7.2.6 Structural features of the *mono*- and *bis*-anions of CP-PAH
    - 7.2.7 Corollary
  - 7.3 Validation
    - 7.3.1 Optimized geometries
    - 7.3.2 Visualization of  $6\pi$  cyclopentadienide sub-structures
    - 7.3.3 High electron affinities of *mono*- and *bis*-CP-PAH
  - 7.4 Conclusions
  - 7.5 Experimental section
- References and notes

<b>8</b>	<b>Novel Cyclohepta-Fused Non-Alternant Polycyclic Aromatic Hydrocarbons: Synthesis and Redox Properties</b>	<b>155</b>
8.1	Introduction	
8.2	Results & Discussion	
8.2.1	Syntheses of cyclohepta[ <i>c,d</i> ]pyrene and cyclohepta[ <i>c,d</i> ]fluoranthene	
8.2.2	Attempted synthesis of cyclohepta[ <i>k,l</i> ]anthracene	
8.2.3	Redox properties of cyclohepta-fused PAH	
8.3	CH-PAH and CP-PAH are <i>anti</i> -symmetric	
8.4	Conclusions	
8.5	Experimental section	
	References and notes	
<b>9</b>	<b>Magnetic Properties of Cyclohepta-Fused Non-Alternant Polycyclic Aromatic Hydrocarbons</b>	<b>183</b>
9.1	Introduction	
9.2	Aromaticity: the magnetic criterion	
9.2.1	<sup>1</sup> H-NMR spectroscopy of CH-PAH	
9.2.2	Current density maps of CH-PAH	
9.2.3	NICS values and <sup>1</sup> H-chemical shifts of CH-PAH	
9.2.4	Magnetic properties of CP-PAH and CH-PAH <i>vs.</i> CP-CH-PAH: a prediction	
9.3	Conclusions	
9.4	Experimental section	
	References and notes	
	<b>Summary</b>	<b>201</b>
	<b>Samenvatting</b>	<b>205</b>
	<b>Dankwoord</b>	<b>209</b>
	<b>Curriculum Vitae</b>	<b>211</b>
	<b>List of Publications</b>	<b>213</b>







# CHAPTER 1

## **Introduction**

## 1.1 Introduction

When burning a candle, driving your car or during an eruption of a volcano (non)-alternant polycyclic aromatic hydrocarbons (PAHs) are formed. In fact, PAH are invariably introduced into our environment as a consequence of incomplete combustion processes, both natural or due to human activity. This makes these molecules abundant. Unfortunately, several representatives possess genotoxic properties, *i.e.* they are environmental pollutants.<sup>1,2</sup> Besides their terrestrial prevalence, (ionized) cyclopenta-fused (CP)-PAH are proposed to constitute up to 20% of all the carbon present in the galaxy.<sup>3</sup> The prevalence of PAH combined with their physico-chemical properties make PAH of interest for a variety of natural sciences, *i.e.* chemistry, physics, biology, medicine, geology and for material science.<sup>4</sup>

A new dimension to non-alternant PAH chemistry was added by the discovery of the fullerenes  $C_{60}$  and  $C_{70}$ , *viz.* 3D closed carbon surfaces, and especially after their isolation the recognition of their remarkable properties.<sup>5,6</sup> The electronic and magnetic properties are strongly affected by changing a  $\pi$ -conjugated 2D arrangement of pentagons and hexagons into a 3D closed carbons surface. Therefore, the theoretical description of both fullerenes and non-alternant PAH gained much attention.<sup>7</sup> For example, the concept of aromaticity in relation with curved molecules that are partly composed of odd-membered rings still intrigues many scientists.<sup>8,9</sup>

After the discovery of fullerenes non-alternant PAH, and primarily cyclopenta-fused PAH, were recognized as model compounds and key sub-structures of classical fullerenes. The term 'buckybowls' was given to large CP-PAH that possess a curved structure.<sup>10-12</sup> This has led to substantial activity to synthesize large and curved CP-PAH in order to enable the study of the effect of pentagons on curvature and ultimately the properties of the molecule. Especially, the number, topology as well as the difference between internal and peripheral cyclopenta-moieties is hereby of interest.<sup>10-12</sup> At that time a drawback was that only lengthy synthetic routes for CP-PAH were available. In recent years, more convenient syntheses were developed, of which many involve Flash Vacuum Thermolysis (FVT) steps.<sup>13-15</sup> Furthermore, besides cyclopenta-fused PAH, the related cyclohepta-fused PAH were recognized as key sub-structures of bended carbon nanotubes.<sup>16,17</sup> However, only a few representatives of this class of molecules are known and their properties have only scarcely been studied.<sup>18-21</sup>

An interesting observation is that both (non)-alternant PAH as well as fullerenes are formed in flames.<sup>1</sup> This suggest that the formation of non-alternant PAH and fullerenes is interrelated under appropriate conditions. Based on this observation, a quest for the synthesis by design of, in first instance  $C_{60}$ , but ultimately new materials with 3D closed (carbon) surfaces starting from non-alternant PAH with the exact carbon topology as the desired molecule arose.<sup>22-</sup>

<sup>24</sup> Hence, in recent years various aspects of non-alternant PAH chemistry (re)gained considerable attention, while they are closely related to the area of fullerene and nano-tube chemistry.

## 1.2 Non-alternant PAH

Alternant PAH are composed of annelated even-membered  $\pi$ -conjugated rings. The carbon atoms in these compounds can be divided into two sets, *viz.* *s* (starred) and *u* (un-starred) with each *s*-carbon having only *u* neighbors and *vice versa*. Non-alternant PAH, in contrast, are  $\pi$ -conjugated compounds that have at least one odd-membered, annelated ring, for example, a pentagon or heptagon.<sup>25</sup> In non-alternant PAH always either two adjacent *s*-carbons or *u*-carbons can be found (see Chart 1). The presence of such an odd-membered ring in the structure has a significant effect on the properties when compared to a structure with only even-membered rings, *i.e.* alternant PAH. As a consequence, an asymmetric charge distribution along the molecule is present. Furthermore, an odd-membered ring can give rise to curvature, which will affect the overlap of the neighboring  $\pi$ -orbitals.<sup>8,26</sup>

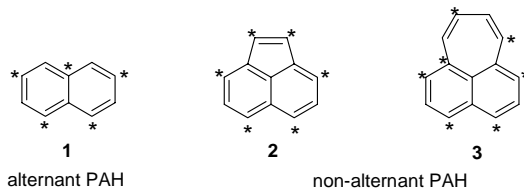


**Chart 1.** Alternant naphthalene (1) *vs.* the non-alternant PAH acenaphthylene (2) and pleiadene (3).

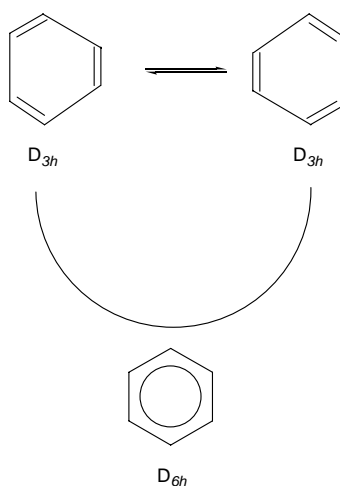
### 1.2.1 Aromaticity: the concept

When Faraday isolated and identified benzene (initially named bicarburet of hydrogen), he entitled it aromatic because of its typical fragrance.<sup>27</sup> The elucidation of its molecular formula ( $C_6H_6$ ) revealed that benzene is an unsaturated compound. However in contrast to alkenes, benzene is reluctant to undergo the classical addition reactions, but instead displays substitution reactions. This unexpected behavior ultimately led to the modern concept of aromaticity. Hence, the term aromaticity has evolved from the fragrance of a compound to a theoretical model. Despite the importance of this concept in organic chemistry, it neither has a precise definition nor is reflected by a direct measurable quantity.<sup>28</sup> This is predominantly caused by the fact that suitable reference systems are required that often are (experimentally) inaccessible. Aromaticity is for example associated with bond length equalization (geometric criterion) and ‘increased stability’ (energy

criterion). However, a still unanswered question is compared to what. As a consequence various criteria for aromaticity exist, both experimental and theoretical. However, no agreement (convergence) exists about *the* criteria for aromaticity. Experimental criteria can be divided into geometric, energetic, chemical reactivity and magnetic criteria. For example, benzene possesses a  $D_{6h}$  instead of  $D_{3h}$  structure, has a lower heat of hydrogenation than an alkene-like reference compound containing three isolated (non-interacting) double bonds, is reluctant to undergo addition reactions and sustains a diatropic ring current due to cyclic  $\pi$ -electron delocalization when exposed to a perpendicular external magnetic field. Most of the models and theories that have been put forward, however, explain only a few of the above-described phenomena.<sup>28</sup>

### 1.2.2 Models for aromaticity

The first model put forward that could rationalize part of the peculiar behavior of benzene was postulated by Kekulé in 1865.<sup>29</sup> Benzene is described as an ‘oscillating’ 1,3,5-cyclohexatriene structure ( $D_{3h}$ ). With a fast equilibrium formation both the substitution behavior of benzene and the structure ( $D_{6h}$ ) could be interpreted. However, its incorrectness became immediately apparent, since all attempts to freeze out this equilibrium failed.



**Scheme 1.** The equilibrium between two 1,3,5-cyclohexatriene ( $D_{3h}$ ) isomers according to Kekulé.<sup>29</sup>

The theoretical description of aromaticity started with the Hückel ‘ $4n+2$ ’-rule derived for planar  $\pi$ -conjugated monocycles.<sup>30,31</sup> In this model (HMO theory), the  $\pi$ -molecular orbital energy-

level diagram can be constructed using the following set of approximations. Only  $\pi$ -electrons are taken into account. As all carbon atoms are treated identically, all Coulomb interactions are equal and set to a value  $\alpha$ . The resonance integrals are set equal to zero for all non-neighboring atoms and equal to  $\beta$  for neighboring atoms. In the case of benzene this leads to three bonding and three *anti*-bonding  $\pi$ -molecular orbitals. The  $\pi$ -electron energy for benzene is  $6\alpha + 8\beta$ , whereas for three (non-interacting) localized bonds the  $\pi$ -electron energy is  $6\alpha + 6\beta$ . Hence, the delocalization energy or the stabilization energy in benzene is  $2\beta$  according to the Hückel model.

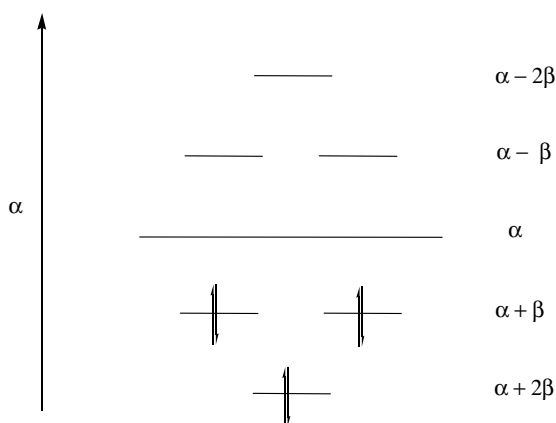


**Figure 1.** Energy levels for the  $\pi$ -molecular orbitals ( $\pi$ -MO's) of benzene according to Hückel (HMO) theory.

The conceptual strength of the Hückel model has had a major impact on the description of aromaticity. Although it was formally derived for planar  $\pi$ -conjugated monocycles, it is frequently used for (polycyclic) alternant PAH. For example, various correlations were found between the  $\epsilon_{\text{LUMO}}/\epsilon_{\text{HOMO}}$  Hückel energies and experimentally accessible physicochemical parameters such as the redox properties.<sup>25</sup> In contrast, however, such correlations could not be obtained for non-alternant PAH.<sup>9,32</sup> This was attributed to be a consequence of the non-symmetrical distribution of the energy levels around the  $\alpha$ -level, which leads to a non-uniform charge distribution in the molecules. However, it could also have its origin in the use of 'exotic' representatives as azulene and pleiadiene for these correlations.

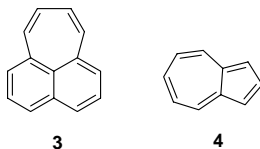


**Chart 2.** The known 'exotic' non-alternant PAH pleiadene (**3**) and azulene (**4**).

A few important comments concerning the applicability of Hückel theory to (non)-alternant-PAH should be made. HMO theory describes aromaticity as a global property (energy criterion) of a compound. However, in the case of PAH the different rings may contribute differently [(local) aromaticity] to the overall (global) aromaticity. The discrepancies that arise when PAH are treated with a model derived for monocycles, led to the development of other (more refined) models and theories. For example, the now refuted ring-perimeter model has been put forward as another model. In this model only the perimeter  $\pi$ -electrons were thought to be of importance.<sup>25</sup> Furthermore, theories were developed in which all possible conjugation pathways were taken into account ('conjugated circuits').<sup>33</sup> Robinson and Clar proposed the theory of the aromatic sextet, *i.e.* the most stable structure in a  $\pi$ -conjugated polycycle will possess the maximum number of benzenoid sextets (Chart 3). This theory describes aromaticity as a local property.<sup>34</sup> In all descriptions that are discussed so far the aromatic properties are attributed to  $\pi$ -electron contributions. However, the papers from Shaik, Hiberty and co-workers seriously attacked this view.<sup>35-37</sup> Their calculations, in which they separated the  $\sigma$ - and  $\pi$ -electron contributions, indicated that not the  $\pi$ -electrons but the  $\sigma$ -electrons favor the  $D_{6h}$  geometry of benzene. *Ab initio* valence bond calculations, however, indicate that a delicate interplay between the  $\sigma$ -system, the  $\pi$ -system and resonance determines the geometry of benzene.<sup>38,39</sup> Hence, the description of the aromaticity of, especially, non-alternant PAH, is still a subject of debate.

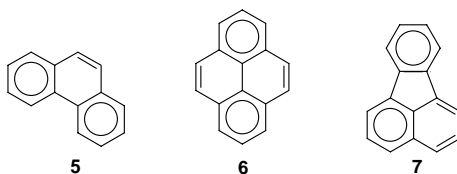


**Chart 3.** Clar representation of phenanthrene (**5**), pyrene (**6**) and fluoranthene (**7**).



### 1.2.3 Aromaticity: the magnetic criterion

One of the criteria for aromaticity in a  $\pi$ -conjugated monocycle is the presence of cyclic electron delocalization, which manifests itself by sustaining a ring current when an external magnetic field is applied.<sup>40</sup> According to Hückel-London theory, a  $\pi$ -conjugated monocycle containing  $4n+2$   $\pi$ -electrons will sustain a diatropic (aromatic) ring current when exposed to a perpendicular external magnetic field, whereas a monocycle with  $4n$   $\pi$ -electrons will display a paratropic (*anti*-aromatic) ring current.<sup>41</sup> Although, ring currents are not directly observable, they can be inferred from integrated properties, such as <sup>1</sup>H-NMR chemical shifts, magnetic anisotropy ( $\Delta\zeta$ ) and exaltation of isotropic magnetic susceptibility ( $\Lambda$ ).<sup>40,42</sup>

Hence, study of the <sup>1</sup>H-NMR chemical shifts,  $\Delta\zeta$  and  $\Lambda$  has become a useful tool to gain insight in the global aromaticity of the  $\pi$ -conjugated polycycle.<sup>43</sup> The magnetic properties of molecules can also be assessed theoretically. In recent years several methods have been developed and are now widely used to evaluate these properties computationally. The <sup>1</sup>H- and <sup>13</sup>C-NMR chemical shifts,  $\Delta\zeta$  and  $\Lambda$ , can be calculated with *ab initio* methods such as Individual Gauges for Localized molecular Orbitals (IGLO) or Gauge Invariant (including) Atomic Orbitals (GAIO).<sup>42</sup> Insight in the *local* aromaticity of the individual rings of a polycycle can be obtained by the calculation of the nucleus independent chemical shift (NICS) values for the distinct rings.<sup>44</sup> In a different approach the non-observable ring currents can be visualized by calculating the all-electron current density maps of the molecule using the continuous transformation of origin of current density method in the diamagnetic zero approximation (CTOCD-DZ).<sup>45,46</sup> A unique feature of the *ipso*centric CTOCD-DZ approach is that a physically realistic analysis of the contributions from the different molecular orbitals to the computed ring currents in terms of occupied to unoccupied transitions is possible.<sup>47</sup> Furthermore, also with this method the experimental <sup>1</sup>H- and <sup>13</sup>C-NMR chemical shifts,  $\Delta\zeta$ ,  $\Lambda$  and NICS can be calculated by integration of the current density maps.<sup>48</sup>

### 1.2.4 Synthesis of non-alternant PAH: the FVT approach

In order to establish the applicability of non-alternant PAH as model compounds for fullerenes and for the identification of potential fullerenes precursors, efficient syntheses of non-alternant PAH had to be accessible. In first instance, the attention was mainly focused on the syntheses and properties of cyclopenta-fused PAH, since these molecules constitute formal building blocks of classical fullerenes, *i.e.* those fullerenes composed of pentagons and hexagons.<sup>14</sup> Furthermore, cyclopenta-fused PAH are also predominantly formed during incomplete combustion and reference compounds are needed to unequivocally identify these pollutants and assess their physicochemical and biological properties (section 1.2.6).<sup>1</sup> Whereas many alternant PAH can be

Chapter 1

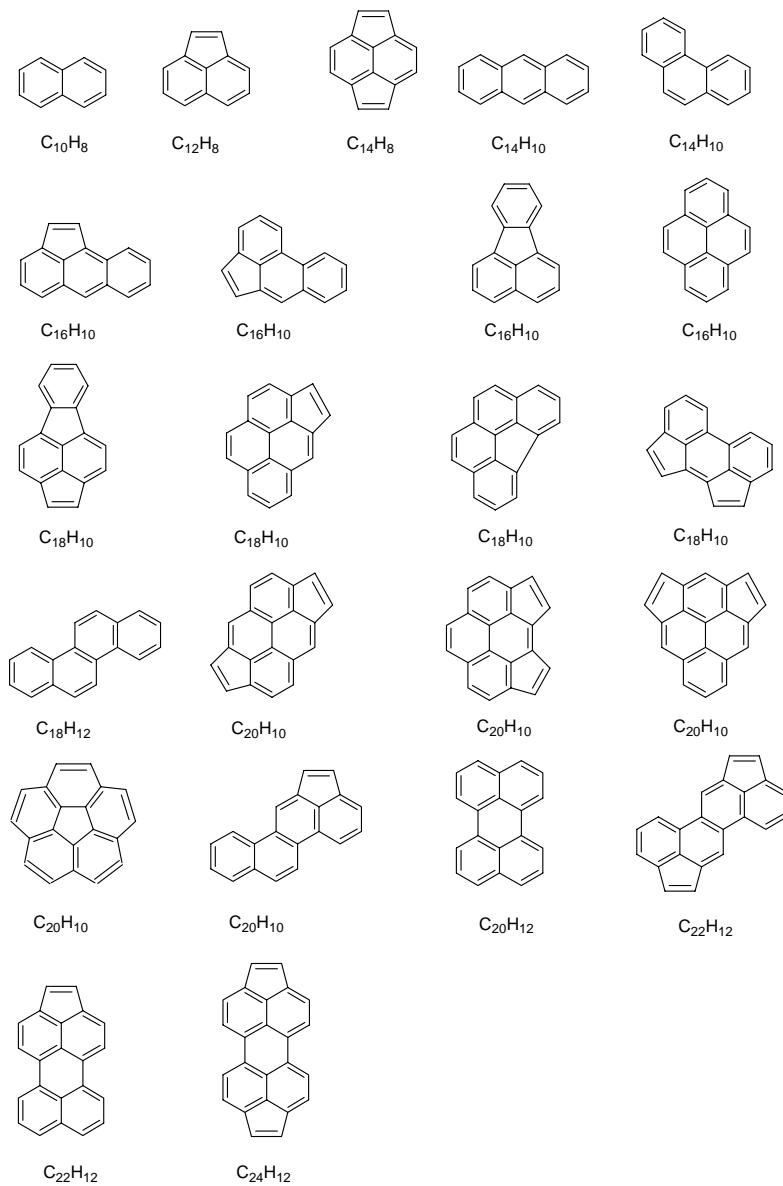


**Chart 4.** Cyclopenta-fused polycyclic aromatic hydrocarbons that have become available by the use of Flash Vacuum Thermolysis (FVT).

isolated from coal tar, for CP-PAH lengthy and difficult classical ‘wet’ syntheses were developed.<sup>34,49-52</sup> Although a recent reported Pd-catalyzed reaction is an important improvement on these syntheses,<sup>53</sup> gas phase reactions by means of Flash Vacuum Thermolysis (FVT) or Flow Pyrolysis (FP) have proven to be the methods of choice for the preparation of CP-PAH.<sup>12,14</sup> Especially, since certain representatives, such as the *bis*-cyclopentapyrene isomers, can hitherto only be obtained by FVT.<sup>15,54</sup> In a typical FVT experiment the pressure is low (0.01 - 0.001 mm Hg), the temperatures are high (600°C - 1200°C) and the residence times of the precursor that has to be sublimed into the hot zone of the furnace are in the order of milliseconds. Under these conditions primarily unimolecular reactions take place. Due to collisions with the walls the precursor gains thermal energy, whereupon it rearranges to the desired CP-PAH. Ethynyl-substituted (E-PAH) or 1-chloroethynyl (‘masked’ E-PAH) have shown to be excellent precursors for CP-PAH. *Via* this approach a large set of *mono*- and *bis*-substituted CP-PAH has been prepared in our laboratory in excellent to reasonable yields and mass recoveries.<sup>14</sup>

In contrast to the availability of a plethora of cyclopenta-fused PAH, other non-alternant PAH such as cyclohepta-fused PAH have not received much attention. Some derivatives of this class of molecules were prepared. Examples are pleiadiene,<sup>21,55</sup> acepleiadiene,<sup>56</sup> dipleiadiene<sup>57</sup> and cyclohepta[*j,k*]phenanthrene (Chart 5).<sup>19</sup> However, in all cases lengthy synthetic routes were employed. A problem hereby is the reactivity of these molecules in solution and the (undesired) formation of mixtures of different constitutional isomers. Whereas cyclopenta-fused PAH cause positive curvature, cyclohepta-fused PAH have also been recognized as interesting synthetic target since the cyclohepta-moiety can induce negative curvature in a graphitic sheet.<sup>17,58,59</sup>

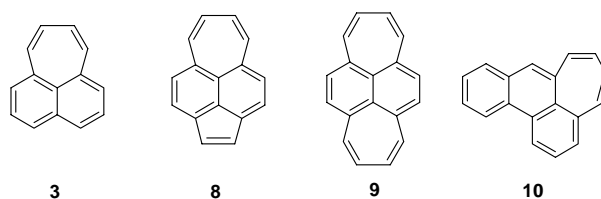


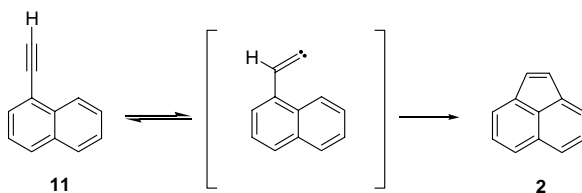
**Chart 5.** The known cyclohepta-fused PAH pleiadiene (3), acepleiadiene (8), dipleiadiene (9) and cyclohepta[*j,k*]phenanthrene (10).

### 1.2.5 Behavior of (CP)-PAH under high temperature conditions

As discussed above, (CP)-PAH are invariably formed during incomplete combustion processes.<sup>1</sup> The recognition that various representatives possess genotoxic properties instigated much activity to unravel their structure, build up, and rearrangement and fragmentation behavior under high

temperature conditions.<sup>2</sup> Valuable information on the formation of (CP)-PAH has been obtained by careful analyses of combustion exhausts with available reference molecules obtained by FVT,<sup>1,60</sup> study of the high temperature rearrangements of abundant (CP)-PAH by independent FVT experiments<sup>12,14</sup> and flame experiments.<sup>61</sup> Since a distinct set of (non)-alternant PAH are invariably formed during combustion processes, the build-up processes do not take place, as might expected, in a chaotic fashion.<sup>62</sup>

The formation of benzene under high temperature in flames has extensively been studied and is proposed to proceed either *via* reaction of two propargyl radicals or by reaction of acetylene with a  $C_4H_x$  species.<sup>63,64</sup> Subsequently, the build up of larger aromatic molecules is proposed to take place *via* accretion of  $C_2H_2$  and other alkene/alkyn-chains to the aromatic core.<sup>64</sup> Accretion of  $C_2H_2$  to PAH leads to the formation of ethynyl-substituted PAH (E-PAH).<sup>65,66</sup> These E-PAH have been identified in combustion mixtures and are expected to be important intermediates since they can rearrange amongst others to CP-PAH.<sup>60</sup> This is proposed to occur *via* ethynyl-ethylidene equilibration followed by C-H insertion of the ethylidene carbene (Scheme 2).<sup>13</sup> Application of FVT has been essential in elucidating the potential of E-PAH as precursors for CP-PAH.<sup>12,14</sup>

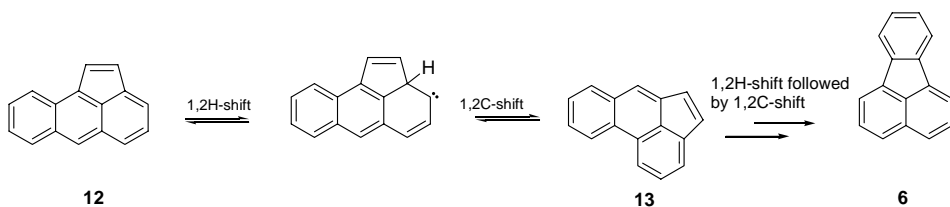


**Scheme 2.** Formation of cyclopenta-fused PAH from the corresponding ethynyl-substituted PAH *via* ethynyl-ethylidene carbene equilibration and C-H insertion of the ethylidene carbene.

Another remarkable property of (non)-alternant PAH is their ability to undergo well-defined skeletal rearrangements/conversions under high temperature conditions. In the case of CP-PAH, these rearrangements mostly proceed *via* ring-contraction/ring-expansion processes involving 1,2-H and 1,2-C shifts and carbene intermediates, and ultimately lead to the formation of the thermodynamic more stable isomer (Scheme 3).<sup>11,12</sup> A vivid example is the rearrangement of acenanthrylene into acephenanthrylene and finally fluoranthene with increasing temperature (Scheme 3).<sup>67</sup> Detailed insight in these rearrangements was obtained by performing FVT experiments at different temperatures followed by pyrolysate analysis.<sup>14</sup> It has become clear that the occurrence of skeletal rearrangements may seriously affect the overall composition and, as a consequence the genotoxic properties of the combustion exhausts.<sup>68</sup> Moreover, these processes

rationalize that during (incomplete) combustion processes only a distinct set of CP-PAH, varying with temperature, is formed. Besides build up and rearrangements, breakdown can occur *via* C<sub>2</sub>- or C<sub>2</sub>H<sub>2</sub>-extrusions from E-PAH or CP-PAH whereupon the original PAH core is recovered.<sup>14</sup>

Although, in recent years much insight has been obtained in the high temperature chemistry of CP-PAH, many issues still remain unresolved. For example, the viability of the ethynyl-ethylidene equilibration and C-H insertion of the ethylidene carbene has been questioned recently on the basis of *ab initio* calculations.<sup>69</sup> The intermediacy of carbene-like species in the skeletal rearrangement is not without flaws. Their reactivity renders them difficult to detect experimentally and hampers the assessment of their properties experimentally. Furthermore, computation of their properties is also not a simple task; in many instances a single configuration is not sufficient, *i.e.* static and dynamic correlations have to be taken into account. From a more practical perspective a question remains why besides CP-PAH no other non-alternant PAH have yet been identified in combustion mixtures, since accretion of other C<sub>n</sub>-fragments should be feasible.<sup>70</sup> Apparently, not all pathways operational under high temperature conditions have yet been elucidated.



**Scheme 3.** Skeletal rearrangement of aceanthrylene (8) to acephenanthrylene (9) and cyclopenta[*c,d*]fluoranthene (10) *via* 1,2-H and 1,2-C shifts involving carbene intermediates.

### 1.2.6 Properties of non-alternant PAH

The annelation of an odd-membered ring, such as a pentagon, to an alternant core considerably affects the properties of the  $\pi$ -conjugated molecule. This is clear from several observations. For example, in some cases the <sup>1</sup>H-NMR chemical shifts of a CP-PAH are shifted up-field with respect to the <sup>1</sup>H-NMR chemical shifts of the related alternant PAH.<sup>15,54</sup> This indicates that upon cyclopenta-fusion the overall aromaticity (global aromaticity) of the molecule will be reduced. Recent theoretical evaluations of the magnetic properties of CP-PAH confirm this observation.<sup>48</sup> Furthermore, CP-PAH have significantly less negative first reduction potentials than the

corresponding PAH.<sup>14</sup> Several CP-PAH give in addition rise to anomalous S<sub>2</sub> fluorescence, which is not observed for the alternant PAH.<sup>71-73</sup>

### 1.3 Fullerenes

The first idea for a hypothetical spherical molecule with 60 carbon atoms arose already in 1970 in a theoretical study related to 'superaromaticity'.<sup>74,75</sup> In 1985, the formation of C<sub>60</sub> and C<sub>70</sub> was for the first time proposed, when persistent features positioned at 720 and 840 a.m.u. in the mass spectrum were observed during laser vaporization of graphite.<sup>5</sup> When the groups of Krätschmer and Huffman produced carbon particles by evaporating graphite in an arc generating soot, under certain experimental conditions additional UV- ('the camel humps') and IR-features were observed in the soot that were not recognized at that time. Later, 'the camel humps' and IR-features were indeed identified as absorption bands of C<sub>60</sub>.<sup>76</sup> Unequivocal evidence for the structure of C<sub>60</sub> and C<sub>70</sub> was eventually obtained after their isolation from this soot by simple extraction followed by characterization.<sup>6,77</sup>

#### 1.3.1 Fullerene formation

Although, C<sub>60</sub> and C<sub>70</sub> can now be obtained in reasonable quantities from the soot obtained by arc-vaporization of graphite, the mechanism by which the fullerenes are formed is still not clear. Several mechanisms have been put forward, but up till now no mechanism can account for all the experimental observations. Two of the proposed mechanisms are the 'pentagon road' and 'the fullerene road'.<sup>78,79</sup> The first involves the introduction of cyclopenta-fused rings in graphitic sheets under high temperature conditions. This leads to curling up of the surface, which will reduce the amount of undesired dangling bonds. Hereupon, the curved graphitic sheet can give closed carbon spheres.

In the fullerene road mechanism, the proposed intermediates are not (curved) graphitic sheets but small closed carbon cages consisting of 30-58 carbon atoms. These small carbon cages are proposed to grow by accretion of C<sub>2</sub> fragments to the cyclopenta-rings.

As stated above, a large set of (CP)-PAH is invariably formed under high temperature conditions in the gas phase, for example in flames. Remarkably, under certain conditions, such as in acetylene and benzene flames, besides (CP)-PAH, fullerenes are also formed.<sup>1,80</sup> Furthermore, the fullerenes C<sub>60</sub> and C<sub>70</sub> are also formed upon pyrolysis of PAH as naphthalene, corannulene.<sup>81-84</sup> Hence, this strongly suggests that a relation exists between the formation of fullerenes and (CP)-PAH under high temperature conditions.

More recently, an even more spectacular relation between (CP)-PAH and fullerene formation in the solid state was proposed, albeit with trepidation because it entails formidable hurdles. This hypothesis is based on the following. On three different locations  $C_{60}$  has been identified in terrestrial hard rocks (geological samples) by geochemists.<sup>85-87</sup> Initially, the presence of  $C_{60}$  was explained by the fact that extraterrestrial bodies must have struck the earth on these sites which led to the extreme conditions (forest fires) to transform carbonaceous matter into fullerenes.<sup>86</sup> Most recently, however, it was proposed that the presence of the fullerenes in the hard rocks might also have a biologic origin with remnants of algae being the carbon source as they could be formed by transformations in the solid state from algae *via* PAH to fullerenes.<sup>88</sup> Hence, under different conditions (solid state *vs.* gas phase and high pressure *vs.* high temperature) similar chemistry is proposed to be operational.

### 1.3.2 Properties of fullerenes

Several aspects of the formation and properties of fullerenes have been or still are subject of intensive research. For example, the fact that 'spherical' molecules are stable under the extreme conditions under which they are formed. The answer to this question appears to have a kinetic origin. Once fullerenes are formed, the barrier to convert them to other constitutional isomers is very high.<sup>89</sup>

The question whether fullerenes have to be considered as 3D aromatic  $\pi$ -conjugated systems or not, has been subject of debate since their initial discovery. Due to the presence of both pentagons (paratropic contributions) and hexagons (diatropic contributions), predictions concerning the global aromaticity of  $C_{60}$  were not easy to make. Magnetic indicators such as NMR chemical shifts seem to indicate that cyclic electron delocalization is present in fullerenes. However, fullerenes are prone to undergo addition reactions, *i.e.* possess alkene-like behavior.<sup>7,90</sup>

In addition, a fascinating property of fullerenes is their high electron affinity, *i.e.* their ability to take up six electrons under mild conditions, forming hexa-anions. This behavior was initially interpreted by considering fullerenes to be build up of 6 pycrylene units. These units can take up two electrons forming cyclopentadienide sub-structures each containing six  $\pi$ -electrons.<sup>91</sup> An important question is whether the facile reduction of  $C_{60}$  and  $C_{70}$  is due to their non-alternant character or due to the curvature. As will be shown in this thesis several aspects of fullerene chemistry can be readily interpreted by studying the properties of the smaller (planar) key sub-structures of which they are composed.

## 1.4 Fullerenes by design; The Schlegel-match proposition

Although,  $C_{60}$  and  $C_{70}$  can now be prepared in reasonable quantities, the arc-vaporization of graphite is reluctant to modification and therefore the properties of these molecules cannot be altered.<sup>92</sup> This initiated the quest to design selective syntheses for, in first instance,  $C_{60}$  and  $C_{70}$ . One approach put forward, is to synthesize (curved) CP-PAH with the aim to subsequently link several together. Various synthetic strategies were developed to obtain these curved sub-structures, *i.e.* 'buckybowls'.<sup>10,93</sup> Despite the fact that the linking of these large buckybowls has not yet been achieved,<sup>94-96</sup> these molecules are interesting model compounds to study the effect of curvature on aromaticity.<sup>97</sup>

Another approach is based on the idea that cyclic polyynes also may be important intermediates in the build up of fullerenes under high temperature conditions. Note that the formation of  $C_{60}$  from an *in-situ* generated cyclic  $C_{30}$  polyynene has been observed to occur under mass spectrometric conditions.<sup>98</sup> Therefore, large cage-like polyynes were designed (Figure 2), which were proposed to rearrange in the mass spectrometer to fullerenes.<sup>98-103</sup> A problem concerning these large cage-like polyynes is their lack of stability. As a consequence, they can only be generated *in-situ* inside the mass spectrometer from a protected precursor. Furthermore, neither experimental nor theoretical proof has been provided that under these conditions the drastic rearrangement of the carbon skeleton takes place as proposed in a unimolecular fashion and that ultimately a closed carbon surface is indeed obtained.<sup>99</sup>

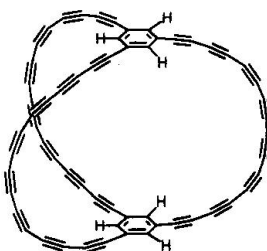


**Figure 2.** Proposed  $C_{60}$  polyynene precursor.

A different approach to access proper unimolecular fullerene precursors is to start with a 2D progenitor that already contains the correct carbon topology as the fullerene that has to be formed. *i.e.* non-alternant PAH (Schlegel-match). Such a precursor for  $C_{60}$  is the  $C_{60}H_{30}$  CP-PAH



Benzo[1,2-*e*:3,4-*e'*:5,6-*e''*]tribenzo[*h*]acephenanthrylene (Figure 3c).<sup>104</sup> To determine the correct carbon topology, a two dimensional projection of the desired fullerene has to be made, *i.e.* a Schlegel map (Figure 3b). In this thesis it will be shown that a prerequisite for the successful conversion of a CP-PAH precursor into a fullerene under relatively mild conditions and without the occurrence of fragmentation, is the presence of this ‘Schlegel-match’.

A tantalizing objective is ultimately the preparation of hitherto unknown materials with closed carbon surfaces of which the properties can be varied by introduction of hetero-atoms, other odd-membered rings or the selective preparation of endohedral materials. In this respect, the synthesis of novel azafullerenes or azafulleranes is of worthwhile objective.<sup>105,106</sup> The presence of nitrogen atoms is expected to have a huge effect on the properties of the molecule. Upon replacement of one carbon atom by one nitrogen atom, an open-shell system is obtained. Therefore, *mono*-azafullerenes were isolated as either dimers or as their hydroazafullerene (azafullerane) derivatives.<sup>107-109</sup> Whilst fullerenes have high electron affinities, *i.e.* are good n-type materials, the presence of nitrogen atoms might render these molecules electropositive, *i.e.* add p-type character.

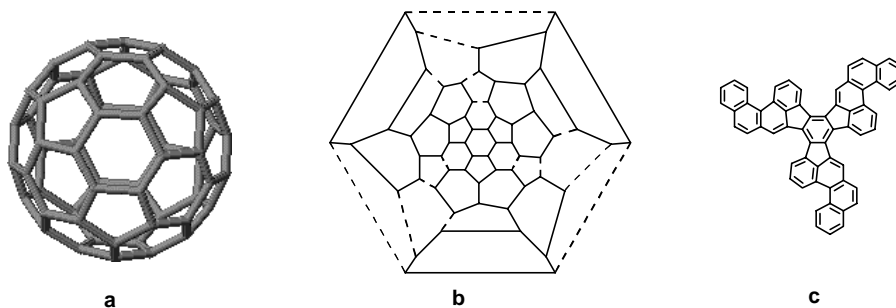


**Figure 3.** **a.**  $C_{60}$  **b.** its 2D projection, *i.e.* Schlegel diagram and **c.** the unimolecular non-alternant precursor  $C_{60}H_{30}$ .

#### 1.4.1 Carbon nanotubes

Shortly after the discovery of the fullerenes, also (multi- and single wall) carbon nanotubes were prepared and identified by a modification of the original procedure.<sup>16</sup> These robust structures combine a set of extraordinary properties, such as a high tensile strength, high thermal conductivity, high current carrying capacity and electronic properties ranging from metallic to *semi*-conducting depending on the helicity of the tube.<sup>110</sup> In the miniaturization in electronics *via* the

'bottom-up' approach, *i.e.* the formation of electronic structures from well-defined nano-scale molecular building blocks, carbon nanotubes are promising candidates.<sup>111-113</sup> The great challenge in carbon nanotube chemistry is still the selective preparation and isolation of tubes with the same length, diameter and helicity.

Carbon nanotubes consist of folded graphene sheets. However, it recently has been shown that bending and coiling in these tubes have their origin in the presence of both a pentagon and a heptagon.<sup>17,59,114</sup> Whereas, the pentagon is responsible for positive curvature, the heptagon is hereby thought to be responsible for the negative curvature (see Figure 4).

These seemingly unwanted defects can lead to interesting modification of the properties of the structure.<sup>110,115</sup> For example, the combination of a pentagon and a heptagon can introduce a junction between two carbon nanotubes with different helicity. Hereby, forming metal - *semi*-conductor, metal - metal or *semi*-conductor - *semi*-conductor molecular nano-scale junctions.<sup>110</sup> Furthermore, calculations predict that in the pentaheptide modification of the graphite sheet in which all hexagonal rings are replaced by pentagons and heptagons, carbon might be metallic.<sup>115-117</sup>

Although, the key sub-structures of classical fullerenes, cyclopenta-fused PAH, have drawn much attention, the other sub-structures of bended and folded nanotubes, cyclohepta-fused PAH, have not. Thus also from this perspective, insight in their structure, stability and electronic properties is of interest to selectively obtain carbon-nanotubes with 'defects' and tune their properties.

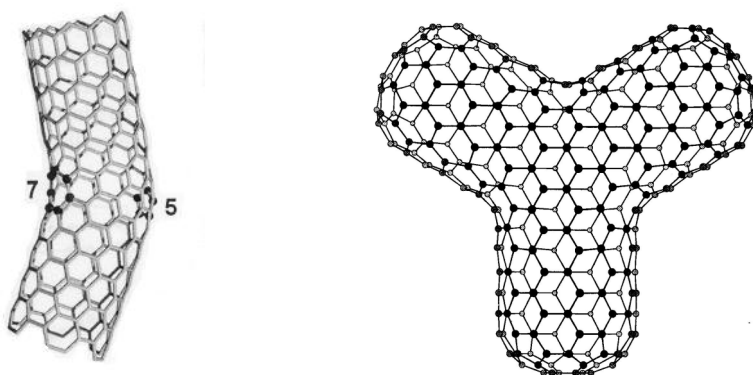


**Figure 4.** Examples of the effect of the presence of heptagons on the structure of closed carbon surfaces.

## 1.5 Corollary

The chemistry of 2D (non)-alternant PAH and 3D closed carbon surfaces as fullerenes, carbon nanotubes and materials yet to be discovered is, as has been shown, intimately related. This connection is present in the gas phase, where both non-alternant PAH and fullerenes can be formed under similar conditions. Hence, study of the build up and rearrangements of non-alternant PAH in the gas phase is of topical interest since it could give information concerning ‘missing links’ connecting the 2D and 3D structures. The relationship between the formation in the gas phase also inspired the quest for the selective synthesis of the fullerenes  $C_{60}$  and  $C_{70}$  starting from non-alternant PAH. This might result in syntheses where the structure and thereby the properties can be tuned. The relation between non-alternant PAH and closed carbon surfaces is also present on a more fundamental level: non-alternant PAH as sub-structures and model compounds to study the effect of odd-membered rings and curvature on the properties of the system.

## 1.6 Outline of this Thesis

The aim of this thesis is to study several aspects of the (2D) chemistry of non-alternant PAH with the objective to gain insight in the chemistry of the larger (3D) closed carbon surfaces.

- In **Part I** of this thesis (**Chapter 2** and **3**) some fundamental rearrangements of alternant PAH and non-alternant CP-PAH in the gas phase are studied.
- In **Part II** (**Chapters 4 – 6**) the selective syntheses of closed carbon surfaces, *i.e.*  $C_{60}$ ,  $C_{70}$  and new azafullerenes starting from non-alternant PAH are described.
- In **Part III** (**Chapters 7 – 9**) the electronic and magnetic properties of two classes of sub-structures of fullerenes and bended carbon nanotubes, *i.e.* cyclopenta- and cyclohepta-fused PAH are discussed.

In **Chapter 2**, the mechanism by which CP-PAH are formed in the gas phase, *i.e.* the rearrangement of ethynyl-substituted PAH to CP-PAH, is studied by FVT of selectively *mono*-deuterated ethynyl-substituted PAH. Besides support for the Brown mechanism, *viz.* ethynyl-ethylidene equilibration followed by C-H insertion of the ethylidene carbene, previously unidentified migrations of the hydrogen along the perimeter of the molecule under FVT conditions were observed. The results affect the interpretation of mechanistic studies of (CP)-PAH under high temperature conditions where deuterium-labels have been employed.

In **Chapter 3** it is shown that a similar process as observed for non-alternant PAH in **Chapter 2**, *viz.* hydrogen migration along the perimeter of a molecule, is also operational in alternant PAH.

In **Chapter 4**, the synthesis of  $C_{60}$  under MALDI TOF-MS conditions is described by ‘zipping up’ of the non-alternant  $C_{60}H_{30}$  PAH benzo[1,2-*e*:3,4-*e'*:5,6-*e''*]tribenzo[*d*]acephenanthrylene, which fulfills our Schlegel-match proposition criterion. The zipping up process is studied by comparison with two sub-structures of the  $C_{60}H_{30}$  precursor, benzo[1,2-*e*:3,4-*e'*:6,5-*e''*]triaceneanthrylene ( $C_{48}H_{24}$ ) and decacycene ( $C_{36}H_{18}$ ). *Semi-empirical* and *ab initio* calculations corroborate the experimental results.

In **Chapter 5**, two possible  $C_{70}$  progenitors, based on the results obtained in Chapter 4 are proposed and their conversion into  $C_{70}$  is studied by *semi-empirical* and *ab initio* calculations. The results show that the progenitors can indeed be converted into  $C_{70}$ , which makes their syntheses worthwhile.

In **Chapter 6**, the Schlegel-match proposition is applied to obtain a novel material with a closed carbon surface; the ionic azafullerane  $C_{57}N_2H_3$ . Its synthesis is achieved by ‘zipping up’ the  $C_{57}H_{33}N_3$  Schlegel-match precursor under MALDI TOF-MS conditions.

In **Chapter 7**, the redox properties of 23 PAH, *mono*-CP-PAH and *bis*-CP-PAH are studied. In contrast to previous studies, a linear correlation between the first reduction potential and the  $-\epsilon_{LUMO}$  energy derived from Hückel (HMO) theory is found. It is shown that the cyclopenta-moiety in externally-fused CP-PAH acts as a *peri*-substituent. A simple HMO model can be used to explain the behavior of *mono*- as well as *bis*-substituted CP-PAH upon reduction. The applicability of HMO theory is validated by *ab initio* calculations.

In **Chapter 8**, the syntheses and rearrangements under FVT conditions of novel CH-PAH are described. The formation of CH-PAH and CP-PAH in the gas phase is interrelated. CH-PAH are shown to be susceptible to oxidation and therefore expected to induce p-type character to the compound. A linear correlation between first oxidation potential and the  $-\epsilon_{HOMO}$  energy derived from HMO theory is found.

Finally, in **Chapter 9** the magnetic properties of a set of CH-PAH are investigated. The presence of CH-moiety leads in most cases to an overall up-field shift of the  $^1H$ -NMR chemical resonances, due to the presence of strong paratropic ring currents in the CH-moiety. It is shown that the presence of both a cyclopenta- and a cyclohepta-moiety in one molecule leads to interesting new properties.

## References

- (1) Lafleur, A. L.; Howard, J. B.; Taghizadeh, K.; Plummer, E. F.; Scott, L. T.; Necula, A.; Swallow, K. C. *J. Phys. Chem.* **1996**, *100*, 17421-17428.
- (2) Jacob, J. *Pure & Appl. Chem.* **1996**, *68*, 301-308.
- (3) Allamandola, L. J. *Topics in Current Chemistry* **1990**, *153*, 1-25.
- (4) Jenneskens, L. W.; Vlietstra, E. J.; Sarobe, M.; Ponzano, S. N. R. *Polycyclic. Aromat. Compd.* **1999**, *10*, 169-178.
- (5) Kroto, H. W.; Heath, J. R.; O'Brien, S. C.; Curl, R. F.; Smalley, R. E. *Nature* **1985**, *318*, 162-163.
- (6) Krätschmer, W.; Lamb, L. D.; Fostiropoulos, K.; Huffman, D. R. *Nature* **1990**, *347*, 354-358.
- (7) Bühl, M.; Hirsch, A. *Chem. Rev.* **2001**, *101*, 1153-1183.
- (8) Haddon, R. C. *Acc. Chem. Res.* **1988**, *21*, 243-249.
- (9) Haddon, R. C. *Phil. Trans. R. Soc. Lond. A* **1993**, *343*, 53-62.
- (10) Mehta, G.; Prakash Rao, H. S. *Tetrahedron* **1998**, *54*, 13325-13370.
- (11) Jenneskens, L. W.; Sarobe, M.; Zwikker, J. W. *Pure & Appl. Chem.* **1996**, *68*, 219-224.
- (12) Scott, L. T. *Pure & Appl. Chem.* **1996**, *68*, 291-300.
- (13) Brown, R. F. C.; Eastwood, F. W. *Synlett* **1993**, 9-19.
- (14) Sarobe, M. *Polycyclic Aromatic Hydrocarbons under High Temperature Conditions. Consequences for Carbon Build up during Combustion and Fullerene Formation Processes.*; Utrecht University: Utrecht, The Netherlands, **1998**.
- (15) Scott, L. T.; Necula, A. *J. Org. Chem.* **1996**, *61*, 386-388.
- (16) Iijima, S. *Nature* **1991**, *56*, 354.
- (17) Iijima, S.; Ichihashi, T.; Ando, Y. *Nature* **1992**, *356*, 776-778.
- (18) Pagni, R. M.; Watson, C. R. *Tetrahedron Lett.* **1973**, *1*, 59-60.
- (19) Pagni, R. M.; Burnett, M.; Hazell, A. C. *J. Org. Chem.* **1978**, *43*, 2750-2752.
- (20) Michl, J. *J. Am. Chem. Soc.* **1976**, 4546-4549.
- (21) Shields, J. E.; Gavrilovic, D.; Kopecky, J.; Hartmann, W.; Heine, H.-G. *J. Org. Chem.* **1974**, *39*, 515-520.
- (22) Gómez-Lor, B.; Koper, C.; Fokkens, R. H.; Vlietstra, E. J.; Cleij, T. J.; Jenneskens, L. W.; Nibbering, N. M. M.; Echavarren, A. M. *Chem. Commun.* **2002**, 370-371.
- (23) Scott, L. T.; Boorum, M. M.; McMahon, B. J.; Hagen, S.; Mack, J.; Blank, J.; Wegner, H.; de Meijere, A. *Science* **2002**, *295*, 1500-1503.
- (24) Boorum, M. M.; Vasil'ev, Y. V.; Drewello, T.; Scott, L. T. *Science* **2001**, *294*, 828-831.
- (25) Streitwieser, A. *Molecular Orbital Theory for Organic Chemists*; Wiley: New York, 1961.

## Chapter 1

- (26) Scott, L. T.; Hashemi, M. M.; Meyer, D. T.; Warren, H. B. *J. Am. Chem. Soc.* **1991**, *113*, 7082-7084.
- (27) Faraday, M. *Phil. Trans.* **1825**, 440.
- (28) See the complete issue of *Chem. Rev.* **2001**, *101*.
- (29) Kekulé, A. *Liebigs. Ann.* **1866**, *137*, 162.
- (30) Hückel, E. *Z. Phys.* **1931**, *70*, 204.
- (31) Hückel, E. *Z. Phys.* **1931**, *72*, 310.
- (32) Fry, A. J.; Foc, P. C. *Tetrahedron* **1986**, *42*, 5255-5266.
- (33) Randic, M.; Trinajstić, N. *J. Am. Chem. Soc.* **1984**, *106*, 4428-4434.
- (34) Clar, E. *Polycyclic Aromatic Hydrocarbons*; Academic Press Inc.: London, 1964.
- (35) Hiberty, P. C.; Shaik, S. S.; Lefour, J. M.; Ohanessian, G. *J. Org. Chem.* **1985**, *50*, 4657.
- (36) Shaik, S. S.; Hiberty, P. C.; Lefour, J. M.; Ohanessian, G. *J. Am. Chem. Soc.* **1987**, *109*, 363.
- (37) Shaik, S. S.; Shurki, A.; Danovich, D.; Hiberty, P. C. *J. Mol. Struct. (Theochem)* **1997**, *398-399*, 155.
- (38) van Lenthe, J. H.; Havenith, R. W. A.; Dijkstra, F.; Jennekens, L. W. *Chem. Phys. Lett.* **2002**, *361*, 203-208.
- (39) Dijkstra, F.; van Lenthe, J. H.; Havenith, R. W. A.; Jennekens, L. W. *Int. J. Quant. Chem.* **2003**, *91*, 566-574.
- (40) Schleyer, P. v. R.; Jiao, H. *Pure & Appl. Chem.* **1996**, *68*, 209-218.
- (41) Coulson, C. A.; Mallion, R. B. *J. Am. Chem. Soc.* **1976**, *98*, 592-598.
- (42) Fleischer, U.; Kutzelnigg, W.; Lazeretti, P.; Muhlenkamp, V. *J. Am. Chem. Soc.* **1994**, *116*, 5298-5306.
- (43) Mitchell, R. H. *Chem. Rev.* **2001**, *101*, 1301-1316.
- (44) Schleyer, P. v. R.; Maerker, C.; Darnsfeld, A.; Jiao, H.; van Eikema Hommes, N. J. R. *J. Am. Chem. Soc.* **1996**, *118*, 6317-6318.
- (45) Steiner, E.; Fowler, P. W. *J. Chem. Soc., Chem. Commun.* **2001**, 2220-2221.
- (46) Steiner, E.; Fowler, P. W. *J. Phys. Chem. A* **2001**, *105*, 9553-9562.
- (47) Zanasi, R.; Lazeretti, P.; Malagoli, M.; Piccinini, F. *J. Chem. Phys.* **1995**, *18*, 7150-7157.
- (48) Havenith, R. W. A.; Jiao, H.; Jennekens, L. W.; van Lenthe, J. H.; Sarobe, M.; Schleyer, P. v. R.; Kataoka, M.; Necula, A.; Scott, L. T. *J. Am. Chem. Soc.* **2002**, *124*, 2363-2370.
- (49) Harvey, R. G. *Polycyclic Aromatic Hydrocarbons*; Wiley-VCH, Inc: New York, 1997.
- (50) Trost, B. M.; Bright, G. M. *J. Am. Chem. Soc.* **1967**, *89*, 4244-4245.
- (51) Tintel, C.; Cornelisse, J.; Lugtenburg, J. *Recl. Trav. Chim. Pays-Bas* **1983**, *102*, 14-20.
- (52) van Dijk, J. T. M.; Hartwijk, A.; Bleeker, A. C.; Lugtenburg, J.; Cornelisse, J. *J. Org. Chem.* **1996**, *61*, 1136.

- (53) Dang, H.; Levitus, M.; Garcia-Garibay, M. A. *J. Am. Chem. Soc.* **2002**, *124*, 136-143.
- (54) Sarobe, M.; Flink, S.; Jenneskens, L. W.; van Poecke, B. L. A.; Zwikker, J. W. *J. Chem. Soc., Chem. Commun.* **1995**, 2415-2416.
- (55) Murata, I.; Nakasuji, K. *Tetrahedron Lett.* **1973**, *1*, 47-50.
- (56) Boekelheide, V.; Vick, G. K. *J. Am. Chem. Soc.* **1956**, *78*, 653.
- (57) Vogel, E.; Neumann, B.; Klug, W.; Schmickler, H.; Lex, J. *Angew. Chem.* **1985**, *97*, 1044-1045.
- (58) Mackay, A. L.; Terrones, H. *Nature* **1991**, *352*, 762.
- (59) Yao, Z.; Postma, H. W. C.; Balents, L.; Dekker, C. *Nature* **1999**, *402*, 273-276.
- (60) Ledesma, E. B.; Kalish, M. A.; Wornat, M. J.; Nelson, P. F.; Mackie, J. C. *Energy & Fuels* **1999**, *13*, 1167-1172.
- (61) Wang, X.; Becker, H.; Hopkinson, A. C.; March, R. E.; Scott, L. T.; Bohme, D. K. *Int. J. Mass Spectrom. Ion Proc.* **1997**, *161*, 69-76.
- (62) Offenberg, J. H.; Eisenreich, S. J.; Chen, L. C.; Cohen, M. D.; Chee, G.; Prophete, C.; Weisel, C.; Lioy, P. J. *Environ. Sci. Technol.* **2003**, *37*, 502-508.
- (63) Miller, J. A.; Melius, C. F. *Combust. Flame* **1992**, *91*, 21.
- (64) Wang, H.; Frenklach, M. *Combust. Flame* **1997**, *110*, 173.
- (65) Necula, A.; Scott, L. T. *J. Am. Chem. Soc.* **2000**, *122*, 1548-1549.
- (66) Bauschlicher, C. W.; Ricca, A. *Chem. Phys. Lett.* **2000**, *326*, 283-287.
- (67) Sarobe, M.; Jenneskens, L. W.; Wesseling, J.; Snoeijer, J. D.; Zwikker, J. W.; Wiersum, U. E. *Liebigs. Ann./Recueil* **1997**, 1207-1213.
- (68) Howard, J. B.; Longwell, J. P.; Marr, J. A.; Pope, C. J.; Busby, W. F., Jr.; Lafleur, A. L.; Taghizadeh, K. *Combust. Flame* **1995**, *101*, 262-270.
- (69) Cioslowski, J.; Schimeczek, M.; Piskorz, P.; Moncrieff, D. J. *J. Am. Chem. Soc.* **1999**, *121*, 3773-3778.
- (70) Kroto, H. W. *J. Chem. Soc., Faraday Trans.* **1990**, *86*, 2465-2468.
- (71) Plummer, B. F.; Al-Saigh, Z. *J. Phys. Chem.* **1983**, *87*, 1579-1582.
- (72) Gooijer, C.; Kozin, I.; Velthorst, N. H.; Sarobe, M.; Jenneskens, L. W.; Vlietstra, E. J. *Spectrochim. Acta* **1998**, *54*, 1443-1449.
- (73) Plummer, B. F.; Al-Saigh, Z.; Arfan, M. *Chem. Phys. Lett.* **1984**, *104*, 389-392.
- (74) Osawa, E. *Kagaku* **1970**, *25*, 854.
- (75) Osawa, E. *Phil. Trans. R. Soc. Lond. A* **1993**, *343*, 9.
- (76) Krätschmer, W.; Huffman, D. R. *Phil. Trans. R. Soc. Lond. A* **1993**, *343*, 33.
- (77) Taylor, R.; Hare, J. P.; Abdul-Sada, A. K.; Kroto, H. W. *J. Chem. Soc., Chem. Commun.* **1990**, 1423-1425.

## Chapter 1

- (78) Smalley, R. E. *Acc. Chem. Res.* **1992**, *25*, 98-105.
- (79) Heath, J. R. *ACS Symp. Ser.* **1991**, *481*, 1.
- (80) Pope, C. J.; Howard, J. B. *Tetrahedron* **1996**, *52*.
- (81) Taylor, R.; Langley, G. J.; Kroto, H. W.; Walton, D. R. M. *Nature* **1993**, *366*, 728.
- (82) Crowley, C.; Kroto, H. W.; Taylor, R.; Walton, D. R. M.; Bratcher, M. S.; Cheng, P. C.; Scott, L. S. *Tetrahedron Lett.* **1995**, *36*, 9215.
- (83) Crowley, C.; Taylor, R.; Kroto, H. W.; Walton, D. R. M.; Cheng, P. C.; Scott, L. S. *Synth. Met* **1996**, *77*, 17.
- (84) Osterodt, J.; Zett, A.; Vogtle, F. *Tetrahedron* **1996**, *52*, 4949-4962.
- (85) Busek, P. R.; Tsipurski, S. J.; Hettich, R. *Nature* **1992**, *247*, 215.
- (86) Becker, L. *Science* **1994**, *256*, 642.
- (87) Jehlicka, J.; Ozawa, M.; Salina, Z.; Osawa, E. *Fullerene Sci. Techn.* **2000**, *8*, 449.
- (88) Heymann, D.; Jenneskens, L. W.; Jehlicka, J.; Koper, C.; Vlietstra, E. J. *Int. J. Astrobiol.* **2003**, *in press*.
- (89) Curl, R. F. *Phil. Trans. R. Soc. Lond. A* **1993**, *343*, 19.
- (90) Poater, J.; Fradera, X.; Duran, M.; Solà, M. *Chem. Eur. J* **2003**, *9*, 1113-1122.
- (91) Wudl, F. *Acc. Chem. Res.* **1992**, *25*, 157-161.
- (92) Goroff, N. S. *Acc. Chem. Res.* **1996**, *29*, 77-83.
- (93) Rabideau, P. W.; Sygula, A. *Acc. Chem. Res.* **1996**, *29*, 235-242.
- (94) Diederich, F.; Rubin, Y. *Angew. Chem. Int. Ed. Engl.* **1992**, *31*, 1101-1123.
- (95) Sastry, G. N.; Jemmis, E. D.; Mehta, G.; Shah, S. R. *J. Chem. Soc., Perkin Trans. 2* **1993**, 1867-1871.
- (96) Faust, R.; Vollhardt, K. P. C. *J. Chem. Soc., Chem. Commun.* **1993**, 1471-1473.
- (97) Preda, D. V.; Scott, L. T. *Tetrahedron Lett.* **2000**, *41*, 9633-9637.
- (98) Diederich, F.; Thilgen, C. *Science* **1996**, *271*, 317-324.
- (99) Bunz, U. H. F.; Rubin, Y.; Tobe, Y. *Chem. Soc. Rev.* **1999**, *28*, 107-119.
- (100) Rubin, Y.; Parker, T. C.; Pastor, S. J.; Jalisatgi, S.; Bouille, C.; Wilkins, C. L. *Angew. Chem. Int. Ed. Engl.* **1998**, *37*, 1226-1229.
- (101) Tobe, Y.; Nakagawa, J.; Kishi, J.; Sonoda, M.; Naemura, K.; Wakabayashi, T.; Shida, T.; Achiba, Y. *Tetrahedron* **2001**, *57*, 3629-3636.
- (102) Tobe, Y.; Furukawa, R.; Sonoda, M.; Wakabayashi, T. *Angew. Chem. Int. Ed. Engl.* **2001**, *113*, 4196-4198.
- (103) Prinzbach, H.; Weiler, A.; Landenberger, P.; Wahl, F.; Wörth, J.; Scott, L. T.; Gelmont, M.; Olevano, D.; Issendorf, B. *Nature* **2000**, *407*, 60-63.



- (104) Sarobe, M.; Fokkens, R. H.; Cleij, T. J.; Jenneskens, L. W.; Nibbering, N. M. M.; Stas, W.; Versluis, C. *Chem. Phys. Lett.* **1999**, *313*, 31-39.
- (105) Hirsch, A.; Nuber, B. *Acc. Chem. Res.* **1999**, *32*, 795-804.
- (106) Hauke, F.; Hirsch, A. *Tetrahedron* **2001**, *57*, 3697-3708.
- (107) Hummelen, J. C.; Knight, B.; Pavlovich, J.; González, R.; Wudl, F. *Science* **1995**, *269*, 1554-1556.
- (108) Keshavarz-K., M.; González, R.; Hicks, R. G.; Srdanov, G.; Srdanov, V. I.; Collins, T. G.; Hummelen, J. C.; Bellavia-Lund, C.; Pavlovich, J.; Wudl, F.; Holczner, K. *Nature* **1996**, *383*, 147-150.
- (109) Nuber, B.; Hirsch, A. *Chem. Commun.* **1996**, 1421-1424.
- (110) Charlier, J.-C. *Acc. Chem. Res.* **2002**, *35*, 1063-1069.
- (111) Batchold, A.; Hadley, P.; Nakanishi, T.; Dekker, C. *Science* **2001**, *294*, 1317-1320.
- (112) Huang, Y.; Duan, X.; Cui, Y.; Lauhon, L. J.; Kim, K.-H.; Lieber, C. M. *Science* **2001**, *294*, 1313-1317.
- (113) Avouris, P. *Acc. Chem. Res.* **2002**, *35*, 1026-1034.
- (114) Kondo, Y.; Takayanagi, K. *Jpn. J. Appl. Phys.* **1999**, *38*, L1208-L1210.
- (115) Terrones, H.; Terrones, M.; Hernández, E.; Grobert, N.; Charlier, J.-C.; Ajayan, P. M. *Phys. Rev. Lett.* **2000**, *84*, 1716-1719.
- (116) Crespi, V. H.; Benedict, L. X.; Cohen, M. L.; Louie, S. G. *Phys. Rev. B.* **1996**, *53*, R13303-R13305.
- (117) Deza, M.; Fowler, P. W.; Shtogrin, M.; Vietze, K. *J. Chem. Inf. Comput. Sci.* **2000**, *40*, 1325-1332.



# Part I

*Rearrangements*



# CHAPTER 2

## Unexpectedly Facile Hydrogen Migrations in Cyclopenta-Fused Polycyclic Aromatic Hydrocarbons under high Temperature Conditions

### Abstract

Flash Vacuum Thermolysis (FVT) of selectively *mono*-deuterated 9-<sup>2</sup>H-ethynylphenanthrene [**1(9-<sup>2</sup>H)**], 1-<sup>2</sup>H-ethynyl-naphthalene [**4(1-<sup>2</sup>H)**] and 1-(1-chloroethenyl)-4-<sup>2</sup>H-naphthalene [**6(4-<sup>2</sup>H)**] gave, according to <sup>1</sup>H-, <sup>2</sup>H- and <sup>13</sup>C-NMR in combination with (GC)-MS and GC-cryo-FT-IR, initially the corresponding cyclopenta-fused polycyclic aromatic hydrocarbons (CP-PAH) expected on the basis of the mechanism proposed by Brown *et al.* Unexpectedly, however, migration of the deuterium atom within the cyclopenta-moiety and from this unit to the aromatic core and *vice versa* takes place. *Ab initio* calculations (B3LYP/TZ2P) were performed on the possible carbene intermediates. The occurrence of these facile hydrogen migrations has important consequences for the interpretation of mechanistic studies on (CP)-PAH under high temperature conditions where deuterium-labels were employed.

## 2.1 Introduction

Experiments have shown that two processes are of main importance for the chemistry of polycyclic aromatic hydrocarbons under high temperature conditions; build up and skeletal rearrangements.<sup>1-5</sup> One of the pathways leading to build up is C<sub>2</sub>H<sub>2</sub> accretion. Upon accretion of C<sub>2</sub>H<sub>2</sub> to small polycyclic aromatic hydrocarbons ethynyl-substituted PAH (E-PAH) are formed.<sup>6-8</sup> These E-PAH have been identified in combustion mixtures, and are considered to be important intermediates in combustion processes since they are direct precursor for cyclopenta-fused PAH (CP-PAH).<sup>9</sup> This is supported by Flash Vacuum Thermolysis (FVT) experiments in which ('masked') E-PAH were found to rearrange to CP-PAH in the dilute gas phase under high temperature conditions.<sup>4,5,10</sup> Brown *et al.* proposed that CP-PAH are generated from their ethynyl-substituted precursors *via* ethynyl-ethylidene carbene equilibration followed by C-H insertion of the ethylidene carbene.<sup>11</sup> However, the intermediacy of ethylidene carbenes was recently refuted on the basis of *ab initio* BLYP/6-311G\*\* calculations. It was found that *after* zero point energy corrections the transition state leading to this carbene is lower in energy than the ethylidene carbene itself.<sup>12</sup>

Another important phenomenon is that CP-PAH may further rearrange to isomeric CP-PAH or PAH *via* skeletal rearrangements.<sup>13</sup> This was rationalized by the occurrence of a ring contraction/ring expansion mechanism involving consecutive 1,2-H/1,2-C shift or *vice versa*.<sup>13,14</sup> Experimental evidence for this mechanism was provided by <sup>13</sup>C-labeling experiments.<sup>15-17</sup> Besides a scientific curiosity, these skeletal rearrangements are of practical relevance since non-mutagenic (CP)-PAH can be converted into mutagenic isomers.<sup>4,5,18</sup> Hence, build-up and rearrangements of CP-PAH under high temperature conditions contribute to the overall toxicity of the combustion mixture formed.

The objectives of this Chapter are twofold. Firstly, the theoretically refuted ethynyl-ethylidene carbene equilibration followed by C-H insertion of the ethylidene carbene is reinvestigated by FVT of selectively *mono*-deuterated E-PAH. Secondly, this approach opens up the opportunity to assess the fate of the deuterium atoms attached to the core of the CP-PAH. Although the behavior of the carbon atoms in (CP)-PAH have been studied by <sup>13</sup>C-labeling experiments,<sup>16,19,20</sup> the behavior of hydrogen atoms has not been considered explicitly.<sup>21</sup> Therefore, selectively deuterated 9-<sup>2</sup>H-ethynylphenanthrene [**1(9-<sup>2</sup>H)**], 1-<sup>2</sup>H-ethynyl-naphthalene [**4(1-<sup>2</sup>H)**], and 1-(1-chloroethenyl)-4-<sup>2</sup>H-naphthalene [**6(4-<sup>2</sup>H)**], a 'masked' E-PAH, are subjected to FVT in the temperature range 700°C - 1000°C (Schemes 1 - 3). The *mono*-deuterated precursors **1(9-<sup>2</sup>H)**, **4(1-<sup>2</sup>H)** and **6(4-<sup>2</sup>H)** are according to the Brown mechanism expected to give the *mono*-deuterated CP-PAH 2-<sup>2</sup>H-acephenanthrylene [**2(5-<sup>2</sup>H)**],<sup>22</sup> 1-<sup>2</sup>H-acenaphthylene [**5(1-<sup>2</sup>H)**]<sup>23</sup> and 5-

<sup>2</sup>H-acenaphthylene [**5(5-<sup>2</sup>H)**], respectively (Schemes 1 - 3).<sup>11</sup> Unexpectedly, the results unequivocally show that besides the formation of the *mono*-deuterated CP-PAH **2(5-<sup>2</sup>H)**, **5(1-<sup>2</sup>H)** and **5(5-<sup>2</sup>H)** *via* ethynyl-ethylidene carbene equilibration followed by C-H insertion of the ethylidene carbene, previously unnoted deuterium migrations do take place within the cyclopentamoiety, from this moiety to the aromatic core and *vice versa*. Hereupon, a set of *mono*-deuterated isotopomers is formed.

## 2.2 Results & Discussion

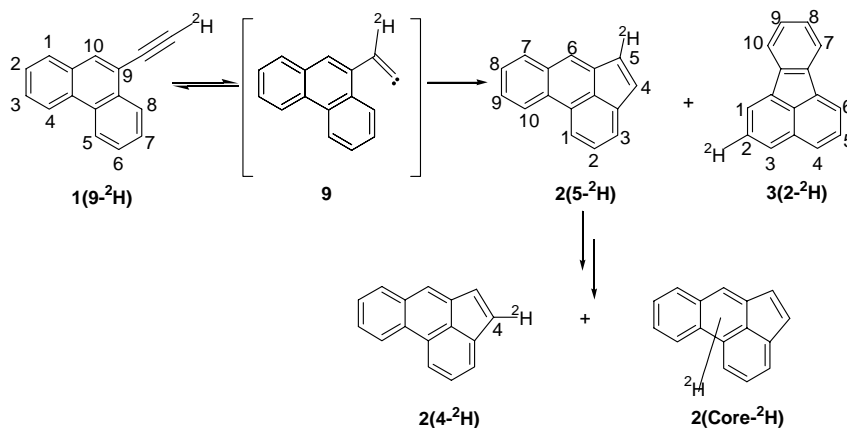
### 2.2.1 FVT of 9-<sup>2</sup>H-Ethynylphenanthrene [**1(9-<sup>2</sup>H)**]

The selectively *mono*-deuterated 9-<sup>2</sup>H-ethynylphenanthrene [**1(9-<sup>2</sup>H)**] was obtained from natural abundance 9-ethynylphenanthrene (**1**) *via* treatment with *n*-butyllithium and subsequent quenching with D<sub>2</sub>O. The degree of deuteration of **1(9-<sup>2</sup>H)** (98%) was established using <sup>1</sup>H-, <sup>2</sup>H, <sup>13</sup>C-NMR and mass spectrometry (GC-MS, direct inlet MS). It is noteworthy that PAH and especially E-PAH as well as CP-PAH readily undergo extrusion of hydrogen atoms and C<sub>2</sub>H<sub>2</sub> fragments under mass spectrometric conditions.<sup>24-26</sup> As a consequence, even after reduction of E.I. from 70 eV to 16 eV, the isotope pattern of *only* the molecular ion of **1(9-<sup>2</sup>H)** could still not be obtained, since hydrogen extrusions are discernible. Fortunately, however, the molecular ion of the *mono*-deuterated compounds possesses the largest intensity and we observed that the degree of hydrogen extrusion from this ion for the different reference samples measured under similar conditions is nearly constant (GC-MS, E.I. 70 eV, for further details see Experimental Section). Hence, throughout this Chapter the isotope patterns of the precursors and the pyrolysate constituents are compared to those measured for the corresponding natural abundance compounds. In line with the presence of *one* deuterium atom, the isotope pattern of **1(9-<sup>2</sup>H)** is shifted by one mass unit ( $m/z$  203) with respect to that of natural abundance **1** ( $m/z$  202), but displays the same intensities. FVT of **1(9-<sup>2</sup>H)** at 700°C [ $p = 1 \cdot 10^{-3}$  mm Hg, sublimation (subl.)  $T = 70$  °C, subl. rate 50 mg $h^{-1}$ ] yields the starting compound (90%) and three acephenanthrylene isotopomers (**2**) (10%) [mass recovery 100%, Table 1,  $M^+$   $m/z$  203 no increase in  $[M-1]^+$  and  $[M+1]^+$  is found in comparison with natural abundance **2** ( $m/z$  202)]. Spectroscopic analyses show that the minor amount of acephenanthrylene has *most* of the deuterium at position C5 [**2(5-<sup>2</sup>H)**, 80%, Table 1]. This is evident from <sup>1</sup>H-NMR where predominantly a broad singlet is present at 7.23 ppm [ $J$  (H4 - <sup>2</sup>H5) < 1Hz, Figure 1A] and from <sup>2</sup>H-NMR [7.12 ppm, **2(5-<sup>2</sup>H)**]. The formation of **2(5-<sup>2</sup>H)** is in accordance with the Brown mechanism (Scheme 1). In contrast to **2**, the starting material [**1(9-<sup>2</sup>H)**] recovered after FVT at 700°C remains unaltered (<sup>1</sup>H-, <sup>2</sup>H- and <sup>13</sup>C-NMR); the deuterium atom is still positioned in the ethynyl-moiety. This is in agreement with the

**Table 1.** Product composition of the pyrolysates obtained after FVT of 9-<sup>2</sup>H-ethynylphenanthrene [**1(9-<sup>2</sup>H)**].

T(°C)	Products formed (%)					Recovery (%)
	<b>1(9-<sup>2</sup>H)</b>	<b>2(4-<sup>2</sup>H)</b>	<b>2(5-<sup>2</sup>H)</b>	<b>2(core-<sup>2</sup>H)<sup>a</sup></b>	<b>3</b>	
700	90	1	8	1	-	100
800	55	4	40	1	-	98
900	trace	20	56	22	2	96
1000	-	30	50	16	4	94

<sup>2</sup>**2(core-<sup>2</sup>H)** represents the different isotopomers of **2** containing one deuterium in the PAH core **2(1-<sup>2</sup>H)** – **2(3-<sup>2</sup>H)** and **2(6-<sup>2</sup>H)** – **2(10-<sup>2</sup>H)**, Scheme 2].



**Scheme 1.** Rearrangement of **1(9-<sup>2</sup>H)** into *mono*-deuterated isotopomers of **2** upon Flash Vacuum Thermolysis (FVT).

occurrence of equilibration between the ethynyl and the ethylidene carbene (1,2-H shift, Scheme 1) at high temperatures. Interestingly, the broad, low intensity signal in between the original doublet at 7.12 ppm in <sup>1</sup>H-NMR reveals that besides **2(5-<sup>2</sup>H)** also a small amount of **2** with deuterium at C4 [**2(4-<sup>2</sup>H)**] is formed. This is confirmed by the presence of a <sup>2</sup>H-NMR resonance at 7.2 ppm. Additionally, also a weak AB pattern [<sup>1</sup>H-NMR:  $J_{AB} = 5.1$  Hz] reveals the presence of acenaphthylene (**2**) with two hydrogen atoms attached to the cyclopenta-moiety! In the 800°C pyrolysate the amount of isotopomers of **2** has increased [**1**: 55%, **2**: 45%, mass recovery 98%,  $M^+$   $m/z$  203 no increase in  $[M-1]^+$  and  $[M+1]^+$  is found in comparison with natural abundance **1** ( $m/z$  202) and **2** ( $m/z$  202)]. As can be seen from Table 1, slightly more of **2(4-<sup>2</sup>H)** is formed. Upon FVT at 900°C the pyrolysate predominantly contains **2(5-<sup>2</sup>H)** and **2(4-<sup>2</sup>H)** (sum 76 %), a trace of



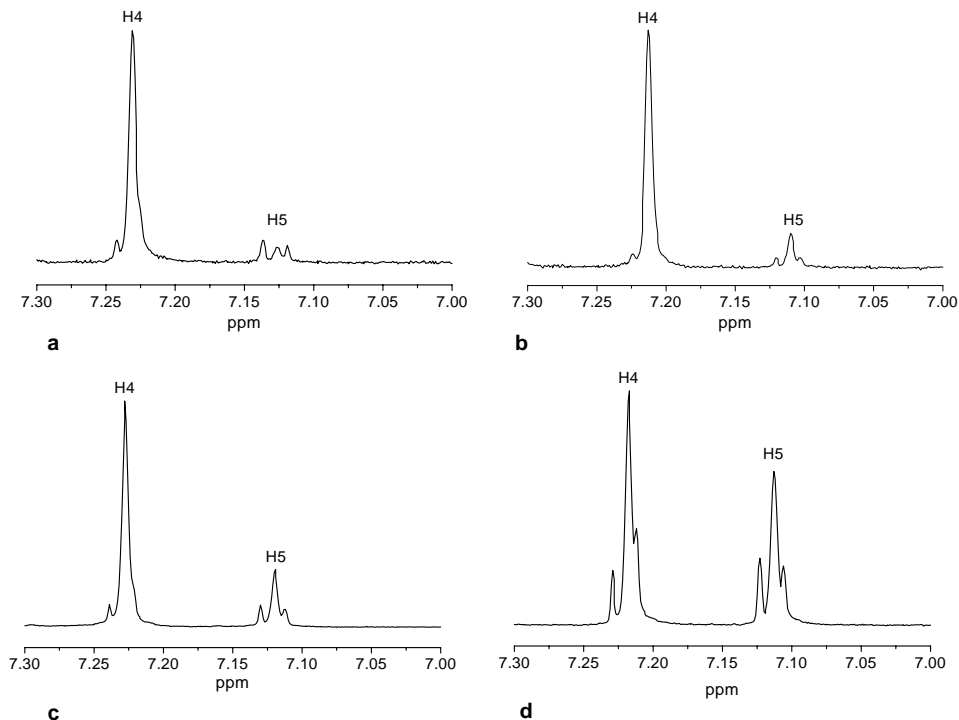


**Figure 1.** Expansions of the signals of the cyclopenta-moiety of **2** (7.3 - 7.0 ppm) in the  $^1\text{H-NMR}$  spectra of pyrolysates obtained after FVT of **1(9- $^2\text{H}$ )** at **a.** 700°C, **b.** 800°C, **c.** 900°C and **d.** 1000°C.

**1(9- $^2\text{H}$ )**, and some fluoranthene (**3**) (2%) [mass recovery 96%,  $\text{M}^+ m/z$  203 no increase in  $[\text{M}-1]^+$  and  $[\text{M}+1]^+$  in comparison with natural abundance **1**, **2** and **3**]. A considerable increase in the amount of **2(4- $^2\text{H}$ )** is observed [*ca.* 20%, Figure 1C and Table 1].  $^2\text{H-NMR}$  spectroscopy confirms that deuterium has migrated within the cyclopenta-moiety (signal at 7.4 ppm). Furthermore, the broadened signals between 7.4 and 8.7 ppm indicate that a deuterium atom in the aromatic core is present. The relative ratio in  $^2\text{H-NMR}$  between the deuterium in the cyclopenta-moiety of **2** [ $^2\text{H-NMR}$ : sum of the resonances at 7.1 and 7.2 ppm] and deuterium in the aromatic core [ $^2\text{H-NMR}$ : sum of the resonances between 7.4 - 8.7 ppm] is similar to the ratio in  $^1\text{H-NMR}$  between the broad singlets and the AB-pattern [between 7.3 and 7.0 ppm, see Figure 1]. Hence, it has to be concluded that in **2** deuterium migrates *from* the cyclopenta-moiety *to* the aromatic core [**2(core- $^2\text{H}$ )**, Scheme 1]. From the data reported in Table 1 it is evident that the amount of **2(core- $^2\text{H}$ )** formed is substantial (22%).

It is noteworthy that the pyrolysate obtained after FVT at 900°C only contains a small amount (2%) of *mono*-deuterated fluoranthene (**3**). This demonstrates that the migration of the deuterium atom from the cyclopenta-moiety to the aromatic core is not directly connected to the known skeletal rearrangements,<sup>22</sup> *i.e.* it thus represents a distinct process, which operates at lower temperatures than the migration of carbon atoms.

In the 1000°C pyrolysate **2** (96%) and **3** (4%) are present (mass recovery 94%,  $M^+ m/z$  203 no increase in  $[M-1]^+$  and  $[M+1]^+$  is found in comparison with natural abundance **2** and **3**). Different isotopomers of **2** are present, from which 50% has the deuterium on the original position [**2(5-<sup>2</sup>H)**], 30% has migrated within the cyclopenta-moiety [**2(4-<sup>2</sup>H)**] and 16% of the deuterium is present in the core [**2(core-<sup>2</sup>H)**]. <sup>2</sup>H-NMR indicates that *all* possible *mono*-deuterated isotopomers with a deuterium atom positioned in the aromatic core are present. Unfortunately, the ratio between the different **2(core-<sup>2</sup>H)** isotopomers could not be determined since the spectral resolution in <sup>2</sup>H-NMR was insufficient. From 900°C only a small amount of **3** is formed. Broad signals positioned in between the original AB-type resonances of natural abundance **3** at 7.96 (H1,6) and 7.86 (H3,4) ppm in <sup>1</sup>H-NMR show that **3(2-<sup>2</sup>H)** is present. These broad signals are a result of the proton-deuterium coupling of H1 with <sup>2</sup>H2 and H3 with <sup>2</sup>H2 ( $J < 2\text{Hz}$ ). The presence of **3(2-<sup>2</sup>H)** is readily explained since at this temperature 56% of **2(5-<sup>2</sup>H)** is present in the pyrolysate, which is *via* skeletal rearrangement a direct precursor for **3** with the deuterium atom positioned at C2 [**3(2-<sup>2</sup>H)**, Scheme 1]. The 900°C pyrolysate contains in addition 20 % **2(4-<sup>2</sup>H)** and 22% **2(core-<sup>2</sup>H)**, which would result in the formation of other *mono*-deuterated isotopomers of **3**. Unfortunately, these isotopomers of **3** could not be detected due to the small amount present (3% of the pyrolysate) and the spectral resolution in <sup>2</sup>H-NMR.

From these results it can be concluded that upon FVT initially the primary product, *i.e.* **2(5-<sup>2</sup>H)**, is formed which is in line with the Brown mechanism (Scheme 1).<sup>11</sup> However, already at low temperature small amounts of other *mono*-deuterated isotopomers [**2(4-<sup>2</sup>H)** and **2(core-<sup>2</sup>H)**] are formed signaling that deuterium migration readily occurs under these conditions. The migration initially takes place within the cyclopenta-moiety and subsequently from this moiety into the aromatic core.

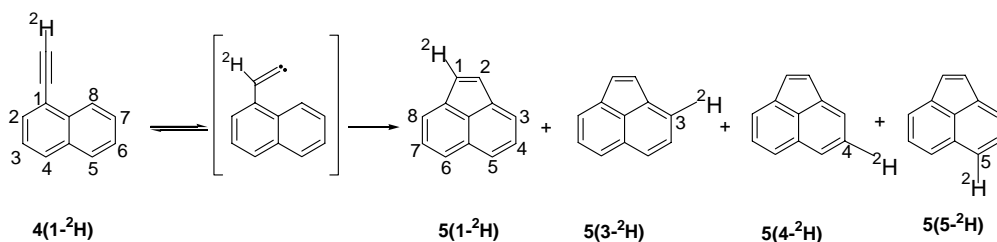
## 2.2.2 FVT of 1-<sup>2</sup>H-Ethynylnaphthalene [**4(1-<sup>2</sup>H)**]

To assess whether the observed deuterium migration in acephenanthrylene (**2**), also takes place in other CP-PAH, the selectively *mono*-deuterated 1-<sup>2</sup>H-ethynylnaphthalene [**4(1-<sup>2</sup>H)**], 97 % *mono*-deuterated according to <sup>1</sup>H-, <sup>2</sup>H-, <sup>13</sup>C-NMR and GC-MS  $M^+ m/z$  153] was subjected to FVT under similar conditions. Although, deuterium migration in the cyclopenta-moiety of **5** will be

degenerate due to its  $C_{2v}$  symmetry, the assignment of *mono*-deuterated isotopomers, after deuterium migration into the naphthalene core will be facilitated. The FVT results of **4(1- $^2\text{H}$ )** [ $1 \cdot 10^{-3}$  mm Hg, subl. T = 50 °C, and subl. rate 60  $\text{mg h}^{-1}$ ] are summarized in Table 2.

**Table 2.** Product composition of the pyrolysates obtained after FVT of 1- $^2\text{H}$ -ethynynaphthalene [**4(1- $^2\text{H}$ )**].

T (°C)	Products formed (%)					Recovery (%)
	<b>4(1-<math>^2\text{H}</math>)</b>	<b>5(1-<math>^2\text{H}</math>)</b>	<b>5(3-<math>^2\text{H}</math>)</b>	<b>5(4-<math>^2\text{H}</math>)</b>	<b>5(5-<math>^2\text{H}</math>)</b>	
700	77	23	-	-	-	98
800	30	70	-	-	-	96
900	-	70	10	10	10	93
1000	-	40	20	20	20	85



**Scheme 2.** Rearrangement of **4(1- $^2\text{H}$ )** into *mono*-deuterated isotopomers of **5** upon Flash Vacuum Thermolysis (FVT).

Upon FVT of **4(1- $^2\text{H}$ )** initially acenaphthylene (**5**) with a deuterium at C1 [**5(1- $^2\text{H}$ )**] is formed (Scheme 2). The 700°C pyrolysate (mass recovery 98%) consists of **4(1- $^2\text{H}$ )** [73%,  $M^+$   $m/z$  153, isotope pattern in agreement with that of natural abundance **4** ( $m/z$  152)] and **5** [23%,  $M^+$   $m/z$  153, isotope pattern in agreement with that of natural abundance **5** ( $m/z$  152)]. In line with expectation, the deuterium in **5** is indeed present in the cyclopenta-moiety [ $^1\text{H}$ -NMR:  $\delta$  7.12 ppm, integral = 1H;  $^2\text{H}$ -NMR 7.12 ppm, Figure 2A]. FVT at 800°C (mass recovery 96%) leads to an increase of the amount of **5** formed [70%,  $M^+$   $m/z$  153, no increase in  $[M-1]^+$  and  $[M+1]^+$  is found in comparison with natural abundance **5**]. Still, most of the deuterium is positioned in the cyclopenta-moiety. However, close scrutiny of  $^2\text{H}$ -NMR spectrum of the 800°C pyrolysate reveals the presence of three additional low intensity peaks (7.8, 7.7 and 7.6 ppm, Figure 2B). These extra deuterium signals are in agreement with the resonances of H5 (7.8 ppm), H3 (7.7 ppm) and H4 (7.6 ppm) of natural abundance **5** in  $^1\text{H}$ -NMR.

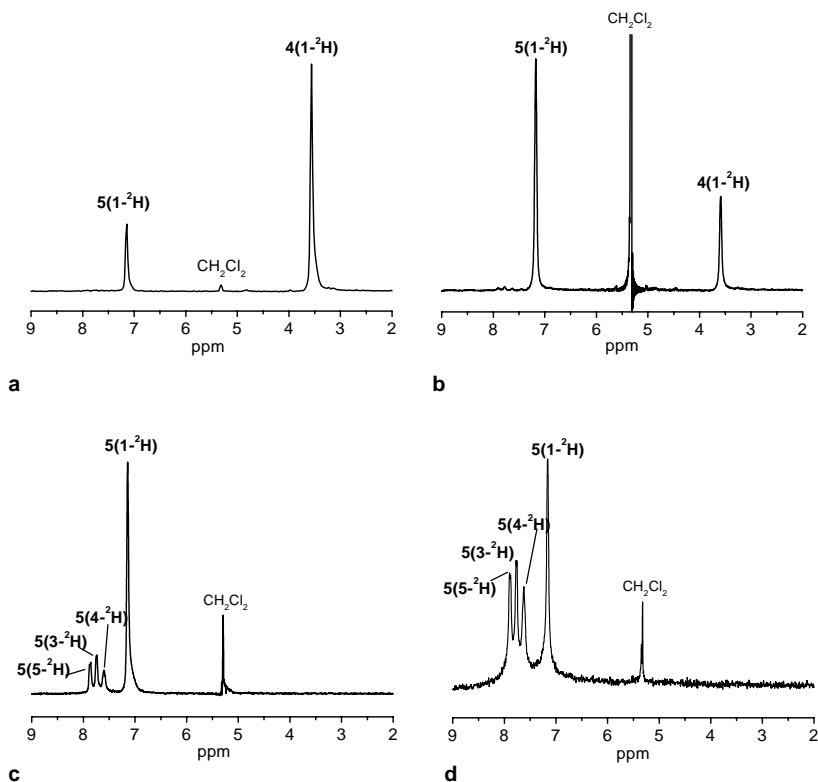


**Figure 2.**  $^2\text{H}$ -NMR spectra (9.0 – 2.0 ppm) of the pyrolysates obtained after FVT of **4(1- $^2\text{H}$ )** at **a.** 700°C, **b.** 800°C, **c.** 900°C, **d.** 1000°C. The different *mono*-deuterated acenaphthylene (**5**) isotopomers are discernible.

Thus, in combination with the MS results, which indicate that only *mono*-deuterated compounds are present, it can be concluded that three isotopomers of **5** with deuterium in the aromatic core [**5(3- $^2\text{H}$ )**, **5(4- $^2\text{H}$ )** and **5(5- $^2\text{H}$ )**] are formed.

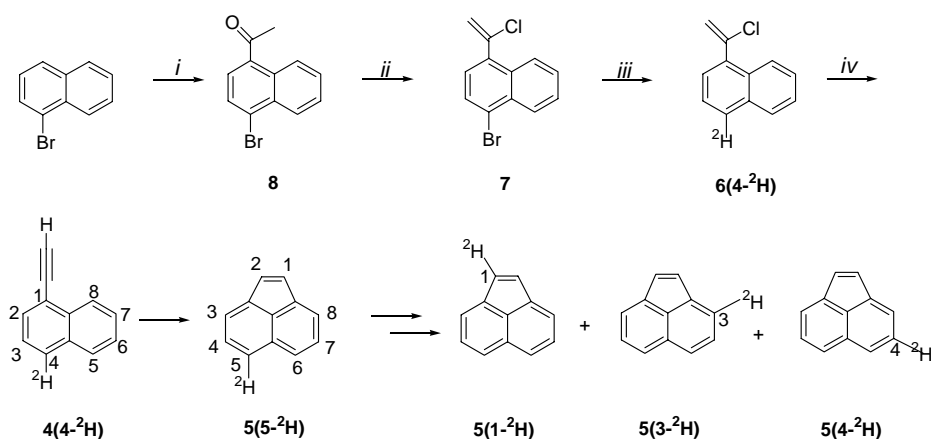
FVT at 900°C of **4(1- $^2\text{H}$ )** (mass recovery 93 %) again only gave *mono*-deuterated **5** [ $\text{M}^+ m/z$  153, isotope pattern in agreement with that of natural abundance **5**]. The constitutional isotopomers with deuterium in the aromatic core [**5(3- $^2\text{H}$ )**, **5(4- $^2\text{H}$ )** and **5(5- $^2\text{H}$ )**] are present [ $^2\text{H}$ -NMR: 7.7, 7.6 and 7.8 ppm; sum *ca.* 30%, Figure 2C]. These isotopomers, **5(3- $^2\text{H}$ )**, **5(4- $^2\text{H}$ )** and **5(5- $^2\text{H}$ )**, are formed in similar amounts (Table 2). At 1000°C (mass recovery 85 %) 60% of **5** [ $\text{M}^+ m/z$  153, isotope pattern is in agreement with that of natural abundance **5**] has a deuterium atom

in the aromatic core. The isotopomers **5(3-<sup>2</sup>H)**, **5(4-<sup>2</sup>H)** and **5(5-<sup>2</sup>H)** are also at this temperature formed in the same ratio. The <sup>1</sup>H-NMR integral ratios show that indeed deuterium has migrated *from* the cyclopenta-moiety *to* the aromatic core since the intensity of the singlet at 7.12 ppm gains intensity with respect to the signals corresponding to the hydrogen in the aromatic core.

Since **5(3-<sup>2</sup>H)**, **5(4-<sup>2</sup>H)** and **5(5-<sup>2</sup>H)** are already discernible upon FVT at 900°C, these isotopomers of **5** cannot be formed by skeletal rearrangements. Flash Vacuum Pyrolysis (FVP) of selectively <sup>13</sup>C-labeled **5** has demonstrated that skeletal rearrangements take only place at elevated temperatures (T > 1000°C).<sup>20</sup> Interestingly, already at this temperature *all* possible isotopomers are formed. This is substantiated by FVT of 1-(1-chloroethenyl)-4-<sup>2</sup>H-naphthalene [**6(4-<sup>2</sup>H)**].

### 2.2.3 FVT of 1-(1-chloroethenyl)-4-<sup>2</sup>H-naphthalene [**6(4-<sup>2</sup>H)**]

To establish whether the reverse process as described for **1(9-<sup>2</sup>H)** and **4(1-<sup>2</sup>H)**, *i.e.* deuterium migration from the aromatic core to the cyclopenta-moiety takes place, 1-(1-chloroethenyl)-4-<sup>2</sup>H-naphthalene [**6(4-<sup>2</sup>H)**] was subjected to FVT (Scheme 3). Compound **6(4-<sup>2</sup>H)**, a 1-chloroethynyl-substituted PAH, is a 'masked' derivative of the E-PAH **4(4-<sup>2</sup>H)**.<sup>27</sup> Selectively *mono*-deuterated **6(4-<sup>2</sup>H)** was prepared as depicted in Scheme 3 (see also Experimental Section). The degree of deuteration of **6(4-<sup>2</sup>H)** was found to be 98% [<sup>1</sup>H-, <sup>2</sup>H-, <sup>13</sup>C-NMR and GC-MS: M<sup>+</sup> *m/z* 189, isotope pattern in agreement with natural abundance **6**].



**Scheme 3.** Synthetic route towards **6(4-<sup>2</sup>H)** [*i.* CH<sub>3</sub>COCl/AlCl<sub>3</sub>, *ii.* PCl<sub>5</sub>/PCl<sub>3</sub>, *iii.* *n*-BuLi/D<sub>2</sub>O, *iv* FVT/-HCl] and subsequent rearrangement of **6(4-<sup>2</sup>H)** into *mono*-deuterated isotopomers of **5** upon Flash Vacuum Thermolysis (FVT).

**Table 3.** Product composition of the pyrolysates obtained after FVT of 1-(1-chloroethenyl)-4-<sup>2</sup>H-naphthalene [**6(4-<sup>2</sup>H)**].

T (°C)	Products formed (%)						Recovery (%)
	<b>6(4-<sup>2</sup>H)</b>	<b>4(4-<sup>2</sup>H)</b>	<b>5(1-<sup>2</sup>H)</b>	<b>5(3-<sup>2</sup>H)</b>	<b>5(4-<sup>2</sup>H)</b>	<b>5(5-<sup>2</sup>H)</b>	
700	trace	70				30	100
800	trace	-	5	-	5	90	95
900	-	-	10	10	10	70	92
1000	-	-	10	10	10	70	80

Upon FVT of **6(4-<sup>2</sup>H)** at 700°C [ $p = 1 \cdot 10^{-3}$  mm Hg, subl. T = 45°C, subl. rate 50 mg h<sup>-1</sup>, mass recovery 100 %] HCl elimination takes place, which results in formation of **4(4-<sup>2</sup>H)**. The formation of **4(4-<sup>2</sup>H)** (70%, Table 3, M<sup>+</sup>  $m/z$  153, isotope pattern in agreement with natural abundance **4**) is evident from the appearance of the ethynyl-signal at 3.54 ppm (<sup>1</sup>H-NMR). The position of the deuterium is determined from the reduced integral of the resonance in <sup>1</sup>H-NMR at 7.90 ppm [H4,5 (1H instead of 2H)], the presence of broad peaks in the AB-pattern at 7.45 ppm (due to  $J_{1H-2H}$ , H3) and the signal at 7.9 ppm in <sup>2</sup>H-NMR. At 700°C the pyrolysate contains besides **4(4-<sup>2</sup>H)** (70%), of acenaphthylene (**5**, 30%). The deuterium in **5** is located at C5 [**5(5-<sup>2</sup>H)**] [<sup>1</sup>H-NMR: reduced integral  $\delta$  7.84 ppm, 1H instead of 2H; <sup>2</sup>H-NMR resonance at  $\delta$  7.9 ppm (broad)]. This is in line with the initial formation of product upon ethynyl-ethylidene carbene rearrangement followed by C-H insertion of the ethylidene carbene (Scheme 3). In the 800°C pyrolysate more acenaphthylene (**5**) is formed [85%, mass recovery 95%, GC-MS: M<sup>+</sup>  $m/z$  153, isotope pattern in agreement with natural abundance **5** ( $m/z$  152)]. <sup>2</sup>H-NMR shows an intensive signal at 7.9 ppm, which corresponds to the presence of **5(5-<sup>2</sup>H)**. In addition, low intensity peaks were present at 7.6 ppm and 7.1 ppm indicating that **5(4-<sup>2</sup>H)** and **5(1-<sup>2</sup>H)** (**5** with one deuterium in the cyclopenta-moiety) are present. A small amount of **5(3-<sup>2</sup>H)** might be present, but the resonance of **5(3-<sup>2</sup>H)** at 7.8 ppm peak could not be observed due to the width of the intensive peak of **5(5-<sup>2</sup>H)** at 7.9 ppm. This means that besides migration to a neighboring site [from **5(5-<sup>2</sup>H)** to **5(4-<sup>2</sup>H)**], indeed deuterium migration from the aromatic core to the cyclopenta-moiety takes place [from **5(5-<sup>2</sup>H)** to **5(1-<sup>2</sup>H)**]. FVT of **6(4-<sup>2</sup>H)** at 900°C (mass recovery 92%) yields **5** as the only product [M<sup>+</sup>  $m/z$  153, isotope pattern in agreement with natural abundance **5** ( $m/z$  152)]. In the <sup>2</sup>H-NMR besides **5(5-<sup>2</sup>H)**, **5(1-<sup>2</sup>H)**, is now clearly detected (7.15 ppm 10 %). From the <sup>1</sup>H-NMR spectra of the 900°C pyrolysate it is deduced that **5(3-<sup>2</sup>H)** is present, as an extra broad peak is visible between the doublet for H4 at 7.76 ppm. The 1000°C pyrolysate (mass recovery 80%) contains increased

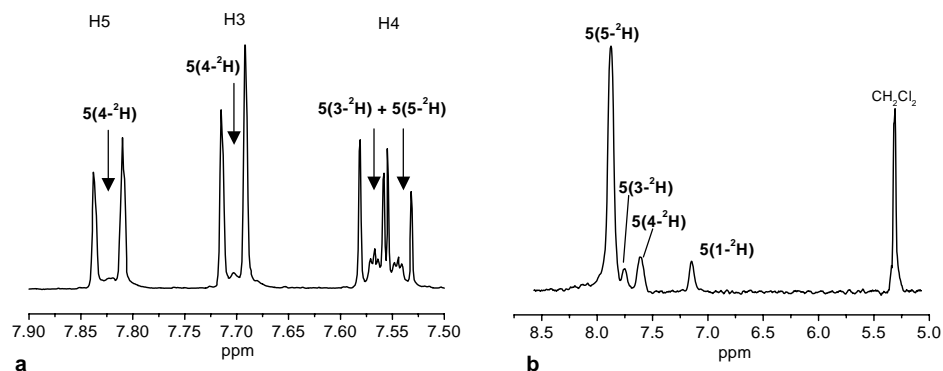


**Figure 3.** a.  $^1\text{H-NMR}$  spectrum (7.9 – 7.5 ppm) of the pyrolysate obtained after FVT of **6(4- $^2\text{H}$ )** at 1000°C. b.  $^2\text{H-NMR}$  spectrum (9.0 – 5.0 ppm) of the pyrolysate obtained after FVT of **6(4- $^2\text{H}$ )** at 1000°C.

amounts of rearranged isotopomers of **5** (Table 3, sum 30%,  $M^+ m/z$  153, isotope pattern in agreement with natural abundance **5**). The presence of all possible *mono*-deuterated isotopomers of **5** [**5(1- $^2\text{H}$ )**, **5(3- $^2\text{H}$ )**, **5(4- $^2\text{H}$ )** and **5(5- $^2\text{H}$ )**] is now evident from the  $^1\text{H-NMR}$  spectrum, where additional broad signals are present at 7.84, 7.71 and 7.58 ppm (Figure 3A) and the  $^2\text{H-NMR}$  spectrum, which displays three additional signals at  $\delta$  7.8, 7.6 and 7.1 ppm (Figure 3B).

These results provide unequivocal proof that indeed migration of deuterium from the aromatic core to the cyclopenta-moiety takes place. In addition, this migration to the cyclopenta-moiety does not seem to be more difficult than migration of deuterium to a neighboring-site; all *mono*-deuterated isotopomers are formed in comparable amounts at the same temperature.

#### 2.2.4 GC-cryo-FT-IR spectroscopy

To obtain further support for the occurrence of deuterium migrations, in addition to NMR, GC-cryo-FT-IR analyses were performed on the pyrolysates obtained after FVT of **4(1- $^2\text{H}$ )**. This technique can give useful information since the products are first separated on a GC-column and the IR spectra are measured at  $-196^\circ$  (see Experimental Section), which generally yields well-resolved vibrations.<sup>28</sup> In addition, the spectra can be readily interpreted making use of computed (RHF/6-31G\*\*) harmonic vibrations of all possible *mono*-deuterated isotopomers of **5**<sup>29,30</sup> and visualization of the vibrational modes using MOLDEN.<sup>31</sup>

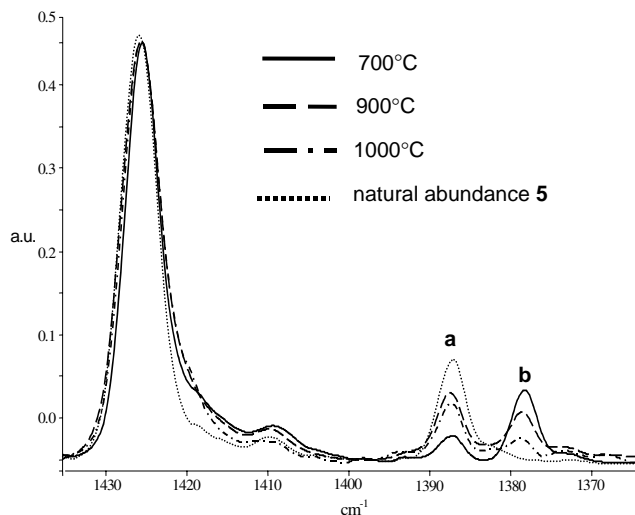


**Figure 4.** Expansion (region: 1435 - 1364  $\text{cm}^{-1}$ ) of the GC-FT-IR spectra of **5** formed upon FVT of **4(1-<sup>2</sup>H)** at 700°C, 900°C and 1000°C. **a.** in-plane bending vibration of H1 and H2 of **5**. **b.** in-plane bending vibration of isomer **5(1-<sup>2</sup>H)**. Vibrations are normalized on  $\nu = 1425 \text{ cm}^{-1}$ .

As discussed above FVT of **4(1-<sup>2</sup>H)** in the temperature range 700°C - 900°C yields starting material and *mono*-deuterated **5**. The IR spectrum of the **4(1-<sup>2</sup>H)** contains a distinct vibration at 2576  $\text{cm}^{-1}$ , which corresponds to the  $\equiv\text{C}-^2\text{H}$  stretch vibration (calc. 2537  $\text{cm}^{-1}$ ). The spectra of **4(1-<sup>2</sup>H)** before and after FVT are identical, which is in line with the occurrence of the proposed ethynyl-ethylidene carbene equilibration mechanism (see also Scheme 2).<sup>11</sup>

All spectra of the *mono*-deuterated isotopomers of **5**, obtained after FVT of **4**, contain low intensity peaks at 2307  $\text{cm}^{-1}$  corresponding to  $=\text{C}-^2\text{H}$  stretch (calc. 2291  $\text{cm}^{-1}$ ). The reduced intensity of this vibration compared to the counterpart in natural abundance **5** [calc. 3042  $\text{cm}^{-1}$  (asymmetric) and 3066  $\text{cm}^{-1}$  (symmetric)] is a consequence of the mass of the deuterium atom. Although, the spectra of **5** obtained after FVT of **4(1-<sup>2</sup>H)** at different temperatures are very similar, careful examination reveals some profound differences in the range 1400  $\text{cm}^{-1}$  - 1300  $\text{cm}^{-1}$  ( $=\text{C}-\text{H}$  in-plane bending) and between 900 - 700  $\text{cm}^{-1}$  ( $=\text{C}-\text{H}$  out-of-plane bending).

The two hydrogen atoms attached to the cyclopenta-carbon atoms (C1 and C2) in natural



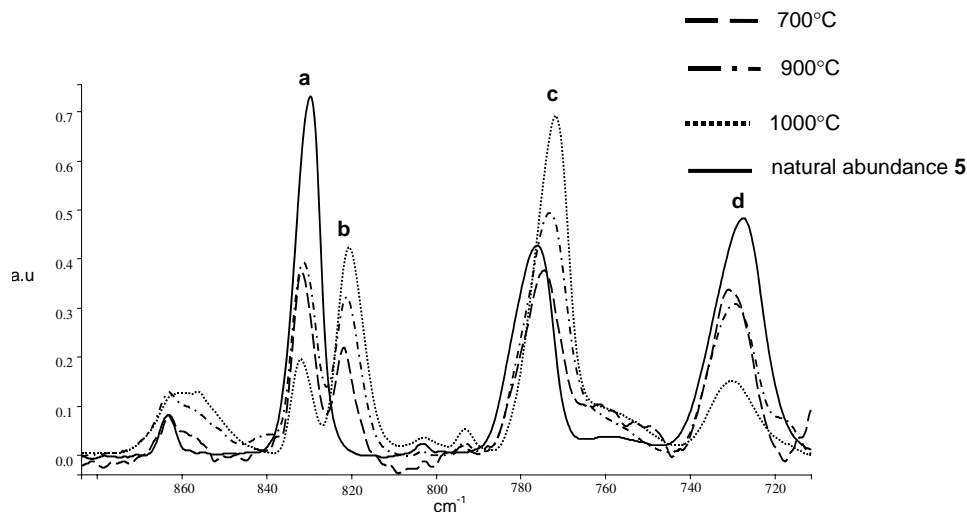


**Figure 5.** Expansion (region: 884 - 711  $\text{cm}^{-1}$ ) of the GC-FT-IR spectra of **5** formed upon FVT of **4(1- $^2\text{H}$ )** at 700°C and 900 °C. Vibrations are normalized on  $\nu$  1425  $\text{cm}^{-1}$ . **a.** symmetric out-of-plane bending =C-H. **b.** shifted symmetric out-of-plane bending =C-H, due to presence of deuterium in CP-moiety. **c.** asymmetric out-of-plane bending =C-H. **d.** symmetric out-of-plane bending of H1, H2, H5 and H6.

abundance **5** have an in-plane bending vibration at 1388  $\text{cm}^{-1}$  (**a**,  $\delta$  in-plane  $\nu_{\text{calc}} = 1379 \text{ cm}^{-1}$ ) (Figure 4). This vibration is absent after FVT at 700°C, but replaced by a new signal at 1378  $\text{cm}^{-1}$  (**b**). This new signal corresponds to the in-plane bending vibration of isomer **5(1- $^2\text{H}$ )** ( $\delta$  in-plane  $\nu_{\text{calc}} = 1363 \text{ cm}^{-1}$ ). In the spectra obtained after FVT at higher temperatures, the vibration at 1378  $\text{cm}^{-1}$  is reduced and the vibration at 1388  $\text{cm}^{-1}$  regains intensity. This gives further support that constitutional isotopomers with deuterium in the aromatic core and two hydrogen atoms attached to the cyclopenta-moiety are present in the pyrolysates after FVT at  $T > 900 \text{ }^\circ\text{C}$ , *i.e.* that migration of the deuterium atom from the cyclopenta-moiety to the aromatic core takes place.

A comparable change in the IR-spectra in the wavenumber range 900  $\text{cm}^{-1}$  – 700  $\text{cm}^{-1}$  is shown in Figure 5. The IR spectrum of **5** displays in this region three major vibrations [exp. 831(**a**), 776(**c**), 729(**d**)  $\text{cm}^{-1}$ ]. The signal (**a**) at 831 $\text{cm}^{-1}$  corresponds to the symmetric out-of-plane bending of all =C-H. The signal (**c**) at 776  $\text{cm}^{-1}$  is an asymmetric out-of-plane bending and the vibration (**d**) at 729  $\text{cm}^{-1}$  is a symmetric vibration of the hydrogens H1, H2, H5, H6 (see Scheme

2). From Figure 5 it is clear that the intensity of the vibration (**a**) at  $831\text{cm}^{-1}$  is reduced after FVT of **4(1-<sup>2</sup>H)** at  $700^\circ\text{C}$ . The new peak at  $821\text{ cm}^{-1}$  (**b**) is caused by the symmetric out-of-plane vibration of **5(1-<sup>2</sup>H)** (calc. shift:  $831\text{ cm}^{-1} - 818\text{ cm}^{-1}$ ; exp. shift  $831 - 821\text{ cm}^{-1}$ ). Again, upon FVT at higher temperature the shifted peak ( $821\text{ cm}^{-1}$ ) is reduced and the original peak at  $831\text{ cm}^{-1}$  regains intensity. This is in line with the presence of constitutional isotopomers of **5** with a deuterium atom in the core and two hydrogen atoms attached to the cyclopenta-moiety.

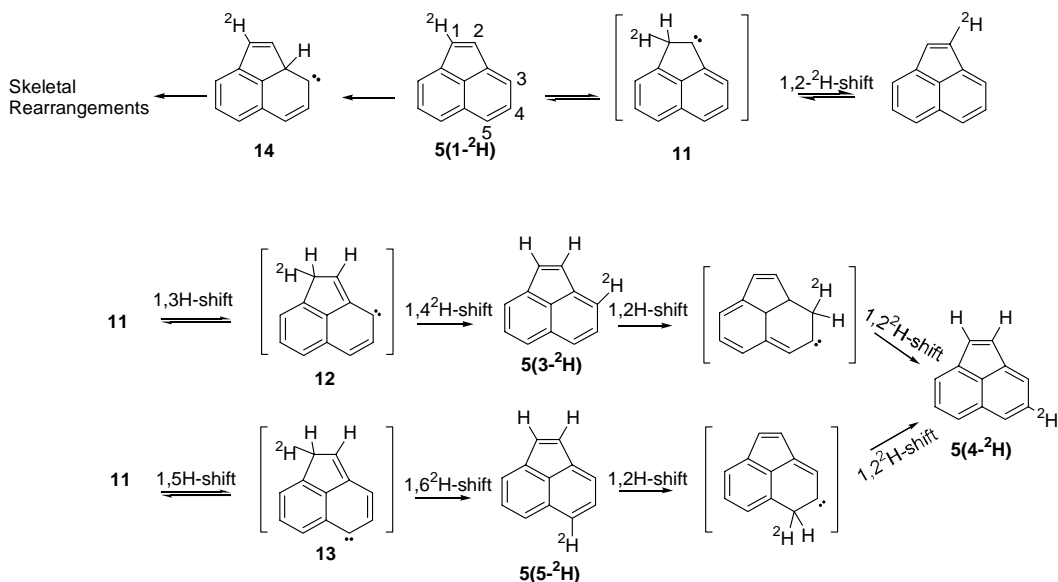
In summary, the GC-cryo-FT-IR-results substantiate that the pyrolysates obtained after FVT in the temperature range  $700^\circ\text{C}$  to  $900^\circ\text{C}$  consist of *mono*-deuterated **5** with a deuterium atom in the cyclopenta-moiety. The IR spectra obtained after pyrolysis at  $1000^\circ\text{C}$  can only be explained if also constitutional isotopomers of the *mono*-deuterated PAH are present with a deuterium atom in the aromatic core.

### 2.3 Mechanistic implications

The results of our experiments show that the initial product formed upon FVT of **1(9-<sup>2</sup>H)** is the CP-PAH **2(5-<sup>2</sup>H)**. The position of the deuterium in **2(5-<sup>2</sup>H)** is in agreement with the mechanism in Scheme 1.<sup>11</sup> However, as discussed above the intermediacy of ethylidene-carbene **9** presented in Scheme 1, has been refuted. Calculations at the BLYP/6-311G\*\* level of theory have indicated that, *after* zero point energy corrections, the transition state leading to **9** is lower in energy than **9** itself.<sup>12</sup> Hence, a one-step mechanism in which 1,2-H shift and insertion of the carbene in the C-H bond occurs was proposed.<sup>12</sup> Although various other mechanisms were also proposed, in none of these the initial step consisted of a 1,2-H shift.<sup>12</sup> Since FVT of **1(9-<sup>2</sup>H)** proves that 1,2-H shift has to take place *before* insertion into the C-H bond of the aromatic core, the intermediacy of ethylidene-carbene **9** is the *only* viable explanation.<sup>32-34</sup>

Unexpected outcomes of the FVT-experiments are that at  $700^\circ\text{C}$  and  $800^\circ\text{C}$  the E-PAH [**1(9-<sup>2</sup>H)**, **4(1-<sup>2</sup>H)** and **4(4-<sup>2</sup>H)**] remained unaltered, *i.e.* with the deuterium atom on the original position. This is in accordance with the *reversible* character of the ethynyl-ethylidene carbene rearrangement (Scheme 1). Furthermore, the FVT-experiments performed on the selectively *mono*-deuterated **1(9-<sup>2</sup>H)** show that migration of the deuterium within the cyclopenta-moiety takes place. In a theoretical study on the topomerization of benzene several unimolecular mechanisms that could be operational under high temperature conditions, *viz.* the benzvalene mechanism, the 1,2-H shifts mechanism involving carbenes intermediates and the dyotropic shift mechanism, have been explored.<sup>35</sup> Of these unimolecular mechanisms *only* the 1,2-H shift mechanism *via* carbene intermediates could account for the experimentally observed migration within the cyclopenta-moiety of CP-PAH. Hence, the most likely rationalization of our results is migrations *via* such

carbene intermediates.<sup>35</sup> In Scheme 4 the deuterium migration in **5** involving carbene **11** is exemplified.



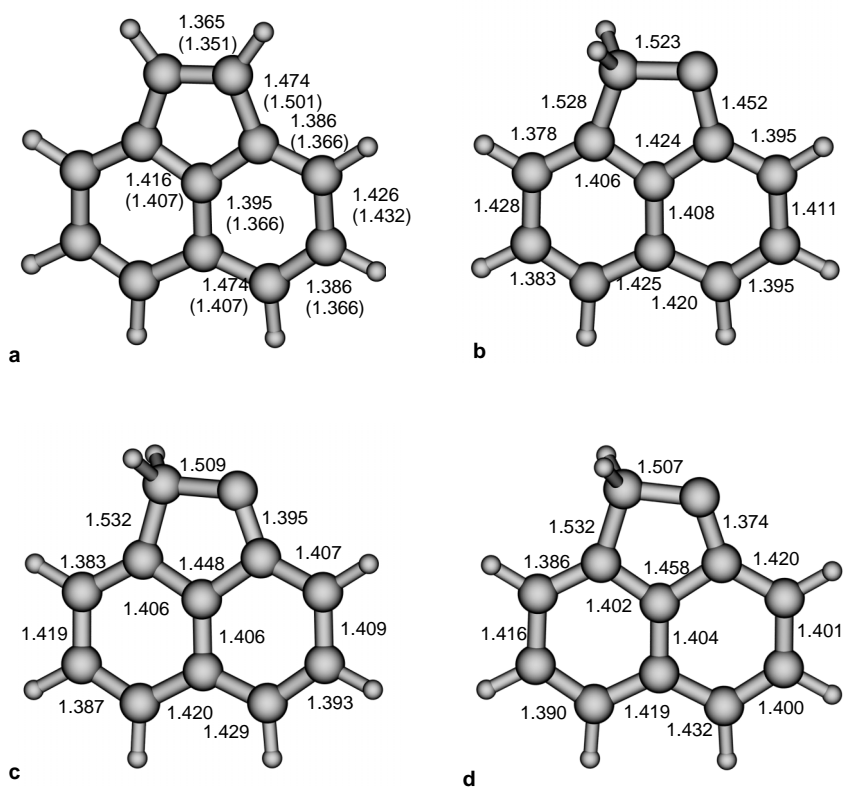
**Scheme 4.** Proposed mechanism for the migration of deuterium within the cyclopenta-moiety and for the migration of deuterium from the cyclopenta-moiety to the aromatic core.

The carbene **11** has a singlet ground state at the B3LYP/TZ2P level of theory. However, the open-shell triplet is only 2.6 kcalmol<sup>-1</sup> and the open-shell singlet only 9.4 kcalmol<sup>-1</sup> higher in energy (Table 4).<sup>36</sup> The relative energy of the closed-shell singlet of **11** with respect to **5** is 64.2 kcalmol<sup>-1</sup> at the B3LYP/TZ2P level of theory. However, the small energy differences make the use of higher levels of theory warranted in order to determine the proper ground state of this carbene. Notwithstanding, the B3LYP/TZ2P optimized geometries of the singlet, open-shell singlet and open-shell triplet of **11** show that in both open-shell species the carbon-carbon bond between the carbene and the aromatic core is significantly shortened with respect to the carbon-carbon bond in the closed-shell singlet (Figure 6). This indicates that in both open-shell species the carbene is in resonance with the aromatic core, which will facilitate migration of a hydrogen atom. Furthermore, both closed-shell and open-shell carbene species of **11** have a lower  $E_{rel}$  than possible radical intermediates formed *via* homolytic C-H cleavage ( $E_{rel}$  *ca.* 100 kcalmol<sup>-1</sup>).<sup>37</sup>

From the FVT experiments of **1(9-<sup>2</sup>H)**, **4(1-<sup>2</sup>H)** and **4(5-<sup>2</sup>H)** it is clear that migration of

**Table 4.** Relative Energies (kcalmol<sup>-1</sup>) at B3LYP/TZ2P level of theory of carbenes **11** and **12** and **13** relative to **5**<sup>a</sup>.

	E <sub>rel</sub>		
	<b>11</b>	<b>12</b>	<b>13</b>
closed-shell singlet	64.2	76.1	89.9
open-shell triplet	66.8	64.8	89.7
open-shell singlet	73.6	68.5	82.9

<sup>a</sup>:  $E_{\text{total}}(\text{B3LYP}/\text{TZ2P}) = -462.189486$  a.u.**Figure 6.** The B3LYP/TZ2P optimized geometries of **a**. acenaphthylene (**5**). The numbers in parenthesis are the RHF/6-31G\*\* bond lengths. **b**. closed-shell singlet **11**, **c**. open-shell triplet **11** and **d**. open-shell singlet **11**.

deuterium to the aromatic core takes place. The most likely pathway presumably involves carbene intermediates.<sup>35</sup> Hence, from **11** 1,3-H shift will lead to hydrogen migration from the aromatic core to the cyclopenta-moiety. Hereby carbene **12** is formed, in which the carbene is located on C3 (Scheme 4). Subsequent 1,4-deuterium shift from the cyclopenta-moiety to the aromatic core, results in an overall migration of a deuterium atom to the aromatic core, *i.e.* conversion of **5(1-<sup>2</sup>H)** into **5(3-<sup>2</sup>H)**. Similarly, *via* 1,5-H shift from **11** the carbene **13** (with carbene on C5, Scheme 4) could be generated and subsequent 1,6-deuterium shift results in the overall conversion of **5(1-<sup>2</sup>H)** in **5(5-<sup>2</sup>H)**. Note that no 1,4-H shift from **11** is possible and therefore **5(4-<sup>2</sup>H)** has to be formed from either **5(3-<sup>2</sup>H)** or **5(5-<sup>2</sup>H)** (see Scheme 4). This implicitly denotes that 1,2-H shifts in the aromatic core should also be viable. Supporting evidence that this is indeed the case is found in the FVT experiments of **6(4-<sup>2</sup>H)**. Here, migration of the deuterium atom to a neighboring position in the aromatic core was observed. B3LYP/TZ2P calculations on carbene **12** (Table 4) show that this intermediate has a triplet ground state at the B3LYP/TZ2P level of theory. This triplet is lower in energy than the triplet of **11** and has a comparable energy as the closed-shell singlet of **11**. Hence, carbene **12** should be accessible from **11**. For comparison, the energy of the closed-shell singlet, open-shell singlet and the open-shell triplet of carbene **13** were calculated (Scheme 4 and Table 4). This intermediate has to be formed before skeletal rearrangements can take place. The calculations show that the energy of carbene **13** is indeed considerably higher than both **11** and **12** (89.9 *vs.* 64.2 and 76.1 kcalmol<sup>-1</sup>, respectively). This is good agreement with the observation that migration of the deuterium atom takes place in a lower temperature range than skeletal rearrangements.

In passing we stipulate that further experiments and calculations are warranted in order to firmly establish the details of the perimeter hydrogen migration process.

## 2.4 Conclusions

FVT experiments on the selectively *mono*-deuterated **1(9-<sup>2</sup>H)**, **4(1-<sup>2</sup>H)** and **4(5-<sup>2</sup>H)** have shown that 1,2-H shift, *i.e.* ethynyl-ethylidene rearrangement, takes place before insertion of the ethylidene carbene in the C-H bond. This is in agreement with the proposed Brown-mechanism.<sup>11</sup> Surprisingly, subsequent hydrogen/deuterium migration takes place within the cyclopenta-moiety and from this moiety to the aromatic core and *vice versa*. Consequently, all possible *mono*-deuterated isotopomers are ultimately formed. All results strongly indicate that deuterium migration takes place in a unimolecular fashion at temperatures significantly lower than those needed for rearrangements of the carbon skeleton (*ca.* 800°C *vs.* 1000°C). A mechanism involving carbene-like intermediates is proposed. In general, it can be concluded that the hydrogen atoms of non-alternant CP-PAH are much more mobile than previously considered. These results observations

will affect the interpretation of several mechanistic studies on the rearrangement of CP-PAH under high temperature conditions where deuterium labels have been utilized.<sup>6,21,38,39</sup> In these studies the mobility of the labels themselves was disregarded in the interpretation of the product composition!

## 2.5 Experimental section

All reactions were carried out under a N<sub>2</sub> atmosphere. All solvents were purified and dried by standard procedures. Melting points are uncorrected. Column chromatography: Merck kieselgel 60 silica (230 - 400 ASTM). <sup>1</sup>H (300.13 MHz) and <sup>13</sup>C (75.47 MHz) NMR spectra were recorded in CD<sub>2</sub>Cl<sub>2</sub>, <sup>2</sup>H (46.07 MHz) NMR spectra were recorded in CH<sub>2</sub>Cl<sub>2</sub>, unless stated otherwise. All chemical shifts reported are in ppm (reference CD<sub>2</sub>Cl<sub>2</sub> δ = 5.32 ppm) and *J* values in Hz. For the <sup>1</sup>H-NMR spectrum multiplicity is denoted as following: s = singlet, d = doublet, t = triplet, dd = double doublet, m = multiplet. In <sup>13</sup>C-NMR the signals are indicated with q = quaternary carbon, t = tertiary carbons and s = secondary carbon. GC-MS spectra were measured on an ATI Unicam Automass System 2 quadrupole mass spectrometer (column J&W Scientific DB-5, length 30 m, ID 0.32 mm and film thickness 0.25 μm; injector temperature 300°C, temperature program 2 min 100°C - 10°Cmin<sup>-1</sup> - 280°C, carrier gas He; mass spectrometer EI 70 eV.)

GC-cryo-FT-IR<sup>28</sup>: GC separations (column: HP-5MS, length 25 m, ID 0.25 mm and film thickness 0.25 μm; injector temperature 275°C, temperature program, 2 min at 80°C and then increased to 290°C (10°Cmin<sup>-1</sup>); carrier gas He). Cryotrap IR detection was carried out with a Digilab FTS-40 Fourier transform instrument equipped with a Digilab Tracer GC interface and A SPC 3200 computer for data acquisition. The temperature of the transfer line and the deposition tip was 275°C; cooling of the IR transparent trapping window to -196°C was carried out with liquid N<sub>2</sub> at a vacuum of 10<sup>-5</sup> Torr. Spectra of the trapped GC-eluates were recorded 'on-the-fly', *i.e.*, a few seconds after deposition by averaging four scans (resolution 8 cm<sup>-1</sup>) every 2s. In addition, post-run scanning (512 scans *ω*-added) of trapped components were performed after completion of the GC-run by repositioning the corresponding window coordinates, *i.e.*, retention times (*t<sub>R</sub>*), into the IR beam (optical resolution 2 cm<sup>-1</sup>). *Caution*: (Non)-alternant (CP)-PAHs are potential genotoxic compounds.

### 9-<sup>2</sup>H-Ethynylphenanthrene [1(9-<sup>2</sup>H)]<sup>22</sup>

To an ice-cooled orange solution of 9-ethynylphenanthrene (**1**) (0.34 mg, 1.7 mmol) in diethyl ether (15 ml), *n*-butyllithium (1.7 ml of a 1.6 M solution in *n*-hexane) was added using a syringe; the reaction mixture turned brown after addition. The reaction mixture was stirred for 1 hr. at room temperature after which a gray suspension was obtained. The reaction mixture was cooled in an ice-bath and D<sub>2</sub>O (2 ml) was added. The organic layer was separated and concentrated *in vacuo*. Yield 0.31 mg (1.5 mmol, 90%) of a brown solid (m.p.

53 - 55°C). <sup>1</sup>H-NMR ( $\delta$ , ppm): 8.74 - 8.66 (2H, m, H4+5), 8.50 - 8.44 (1H, m, H1), 8.08 (1H, s, H9), 7.90 (1H, dd, *J* 1.4/7.7, H8), 7.76 - 7.60 (3H, m, H2+3+6+7). <sup>2</sup>H-NMR ( $\delta$ , ppm):  $\delta$  3.57 (s). <sup>13</sup>C-NMR ( $\delta$ , ppm):  $\delta$  133.2 (t), 131.3 (q), 131.2 (q), 130.7 (q), 130.3 (q), 128.8 (t), 128.1 (t), 127.5 (t), 127.5 (t), 127.4 (t), 126.9 (t), 123.1 (t), 122.9 (t), 118.8 (q). GC-MS *m/z* 203 (M<sup>+</sup>).  $\nu$  3284 ( $\equiv$ C-H stretch), 3059 (=C-H stretch), 2576 ( $\equiv$ C-<sup>2</sup>H stretch), 2103 (C $\equiv$ C-<sup>2</sup>H stretch) cm<sup>-1</sup>. Degree of deuteration 98% according to <sup>1</sup>H-NMR and GC-MS.

### 1-<sup>2</sup>H-Ethynyl-naphthalene [4(1-<sup>2</sup>H)]<sup>40</sup>

To an ice-cooled solution of 1-ethynyl-naphthalene (**4**) (0.28 g, 1.84 mmol) in diethyl ether (5 ml) *n*-butyllithium (1.8 ml of a 1.6 M solution in *n*-hexane) was added with a syringe. After addition the reaction mixture became a dark red solution. The reaction mixture was stirred for 2 hr. at room temperature after which D<sub>2</sub>O (4 ml) was added. The organic layer was separated and concentrated *in vacuo*. Yield 0.23 g (1.57 mmol, 85.0 %) of a reddish oil. <sup>1</sup>H-NMR ( $\delta$ , ppm): 8.40 (1H, d, *J* 8.2), 7.91 (2H, d, *J* 8.4), 7.78 (1H, d, *J* 7.1), 7.64 (2H, m), 7.49 (1H, t, *J* 7.4), 3.56 (s). <sup>2</sup>H-NMR ( $\delta$ , ppm):  $\delta$  3.61 (s). <sup>13</sup>C-NMR ( $\delta$ , ppm): 133.7 (q), 133.4 (q), 131.5 (t), 129.6 (t), 128.6 (t), 127.3 (t), 126.8 (t), 126.1 (t), 125.4 (t), 120.0 (q). GC-MS *m/z* 153 (M<sup>+</sup>)  $\nu$  3282 ( $\equiv$ C-H stretch), 3057 (=C-H stretch), 2576 ( $\equiv$ C-<sup>2</sup>H stretch), 2103 (C $\equiv$ C-<sup>2</sup>H stretch) cm<sup>-1</sup>. Degree of deuteration 97% according to <sup>1</sup>H-NMR and GC-MS.

### 1-(1-Chloroethenyl)-4-<sup>2</sup>H-naphthalene [6(4-<sup>2</sup>H)]

A solution of 1-(1-chloroethenyl)-4-bromonaphthalene (**9**) (0.51 g, 1.9 mmol) in THF was cooled to -40°C. *n*-Butyllithium (2 ml of 1.6 M solution in *n*-hexane) was added using a syringe. After stirring for 6 hr at -40°C D<sub>2</sub>O (4 ml) was added. The organic layer was separated and concentrated *in vacuo*. The resulting oil was purified by column chromatography (silica, eluent *n*-hexane). Yield 0.21 g (1.1 mmol, 60%) of a colorless oil. <sup>1</sup>H-NMR ( $\delta$ , ppm): 8.22 (1H, dd, *J* 2.1, 7.4) 7.92 (1H, dd, *J* 2.2/7.8), 7.61 (4H, m), 5.88 (1H, d, *J* 1.3), 5.60 (1H, d, *J* 1.2). <sup>2</sup>H-NMR ( $\delta$ , ppm): 7.9 (s). <sup>13</sup>C-NMR ( $\delta$ , ppm): 138.7 (q), 137.0 (q), 133.9 (q), 129.5 (t), 127.0 (t), 126.9 (t), 126.5 (t), 125.5 (t), 125.2 (t), 118.1 (q). GC-MS *m/z* 187 (M<sup>+</sup>). Degree of deuteration 98% according to <sup>1</sup>H-NMR and GC-MS.

### 1-(1-Chloroethenyl)-4-bromonaphthalene (7)

A mixture of 1-(1-acetyl)-4-bromonaphthalene (**8**) (2.00 g, 8.0 mmol) and PCl<sub>5</sub> (2.5 g, 12.0 mmol) in PCl<sub>3</sub> (60 ml) was stirred at room temperature for 24 hr. The reaction mixture was hydrolyzed by pouring it on ice (150 g). The organic layer was separated, washed with a saturated solution of sodium bicarbonate (50 ml) and water (50 ml), dried over magnesium sulfate, filtered and concentrated *in vacuo*. Crude 1-(1-chloroethenyl)-4-bromonaphthalene (**7**) (1.96 g, 7.3 mmol, 91%) was purified by flash chromatography (silica, eluent *n*-hexane: dichloromethane 9:1). Yield 1.8 g (6.7 mmol, 84%) of a yellow oil. <sup>1</sup>H-NMR ( $\delta$ , ppm): 8.28 (1H, m), 8.17 (1H, m), 7.73 (1H, d, *J* 7.7), 7.59 (2H, m), 7.32 (1H, d, *J* 7.7), 5.82 (1H, d, *J* 1.2), 5.52 (1H, d, *J* 1.2). <sup>13</sup>C-NMR ( $\delta$ ,

ppm): 137.7 (q), 136.8 (q), 132.0 (q), 131.6 (q), 129.2 (t), 127.7 (t) 127.6 (t), 127.4 (t), 126.9 (t), 125.9 (t), 124.4 (q), 118.3 (s).

### 1-(1-Acetyl)-4-bromonaphthalene (**8**)

To a cooled suspension (0 °C, ice bath) of anhydrous AlCl<sub>3</sub> (8.48 g, 62.8 mmol) in dichloromethane (125 ml), acetylchloride (4.17 g, 53.1 mmol) was added under stirring. When a clear solution was formed, 10.0 g (48.3 mmol) of 1-bromonaphthalene was added from a dropping funnel. After stirring the reaction mixture overnight 125 ml of a 0.5 M HCl solution was added. The organic layer was separated, washed with a saturated sodium bicarbonate solution (75 ml) and water (75 ml), dried over magnesium sulfate, filtered and concentrated *in vacuo*. Crude 1-(1-chloroethenyl)-4-bromonaphthalene (**8**) was obtained in a yield of 10.17 g (40.8 mmol, 85%). The crude mixture was purified by recrystallization of its picric acid. The crude mixture was dissolved in boiling ethanol (100 ml) after which picric acid (9.5 g, 41.4 mmol) was added. Upon cooling to room temperature yellow crystals precipitated, which were filtered off and recrystallized from ethanol (1 gml<sup>-1</sup>). To obtain pure **8** its picric salt was dissolved in CH<sub>2</sub>Cl<sub>2</sub> (100 ml) and washed with NH<sub>4</sub>OH (4 x 50 ml). The organic phases were separated and concentrated *in vacuo*. Compound **8** was obtained as a white solid. Yield 6.1 g (24.5 mmol, 60%, m.p. 47 - 49°C). <sup>1</sup>H-NMR (δ, ppm): δ 8.72 (1H, m), 8.32 (1H, m), 7.81 (1H, d, *J* 7.8) 7.71 (1H, d, *J* 7.8), 7.64 (2H, m), 2.70 (3H, s). <sup>13</sup>C-NMR (δ, ppm): δ 201.0 (q), 135.4 (q), 132.4 (q), 131.2 (q), 128.7 (t), 128.7 (t), 128.3 (t), 128.2 (q), 127.8 (t), 127.6 (t), 126.4 (t), 30.0 (s).

### Flash Vacuum Thermolysis General Procedure<sup>10</sup>

A Thermolyne 21100 furnace containing an unpacked quartz tube (length 40 cm and diameter 2.5 cm) was used for all FVT experiments Aliquots (ca. 50 mg) of the precursors were slowly sublimed into the quartz tube at a pressure of 10<sup>-3</sup> mm Hg. The pyrolysates were rinsed from the quartz tube with dry CH<sub>2</sub>Cl<sub>2</sub> and directly stored under N<sub>2</sub> atmosphere. The pyrolysate product composition was determined by <sup>1</sup>H-, <sup>2</sup>H- and <sup>13</sup>C-NMR, capillary GC, GC-MS and GC-cryo-FT-IR.

### *Ab initio* Calculations

The geometries of natural abundance and all *mono*-deuterated of **5** were optimized at the RHF/6-31G\*\* level of theory. All geometries were minima since no negative vibrations were found in the Hessian calculations. A scaling factor was applied to match the calculated to the experimental vibrations. This factor was 0.90 for the region 4000 - 1200 cm<sup>-1</sup> and 0.85 for the region 1200 - 600 cm<sup>-1</sup>. For a match with the experimental vibrations, the calculated vibrations were assigned using the program MOLDEN.<sup>31</sup> The match between the experimental and calculated RHF/6-31G\*\* spectra was in agreement with that reported for vibrations calculated at the B3LYP/6-31G\*\* level of theory.<sup>29,30</sup> The closed-shell carbene species were optimized at B3LYP/TZ2P level of theory. The UB3LYP/TZ2P method was employed for open-shell singlets and



triplets. The TZ2P basis was constructed from Hunzinger's TZ basis<sup>41</sup> augmented with two sets of polarization functions;  $\alpha_d(\text{C}) = 1.5, 0.375$  and  $\alpha_p(\text{H}) = 1.5, 0.375$ .<sup>35</sup> All calculations were performed using the GAMESS-UK package.<sup>42</sup>

## References and notes

- (1) Lafleur, A. L.; Howard, J. B.; Taghizadeh, K.; Plummer, E. F.; Scott, L. T.; Necula, A.; Swallow, K. C. *J. Phys. Chem.* **1996**, *100*, 17421-17428.
- (2) Wang, H.; Frenklach, M. *J. Phys. Chem.* **1994**, *98*, 11465.
- (3) Wang, X.; Becker, H.; Hopkinson, A. C.; March, R. E.; Scott, L. T.; Bohme, D. K. *Int. J. Mass Spectrom. Ion Proc.* **1997**, *161*, 69-76.
- (4) Jenneskens, L. W.; Sarobe, M.; Zwikker, J. W. *Pure & Appl. Chem.* **1996**, *68*, 219-224.
- (5) Scott, L. T. *Pure & Appl. Chem.* **1996**, *68*, 291-300.
- (6) Necula, A.; Scott, L. T. *J. Am. Chem. Soc.* **2000**, *122*, 1548-1549.
- (7) Bauschlicher, C. W.; Ricca, A. *Chem. Phys. Lett.* **2000**, *326*, 283-287.
- (8) Bockhorn, H.; Fetting, F.; Wenz, H. W. *Ber. Bunsenges. Phys. Chem.* **1983**, *87*, 1067-1073.
- (9) Lafleur, A. L.; Gagel, J. J.; Longwell, J. P.; Monchamp, P. A. *Energy & Fuels* **1988**, *2*, 709.
- (10) Brown, R. F. C. *Pyrolytic Methods in Organic Chemistry*; Academic Press: New York, **1980**; Vol. 41.
- (11) Brown, R. F. C.; Eastwood, F. W. *Synlett* **1993**, 9-19.
- (12) Cioslowski, J.; Schimeczek, M.; Piskorz, P.; Moncrieff, D. J. *Am. Chem. Soc.* **1999**, *121*, 3773-3778.
- (13) Sarobe, M. *Polycyclic Aromatic Hydrocarbons under High Temperature Conditions. Consequences for Carbon Build Up During Combustion and Fullerene Formation Processes.*; Utrecht University: Utrecht, The Netherlands, **1998**.
- (14) Scott, L. T.; Roelofs, N. H. *J. Am. Chem. Soc.* **1987**, *109*, 5461-5465.
- (15) Scott, L. T. *Acc. Chem. Res.* **1982**, *15*, 52-58.
- (16) Scott, L. T.; Hashemi, M. M.; Schultz, T. H.; Wallace, M. B. *J. Am. Chem. Soc.* **1991**, *113*, 9692-9693.
- (17) Scott, L. T.; Kirms, M. A. *Tetrahedron Lett.* **1982**, *23*, 1859-1862.
- (18) Howard, J. B.; Longwell, J. P.; Marr, J. A.; Pope, C. J.; Busby, W. F., Jr.; Lafleur, A. L.; Taghizadeh, K. *Combust. Flame* **1995**, *101*, 262-270.
- (19) Scott, L. T.; Roelofs, N. H.; Tsang, T.-H. *J. Am. Chem. Soc.* **1987**, *109*, 5456-5461.
- (20) Scott, L. T.; Roelofs, N. H. *Tetrahedron Lett.* **1988**, *29*, 6857-6860. These experiments were performed under slightly different conditions as our experiments (FVP vs. FVT). The pressure under FVP conditions is usually higher than under FVT conditions, which will

enhance the occurrence of skeletal rearrangements. Hence, under FVT conditions skeletal rearrangement are expected to take place at even higher temperatures.

- (21) Brooks, M. A.; Scott, L. T. *J. Am. Chem. Soc.* **1999**, *121*, 5444-5449. For the PAH radicals it was observed that 1,2-H shifts are operational under high temperature conditions
- (22) Sarobe, M.; Jenneskens, L. W.; Wesseling, J.; Snoeijer, J. D.; Zwikker, J. W.; Wiersum, U. E. *Liebigs. Ann./Recueil* **1997**, 1207-1213.
- (23) Brown, R. F. C.; Eastwood, F. W.; Jackman, G. P. *Aust. J. Chem.* **1977**, *30*, 1757.
- (24) Ling, Y.; Lifshitz, C. *J. Phys. Chem.* **1998**, *102*, 708-716.
- (25) Gotkis, Y.; Oleinikova, M.; Naor, M.; Lifshitz, C. *J. Phys. Chem.* **1993**, *97*, 12282-12290.
- (26) Ling, Y.; Martin, J. M. L.; Lifshitz, C. *J. Phys. Chem.* **1997**, *101*, 219-226.
- (27) The conversion of 1-chloroethynyl-substituted PAH in their ethynyl-substituted analogues takes place quantitatively at low temperature.<sup>4,5</sup>
- (28) Visser, T.; Sarobe, M.; Jenneskens, L. W.; Wesseling, J. *Fuel* **1998**, *77*, 913-920.
- (29) Bauschlicher, C. W.; Hudgins, D. M.; Allamandola, L. J. *Theor. Chem. Acc* **1999**, *103*, 154-162.
- (30) Banisaukas, J.; Szczepanski, J.; Eyler, J.; Vala, M.; Hirata, S.; Head-Gordon, M.; Oomens, J.; Meijer, G.; Helden, G. v. *J. Phys. Chem. A* **2003**, *107*, 782-793.
- (31) Schaftenaar, G. ; CAOS/CAMM center: Nijmegen, 1991.
- (32) Sarobe, M.; Jenneskens, L. W.; Kleij, A.; Petroutsa, M. *Tetrahedron Lett.* **1997**, *38*, 7255-7258.
- (33) Scott, L. T.; Necula, A. *Tetrahedron Lett.* **1997**, *38*, 1877-1880.
- (34) Sarobe, M.; Jenneskens, L. W.; Steggink, R. G. B.; Visser, T. *J. Org. Chem.* **1999**, *64*, 3861-3866.
- (35) Bettinger, H. F.; Schreiner, P. R.; Schaefer, H. F.; Schleyer, P. v. R. *J. Am. Chem. Soc.* **1998**, *120*, 5741-5750.
- (36) The energies of the open-shell species are given for completeness. Recent investigations in our laboratory, however, have shown that B3LYP might give unreliable, *i.e.* converged, results in the case of open-shell singlets.
- (37) Cioslowski, J.; Liu, G.; Martinov, M.; Piskorz, P.; Moncrieff, D. *J. Am. Chem. Soc.* **1996**, *118*, 5261-5264.
- (38) Schulz, K.; Hofmann, J.; Zimmermann, G. *Eur. J. Org. Chem.* **1999**, 3407-3412.
- (39) Anderson, M. R.; Brown, R. F. C.; Coulston, K. J.; Eastwood, F. W.; Ward, A. *Aust. J. Chem.* **1990**, *43*, 1137-1150.
- (40) Okamoto, Y.; Chellappa, K. L.; Kunchu, S. K. *J. Org. Chem.* **1972**, *37*, 318.
- (41) Huzinaga, S. *J. Chem. Phys.* **1965**, *42*, 1293.

- (42) Guest, M. F.; van Lenthe, J. H.; Kendrick, J.; Schöffel, K.; Sherwood, P.; Harrison, R. J. *GAMESS-UK, a package of ab initio programs*, **1998**. With contributions from Amos, R.D.; Buenker, R.J., Dupuis M; Handy, N.C.; Hillier, I.; Knowles, P.J.; Bonacic-Koutecky, V.; von Niessen, W.; Saunders, V.R.; Stone, A.J. Derived from the original GAMESS code by: Dupuis, M.; Spangler, D.; Wendolowski, J., NRCC Software Catalog, vol. 1, programs no. QG01 (GAMESS), **1980**.



# CHAPTER 3

## FVT of 1-<sup>2</sup>H-naphthalene and 2-<sup>2</sup>H-naphthalene; Hydrogen Migration along a PAH Perimeter

### Abstract

Flash vacuum thermolysis (FVT) of 1-<sup>2</sup>H-naphthalene (**1**) or 2-<sup>2</sup>H-naphthalene (**2**) shows that in the temperature range 800°C – 1000°C **1** is converted into **2** and *vice versa* with excellent mass recoveries. Hence, hydrogen migration takes place presumably *via* 1,2-H shifts involving carbene intermediates, but at higher temperatures than within the cyclopenta-moiety of the non-alternant cyclopenta-fused polycyclic aromatic hydrocarbons (CP-PAH). This interpretation is supported by *ab initio* B3LYP/TZVP calculations.

### 3.1 Introduction

In the previous Chapter we have shown for the first time that at elevated temperatures in the diluted gas phase the hydrogen atoms of non-alternant cyclopenta-fused polycyclic aromatic hydrocarbons (CP-PAH) migrate along the perimeter of the molecule. Remarkably, hydrogen migration within the cyclopenta-moieties was already observed at a relatively low temperature (700°C). At higher temperatures (900°C) the cyclopenta-hydrogen atoms were shown to migrate to the aromatic core and *vice versa*. Moreover, the migration of the hydrogen atoms is a distinct process that is not connected to well-known skeletal rearrangements that occur at higher temperatures.<sup>1,2</sup> These results have important consequences for the interpretation of mechanistic studies on (CP)-PAH under high temperature conditions where <sup>2</sup>H-labeling has been used.<sup>3-6</sup>

An interesting question that remains to be addressed, is whether the hydrogen atoms attached to the core of an *alternant* PAH also possess a propensity to migrate along the PAH perimeter under these similar conditions. Tentative evidence for the viability of this process is provided by the results of the Flash Vacuum Thermolysis (FVT) experiments of 1-(1-chloroethenyl)-4-<sup>2</sup>H-naphthalene, a precursor for acenaphthylene with one deuterium atom present in the aromatic core. Upon FVT deuterium migration from the aromatic core to the cyclopenta-moiety was observed (Chapter 2).

To elucidate if hydrogen migration along a PAH perimeter in the temperature range 700°C – 1000°C is feasible selectively *mono*-deuterated 1-<sup>2</sup>H-naphthalene (**1**) and 2-<sup>2</sup>H-naphthalene (**2**) were subjected to FVT. Here, it is shown that hydrogen migrations along the alternant perimeter indeed occur, under similar conditions as migration of the deuterium atom from the cyclopenta-moiety to the aromatic core and *vice versa* in the related CP-PAH, acenaphthylene (see Chapter 2). *Ab initio* (B3LTP/TZVP) calculations indicate that also in this case 1,2-H shifts and carbene intermediates play an important role.

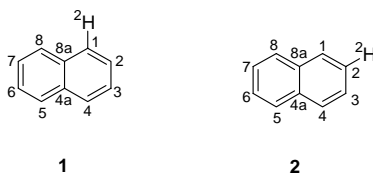


Chart 1

## 3.2 Results & Discussion

### 3.2.1 FVT of 1-<sup>2</sup>H-naphthalene (**1**)

Selectively *mono*-deuterated 1-<sup>2</sup>H-naphthalene (**1**) and 2-<sup>2</sup>H-naphthalene (**2**) were synthesized from the corresponding *mono*-bromo-substituted naphthalenes by treatment with *n*-butyllithium followed by quenching with D<sub>2</sub>O [95 - 98% <sup>2</sup>H see Experimental Section]. The position of the deuterium isotope and the degree of deuteration was unequivocally established by <sup>2</sup>H-NMR and the isotope induced shift <sup>13</sup>C-NMR chemical shift (quantitative <sup>13</sup>C-NMR).<sup>7,8</sup> Further support was obtained by direct inlet electron ionization mass spectrometry (direct inlet E.I. MS) performed at 16 eV (see Experimental Section).<sup>9</sup>

Compounds **1** and **2** were subjected to FVT [ $p = 1 \cdot 10^{-3}$  mm Hg, sublimation (subl.) temperature 30°C, subl. rate 60 mg·h<sup>-1</sup>] in the temperature range 700°C – 1000°C; mass recoveries were excellent (> 90%, Table 1). Pyrolysate analyses by capillary GC-MS and direct inlet E.I. MS showed that only *mono*-deuterated naphthalene is present after FVT of **1** at 800°C. Only the molecular ion (M<sup>+</sup>) at  $m/z$  is 129 is present with the correct isotope pattern; no increase of the signals of [M-1]<sup>+</sup> or [M+1]<sup>+</sup> is observed (Table 2). Hence, only *mono*-deuterated compounds are present. Notwithstanding, the <sup>2</sup>H-NMR spectrum of the 800°C pyrolysate shows two distinct signals; positioned at  $\delta = 7.8$  ppm of **1** and an extra signal at  $\delta = 7.5$  ppm. The latter corresponds to the <sup>2</sup>H-NMR resonance expected for 2-<sup>2</sup>H-naphthalene (**2**) (Chart 1).

**Table 1.** Pyrolysate composition after FVT of **1** and **2**.

T (° C)	FVT of <b>1</b>	FVT of <b>2</b>	mass recovery (%)
	% <b>2</b>	% <b>1</b>	
700	trace	-	98
800	4	trace	95
900	10	5	95
1000	25	30	90

With increasing temperature the intensity of the  $\delta(^2\text{H}) = 7.5$  ppm resonance increases (see Table 1 and Figure 1A). At 1000°C the pyrolysate contained 25 % of **2**. Additional support for the presence of **2** in the 1000°C pyrolysate of **1** was obtained by quantitative <sup>13</sup>C-NMR in the presence of Cr(acac)<sub>3</sub> as a relaxation agent. A triplet at  $\delta = 125$  ppm with the characteristic  $J_{\text{C-}^2\text{H}}$  ( $J$  24 Hz) is visible as expected for the presence of **2** (see Experimental Section). The integral ratio between the triplets of C1-<sup>2</sup>H (127 ppm) and C2-<sup>2</sup>H (125 ppm) shows that *ca.* 25% of **2** is present.

**Table 2.** Pyrolysate composition (massa %) determined by Direct Inlet EL-MS (E.I. 16 eV).

deuterium content	FVT of <b>1</b>			FVT of <b>2</b>		
	0 <sup>a</sup>	mono <sup>b</sup>	di <sup>c</sup>	0 <sup>a</sup>	mono <sup>b</sup>	di <sup>c</sup>
T (°C)						
700	-	100	-	-	100	-
800	-	100	-	-	100	-
900	5	90	5	6	88	6
1000	10	80	10	10	80	10

<sup>a</sup> natural abundance naphthalene. <sup>b</sup> *mono*-deuterated naphthalene. <sup>c</sup> *di*-deuterated naphthalene.

Inspection of the data in Table 2 indicates that while in the 700°C and 800°C pyrolysates only *mono*-deuterated naphthalene is present, after FVT at 900°C and 1000°C some natural abundance and *di*-deuterated naphthalene is formed. This is established from isotope pattern analysis of the direct inlet E.I MS spectra. A minor increase in both [M-1]<sup>+</sup> and [M+1]<sup>+</sup> was observed. This suggests that whereas in the lower temperature range only unimolecular processes occur, at higher temperatures additional bimolecular processes have to contribute.

### 3.2.2 FVT of 2-<sup>2</sup>H-naphthalene (**2**)

To validate the occurrence of hydrogen migration along the naphthalene perimeter, 2-<sup>2</sup>H-naphthalene (**2**) was subjected to FVT. Again, in the <sup>2</sup>H-NMR spectrum an additional signal corresponding to **1** [ $\delta = 7.8$  ppm, 1 *ca.* 5%] was present after FVT of **2** at 900°C. Direct inlet E.I. MS and detailed isotope pattern analysis shows that this pyrolysate mainly consists of *mono*-deuterated naphthalenes. However, in addition small amounts of natural abundance naphthalene and *di*-deuterated naphthalene are present. After FVT at 1000°C the signal in <sup>2</sup>H-NMR corresponding to **1** increased to 30% (Table 1 and Figure 1B). At this temperature still mainly *mono*-deuterated naphthalene isotopomers are present. Further support for the presence of **1** in the 1000°C pyrolysate of **2** was again obtained by quantitative <sup>13</sup>C-NMR spectroscopy. Here, a triplet ( $J_{C-2H}$  24Hz) is visible at 127 ppm, which corresponds to C1 in **1** and the integral of  $\delta(^{13}C)$  at 127.2 ppm (C2) was reduced. The integral ratio between the two triplets indicates that *ca.* 30% of **1** is present.

These observations indicate that hydrogen migrations along the perimeter are indeed also feasible in alternant PAH. These migrations take place at higher temperatures (800°C for **1** and 900°C for **2**) than the migrations of the deuterium atom within the cyclopenta-moiety of the non-



alternant CP-PAH (*ca.* 700°C), but at similar temperatures as the migration of the cyclopentamoiety to the alternant core.

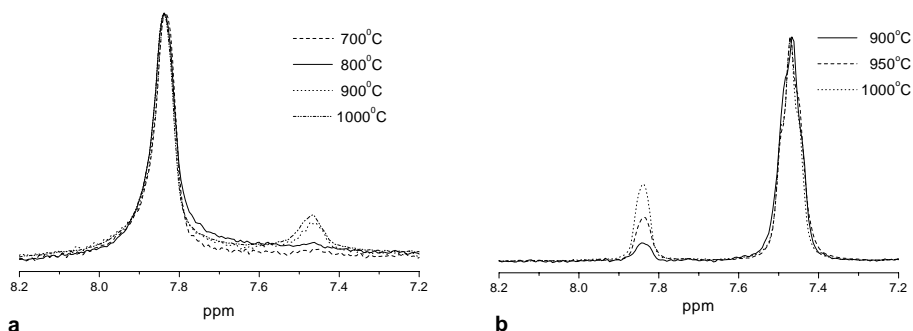


**Figure 1.**  $^2\text{H}$ -NMR spectra (8.2 – 7.2 ppm) obtained after pyrolysis of **a.** 1- $^2\text{H}$ -naphthalene (**1**) and **b.** 2- $^2\text{H}$ -naphthalene (**2**) at different temperatures.

### 3.2.3 GC-cryo-FT-IR spectroscopy

Further support for the occurrence of deuterium migrations is provided by GC-cryo-FT-IR spectra of **1**, **2** and the 1000°C pyrolysates of **1** and **2**. GC-cryo-FT-IR spectroscopy is an excellent method to obtain well-resolved IR spectra, since the IR spectra are recorded at  $-196^\circ\text{C}$  (see Experimental Section).<sup>10</sup>

In Figure 2A and 2B, GC-cryo-FT-IR-spectra (range  $600\text{ cm}^{-1}$  –  $1400\text{ cm}^{-1}$ ) of **1** and **2** are shown. The presence of the deuterium atom at either C1 or C2 leads to clear-cut differences between the two IR spectra (characteristic vibrations for **1** are marked with \*, for **2** with •). From Figure 2C, where the IR spectrum of the 1000°C pyrolysate of **1** is displayed, it can be seen that mainly 1- $^2\text{H}$ -naphthalene (**1**) is present. However, additional vibrations are discernible at, for example,  $\nu$  760, 905, 923 and  $1272\text{ cm}^{-1}$  (marked with •). These new peaks correspond to vibrations of 2- $^2\text{H}$ -naphthalene (**2**) (Figure 2B). The IR spectrum of the 1000°C pyrolysate of **2** shows similar features (Figure 1D). The major component is **2**, but new vibrations that are present at  $780$ ,  $807$  and  $815\text{ cm}^{-1}$  (marked with \*) can be assigned to **1** (Figure 1A). Besides the formation of the corresponding *mono*-deuterated isomer by migration of the deuterium atom, IR analyses also reveals the presence of a small amount of natural abundance naphthalene in the pyrolysates obtained after FVT at  $1000^\circ\text{C}$  [ $\nu$  960, 1007,  $1388\text{ cm}^{-1}$  (marked with x), *ca.* 10%]. Since the IR spectra of the pyrolysates can be fully accounted for by the presence of **1**, **2** and some natural

abundance naphthalene, this provides strong evidence that a distinct process should be responsible for the deuterium migration.<sup>11</sup>

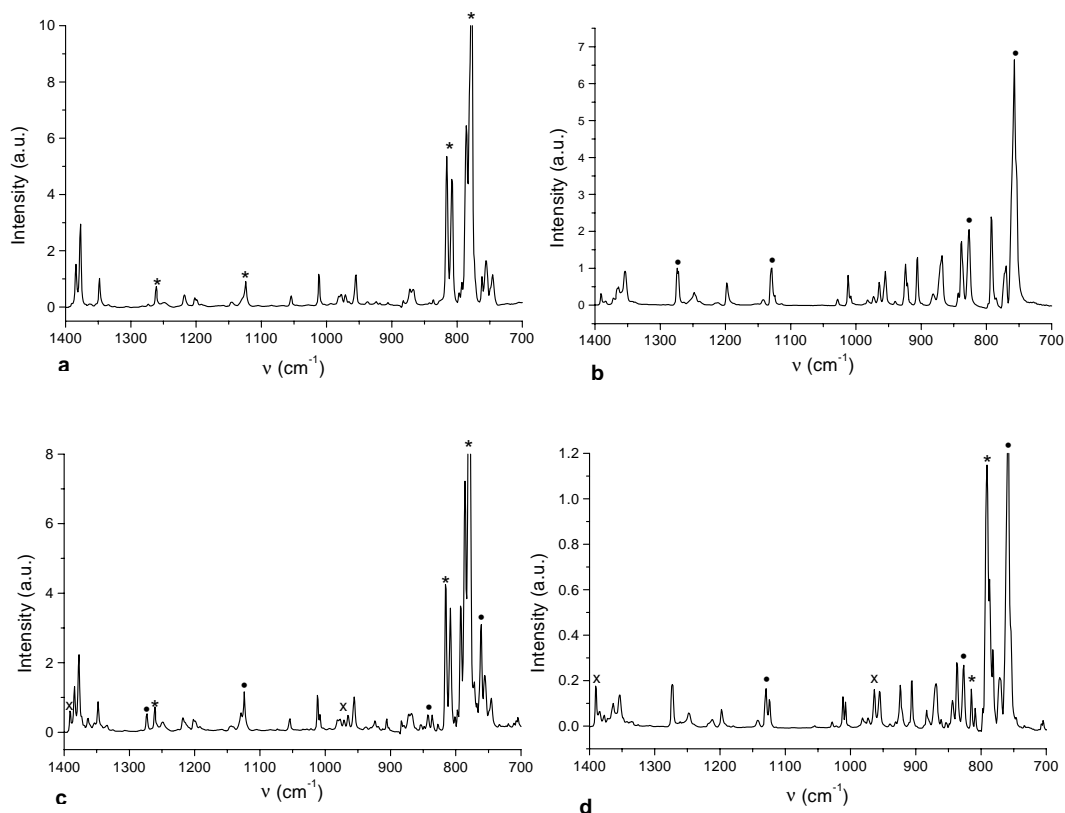


**Figure 2.** GC-cryo-FT-IR spectra (range 1400 – 700  $\text{cm}^{-1}$ ) of **a.** 1-<sup>2</sup>H-naphthalene (**1**) (characteristic peaks are marked \*), **b.** 2-<sup>2</sup>H-naphthalene (**2**) (characteristic peaks are marked with •), **c.** 1000°C pyrolysate of **1** (peaks corresponding to **2** are marked with •, peaks corresponding to natural abundance naphthalene with x) and **d.** 1000°C pyrolysate of **2** (peaks corresponding to **1** are marked with \*, peaks corresponding to natural abundance naphthalene with x).

### 3.3 Mechanistic considerations

An important question to account for the observed deuterium migrations is whether the processes taking place are unimolecular. Radical processes in the case of naphthalene would give naphthyl

radicals, which by recombination are known to give the three isomeric 1,1-, 1,2- and 2,2-binaphthyl.<sup>12,13</sup> Investigations, also in our group, have shown that under FVT conditions, radical processes take place from 1100°C and indeed result in the formation of all possible isomeric binaphthyls.

The high mass recoveries (Table 1) indicate, however, that no radical processes take place. Notwithstanding, the presence of some natural abundance naphthalene and *di*-deuterated naphthalene in the 900°C and 1000°C pyrolysates (Table 2) indicate that in the high temperature region additional (bimolecular) processes have to contribute. Therefore, all pyrolysates were checked for the presence of trace of amounts of binaphthyl compounds by capillary GC-analysis using all possible binaphthyls as reference compounds (see Experimental Section). However, no trace of any of the binaphthyls (< 0.05%) were detected in all pyrolysates. These observations indicate that the additional processes that contribute at high temperatures do not proceed *via* free radical intermediates.

The most likely unimolecular process that accounts for our observations in the low temperature regime, are 1,2-H shifts and the involvement of carbene intermediates (Scheme 1). Here, the 1,2-H shifts and carbene intermediates responsible for the migration of the deuterium are shown. The different closed-shell carbenes **3**, **4** and **5**, and the transition states (TS) are calculated at the B3LYP/TZVP level of theory (Table 3). As can be seen, the relative energies of carbenes **3** and **4** are similar ( $E_{\text{rel}}$  83.5 and 82.6 kcalmol<sup>-1</sup>, respectively, relative to naphthalene). The corresponding transition states are only slightly higher in energy (TS**3**: 88.0 and TS**4**: 86.7 kcalmol<sup>-1</sup>). Carbene **5** is considerable higher in energy than **3** and **4** ( $E_{\text{rel}}$  94.5 kcalmol<sup>-1</sup>), which is in accordance with the fact that here the aromaticity of two rings is destroyed.

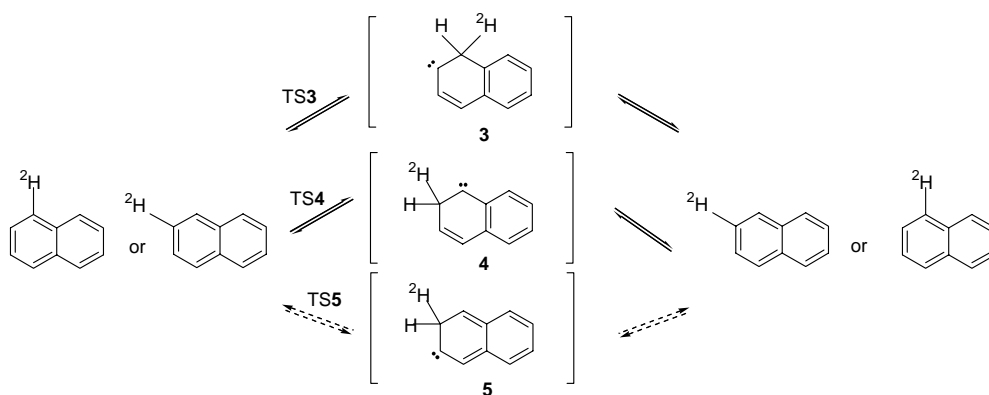
Note that all carbenes have significant higher relative energies (*ca.* 20 kcalmol<sup>-1</sup>) than the carbene intermediates of the CP-PAH discussed in Chapter 2. This is in line with the observation that deuterium migration in alternant PAH (from *ca.* 900°C) takes place at higher temperatures than deuterium migration within the cyclopenta-moiety of CP-PAH (from *ca.* 700°C). This is also in agreement with the occurrence of deuterium migration from the cyclopenta-moiety to the aromatic core, which takes place from 900°C (Chapter 2). The formation of all isotopomers with deuterium in the aromatic core in similar amounts could only be explained when 1,2-H shifts in the alternant core are feasible.

The presence of some natural abundance and *di*-deuterated naphthalene in the 900°C and 1000°C pyrolysates, cannot be accounted for by the carbene mechanism. The fact that the total deuterium content of the pyrolysate does not change (Table 2) suggests that at higher temperature bimolecular processes (H, <sup>2</sup>H transfer) begin to contribute.

**Table 3.** Relative energies (kcalmol<sup>-1</sup>) at the B3LYP/TZVP level of theory of the closed-shell singlets of carbenes **3** - **5** and transitions states **3** - **5** relative to natural abundance naphthalene.<sup>a</sup>

carbene	E <sub>rel</sub>	TS	E <sub>rel</sub>
<b>3</b>	83.5	<b>3</b>	88.0
<b>4</b>	82.6	<b>4</b>	86.7
<b>5</b>	94.5	<b>5</b>	99.6

<sup>a</sup>E<sub>total</sub> naphthalene = -386.015583 a.u.



**Scheme 1.** Proposed mechanism for the migration of the deuterium along the perimeter of the alternant PAH naphthalene.

### 3.4 Conclusions

These observations give the first experimental evidence that hydrogen atoms in *alternant* PAH are mobile and migrate under FVT conditions from *ca.* 800°C, when no skeletal rearrangements are operational.<sup>14</sup> This gives further support for the mechanism proposed in Chapter 2 for the migration of the deuterium atom from the cyclopenta-moiety to the aromatic core and *vice versa*; 1,2-H/1,2-<sup>2</sup>H shifts in the alternant core are feasible. Further research in the field of the high temperature chemistry of deuterated PAH is warranted.

### 3.5 Experimental section

Reactions were carried out under a N<sub>2</sub> atmosphere. Solvents were dried and purified using standard procedures. Commercially available reagents were used without further purification. <sup>1</sup>H (300.13 MHz) and <sup>13</sup>C (75.47 MHz) NMR spectra were recorded on a Bruker AC 300 spectrometer and a Varian 300 NMR using CD<sub>2</sub>Cl<sub>2</sub> as the solvent. Chemical shifts (in ppm) are given relative to CD<sub>2</sub>Cl<sub>2</sub> (5.32 ppm) in the case of <sup>1</sup>H-NMR and 53.00 ppm in the case of <sup>13</sup>C-NMR. *J* values are given in Hz. <sup>2</sup>H (46.07 MHz) NMR spectra were recorded in CH<sub>2</sub>Cl<sub>2</sub>, with the natural abundance <sup>2</sup>H present in CH<sub>2</sub>Cl<sub>2</sub> as the reference (5.32 ppm). Quantitative <sup>13</sup>C-NMR was performed in CD<sub>2</sub>Cl<sub>2</sub> with Cr(acac)<sub>3</sub> to enhance relaxation processes and d1 = 20 s, at = 0.8s. In <sup>13</sup>C-NMR the signals are indicated with q = quaternary carbon, t = tertiary carbon. GC-analysis was performed using a Varian 3800 (column: J&W Scientific DB-5, length 30m, ID 0.3 mm, film thickness 0.1μm) with FID detection. Flow control assured reproducibility of the retention times.

GC-cryo-FT-IR<sup>10</sup>: GC separations (column: HP-5MS, length 25 m, ID 0.25 mm and film thickness 0.25 μm; injector temperature 275°C, temperature program, 2 min at 80°C and then increased to 290°C (10°C min<sup>-1</sup>); carrier gas He). Cryotrap IR detection was carried out with a Digilab FTS-40 Fourier transform instrument equipped with a Digilab Tracer GC interface and A SPC 3200 computer for data acquisition. The temperature of the transfer line and the deposition tip was 275°C; cooling of the IR transparent trapping window to -196°C was carried out with liquid N<sub>2</sub> at a vacuum of 10<sup>-5</sup> Torr. Spectra of the trapped GC-eluates were recorded 'on-the-fly', *i.e.*, a few seconds after deposition by averaging four scans (resolution 8 cm<sup>-1</sup>) every 2 s. In addition, post-run scanning (512 scans co-added) of trapped components were performed after completion of the GC-run by repositioning the corresponding window coordinates, *i.e.*, retention times (*t<sub>R</sub>*), into the IR beam (optical resolution 2 cm<sup>-1</sup>).

Direct Inlet Electron Ionization (EI) mass spectrometry was carried out using a JEOL JMS SX102/102A four-sector mass spectrometer (Akishima Tokyo, Japan), coupled to a JEOL MS/MP700 data system. The samples were introduced into the ion source with a direct insertion system (probe temperature between 45°C and 70°C). The electron energy was 16 eV; the ion source temperature was 150°C.

*Caution:* PAH are potential genotoxic compounds.

#### General Flash Vacuum Thermolysis Procedure<sup>15</sup>

A commercial Thermolyne 21100 tube furnace containing an unpacked quartz tube (length 40 cm and diameter 2.5 cm) was used in all FVT experiments. The pressure during all FVT-experiment was 1·10<sup>-3</sup> mmHg. Two consecutive cold traps (N<sub>2</sub> (l)) were used to trap all naphthalene formed. The products were rinsed from either the tube or the cold-traps with distilled CH<sub>2</sub>Cl<sub>2</sub>, after which the pyrolysate composition was determined by capillary GC and <sup>1</sup>H-NMR and GC-MS.

**Ab initio Calculations**

The carbene species and the corresponding transition states were calculated at the B3LYP/TZVP level of theory. Minima and transition states were identified by harmonic analysis. All calculations were performed using the GAMESS-UK package.<sup>16</sup>

**1-<sup>2</sup>H-naphthalene (1)<sup>8</sup>**

To an ice-cooled solution of 1-bromonaphthalene (2.3 g, 11.0 mmol) in diethylether (50 ml) *n*-butyllithium (9 ml, 14.0 mmol of a 1.6 M solution in *n*-hexane) was added. After stirring the reaction mixture at room temperature for 2 hr., D<sub>2</sub>O (5 ml) was added. The organic layer was separated, dried and concentrated *in vacuo*. The resulting white solid was purified by flash chromatography (silica, eluent *n*-hexane). Yield 1.2 g of a white solid (80%, 9.4 mmol, 98% <sup>2</sup>H).

<sup>1</sup>H-NMR ( $\delta$  in ppm): 7.87 (3H, m), 7.50 (4H, m).

<sup>13</sup>C-NMR ( $\delta$  in ppm): 132.8 (q, C4a), 132.8 (q, C8a), 127.3 (t, C1, triplet *J* 24), 127.3 (s, C4 and C5), 127.2 (s, C8), 125.2 (t, C3, C6 and C7), 125.1 (t, C2).

<sup>2</sup>H-NMR ( $\delta$  in ppm): 7.8 (broad s)

EI-MS: *m/z* 129 (M<sup>+</sup>, 100%), 130 ([M+1]<sup>+</sup>, 11.06 %), 128 ([M-1]<sup>+</sup>, 6.93 %)

**2-<sup>2</sup>H-naphthalene (2)<sup>8</sup>**

A similar procedure as used for **1** was followed, this time starting from 2-bromonaphthalene. Yield 95% (96% <sup>2</sup>H).

<sup>1</sup>H-NMR ( $\delta$  in ppm): 7.87 (4H, m), 7.50 (3H, m)

<sup>13</sup>C-NMR ( $\delta$  in ppm): 132.9 (q, C4a and C8a), 127.3 (t, C4, C5 and C8), 127.2 (t, C1), 125.3 (t, C2, triplet *J* 24), 125.2 (t, C6 and C7), 125.1 (t, C3).

<sup>2</sup>H-NMR ( $\delta$  in ppm): 7.5 (broad s)

EI-MS: *m/z* 129 (M<sup>+</sup>, 100%), 130 ([M+1]<sup>+</sup>, 11.04 %), 128 ([M-1]<sup>+</sup>, 8.48%).

## References and notes

- (1) Sarobe, M. Polycyclic Aromatic Hydrocarbons under High Temperature Conditions. Consequences for Carbon Build up during Combustion and Fullerene Formation Processes.; Utrecht University: Utrecht, The Netherlands, **1998**.
- (2) Scott, L. T. Pure & Appl. Chem. **1996**, 68, 291-300.
- (3) Necula, A.; Scott, L. T. J. Am. Chem. Soc. **2000**, 122, 1548-1549.
- (4) Brooks, M. A.; Scott, L. T. J. Am. Chem. Soc. **1999**, 121, 5444-5449.
- (5) Anderson, M. R.; Brown, R. F. C.; Coulston, K. J.; Eastwood, F. W.; Ward, A. Aust. J. Chem. **1990**, 43, 1137-1150.
- (6) Schulz, K.; Hofmann, J.; Zimmermann, G. Eur. J. Org. Chem. **1999**, 3407-3412.
- (7) Hoffman, R. E.; Treitel, N.; Shabtai, E.; Benschafut, R.; Rabinovitz, M. J. Chem. Soc., Perkin Trans. 2 **2000**, 1007-1011.
- (8) Martin, R. H.; Moriau, J.; Defay, N. Tetrahedron **1974**, 30, 179-185.
- (9) In contrast to what was observed for the non-alternant CP-PAH,<sup>17</sup> fragmentation of the molecular ion of naphthalene under mass spectrometric conditions could be reduced using direct inlet MS and lowering of the E.I. from 70 to 16 eV.
- (10) Visser, T.; Sarobe, M.; Jenneskens, L. W.; Wesseling, J. Fuel **1998**, 77, 913-920.
- (11) This assignment is supported by *ab initio* computations.
- (12) Badger, G. M.; Whittle, C. P. Aust. J. Chem. **1963**, 16, 440-444.
- (13) Badger, G. M.; Kimber, R. W. L.; Novotny, J. Aust. J. Chem. **1964**, 17, 778-786.
- (14) Scott, L. T.; Agopian, G. K. J. Am. Chem. Soc. **1977**, 99, 4506.
- (15) Brown, R. F. C. Pyrolytic Methods in Organic Chemistry; Academic Press: New York, 1980; Vol. 41.
- (16) Guest, M. F.; van Lenthe, J. H.; Kendrick, J.; Schöffel, K.; Sherwood, P.; Harrison, R. J. GAMESS-UK, a package of ab initio programs, **1998**. With contributions from Amos, R.D.; Buenker, R.J., Dupuis M; Handy, N.C.; Hillier, I.; Knowles, P.J.; Bonacic-Koutecky, V.; von Niessen, W.; Saunders, V.R.; Stone, A.J. Derived from the original GAMESS code by: Dupuis, M.; Spangler, D.; Wendolowski, J., NRCC Software Catalog, vol. 1, programs no. QG01 (GAMESS), **1980**.
- (17) Lifshitz, C.; Ling, Y.; Martin, J. M. L. Adv. Mass. Spectrom. **1998**, 14.





# Part II

*The Schlegel-Match Proposition*



# CHAPTER 4

## **Benzo[1,2-*e*:3,4-*e'*:5,6-*e''*]tribenzo[*l*]acephenanthrylene (C<sub>60</sub>H<sub>30</sub>): a Progenitor of C<sub>60</sub>. Its Stepwise Conversion into C<sub>60</sub>.**

### **Abstract**

The C<sub>60</sub>H<sub>30</sub> PAH benzo[1,2-*e*:3,4-*e'*:5,6-*e''*]tribenzo[*l*]acephenanthrylene (**4**, C<sub>3</sub>) which possesses a carbon topology that is a Schlegel-match for C<sub>60</sub>, is converted into C<sub>60</sub> by fifteen-fold H<sub>2</sub> losses and ring closures. This conversion of **4** in C<sub>60</sub> is achieved by matrix-assisted-laser-desorption-ionization time-of-flight mass spectrometry [MALDI TOF-MS (positive-ion mode)] at various laser fluences. The *in-source* and *post-source* decay MALDI TOF mass spectra show that **4** 'zips up' in a stepwise fashion. In this 'zipping up' process (H<sub>2</sub> loss followed by ring closure) the inner core hydrogen atoms are eliminated first as is demonstrated by comparison with its sub-structures benzo[1,2-*e*:3,4-*e'*:6,5-*e'*]triacephenanthrylene C<sub>48</sub>H<sub>24</sub> (**3**) and decacyclene C<sub>36</sub>H<sub>18</sub> (**2**). The occurrence of fifteen-fold consecutive intramolecular H<sub>2</sub> losses and ring closures is supported by *semi-empirical* RHF/AM1 and UHF/AM1 and *ab initio* (RHF/6-31G\*\*/RHF/AM1, B3LYP/6-31G\*\*/RHF/AM1, UB3LYP/6-31G\*\*/UHF/AM1) calculations.

## 4.1 Introduction

Although substantial amounts of  $C_{60}$  and  $C_{70}$  can be obtained by arc/laser vaporization of graphite,<sup>1,2</sup> the underlying mechanism of fullerene formation is still not fully resolved and from a synthetic perspective not readily amendable to modifications. This obstructs the development of the selective preparation of  $C_{60}$ ,  $C_{70}$  and ultimately other fullerenes.<sup>3</sup> Hence, a quest for rational fullerene syntheses was instigated.

Hitherto, various approaches have been put forward. In one approach the synthesis of 'bucky-bowls', *i.e.* large bowl-shaped polycyclic aromatic hydrocarbons (PAH), is pursued.<sup>4-11</sup> Although, the conversion of 'bucky-bowls' into closed carbon surfaces has not yet been achieved,<sup>12-14</sup> these molecules are of interest in their own right since they possess curvature and represent topological fullerene sub-structures.<sup>15</sup>

More recently, *unimolecular* fullerene progenitors became synthetic targets. For example, a cage-like  $C_{60}H_6$  polyene was proposed as a penultimate precursor for  $C_{60}$ . This polyene, which could only be generated *in-situ*, gave  $C_{60}$  after six-fold hydrogen losses under FT-ICR LD<sup>16</sup> or LDI TOF-MS conditions.<sup>17</sup> However, the unimolecular nature of the conversion process is questioned as both build-up and degradation of the  $C_{60}H_6$  carbon skeleton occurs in the mass spectrometer. Additionally, it is still ambiguous to what extent the proposed drastic cyclization of the polyene skeleton into the icosahedral  $C_{60}$  closed carbon surface is feasible.<sup>18</sup> Notwithstanding, *via* a similar approach  $C_{36}$  was prepared from an *in-situ* generated polyene  $C_{36}Cl_8$ .<sup>19</sup> Following a similar approach, compelling evidence was given that the smallest possible fullerene,  $C_{20}$ , is accessible from a *per*-brominated dodecahedrane cage.<sup>20</sup>

In a completely different approach, two polycyclic aromatic hydrocarbons, which already contain the *right* carbon atom topology of the  $C_{60}$  Schlegel diagram, were envisaged as unimolecular precursors for  $C_{60}$ , *i.e.* 1,3,5-(tribenzo[*d*]phenanthren-5-yl)benzene [ $C_{60}H_{36}$  ( $C_3$  symmetry)]<sup>21</sup> and benzo[1,2-*e*:3,4-*e'*:5,6-*e''*]tribenzo[*h*]acephenanthrylene [ $C_{60}H_{30}$  (**4**,  $C_3$ )].<sup>22</sup> The proposal of these PAH precursors was inspired by the fact that in suitable flames the formation of PAH and the fullerenes  $C_{60}$  and  $C_{70}$  appear to be interrelated.<sup>23</sup> Unfortunately, the  $C_{60}H_{36}$  precursor, containing a 1,3,5-substituted benzene core, readily decomposed under the conditions needed for the required consecutive cyclodehydrogenations, *viz.*  $H_2$  losses and ring closures that will lead to increased curvature and, finally, a closed carbon surface.<sup>21</sup>

Initially, the synthesis of the other unimolecular progenitor, **4** (Chart 1), was attempted *via* the  $S_8$ -mediated trimerization of the dihydroPAH 4,5-dihydro[*h*]benzacephenanthrylene. Unfortunately, however, this yielded predominantly the isomer **5** ( $C_1$ ) and only to a minor extent the desired **4** ( $C_3$ ) isomer (Chart 1). This is attributed to the lack of *regio*-chemical control of the  $S_8$ -

mediated trimerization reaction that involves radical intermediates.<sup>22</sup> Since these large PAH are sparingly soluble, the separation of the two isomers was not achieved. Note, however, that if no rearrangements of the carbon skeleton take place under the zip up conditions, the C<sub>7</sub> isomer is no suitable precursor for C<sub>60</sub> (Chart 1). Indeed, it was shown that **5** could not be converted in C<sub>60</sub> by matrix-assisted LDI TOF-MS [MALDI TOF-MS (positive-ion mode)] but only yielded curved C<sub>60</sub>H<sub>12</sub>/C<sub>60</sub>H<sub>10</sub> PAHs.

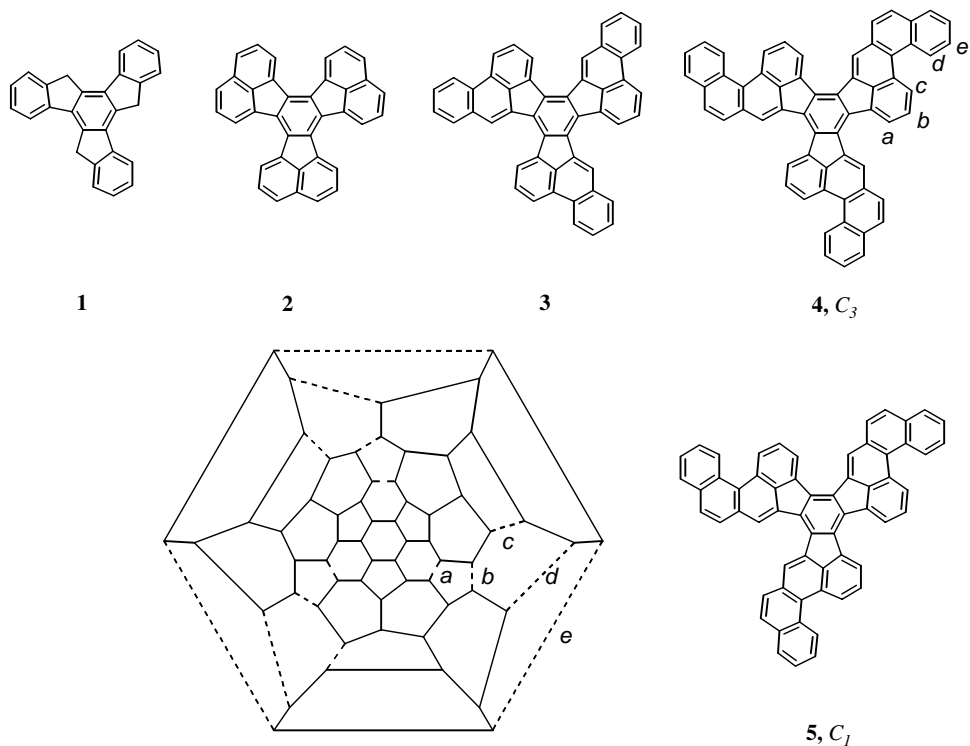


**Chart 1**

Recently, however, two *regio*-controlled synthesis of **4** have been reported. One based on the application of the Pd-catalyzed intramolecular arylation on a derivative of truxene **1** (Chart 1) by the group of Echavarren in Spain.<sup>24</sup> Another synthesis of **4** was reported by Scott and *co*-workers, which is based on the trimerization of 5*H*-benzo[*f*]acephenanthrylen-4-one catalyzed by TiCl<sub>4</sub>.<sup>25</sup> The synthesis of Scott *et al.* was later applied for the preparation of a chlorinated derivative of **4** in 11 steps from 1-bromo-4-chlorobenzene.<sup>26</sup> Although, their initial objective was

chlorine substitution at positions **a** (Chart 1), this failed due to severe steric congestion at this position.<sup>25</sup> Hence, hitherto only a derivative with chlorines at positions **c** could be prepared. Upon FVT of this chlorinated derivative of **4**, the pyrolysate was shown to contain C<sub>60</sub> in only 0.1 - 1.0% which could be isolated after laborious preparative HPLC.<sup>26</sup> This indicates that chlorine substitution at position **c** has a minor beneficial effect.

In this Chapter the results of the collaboration between the group of Echavarren and our group, which resulted in the controlled and stepwise conversion of **4** (C<sub>3</sub>) into C<sub>60</sub> by fifteen-fold consecutive intramolecular H<sub>2</sub> losses under MALDI TOF-MS conditions is described.<sup>27</sup> The results are compared with those independently reported by the Boston-Warwick group, who achieved the conversion of **4** into C<sub>60</sub> under LDI TOF-MS conditions<sup>25</sup> and by FVT.<sup>26</sup>

It is shown that the correct carbon topology of **4** is a prerequisite for its conversion into C<sub>60</sub> by fifteen-fold intramolecular cyclodehydrogenations. The sub-structures of **4**, C<sub>48</sub>H<sub>24</sub> (**3**, C<sub>3</sub>) and C<sub>36</sub>H<sub>18</sub> (**2**, D<sub>3</sub>) (Chart 1), which possess similar inner cores, but lack distinct parts of the outer annelated hexagons, are shown to undergo besides initial cyclodehydrogenations also fragmentation reactions. In addition, a comparison of the initial cyclodehydrogenation behavior of **3** and **2** with those of **4** reveals that curling up of the surface of **4** occurs from the inside outwards in consecutive steps. This is corroborated by *semi*-empirical (RHF/AM1 and UHF/AM1) and *ab initio* (RHF/6-31G\*/RHF/AM1, B3LYP/6-31G\*/RHF/AM1, UB3LYP/6-31G\*/UHF/AM1) calculations.

## 4.2 Results & Discussion

### 4.2.1 Zipping up of C<sub>60</sub>H<sub>30</sub> to C<sub>60</sub> by MALDI TOF-MS

To induce fifteen-fold consecutive H<sub>2</sub> losses and ring closures, **4** was subjected to MALDI TOF-MS conditions at different laser fluences.<sup>27</sup> At a laser fluence of 1800 (*ca.* 8 μJ pulse<sup>-1</sup>) only the radical cation of **4** (**4**<sup>+</sup>) (*m/z* 750) is observed [natural isotope pattern: *calc.* *m/z* 750 (100 %), 751 (67 %), 752 (22 %) and 753 (6 %); *found* *m/z* 750 (100 %), 751 (70 %), 752 (33 %) and 753 (10 %)]. When the laser fluence is increased to 1900 (*ca.* 12 μJ pulse<sup>-1</sup>) **4**<sup>+</sup> undergoes up to three-fold H<sub>2</sub> losses giving C<sub>60</sub>H<sub>28</sub><sup>+</sup>, C<sub>60</sub>H<sub>26</sub><sup>+</sup> and C<sub>60</sub>H<sub>24</sub><sup>+</sup> [*m/z* 748 (11 %), 746 (3 %) and 744 (2 %)] (Figure 1A). A further increase of the laser fluence to 2200 (*ca.* 440 μJ pulse<sup>-1</sup>) leads to consecutive cyclodehydrogenations from *m/z* 750 down to *m/z* 720, *i.e.* C<sub>60</sub> [*m/z* 748 (85 %), 746 (72 %), 744 (43 %), 742 (23 %), 740 (10 %), 738 (6 %), 736 (5 %), 734 (4 %), 732 (3 %), 730 (2 %), 728 (1 %), 726 (2 %), 724 (2 %), 722 (6 %) and 720 (5 %)] (Figure 1B). Isotope pattern analysis in the mass range *m/z* 720 to *m/z* 725 shows that both C<sub>60</sub><sup>+</sup> and C<sub>60</sub>H<sub>2</sub><sup>+</sup> are formed [*ratio* 1 : 1, natural isotope pattern: *calc.* *m/z* 720 (4.9%), 721 (3.3%), 722 (6.0%), 723 (3.5%), 724 (1.1%) and 725 (0.3%); *found*

## A Progenitor of C<sub>60</sub> and Its Stepwise Conversion into C<sub>60</sub>

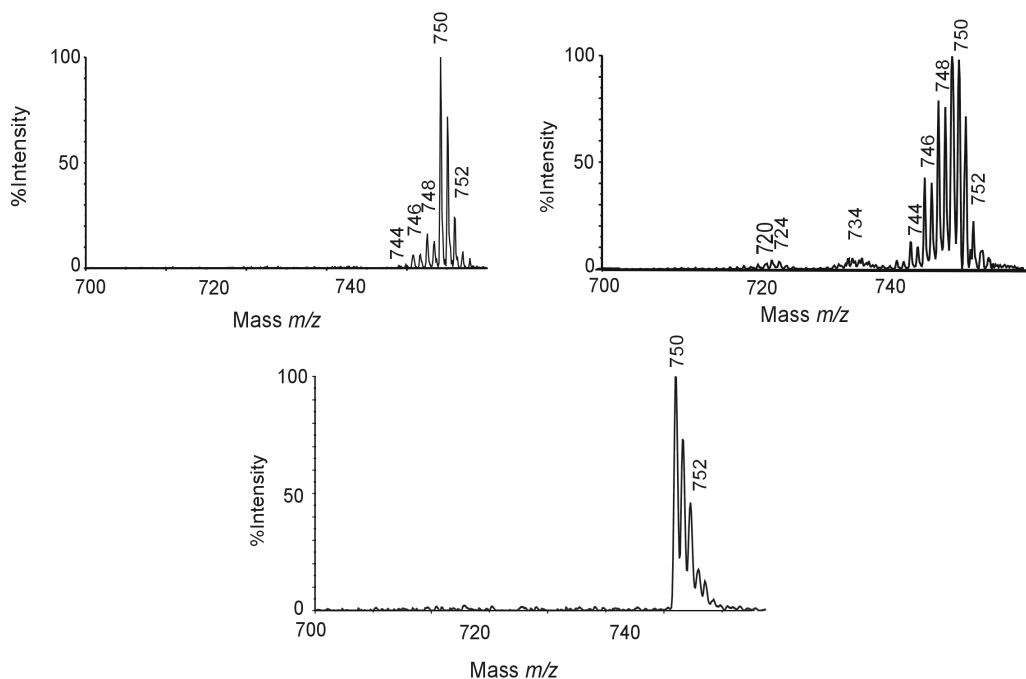


**Figure 1.** *In-source* MALDI TOF mass spectra of **4** a. laser fluence of 1900 (positive-ion mode), b. laser fluence of 2200 (positive-ion mode) and c. laser fluence of 2200 (negative-ion mode).<sup>28</sup>

$m/z$  720 (5.0%), 721 (3.5%), 722 (6.0%), 723 (3.6%), 724 (2.0%), and 725 (0.9%)]. As can be seen from Figure 1B two distinct mass clusters are present around  $m/z$  734 and  $m/z$  724. Notice that the fifteen-fold consecutive cyclodehydrogenations are only visible in the positive-ion mode mass spectra. This is illustrated by the MALDI TOF-MS (negative-ion mode) *in-source* spectrum of **4**<sup>-</sup> at a laser fluence of 2200 (*ca.* 440  $\mu\text{J}/\text{pulse}^{-1}$ ) (Figure 1C); only the molecular ion is found. Hence, the formation of the radical cation of **4** is essential for its conversion into C<sub>60</sub>.

For the zipping up of **4**<sup>+</sup> to C<sub>60</sub> two distinct thresholds are present. At the first threshold **4**<sup>+</sup> and its cyclodehydrogenation products C<sub>60</sub>H<sub>28</sub><sup>+</sup>, C<sub>60</sub>H<sub>26</sub><sup>+</sup>, and C<sub>60</sub>H<sub>24</sub><sup>+</sup> are discernible, whereas at the second threshold cyclodehydrogenations occur from **4**<sup>+</sup> down to C<sub>60</sub><sup>+</sup>. In our experiments neither skeletal fragmentation nor build up, such as incorporation of fragments or ion-molecule reactions, take place as is apparent from the ‘clean’ MS-spectra. It is documented that PAH are susceptible to loss and accretion of H, H<sub>2</sub> and C<sub>2</sub>H<sub>2</sub>, while fullerenes generally only undergo extrusion and build up involving ‘C<sub>2</sub>’-units.<sup>29-32</sup>

Unambiguous evidence for the unimolecular transformation of  $4^+$  into  $C_{60}$  is obtained from *post-source-decay* (PSD) experiments. In these experiments  $4^+$  is isolated prior to TOF-MS analysis (Figure 2A). The PSD spectrum is nearly identical to the corresponding *in-source* spectrum. This demonstrates that the consecutive cyclodehydrogenation products all originate from  $4^+$ . Also in the PSD spectrum the three distinct regions are discernible; from  $m/z$  750-744,  $m/z$  734-730 and  $m/z$  722-720. This well-defined pattern, which displays a gradual decrease in intensity, implies that the cyclodehydrogenations indeed take place in a controlled and stepwise fashion. Additional compelling evidence is provided by the PSD spectrum of an intermediate ion, *i.e.*  $C_{60}H_{26}$  ( $m/z$  746), which is formed after two successive  $H_2$  losses and ring closures from  $C_{60}H_{30}^+$  ( $m/z$  750) (Figure 2B). Upon isolation of this ion, the same pattern of cyclodehydrogenations leading to  $C_{60}$  is discernible. Hence, under the given MALDI TOF-MS conditions (positive-ion mode)  $C_{60}$  is formed from  $4^+$  *without* any skeletal rearrangements. These results rationalize that in our previous experiment the wrong isomer **5** ( $C_7$ ) only gave the curved PAHs  $C_{60}H_{12}$  and  $C_{60}H_{10}$  under similar MALDI TOF-MS conditions.<sup>22</sup>

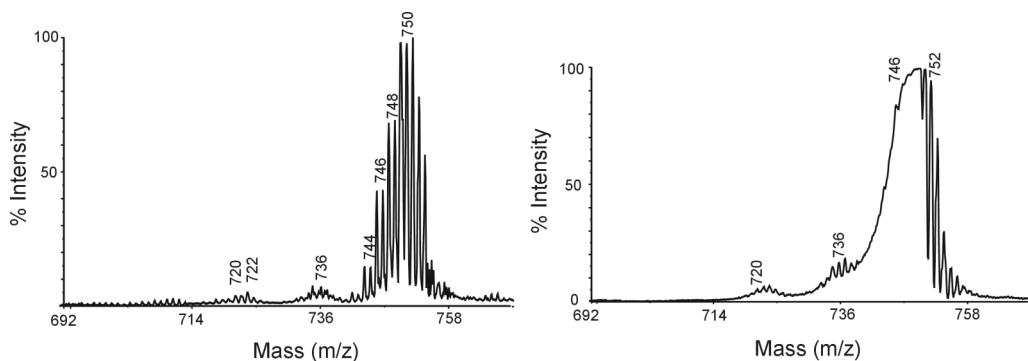


**Figure 2.** *Post-Source Decay* (PSD) MALDI TOF mass spectra of  $4^+$  at a laser fluence of 2200 (positive-ion mode). **a.** Isolation of  $m/z$  750 ( $C_{60}H_{30}^+$ ) and **b.** isolation of  $m/z$  746 ( $C_{60}H_{26}^+$ ).

#### 4.2.2 The effect of laser fluence

An unexpected difference between our results described here and those reported by the Boston-Warwick group<sup>25</sup> is that they observed, besides the formation of  $C_{60}$ , extensive fragmentation and build-up reactions under their apparently similar LDI TOF-MS conditions ( $N_2$  laser 337 nm, laser pulse 3 ns).<sup>25</sup> The only variation is that in the LDI TOF-MS experiments no matrix was used. It is



## A Progenitor of C<sub>60</sub> and Its Stepwise Conversion into C<sub>60</sub>

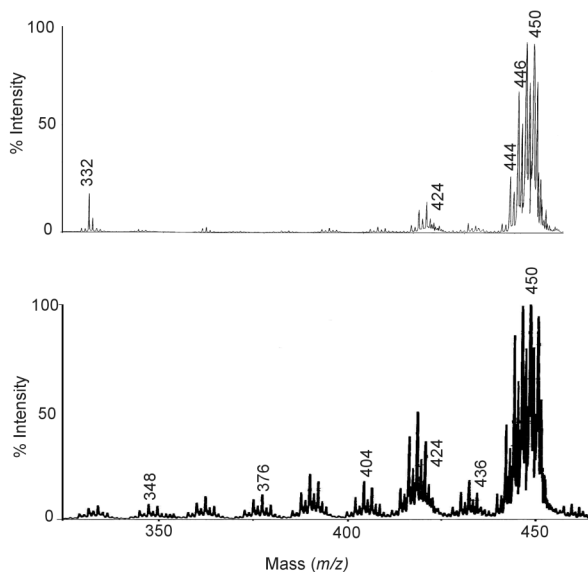


**Figure 3.** Post-source decay (PSD) MALDI TOF mass spectra of  $2^+$  (positive-ion mode). **a.** at a laser fluence of 2300, **b.** At a laser fluence of 3000.

known that the use of a matrix can have an effect on the extent in which fragmentation and build up take place during (MA)LDI TOF-MS.<sup>33</sup> Therefore, we repeated the (MA)LDI TOF-MS experiments on  $4^+$  without a matrix and using different matrices. In all cases similar results were found. Therefore, we attribute the apparent discrepancy to differences in the employed laser fluence.

This prompted us to subject key sub-structures of **4** with comparable innercores, *i.e.* benzo[1,2-*e*:3,4-*e'*:6,5-*e''*]triacenanthrylene (**3**, C<sub>48</sub>H<sub>24</sub>, C<sub>3</sub>) and decacyclene (**2**, C<sub>36</sub>H<sub>18</sub>, D<sub>3</sub>) (Chart 1) to MALDI TOF-MS conditions. For **3** and **2** it is expected that the cyclodehydrogenations of the first six hydrogen atoms will occur under similar conditions as for **4**.

MALDI TOF-MS on the smallest sub-structure of **4**, decacyclene (**2**), shows that at a laser fluence of 1900 the radical cation  $2^+$  is observed [ $m/z$  450 (100%), 451 (41%), 452 (9%)]. Upon increase of the laser fluence to 2300 three-fold H<sub>2</sub> losses and ring closures occur giving C<sub>36</sub>H<sub>16</sub><sup>+</sup>, C<sub>36</sub>H<sub>14</sub><sup>+</sup>, C<sub>36</sub>H<sub>12</sub><sup>+</sup> [ $m/z$  448 (100%), 446 (75%), 444 (30%)]. However, already at this laser fluence additional low intensity mass clusters are observed [ $m/z$  436 C<sub>35</sub>H<sub>16</sub>, '-CH<sub>2</sub>', *i.e.* C<sub>2</sub>H<sub>2</sub> loss followed by nH<sub>2</sub> loss, 16% and  $m/z$  424 C<sub>34</sub>H<sub>16</sub>, -C<sub>2</sub>H<sub>2</sub>, 16%]. Their presence indicates that fragmentation already sets in. A PSD experiment (laser fluence 2300) in which  $2^+$  ( $m/z$  450) was

isolated, shows that the fragmentation processes originate from the molecular ion (Figure 3A). Further increase of the laser fluence to 2600 results in a more pronounced appearance of the additional mass clusters. At a laser fluence of 3000 a regular pattern of mass clusters attributed to consecutive 'CH<sub>2</sub>' and C<sub>2</sub>H<sub>2</sub> fragmentation is clearly present (Figure 3B). This fragmentation pattern consists of clusters with comparable intensities separated by 14 a.m.u.. Apparently, at this laser fluence breakdown of 2<sup>+</sup> takes place by elimination of C<sub>2</sub>H<sub>2</sub> followed by nH<sub>2</sub> loss.

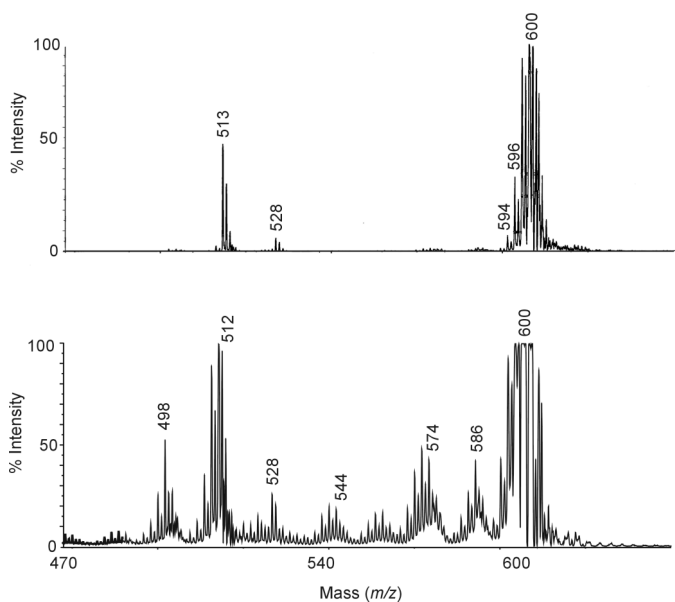


**Figure 4.** Post-source decay (PSD) MALDI TOF mass spectra of 3<sup>+</sup> (positive-ion mode) **a.** at a laser fluence of 2300, **b.** at a laser fluence of 2600.

MALDI TOF-MS experiments (positive-ion mode) using various laser fluences on the larger sub-structure of **4**, e.g. C<sub>48</sub>H<sub>24</sub> **3**, gave comparable results. At a laser fluence of 1850 the radical cation 3<sup>+</sup> is observed [ $m/z$  600 (100%), 601 (48%), 602 (2%)]. However already minor traces of one-fold H<sub>2</sub> loss are discernible, which become more clearly visible at a laser fluence of 1950 [ $m/z$  600 (100%), 598 (10%)]. The products formed upon the three possible H<sub>2</sub> losses and ring closures giving C<sub>48</sub>H<sub>22</sub><sup>+</sup>, C<sub>48</sub>H<sub>20</sub><sup>+</sup> and C<sub>48</sub>H<sub>18</sub><sup>+</sup> are present at a laser fluence of 2300 [ $m/z$  600 (100%), 598 (93%), 596 (73%), 594 (18%)]. At this laser fluence additional mass clusters appear positioned around  $m/z$  586 (C<sub>47</sub>H<sub>22</sub><sup>+</sup>, -'CH<sub>2</sub>', 21%) and at  $m/z$  574 (C<sub>46</sub>H<sub>22</sub><sup>+</sup>, -C<sub>2</sub>H<sub>2</sub>, 15%). Again a PSD experiment (laser fluence 2300) assures that these new mass clusters originate from the PAH

precursor (Figure 4A). A regular repeating pattern due to fragmentation with mass clusters separated by 14 a.m.u., comparable to that observed for  $2^+$ , is formed at a laser fluence 2600 (Figure 4B).

Next we turn to the MALDI TOF mass spectra of  $4^+$  obtained using higher laser fluences. Only, when a laser fluence of 2500 is applied, the appearance of the MALDI TOF-MS spectrum changes from that discussed in paragraph 4.2.1. The mass clusters possess a less defined pattern. Increase of the laser fluence to 2600 gives a comparable fragmentation pattern as observed for both  $3^+$  and  $2^+$  (Figure 5). From a PSD experiment (laser fluence 2600) on the  $4^+$   $m/z$  750 it is clear that this fragmentation has its origin in the PAH precursor.

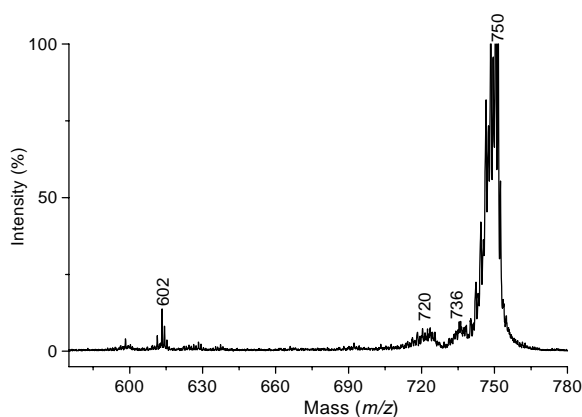


**Figure 5.** Post-source decay (PSD) MALDI TOF mass spectrum of  $4^+$  (positive-ion mode) at a laser fluence of 2600.

### 4.3 Corollary

From these experiments it can be concluded that the threshold for the zipping-up process for  $2^+$ ,  $3^+$  and  $4^+$  is nearly identical in all cases (laser fluence 2200 - 2300). At this threshold all possible cyclodehydrogenations are observed. This means that three-fold  $H_2$  losses and ring closures occur in the case of both  $2^+$  and  $3^+$  while  $4^+$  is converted into  $C_{60}^+$ . It can be concluded that consecutive intramolecular  $H_2$  losses and ring closures occur from the inner core outwards. Furthermore, the PSD experiment in which  $m/z$  746 is isolated prior to TOF-MS analysis, proves that hydrogen losses occur stepwise. Already at the threshold, fragmentation is observed for  $2^+$  and  $3^+$ , whereas fragmentation is absent at this laser fluence for  $4^+$ . PSD experiments elucidate

that fragmentation takes place from the radical cation of the PAH-precursors. At a laser fluence of *ca.* 2600 a distinct fragmentation pattern is observed for all compounds due to subsequent loss of  $C_2H_2$  followed by  $nH_2$  loss. Apparently, the PAH precursors  $2^+$ ,  $3^+$ , and  $4^+$  are stable up to this laser fluence (see Experimental Section). These observations explain the different results obtained by Scott *et al.*<sup>25</sup> The laser fluence in their experiment must have been above the threshold for fragmentation.

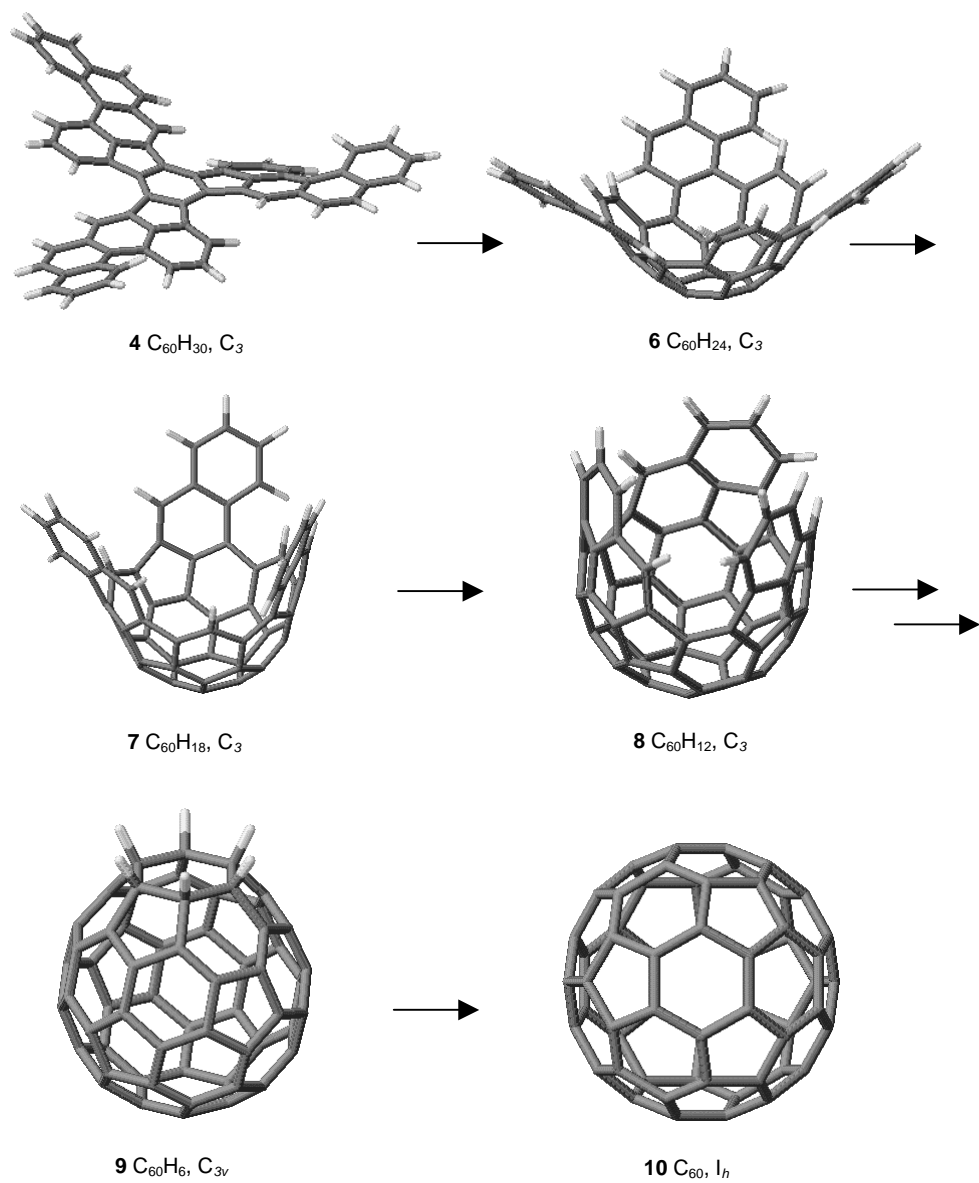
#### 4.4 The Zipping-up Process of $C_{60}H_{30}$ to $C_{60}$

Insight into the conversion of **4** into  $C_{60}$  is obtained by both *semi*-empirical and *ab initio* single point calculations on the possible intermediates. Interestingly, the results indicate that cyclodehydrogenations occur with *regio*-chemical control. From Scheme 1 it can be seen that **4** has a propeller-like structure in which the innermost symmetry related non-bonded hydrogen atoms  $H_a$  are sterically congested [ $H_a \cdots H$  1.89 Å]. Similar as in the optimized geometry of **4**, the innermost hydrogens of **2** and **3** are also congested [**2**:  $H_a \cdots H_a$  1.90 Å, **3**:  $H_a \cdots H$  1.90 Å]. Thus, in line with the experimental results the hydrogen  $H_a$  of **4** will be susceptible to undergo ring-closure giving the bowl-shaped  $C_{60}H_{24}$  (**6**,  $C_3$ ) in which three other non-bonded hydrogen pairs  $H_b$  [**6**:  $H_b \cdots H$ , 2.01 Å] become congested (Scheme 1); this will facilitate  $C_{60}H_{18}$  (**7**,  $C_3$ ) formation. In  $C_{60}H_{18}$  the hydrogen  $H_c$  [**7**:  $H_c \cdots H$  2.14 Å] are prone to undergo cyclodehydrogenation towards  $C_{60}H_{12}$  (**8**,  $C_3$ ). Other possible isomers of  $C_{60}H_{24}$  and  $C_{60}H_{18}$  formed upon loss of  $H_c$  respectively instead of  $H_a$  and  $H_b$  all possess considerably higher energies.<sup>34</sup>

The energy needed ( $\Delta H_f$ ) for the three-fold  $H_2$  losses in the five consecutive cyclodehydrogenation cycles is depicted in Table 1. The first three dehydrogenation cycles from  $C_{60}H_{30}$  (**4**) to  $C_{60}H_{24}$  (**6**),  $C_{60}H_{18}$  (**7**) and finally  $C_{60}H_{12}$  (**8**) have comparable  $\Delta H_f$  values of 134.5, 144.7 and 151.5 kcalmol<sup>-1</sup>, respectively. The  $\Delta H_f$  value per  $H_2$  loss and ring closure (Table 2) is between 40 and 50 kcalmol<sup>-1</sup>. Similar values for  $\Delta H_f$  per  $H_2$  loss and ring closure are found for **2** and **3** (Table 3 and 4). This supports our contention that **2**, **3** and **4** possess similar inner cores and, thus, will behave similarly under the applied cyclodehydrogenation conditions.

Cyclodehydrogenation from  $C_{60}H_{12}$  (**8**) to  $C_{60}H_6$  could either yield a ring-opened isomer of  $C_{60}H_6$ , *via* ring-closure and three-fold  $H_2$  losses, or a ring-closed isomer of  $C_{60}H_6$  (**9**), *via* a 2+2+2 cycloaddition (Scheme 6).<sup>27</sup> The ring-closed isomer **9** is a fullerane of which several representatives have been synthesized by hydrogenation of  $C_{60}$ .<sup>35,36</sup> It is known that in the case of fullerenes the AM1 results ( $\Delta H_f$ ) may be unreliable.<sup>37</sup> Therefore, single-point *ab initio* calculations were performed [RHF/6-31G\*//RHF/AM1, B3LYP/6-31G\*//RHF/AM1 and UB3LYP/6-31G\*//UHF/AM1] on the structures that can be formed upon three-fold  $H_2$  losses and ring

A Progenitor of  $C_{60}$  and Its Stepwise Conversion into  $C_{60}$



Scheme 1. Optimized RHF/AM1 structures of 4 and 6 - 10.

**Table 1.** *Semi*-empirical AM1 ( $\Delta H_r$ ) and single point *ab initio*  $\Delta E_r$  values (in kcalmol<sup>-1</sup>) for the five cyclodehydrogenation cycles of **4** ( $C_{60}$ ).

Compound (symmetry)	AM1		6-31G*		
	neutral (RHF)	radical cation (UHF)	RHF	B3LYP	radical cation UB3LYP
	$\Delta H_r$	$\Delta H_r$	$\Delta E_r$	$\Delta E_r$	$\Delta E_r$
$C_{60}H_{30}$ ( <b>4</b> , $C_3$ )	<sup>a</sup>	<sup>b</sup>			
$C_{60}H_{24}$ ( <b>6</b> , $C_3$ )	134.5	148.0 <sup>c</sup>	146.1	117.3	129.7
$C_{60}H_{18}$ ( <b>7</b> , $C_3$ )	144.7	146.2	145.1	130.1	118.7
$C_{60}H_{12}$ ( <b>8</b> , $C_3$ )	151.5	155.5	149.2	120.3	132.7
$C_{60}H_6$ ( <b>9</b> , $C_{3v}$ ) rc <sup>d</sup>	88.1	97.6	100.8	88.9	85.7
$C_{60}H_6$ ( $C_{3v}$ ) ro <sup>d</sup>	97.1	108.5	118.5	97.5	100.2
$C_{60}H_4$ ( $C_3$ ) rc <sup>d</sup>	26.9	21.9	29.1	23.1	18.0
$C_{60}H_2$ ( $C_{2v}$ ) rc <sup>d</sup>	39.0	40.8	20.9	14.3	36.7
$C_{60}$ ( <b>10</b> , $I_h$ )	42.1 (0)	50.0	28.8	21.9	19.2

<sup>a</sup>  $\Delta H_r[C_{60}H_{30}$  (**4**,  $C_3$ )] RHF/AM1 = 346.5 kcalmol<sup>-1</sup><sup>b</sup>  $\Delta H_r(C_{60}H_{30}^{\bullet})$  UHF/AM1 = 496.5 kcalmol<sup>-1</sup><sup>c</sup> In the case of UHF/AM1 no symmetry was found.<sup>d</sup> rc = ring-closed isomer; ro = ring-opened isomer.<sup>34</sup>

closures from  $C_{60}H_{30}$  (**4**) [ $C_{60}H_{24}$  (**6**),  $C_{60}H_{18}$  (**7**),  $C_{60}H_{12}$  (**8**) and  $C_{60}H_6$  (**9**) and  $C_{60}$  (**10**)] to validate the results (Table 1 and Scheme 1).

Both the AM1 and *ab initio* results predict that the ring-closed isomer of  $C_{60}H_6$  (**9**) is more stable than its ring-opened isomer (RHF/AM1: 9.0 kcalmol<sup>-1</sup> and B3LYP/6-31G\*//RHF/AM1: 8.6 kcalmol<sup>-1</sup> and RHF/6-31G\*//RHF/AM1: 17.7 kcalmol<sup>-1</sup>). The conversion of  $C_{60}H_{12}$  (**8**) into the ring-closed fullerene  $C_{60}H_6$  (**9**) and the subsequent conversion of **9** into  $C_{60}$  (**10**) have a significantly lower  $\Delta H_r$  than the previous cyclodehydrogenation steps [RHF/AM1: 88.1 and 108.0 kcalmol<sup>-1</sup>, respectively; B3LYP/6-31G\*//RHF/AM1: 88.9 and 59.3 kcalmol<sup>-1</sup>, respectively and RHF/6-31G\*//RHF/AM1: 100.8 and 78.8 kcalmol<sup>-1</sup>, respectively]. This is due to the less drastic skeletal rearrangements that have to take place. Hence, this supports that in going from  $C_{60}H_{12}$  to  $C_{60}H_6$  ring closure *via* a 2+2+2 cycloaddition will occur.

Since all cyclodehydrogenations are only discernible in the positive-ion mode under MALDI TOF-MS conditions, radical cations are involved in the ‘zipping-up’ mechanism. Therefore, computations were also performed on the radical cations of compounds **2** and **6** – **10**

**Table 2.** *Semi*-empirical RHF/AM1  $\Delta H_f^\circ$  and  $\Delta H_r$  values (in kcalmol<sup>-1</sup>) for the products obtained *via* stepwise H<sub>2</sub> loss and ring closure from **4** (C<sub>3</sub>).

Compound <sup>a</sup> (symmetry)	neutral (RHF)	
	$\Delta H_f^\circ$	$\Delta H_r$
C <sub>60</sub> H <sub>30</sub> ( <b>4</b> , C <sub>3</sub> )	346.5	
C <sub>60</sub> H <sub>28</sub> (C <sub>1</sub> )	387.0	40.5
C <sub>60</sub> H <sub>26</sub> (C <sub>1</sub> )	436.0	49.0
C <sub>60</sub> H <sub>24</sub> ( <b>6</b> , C <sub>3</sub> )	481.0	45.0
C <sub>60</sub> H <sub>22</sub> (C <sub>1</sub> )	528.9	47.9
C <sub>60</sub> H <sub>20</sub> (C <sub>1</sub> )	577.1	48.2
C <sub>60</sub> H <sub>18</sub> ( <b>7</b> , C <sub>3</sub> )	625.7	48.6
C <sub>60</sub> H <sub>16</sub> (C <sub>1</sub> )	675.2	49.5
C <sub>60</sub> H <sub>14</sub> (C <sub>1</sub> )	725.7	50.5
C <sub>60</sub> H <sub>12</sub> ( <b>8</b> , C <sub>3</sub> )	777.2	51.5
C <sub>60</sub> H <sub>10</sub> (C <sub>1</sub> )	810.0	32.8
C <sub>60</sub> H <sub>8</sub> (C <sub>1</sub> )	842.7	32.7
C <sub>60</sub> H <sub>6</sub> (rc) <sup>b</sup> ( <b>9</b> , C <sub>3i</sub> )	865.3	22.6
C <sub>60</sub> H <sub>6</sub> (ro) <sup>b</sup> (C <sub>3i</sub> )	874.3	9.0
C <sub>60</sub> H <sub>4</sub> (rc) (C <sub>3</sub> )	892.2	26.9
C <sub>60</sub> H <sub>2</sub> (rc) (C <sub>2v</sub> )	931.2	39.0
C <sub>60</sub> ( <b>10</b> , I <sub>h</sub> )	973.3	42.1

<sup>a</sup> Only the most stable isomers are reported; for a complete overview of all possible isomers (C<sub>6</sub>H<sub>2</sub>) and their optimized RHF/AM1 geometries.<sup>34</sup>

<sup>b</sup> rc = ring-closed isomer; ro = ring-opened isomer.<sup>34</sup>

**Table 3.** *Semi*-empirical RHF/AM1  $\Delta H_f^\circ$  and  $\Delta H_r$  values (in kcalmol<sup>-1</sup>) for the products obtained *via* stepwise H<sub>2</sub> loss and ring closure from **3** (C<sub>3</sub>).<sup>34</sup>

Compound (symmetry)	Neutral (RHF)	
	$\Delta H_f^\circ$	$\Delta H_r$
C <sub>48</sub> H <sub>24</sub> ( <b>3</b> , C <sub>3</sub> )	274.6	
C <sub>48</sub> H <sub>22</sub> (C <sub>1</sub> )	316.6	42.0
C <sub>48</sub> H <sub>20</sub> (C <sub>1</sub> )	367.8	51.2
C <sub>48</sub> H <sub>18</sub> (C <sub>3</sub> )	415.4	47.6

**Table 4.** *Semi*-empirical RHF/AM1  $\Delta H_f^\circ$  and  $\Delta H_r$  values (in kcalmol<sup>-1</sup>) for the products obtained *via* stepwise H<sub>2</sub> loss and ring closure from **2** (D<sub>3</sub>).<sup>34</sup>

Compound (symmetry)	Neutral (RHF)	
	$\Delta H_f^\circ$	$\Delta H_r$
C <sub>36</sub> H <sub>18</sub> ( <b>2</b> , D <sub>3</sub> )	228.8	
C <sub>36</sub> H <sub>16</sub> (C <sub>1</sub> )	270.0	41.2
C <sub>36</sub> H <sub>14</sub> (C <sub>1</sub> )	321.0	51.0
C <sub>36</sub> H <sub>12</sub> (C <sub>3</sub> )	369.1	48.1

depicted in Scheme 8. Their geometries were re-optimized at the *semi*-empirical UHF/AM1 level of theory. In addition, energy differences ( $\Delta E_r$ ) were also re-calculated at the UB3LYP/6-31G\*\*//UHF/AM1 level of theory to verify if the observed trends found by RHF/AM1 for closed-shell species still hold when radical cations are considered.

Table 1 indeed shows that similar results are attained for the corresponding radical cations. Again, the first three dehydrogenation cycles (from **4** to **8**) have higher  $\Delta H_r$ /  $\Delta E_r$  values than the following dehydrogenation cycles. Moreover, the formation of the ring-closed, fullerane intermediate [ $C_{60}H_6$  (**9**)] is favoured (UHF/AM1: 10.9 kcalmol<sup>-1</sup>, UB3LYP/6-31G\*\*//UHF/AM1: 14.5 kcalmol<sup>-1</sup>).

## 4.5 Conclusions

In a collaboration, the selective and stepwise conversion of the non-alternant PAH  $C_{60}H_{30}$  (**4**) into  $C_{60}$  is achieved. PSD experiments on the molecular ion show that the processes take place in a unimolecular fashion. Furthermore, evidence is provided for the stepwise nature of the  $H_2$  losses and ring closures from a PSD experiment in which an intermediate ion  $6^+$  ( $C_{60}H_{24}^+$   $m/z$  746) was isolated which also converted into  $C_{60}$  (**10**). A comparison of the behavior of  $4^+$  under similar MALDI TOF-MS conditions with that of its sub-structures  $2^+$  and  $3^+$  revealed that the innermost hydrogen are eliminated first. This observation is confirmed by the calculations on the subsequent  $H_2$  losses from **4**, **2** and **3**. Whereas in the case of  $2^+$  the threshold for zipping up is significant lower than the threshold for fragmentation, this is not the case for  $3^+$  and  $2^+$ . The correct carbon topology seems therefore essential for the successful conversion of  $C_{60}H_{30}$  (**4**) into  $C_{60}$  (**10**).

## 4.6 Experimental Section

Compounds **3** and **4** were synthesized by the group of Echavarren (Spain); details of the synthesis of **1** – **4** are described elsewhere.<sup>38,39</sup>

### MALDI TOF-MS

Matrix-Assisted-Laser-Desorption-Ionisation (MALDI) Time-of-Flight mass spectrometry (TOF-MS)<sup>40</sup> experiments were done using a Voyager-DE-RP MALDI-TOF mass spectrometer (Applied Biosystems/PerSeptive Biosystems, Inc., Framingham, MA, USA) equipped with delayed extraction.<sup>41</sup> A 337 nm UV  $N_2$  laser producing 3ns pulses was used and the mass spectra were obtained in the linear and reflectron mode. Samples were prepared either by mixing 10  $\mu$ l of a toluene solution of the sample with 30  $\mu$ l



of a solution of 3 mgL<sup>-1</sup> 2,5-dihydroxybenzoic acid in toluene or by using the toluene solution *without* the matrix. One  $\mu$ l of the solution was loaded on a gold-sample plate, the solvent was removed in warm air and the sample transferred to the vacuum of the mass spectrometer for analysis. *Post-Source-Decay* (PSD) experiments were obtained by adjusting the voltage applied to the reflector (Mirror Ratio setting). MALDI/PSD spectra record the fragment ions of spontaneously decomposing ions.

### Computational Methods

*Semi*-empirical computations (RHF/AM1) were performed using MOPAC 7.0<sup>42</sup> to optimize the geometries of all the possible intermediates formed from C<sub>60</sub>H<sub>30</sub> (4), C<sub>48</sub>H<sub>24</sub> (3) and C<sub>36</sub>H<sub>18</sub> (2) upon consecutive cyclodehydrogenations (H<sub>2</sub> losses and ring closures). *Ab initio* calculations were performed on the AM1 geometries at either RHF/6-31G\* or B3LYP/6-31G\* levels of theory using GAMESS-UK.<sup>43</sup> The geometries of the radical cation species were optimized using open-shell UHF/AM1. With UHF/AM1 substantial spin contamination was observed ( $s^2 > 4$ ). In addition, single point *ab initio* calculations were performed on these geometries using UB3LYP/6-31G\*. In the case of the *semi*-empirical AM1 method  $\Delta H_r$  is defined as  $\Delta \Delta H_r^0$ . Note that the experimental  $\Delta H_r^0$  value for H<sub>2</sub> (0.0 kcalmol<sup>-1</sup>) is used. In the case of the single point *ab initio* calculations  $\Delta E_r = [E_{\text{total}}(\text{PAH} - 3\text{H}_2) + 3E_{\text{total}}(\text{H}_2)] - E_{\text{total}}(\text{PAH})$ .  $E_{\text{total}}(\text{H}_2)$  RHF/6-31G\*\*/RHF/AM1 = -1.124471 a.u.  $E_{\text{total}}(\text{H}_2)$  B3LYP/6-31G\*\*/RHF/AM1 = -1.172050 a.u.,  $E_{\text{total}}(\text{H}_2)$  UB3LYP 6-31G\*\*/UHF/AM1 = -1.172050 a.u. The hydrogen bond distance after RHF/AM1 (UHF/AM1) optimisation is 0.667 (0.979) Å.<sup>42</sup>

### References and notes

- (1) Krätschmer, W.; Lamb, L. D.; Fostiropoulos, K.; Huffman, D. R. *Nature* **1990**, *347*, 354-358.
- (2) Taylor, R.; Hare, J. P.; Abdul-Sada, A. K.; Kroto, H. W. *J. Chem. Soc., Chem. Commun.* **1990**, 1423-1425.
- (3) Goroff, N. S. *Acc. Chem. Res.* **1996**, *29*, 77-83.
- (4) Rabideau, P. W.; Sygula, A. *Acc. Chem. Res.* **1996**, *29*, 235-242.
- (5) Mehta, G.; Prakash Rao, H. S. *Tetrahedron* **1998**, *54*, 13325-13370.
- (6) Scott, L. T. *Pure & Appl. Chem.* **1996**, *68*, 291-300.
- (7) Scott, L. T.; Bronstein, H. E.; Preda, D. V.; Ansems, R. B. M.; Bratcher, M. S.; Hagen, S. *Pure & Appl. Chem.* **1999**, *71*, 209-219.
- (8) Mehta, G.; Sarma, S. *Chem. Commun.* **2000**, 19-20.
- (9) Ansems, R. B. M.; Scott, L. T. *J. Am. Chem. Soc.* **2000**, *122*, 2719-2724.
- (10) Reisch, H. A.; Bratcher, M. S.; Scott, L. T. *Org. Lett.* **2000**, *2*, 1427-1430.

- (11) Sygula, A.; Xu, G.; Marcinow, Z.; Rabideau, P. W. *Tetrahedron* **2001**, *57*, 3637-3644.
- (12) Diederich, F.; Rubin, Y. *Angew. Chem. Int. Ed. Engl.* **1992**, *31*, 1101-1123.
- (13) Sastry, G. N.; Jemmis, E. D.; Mehta, G.; Shah, S. R. *J. Chem. Soc., Perkin Trans. 2* **1993**, 1867-1871.
- (14) Faust, R.; Vollhardt, K. P. C. *J. Chem. Soc., Chem. Commun.* **1993**, 1471-1473.
- (15) Preda, D. V.; Scott, L. T. *Tetrahedron Lett.* **2000**, *41*, 9633-9637.
- (16) Rubin, Y.; Parker, T. C.; Pastor, S. J.; Jalisatgi, S.; Boule, C.; Wilkins, C. L. *Angew. Chem. Int. Ed. Engl.* **1998**, *37*, 1226-1229.
- (17) Tobe, Y.; Nakagawa, J.; Kishi, J.; Sonoda, M.; Naemura, K.; Wakabayashi, T.; Shida, T.; Achiba, Y. *Tetrahedron* **2001**, *57*, 3629-3636.
- (18) Bunz, U. H. F.; Rubin, Y.; Tobe, Y. *Chem. Soc. Rev.* **1999**, *28*, 107-119.
- (19) Tobe, Y.; Furukawa, R.; Sonoda, M.; Wakabayashi, T. *Angew. Chem. Int. Ed. Engl.* **2001**, *40*, 4072-4074.
- (20) Prinzbach, H.; Weiler, A.; Landenberger, P.; Wahl, F.; Wörth, J.; Scott, L. T.; Gelmont, M.; Olevano, D.; Issendorf, B. *Nature* **2000**, *407*, 60-63.
- (21) Plater, M. J. *J. Chem. Soc., Perkin Trans. 1* **1997**, 2897-2901.
- (22) Sarobe, M.; Fokkens, R. H.; Cleij, T. J.; Jenneskens, L. W.; Nibbering, N. M. M.; Stas, W.; Versluis, C. *Chem. Phys. Lett.* **1999**, *313*, 31-39.
- (23) Lafleur, A. L.; Howard, J. B.; Taghizadeh, K.; Plummer, E. F.; Scott, L. T.; Necula, A.; Swallow, K. C. *J. Phys. Chem.* **1996**, *100*, 17421-17428.
- (24) González, J. J.; García, N.; Gómez-Lor, B.; Echavarren, A. M. *J. Org. Chem.* **1997**, *62*, 1286.
- (25) Boorum, M. M.; Vasil'ev, Y. V.; Drewello, T.; Scott, L. T. *Science* **2001**, *294*, 828-831.
- (26) Scott, L. T.; Boorum, M. M.; McMahon, B. J.; Hagen, S.; Mack, J.; Blank, J.; Wegner, H.; de Meijere, A. *Science* **2002**, *295*, 1500-1503.
- (27) Gómez-Lor, B.; Koper, C.; Fokkens, R. H.; Vlietstra, E. J.; Cleij, T. J.; Jenneskens, L. W.; Nibbering, N. M. M.; Echavarren, A. M. *Chem. Commun.* **2002**, 370-371.
- (28) Minor decomposition products were found in the MALDI TOF mass spectrum of **4** obtained with a laser fluence of 2200 at  $m/z$  602, 612 and 620.
- (29) Lifshitz, C.; Ling, Y.; Martin, J. M. L. *Adv. Mass. Spectrom.* **1998**, *14*.
- (30) Gotkis, Y.; Oleinikova, M.; Naor, M.; Lifshitz, C. *J. Phys. Chem.* **1993**, *97*, 12282-12290.
- (31) Budyka, M. F.; Zyubina, T. S.; Ryabenko, A. G.; Muradyan, V. E.; Esipov, S. E.; Cherepanova, N. I. *Chem. Phys. Lett.* **2002**, *354*, 93-99.
- (32) Yeretjian, C.; Hansen, K.; Diederich, F. *Nature* **1992**, *359*, 44.

- (33) Yoshimura, K.; Przybilla, L.; Ito, S.; Brand, J. D.; Wehmeir, M.; Räder, H. J. M., K. *Macromol. Chem. Phys.* **2001**, *202*, 215-222.
- (34) Koper, C.; Ruiz, M.; de Frutos, Ó.; González-Cantalapiedra, E.; Fokkens, R. H.; Nibbering, N. M. M.; Cárdenas, D. J.; Santos, A.; Gómez-Lor, B.; Jenneskens, L. W.; Echavarren, A. M. *Chem. Eur. J* **2003**, *in press*.
- (35) Henderson, C. C.; Cahill, P. A. *Science* **1993**, *259*, 1885-1887.
- (36) Meier, M. S.; Weedon, B. R.; Spielmann, H. P. J. *Am. Chem. Soc.* **1996**, *118*, 11682-11683.
- (37) Henderson, C. C.; Rohlfing, C. M.; Cahill, P. A. *Chem. Phys. Lett.* **1993**, *213*, 383-388.
- (38) Gómez-Lor, B.; de Frutos, O.; Echavarren, A. M. J. *Chem. Soc. , Chem. Commun.* **1999**, 2431-2432.
- (39) de Frutos, Ó.; Gómez-Lor, B.; Granier, T.; Monge, M. A.; Gutiérrez-Puebla, E.; Echavarren, A. M. *Angew. Chem. Int. Ed. Engl.* **1999**, *38*, 204-207.
- (40) Karas, M.; Bahr, U.; Hillenkamp, F. *Int. J. Mass Spectrom. Ion Proc.* **1987**, *78*, 53-68.
- (41) Vestal, M. L.; Juhasz, P.; Martin, S. A. *Rapid Commun. Mass Spectrom.* **1995**, *9*, 1044-1050.
- (42) Dewar, M. J. S.; Zoebisch, E. G.; Healy, E. F.; Stewart, J. J. P. J. *Am. Chem. Soc.* **1985**, *107*, 3902-3909.
- (43) Guest, M. F.; van Lenthe, J. H.; Kendrick, J.; Schöffel, K.; Sherwood, P.; Harrison, R. J. *GAMESS-UK, a package of ab initio programs*, **1998**. With contributions from: Amos, R.D., Buenker, R.J.; Dupuis, M.; Handy, N.C.; Hillier, I; Knowles, P.J.; Bonacic-Koutecky, V.; von Niessen, W.; Saunders, V.R.; Stone, A.J. Derived from the original GAMESS code by: Dupuis, M.; Spangler, D.; Wendolowski, J.; NRCC Software Catalog, vol. 1, program no. QG01 (GAMESS), **1980**.



# CHAPTER 5

## Identification of C<sub>70</sub> Progenitors

### Abstract

Two unimolecular progenitors for C<sub>70</sub> are proposed, *viz.* the C<sub>70</sub>H<sub>40</sub> corannulene derivative **1** and the C<sub>70</sub>H<sub>40</sub> belt-like compound **2**. *Semi*-empirical (RHF/AM1 and UHF/AM1) and *ab initio* (RHF/6-31G\*\* and (U)B3LYP/6-31G\*\*) calculations on closed-shell intermediates and their related open-shell radical cations indicate that both progenitors can be converted into C<sub>70</sub> by cyclodehydrogenations, *i.e.* consecutive H<sub>2</sub> losses and ring closures. Hence, these results make the syntheses of **1** and **2** worthwhile to pursue.

## 5.1 Introduction

In Chapter 4 it has been shown that non-alternant polycyclic aromatic hydrocarbons (PAH) with the correct carbon topology are valuable precursors for closed carbon surfaces. This exact carbon topology can be determined from a 2D projection of the desired 3D molecule, *i.e.* the Schlegel diagram proposition. Conversion of the 2D non-alternant PAH into the closed carbon surface was in the case of the  $C_{60}$  precursor,  $C_{60}H_{30}$ , achieved by fifteen-fold consecutive  $H_2$  losses and ring closures induced by matrix-assisted-laser-desorption-ionization time-off-flight mass spectrometry (MALDI TOF-MS) in the positive-ion mode. The congestion of the innermost non-bonding hydrogen atoms makes these hydrogen susceptible to undergo elimination and ring closure. As a consequence, cyclodehydrogenation leads to curling up of the carbon skeleton, whereupon the next set of inner-core non-bonded hydrogen atoms become sterically congested and, thus, susceptible to undergo the next set of cyclodehydrogenations ('zipping up'). Therefore, this 'zipping up process' occurs with *regio*-chemical control from the inside outwards.<sup>1,2</sup>

This exciting achievement renders the identification of unimolecular PAH precursors for other known and ultimately unknown fullerenes a topical issue. Progenitors for  $C_{70}$  are the subject of this Chapter.

The most favorable unimolecular precursor for  $C_{70}$  is anticipated to be a non-alternant PAH, which contains the same carbon topology as the  $C_{70}$  Schlegel diagram. Therefore, we propose the still elusive corannulene derivative (**1**,  $C_{70}H_{40}$ ) (Chart 1) as a progenitor for  $C_{70}$  and scrutinize the required consecutive cyclodehydrogenations computationally by *semi*-empirical (RHF/AM1) and *ab initio* (RHF/6-31G\*\* and B3LYP/6-31G\*\*) methods. Since under MALDI TOF-MS conditions radical cations are essential for the conversion of  $C_{60}H_{30}$  into  $C_{60}$ ,<sup>1</sup> the radical cations of selected intermediates were also studied using UHF/AM1 and UB3LYP/6-31G\*\*. As a corollary a second  $C_{70}$  progenitor, *i.e.* belt-like compound **2**, is identified.

## 5.2 Results & Discussion

### 5.2.1 *Semi*-empirical AM1 calculations

As required  $C_{70}H_{40}$  (**1**) ( $C_1$  symmetry) has the exact carbon atom topology as the  $C_{70}$  Schlegel diagram and the structure is based on the corannulene-cap of  $C_{70}$  (Chart 1). Although **1** still remains elusive, the synthesis of a part of its structure is currently subject of investigation.<sup>3,4</sup> Hence, it is envisaged that **1** will ultimately be a viable synthetic target.

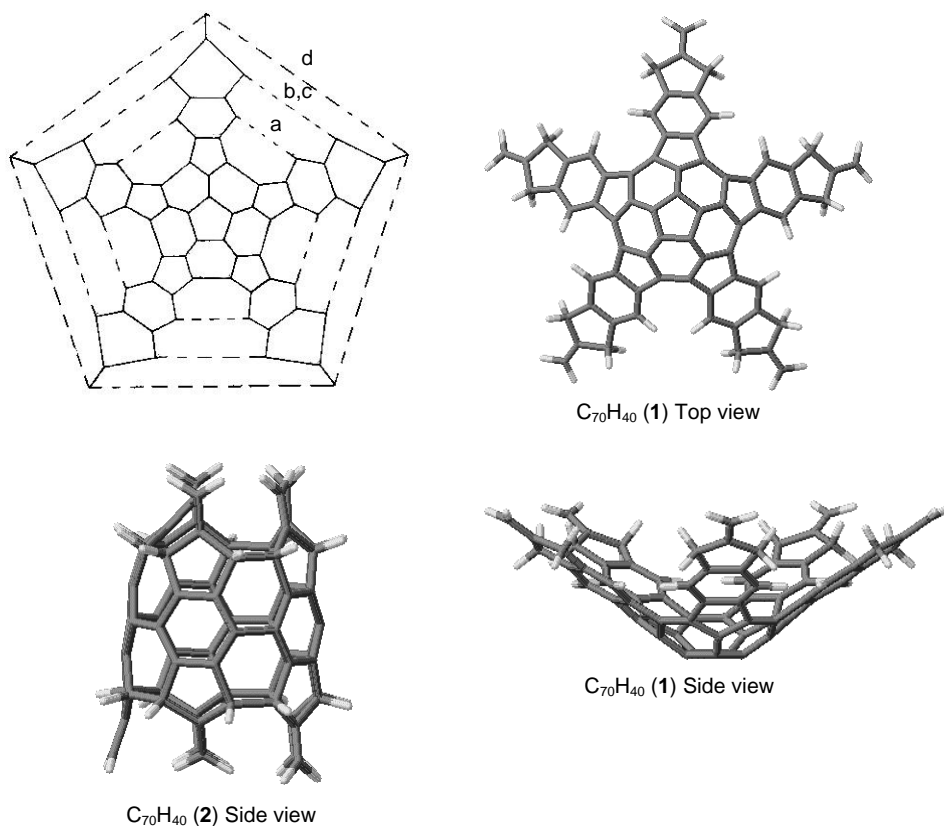


**Chart 1.**  $C_{70}$  Schlegel diagram containing  $C_{70}H_{40}$  (1), and B3LYP/6-31G\*\* optimized structures of  $C_{70}H_{40}$  (1) and  $C_{70}H_{40}$  (2).

The optimized geometry of **1** is depicted in Figure 1. The inner-most non-bonded hydrogen atom pairs  $H_a \cdots H_a$  are positioned within the sum of their Van der Waals radii  $[H_a \cdots H_{a(\max)} 1.83 \text{ \AA}]^5$  and therefore expected to be susceptible to undergo  $H_2$  loss and ring closure.<sup>1</sup> The dotted lines in the  $C_{70}$  Schlegel diagram represent the carbon-carbon bonds that have to be formed in the four distinct cyclodehydrogenation cycles involving  $H_a$ ,  $H_b$ ,  $H_c$  and  $H_d$ , respectively (Chart 1). Notice that *five*  $H_2$  losses and ring closures per cycle are needed. Hence, within each cycle different possibilities exist for the sequence of these consecutive  $H_2$  losses and ring closures. After the formation of one carbon-carbon bond, the next bond can be formed at either a neighboring or at a non-neighboring site. This will result in the formation of two different

$C_{70}H_x$  isomers after the second as well as the third  $H_2$  loss and ring closure in each distinct cycle (Table 1, see also ref. 25 for plots of the optimized AM1 structures of all possible intermediates).

Upon the first formal  $H_2$  loss and ring closure from  $C_{70}H_{40}$  (**1**),  $C_{70}H_{38}$  is obtained, which is *ca.* 47 kcalmol<sup>-1</sup> higher in energy. The introduction of an extra six-membered ring leads to further deformation of the initial bowl-shaped structure. The remaining non-bonded hydrogen atom pairs  $H_a \cdots H_a$ , however, are still positioned within the sum of their Van der Waals radii [ $H_a \cdots H_a$  *ca.* 1.90 Å]. A second  $H_2$  loss and ring closure may result in two different  $C_{70}H_{36}$  isomers; one isomer with the new six-membered rings at a neighboring position, while the other will have the new six-membered rings at a non-neighboring position. According to the AM1 results the two  $C_{70}H_{36}$  isomers are almost equally stable [ $\Delta\Delta H_f^\theta(\text{neighboring} - \text{non-neighboring}) = 0.5$  kcalmol<sup>-1</sup>, Table 1]. The  $\Delta H_r$  for the conversion of  $C_{70}H_{38}$  into the different  $C_{70}H_{36}$  isomers is similar to the  $\Delta H_r$  for the conversion of  $C_{70}H_{40}$  into  $C_{70}H_{38}$  (*ca.* 47 kcalmol<sup>-1</sup>, see Table 1). In analogy, two  $C_{70}H_{34}$  isomers, which again have comparable  $\Delta H_f^\theta$  values [ $\Delta\Delta H_f^\theta(\text{neighboring} - \text{non-neighboring}) = 0.7$  kcalmol<sup>-1</sup>, Table 1], can be formed from the two  $C_{70}H_{36}$  isomers ( $\Delta H_r$  *ca.* 47 kcalmol<sup>-1</sup>). In the next step only one isomer of  $C_{70}H_{32}$  is accessible ( $\Delta H_r = 45.8$  kcalmol<sup>-1</sup>). The important outcome for the initial cyclodehydrogenation cycle is that the neighboring and non-neighboring isomers of  $C_{70}H_{36}$  and  $C_{70}H_{34}$ , respectively, have comparable energies. In addition, independent of the sequence of  $H_2$  losses and ring closures, the next set of hydrogen atoms from the  $H_a$  series will be positioned within the sum of their Van der Waals radii due the increase in curvature and, therefore, will be susceptible to undergo further cyclodehydrogenations. This makes the loss of the non-bonded  $H_a$  pairs followed by six-membered ring formation feasible from all different isomers. Overall five-fold  $H_2$  losses and six-membered ring formations will lead to the 'cup-shaped'  $C_{70}H_{30}$  ( $C_7$  symmetry; overall conversion  $\Delta H_r = 230.8$  kcalmol<sup>-1</sup>, Figure 1 and Table 1).

In this cup-shaped structure the inner-most, non-bonded hydrogen atoms [ $H_b \cdots H_b$  *ca.* 1.90 Å, Chart 1] are sterically congested. Another five-fold cyclodehydrogenation cycle now involving  $H_b$ , which is comparable to the five-fold  $H_2$  losses and ring closures of  $H_a$ , will give the 'egg-shaped'  $C_{70}H_{20}$  ( $C_5$  symmetry). Interestingly,  $\Delta H_r$  values for these cyclodehydrogenations are significantly smaller [*ca.* 11 - 28 *vs.* 45 - 47 kcalmol<sup>-1</sup> per  $H_2$  loss and ring closure (Table 1)]. This is attributed to the fact that in the conversion of  $C_{70}H_{40}$  to  $C_{70}H_{30}$  the imposed deformation of the carbon skeleton is more severe ('bowl-like' to 'cup-shaped') compared to the transformation of  $C_{70}H_{30}$  into  $C_{70}H_{20}$  ('cup-shaped' to 'egg-shaped'). The overall conversion of  $C_{70}H_{30}$  into  $C_{70}H_{20}$  has an overall  $\Delta H_r$  of 92.8 kcalmol<sup>-1</sup>.

In  $C_{70}H_{20}$  both the non-bonded hydrogen atoms  $H_c \cdots H_c$  (*ca.* 2.12 Å) and  $H_a \cdots H_a$  (*ca.* 2.00 Å) become sterically congested. Five-fold  $H_2$  losses of neighboring  $H_c$  atoms will lead to carbon-



**Table 1.** RHF/AM1  $\Delta H_r$  values (in kcalmol<sup>-1</sup>) for consecutive H<sub>2</sub> losses and ring closures from C<sub>70</sub>H<sub>40</sub> (**1**) down to C<sub>70</sub> (see text).

	Ring-opened pathway				Ring-closed pathway			
	Neighboring		Non-Neighboring		Neighboring		Non-Neighboring	
	Sym	$\Delta H_r$	Sym	$\Delta H_r$	Sym	$\Delta H_r$	Sym	$\Delta H_r$
C <sub>70</sub> H <sub>40</sub> ( <b>1</b> ) <sup>a</sup>	<i>C<sub>1</sub></i>							
C <sub>70</sub> H <sub>38</sub>	<i>C<sub>1</sub></i>	46.9						
C <sub>70</sub> H <sub>36</sub>	<i>C<sub>1</sub></i>	47.4	<i>C<sub>1</sub></i>	46.9				
C <sub>70</sub> H <sub>34</sub>	<i>C<sub>1</sub></i>	46.2	<i>C<sub>1</sub></i>	47.4				
C <sub>70</sub> H <sub>32</sub>	<i>C<sub>s</sub></i>	45.8						
C <sub>70</sub> H <sub>30</sub>	<i>C<sub>1</sub></i>	44.5						
C <sub>70</sub> H <sub>28</sub>	<i>C<sub>1</sub></i>	17.6						
C <sub>70</sub> H <sub>26</sub>	<i>C<sub>1</sub></i>	17.7	<i>C<sub>1</sub></i>	28.8				
C <sub>70</sub> H <sub>24</sub>	<i>C<sub>1</sub></i>	18.5	<i>C<sub>1</sub></i>	26.3				
C <sub>70</sub> H <sub>22</sub>	<i>C<sub>1</sub></i>	28.1						
C <sub>70</sub> H <sub>20</sub>	<i>C<sub>s</sub></i>	10.9						
C <sub>70</sub> H <sub>18</sub>	<i>C<sub>s</sub></i>	20.0			<i>C<sub>s</sub></i>	-3.3		
C <sub>70</sub> H <sub>16</sub>	<i>C<sub>1</sub></i>	27.3	<i>C<sub>1</sub></i>	19.8	<i>C<sub>s</sub></i>	9.5	<i>C<sub>s</sub></i>	5.0
C <sub>70</sub> H <sub>14</sub>	<i>C<sub>s</sub></i>	26.3	<i>C<sub>1</sub></i>	26.2	<i>C<sub>s</sub></i>	9.0	<i>C<sub>s</sub></i>	19.5
C <sub>70</sub> H <sub>12</sub>	<i>C<sub>s</sub></i>	25.7			<i>C<sub>s</sub></i>	35.2		
C <sub>70</sub> H <sub>10</sub>	<i>C<sub>5v</sub></i>	31.7 <sup>b</sup>			<i>C<sub>5v</sub></i>	-19.6 <sup>c</sup>		
C <sub>70</sub> H <sub>8</sub>	<i>C<sub>1</sub></i>	14.3				37.4		
C <sub>70</sub> H <sub>6</sub>	<i>C<sub>s</sub></i>	25.3	<i>C<sub>s</sub></i>	21.0	<i>C<sub>s</sub></i>	41.0	<i>C<sub>s</sub></i>	-39.9
C <sub>70</sub> H <sub>4</sub>	<i>C<sub>s</sub></i>	24.8	<i>C<sub>s</sub></i>	34.9		40.5	<i>C<sub>s</sub></i>	41.1
C <sub>70</sub> H <sub>2</sub>	<i>C<sub>s</sub></i>	12.7			<i>C<sub>s</sub></i>	40.8		
C <sub>70</sub>	<i>D<sub>5h</sub></i>	26.4			<i>D<sub>5h</sub></i>	44.0		

<sup>a</sup> $\Delta H_r^0$ (C<sub>70</sub>H<sub>40</sub>) = 504.2 kcalmol<sup>-1</sup>; <sup>b</sup>Ring-opened C<sub>70</sub>H<sub>10</sub> (C<sub>70</sub>H<sub>10a</sub> in text and Figure 1 with  $\Delta H_r^0$  = 958.5 kcalmol<sup>-1</sup>); <sup>c</sup>Ring-closed C<sub>70</sub>H<sub>10</sub> (C<sub>70</sub>H<sub>10b</sub> in text and Figures 1 and 2 with  $\Delta H_r^0$  = 858.5 kcalmol<sup>-1</sup>).

carbon double bond formation and finally the ring-opened isomer C<sub>70</sub>H<sub>10a</sub> (*C<sub>5v</sub>* symmetry). In contrast, loss of *Ha* followed by five-fold six membered ring formation will give the ring-closed isomer C<sub>70</sub>H<sub>10b</sub> (*C<sub>5v</sub>* symmetry). In line with the *semi*-empirical AM1 and *ab initio* results discussed in Chapter 4,<sup>1</sup> the ring-closed isomer C<sub>70</sub>H<sub>10b</sub> is more stable than its ring-opened counterpart (C<sub>70</sub>H<sub>10a</sub>, Figure 1 and Table 1). The first H<sub>2</sub> loss and ring closure from C<sub>70</sub>H<sub>20</sub> to ‘ring-closed’

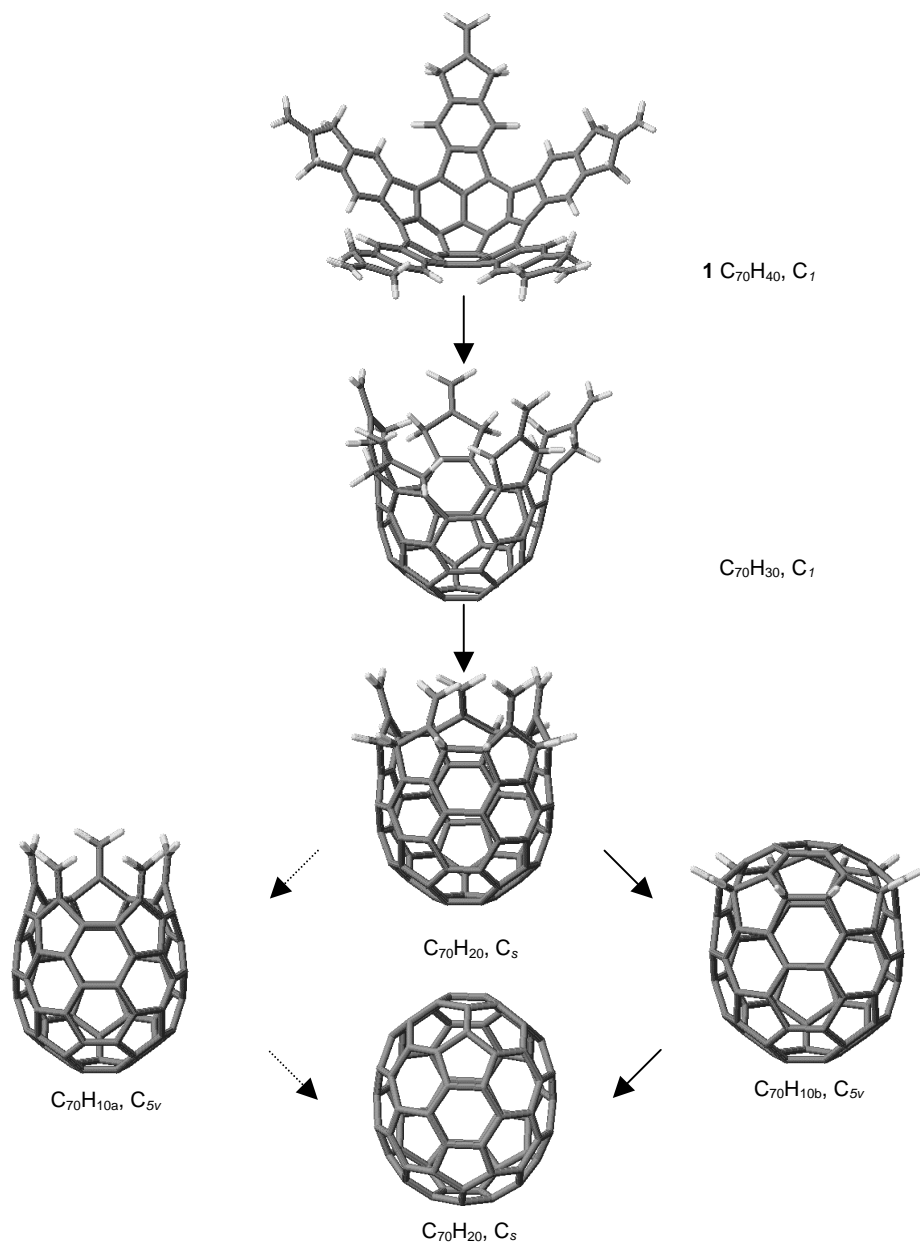


**Figure 1.** B3LYP/6-31G\*\* optimized structures of **1** (C<sub>70</sub>H<sub>40</sub>) and the derived intermediates C<sub>70</sub>H<sub>30</sub>, C<sub>70</sub>H<sub>20</sub>, C<sub>70</sub>H<sub>10a</sub> and C<sub>70</sub>H<sub>10b</sub>, and C<sub>70</sub>.

C<sub>70</sub>H<sub>18</sub> is even predicted to be exothermic (Table 1). Notice that ring-closed C<sub>70</sub>H<sub>10b</sub> represents a C<sub>70</sub> fullerane (hydrofullerene)<sup>6-11</sup> that consists of two distinct parts; an egg-shaped  $\pi$ -conjugated system topped of by a [5]radialene cap.

From ring-opened C<sub>70</sub>H<sub>10a</sub> five-fold cyclodehydrogenations involving *Ha* will result in the formation of the corannulene cap of C<sub>70</sub>, *i.e.* the formation of six six-membered rings and one five-membered ring. To convert ring-closed C<sub>70</sub>H<sub>10b</sub> into C<sub>70</sub> five-fold H<sub>2</sub> losses have to take place. Notice that there is a large difference in  $\Delta H_r$  for the conversion of C<sub>70</sub>H<sub>10a</sub> and C<sub>70</sub>H<sub>10b</sub> into C<sub>70</sub> [Table 2; RHF/AM1: 103.5 and 203.7 kcalmol<sup>-1</sup>, respectively] (*vide infra*).

The available experimental results on the cyclodehydrogenation of C<sub>60</sub>H<sub>30</sub> to C<sub>60</sub> using MALDI TOF-MS have shown that only cyclodehydrogenations occurred from the radical cation C<sub>60</sub>H<sub>30</sub><sup>+</sup> (Chapter 4); no cyclodehydrogenations were observed for the related radical anions (MALDI TOF-MS negative-ion mode).<sup>1,12</sup> Therefore, the radical cations of the intermediates displayed in Figure 1 were also studied using UHF/AM1. From Table 2 it can be concluded that in accordance with the RHF/AM1 results, the UHF/AM1 calculations show that the first five-fold cyclodehydrogenation cycle is the most endothermic [ $\Delta H_r = 231.4$  kcalmol<sup>-1</sup>]. Notice, however, that UHF/AM1 gives considerable spin contamination ( $s^2 > 4$ ). Furthermore, the conversion of C<sub>70</sub>H<sub>20</sub> to the ring-closed isomer C<sub>70</sub>H<sub>10b</sub> is found to be more favorable than the ring-opened isomer (C<sub>70</sub>H<sub>10a</sub>). Previous computational studies on fullerenes have shown that *semi*-empirical methods, such as AM1, are not always capable to correctly predict the (relative) energy order of fullerane isomers.<sup>13,14</sup> Therefore, we were prompted to perform *ab initio* RHF/6-31G\*\* and B3LYP/6-31G\*\* calculations on all proposed intermediates depicted in Figure 1 in order to establish if the formation of the ring-closed isomer C<sub>70</sub>H<sub>10b</sub> is indeed more favored. In addition for the related radical cations the UB3LYP/6-31G\*\* method was used.

### 5.2.2 *Ab initio* calculations

In Table 2 the *semi*-empirical reaction enthalpies ( $\Delta H_r$ ) and the *ab initio* reaction energies ( $\Delta E_r$ ) for the cyclodehydrogenations of both neutral as well as radical cations species of the intermediates depicted in Figure 1 are presented.

First, RHF/6-31G\*\* and B3LYP/6-31G\*\* calculations on the closed-shell intermediates were performed. The results at both *ab initio* levels of theory are in reasonable agreement and show similar trends as found using the *semi*-empirical AM1/RHF method. Only a marked difference is observed for the  $\Delta E_r$  values of the last step in the cyclodehydrogenation cycle forming C<sub>70</sub> from the fullerane-type intermediate C<sub>70</sub>H<sub>10b</sub>. This conversion is considerable less endothermic at the *ab*

**Table 2.** Reaction energies ( $\Delta H_r$  and  $\Delta E_r$  in kcalmol<sup>-1</sup>) for the closed-shell intermediates and the related open-shell, radical cations derived from C<sub>70</sub>H<sub>40</sub> (**1**) and C<sub>70</sub>H<sub>40</sub><sup>•+</sup> (**1**<sup>•+</sup>), respectively, as depicted in Figure 1.

Reaction		Closed-shell intermediate			Open-shell radical cation	
		$\Delta H_r$ RHF/AM1 <sup>a</sup>	$\Delta E_r$ RHF/6- 31G** <sup>b</sup>	$\Delta E_r$ B3LYP/6- 31G** <sup>c</sup>	$\Delta H_r$ UHF/AM1 <sup>a</sup>	$\Delta E_r$ UB3LYP/6- 31G** <sup>d</sup>
C <sub>70</sub> H <sub>40</sub> ( <b>1</b> )	→ C <sub>70</sub> H <sub>30</sub>	230.8	253.1	244.6	231.4	245.9
C <sub>70</sub> H <sub>30</sub>	→ C <sub>70</sub> H <sub>20</sub>	92.8	108.8	135.8	100.6	95.9
C <sub>70</sub> H <sub>20</sub>	→ C <sub>70</sub> H <sub>10a</sub> <sup>e</sup>	130.9	96.2	102.3	113.0	56.7
C <sub>70</sub> H <sub>20</sub>	→ C <sub>70</sub> H <sub>10b</sub> <sup>f</sup>	30.8	58.6	82.0	20.0	45.2
C <sub>70</sub> H <sub>10a</sub>	→ C <sub>70</sub>	103.5	83.7	91.8	120.8	69.0
C <sub>70</sub> H <sub>10b</sub>	→ C <sub>70</sub>	203.7	127.7	112.2	210.0	80.6

<sup>a</sup>C<sub>70</sub>H<sub>40</sub> (**1**): RHF/AM1,  $\Delta H_r^0 = 504.2$  kcalmol<sup>-1</sup> and C<sub>70</sub>H<sub>40</sub><sup>•+</sup> (**1**<sup>•+</sup>): UHF/AM1,  $\Delta H_r^0 = 668.7$  kcalmol<sup>-1</sup>; <sup>b</sup>E<sub>total</sub> C<sub>70</sub>H<sub>40</sub> (**1**, RHF/6-31G\*\*) = -2674.063906 a.u.; <sup>c</sup>E<sub>total</sub> C<sub>70</sub>H<sub>40</sub> (**1**, B3LYP/6-31G\*\*) = -2691.524743 a.u.; <sup>d</sup>E<sub>total</sub> C<sub>70</sub>H<sub>40</sub><sup>•+</sup> (**1**<sup>•+</sup>, UB3LYP/6-31G\*\*) = -2691.295990 a.u. <sup>e</sup>Ring-opened C<sub>70</sub>H<sub>10</sub> (C<sub>70</sub>H<sub>10a</sub> in text and Figure 1). <sup>f</sup>Ring-closed C<sub>70</sub>H<sub>10</sub> (C<sub>70</sub>H<sub>10b</sub> in text and Figure 1).

*initio* level of theory (RHF/6-31G\*\* 127.7 and B3LYP/6-31G\*\* 112.2 kcalmol<sup>-1</sup>), which is in agreement with experimental observations that fullerenes more readily expel hydrogen atoms.<sup>10,15</sup>

The corresponding radical cations were calculated using the UB3LYP/6-31G\*\* method. The five-fold cyclodehydrogenation cycle required for the conversion of C<sub>70</sub>H<sub>40</sub> into C<sub>70</sub>H<sub>30</sub> is again found to be the most endothermic cycle [ $\Delta E_r = 245.9$  kcalmol<sup>-1</sup>, compare UHF/AM1:  $\Delta H_r = 231.4$  kcalmol<sup>-1</sup>, Table 2]. However, the following cyclodehydrogenation cycles from C<sub>70</sub>H<sub>30</sub> to C<sub>70</sub> require considerable less energy when radical cations are calculated by the UB3LYP/6-31G\*\* method. In general, the *ab initio* results confirm that the formation of the ring-closed isomer C<sub>70</sub>H<sub>10b</sub> from C<sub>70</sub>H<sub>20</sub> is more favorable than the formation of the ring-opened isomer C<sub>70</sub>H<sub>10a</sub> (Table 2). The lower  $\Delta E_r$  values in comparison to the related  $\Delta H_r$  (AM1) values computed for C<sub>70</sub> formation from the fullerene C<sub>70</sub>H<sub>10b</sub> at the *ab initio* level in combination with its more facile formation indicates that C<sub>70</sub>H<sub>10b</sub> will be an important intermediate.

The energy needed for each H<sub>2</sub> loss and ring closure in the first cyclodehydrogenation cycle, which is the most energy-demanding cycle, is comparable to that found for cyclodehydrogenation of C<sub>60</sub>H<sub>30</sub> to C<sub>60</sub>H<sub>24</sub> (AM1: 47 *vs.* 40 kcalmol<sup>-1</sup> per H<sub>2</sub> loss and ring closure,

**Table 3.** Reaction energies ( $\Delta H_r$  and  $\Delta E_r$  in kcalmol<sup>-1</sup>) for the closed-shell intermediates and the related open-shell radical cations derived from C<sub>70</sub>H<sub>40</sub> (**2**) and C<sub>70</sub>H<sub>40</sub><sup>+</sup> (**2**<sup>+</sup>), respectively, as depicted in Figure 2.

Reaction		Closed-shell intermediate			Open-shell radical cation		
		$\Delta H_r$ RHF/AM1 <sup>a</sup>	$\Delta E_r$ RHF/6- 31G** <sup>b</sup>	$\Delta E_r$ B3LYP/6- 31G** <sup>c</sup>	$\Delta H_r$ UHF/AM1 <sup>a</sup>	$\Delta E_r$ UB3LYP/6- 31G** <sup>d</sup>	
C <sub>70</sub> H <sub>40</sub> ( <b>2</b> )	→	C <sub>70</sub> H <sub>30</sub>	30.2	56.7	41.6	31.6	46.7
C <sub>70</sub> H <sub>30</sub>	→	C <sub>70</sub> H <sub>20</sub>	29.6	73.2	39.5	28.3	44.8
C <sub>70</sub> H <sub>20</sub>	→	C <sub>70</sub> H <sub>10b</sub>	194.2	93.9	65.7	202.9	85.6
C <sub>70</sub> H <sub>10b</sub>	→	C <sub>70</sub>	203.5	127.7	112.2	213.8	80.6

<sup>a</sup>C<sub>70</sub>H<sub>40</sub> (**2**): RHF/AM1,  $\Delta H_r^\beta = 604.5$  kcalmol<sup>-1</sup> and C<sub>70</sub>H<sub>40</sub><sup>+</sup> (**2**<sup>+</sup>): UHF/AM1,  $\Delta H_r^\beta = 757.9$  kcalmol<sup>-1</sup>; <sup>b</sup>E<sub>total</sub> C<sub>70</sub>H<sub>40</sub> (**2**, RHF/6-31G\*\*) = -2673.752468 a.u.; <sup>c</sup>E<sub>total</sub> C<sub>70</sub>H<sub>40</sub> (**2**, B3LYP/6-31G\*\*) = -2691.221150 a.u.; <sup>d</sup>E<sub>total</sub> C<sub>70</sub>H<sub>40</sub><sup>+</sup> (**2**<sup>+</sup>, UB3LYP/6-31G\*\*) = -2691.028027 a.u.

Chapter 4).<sup>1</sup> For the following cyclodehydrogenation cycles the  $\Delta H_r$  per H<sub>2</sub> loss and ring closure in the conversion of C<sub>70</sub>H<sub>40</sub> into finally C<sub>70</sub> are even lower (Table 1). After each cyclodehydrogenation cycle the next series of hydrogen atoms become sterically congested and, thus, susceptible to undergo H<sub>2</sub> loss and ring closure. Hence, different routes, proceeding through different intermediates might occur, but all will eventually lead to C<sub>70</sub>.

The results of these calculations show that cyclodehydrogenations towards ring-closed C<sub>70</sub>H<sub>10b</sub> are more facile. Presumably, while a [5]radialene-like cap is formed. As a corollary another pathway to C<sub>70</sub> becomes conceivable in which these types of intermediates play a more pronounced role. The amount of curvature that has to be introduced in going from C<sub>70</sub>H<sub>40</sub> to C<sub>70</sub>H<sub>10b</sub> is another factor that will influence the ease with which a precursor can be converted into C<sub>70</sub>. In view of these considerations another isomer of C<sub>70</sub>H<sub>40</sub> (**2**), which does not fit the C<sub>70</sub> Schlegel diagram, but has a belt-like structure, might also be a progenitor for C<sub>70</sub> (Figure 2). The  $\Delta H_r$  and  $\Delta E_r$  values for the conversion of **2** into C<sub>70</sub> are computed following the above mentioned approach; the results are depicted in Table 3. The first cyclodehydrogenation cycle from **2** into C<sub>70</sub>H<sub>30</sub> is noticeably less endothermic than the corresponding cycle in the conversion of **1** [ $\Delta H_r = 230.8$  vs. 30.2 kcalmol<sup>-1</sup> (RHF/AM1) and  $\Delta E_r = 244.6$  vs. 41.6 kcalmol<sup>-1</sup> (B3LYP/6-31G\*\*)]. Clearly, this marked reduction in both  $\Delta H_r$  and  $\Delta E_r$  is due to the fact that in the case of **2** the belt-

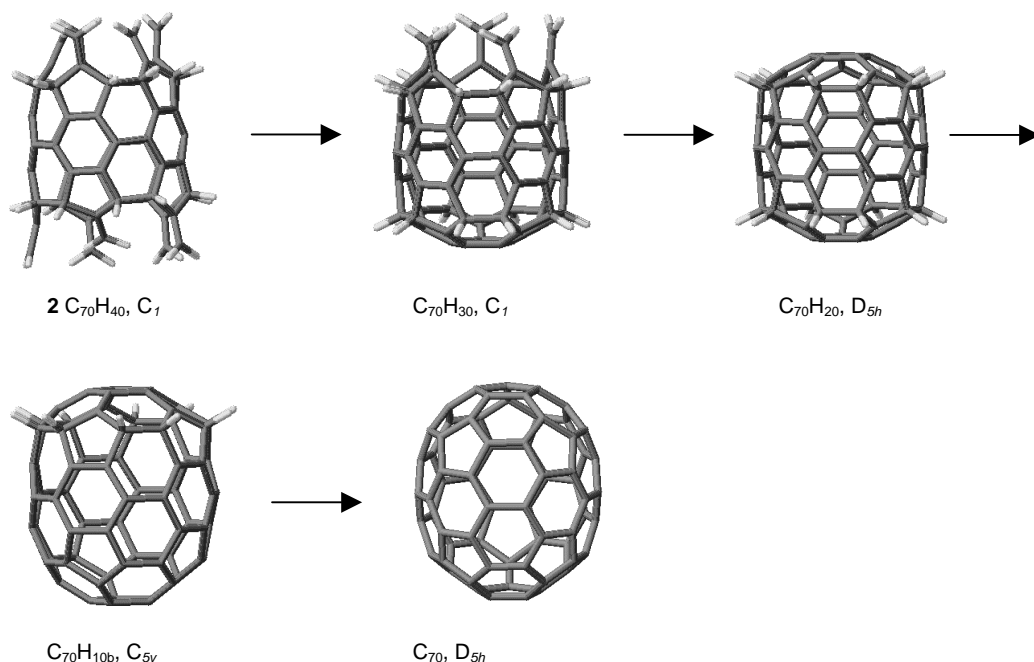


**Figure 2.** B3LYP/6-31G\*\* Optimized structures of the belt-like  $\text{C}_{70}\text{H}_{40}$  (**2**) and the derived intermediates  $\text{C}_{70}\text{H}_{30}$ ,  $\text{C}_{70}\text{H}_{20}$  and  $\text{C}_{70}\text{H}_{10b}$ , and  $\text{C}_{70}$ .

like structure already contains substantial strain energy. The last two steps from  $\text{C}_{70}\text{H}_{20}$  into  $\text{C}_{70}\text{H}_{10}$ , and,  $\text{C}_{70}\text{H}_{10}$  into  $\text{C}_{70}$  have  $\Delta H_r$  and  $\Delta E_r$  values that are comparable to those found for the conversion of **1** into  $\text{C}_{70}$ . The  $\text{C}_{70}\text{H}_{20}$  isomer contains a belt composed of biphenyl-units closed by two [5]radialene caps.

Belt-like structures were recognized previously as interesting synthetic targets.<sup>16-18</sup> These belt-shaped molecules are of relevance because of their structural similarity to carbon nanotubes and their utility in host-guest chemistry. Furthermore, compound **2** also represents a small, rim-functionalized fullerene pipe.<sup>19</sup> Recently, rim functionalization of fullerene pipes, has shown to lead to soluble materials.<sup>20,21</sup> With the proper functionalities attached to the rim this may provide a tool to convert pipes into tubes.

### 5.3 Conclusions

The computational results presented in this Chapter indicate that the C<sub>70</sub>H<sub>40</sub> corannulene derivative (**1**) might be a proper progenitor for C<sub>70</sub>, which can be converted stepwise *via* consecutive cyclodehydrogenations. Although, the initial steps in the zipping up process from C<sub>70</sub>H<sub>40</sub> to C<sub>70</sub>H<sub>30</sub> and, finally, to C<sub>70</sub>H<sub>20</sub> are strongly endothermic processes, the conversion of C<sub>70</sub>H<sub>20</sub> into the ring-closed C<sub>70</sub>H<sub>10b</sub> is considerable less endothermic. A similar phenomenon was observed in the conversion of C<sub>60</sub>H<sub>30</sub> into C<sub>60</sub>; the formation of a ring-closed C<sub>60</sub>H<sub>6</sub> intermediate was favored.<sup>24</sup> The relative stability of the ring-closed intermediates points to another progenitor for C<sub>70</sub>, *i.e.* belt-like compound **2**. If extended homologues of **2** will become synthetically accessible, for example, by selective functionalization of the rims of recently identified fullerene pipes, closed tube-like structures will be accessible by design. This is of interest for the selective synthesis of endohedral fullerenes and carbon nanotubes.

### Acknowledgement

The Stichting Nationale Computerfaciliteiten (National Computing Facilities Foundation, NCF) and NWO are acknowledged for the use of supercomputer facilities.

### 5.4 Experimental Section

#### Computational Methods

All intermediates formed upon consecutive H<sub>2</sub> loss and ring closure from C<sub>70</sub>H<sub>40</sub> were optimized by *semi*-empirical computations (RHF/AM1) using MOPAC 7.0 until GNORM < 0.05.<sup>22</sup> Minima were characterized by Hessian calculations; no imaginary vibrations were found. Selected intermediates were subsequently studied at the *ab initio* level of theory using Gamess-UK Hartree-Fock (RHF) and DFT (B3LYP) calculations in the 6-31G\*\* basis.<sup>23</sup> Related radical cation species were further studied using UHF/AM1 and UB3LYP/6-31G\*\* methods. UHF/6-31G\*\* was not applied since it is known to give severe spin contamination. As shown below and in line with recent reports UB3LYP is a good method for the calculation of open-shell species as no spin contamination is observed.<sup>24</sup> Plots of all RHF/AM1 optimized geometries reported in Table 1 are shown in the Supporting Information of ref. 25. Cartesian coordinates of all *ab initio* optimized geometries depicted in Figures 1 and 2 [closed-shell intermediates (RHF/6-31G\*\* and B3LYP/6-31G\*\*) and related open-shell radical cations (UB3LYP/6-31G\*\*)] are also presented in the Supporting Information of ref. 25. Comparable geometries were found for both closed-shell intermediates and their related open-shell, radical cation species calculated at similar levels of theory (RHF/AM1 *vs.*

UHF/AM1 and B3LYP/6-31G\*\* vs. UB3LYP/6-31G\*\*). When the *semi*-empirical AM1 method was used  $\Delta H_r$  is defined as  $[\Delta H_f^0(\text{PAH-xH}_2) + x\Delta H_f^0(\text{H}_2)] - \Delta H_f^0(\text{PAH})$  where  $\Delta H_f^0(\text{H}_2) = 0 \text{ kcalmol}^{-1}$  (RHF/AM1:  $\text{H}_2$  bond length = 0.667 Å; UHF/AM1:  $\text{H}_2^+$  bond length = 0.979 Å). In the case of *ab initio* methods  $\Delta E_r$  is defined as  $[\Delta E_r(\text{PAH-5H}_2) + 5\Delta E_r(\text{H}_2)] - \Delta E_r(\text{PAH})$ . RHF/6-31G\*\*:  $E_{\text{total}}(\text{H}_2) = -1.131333 \text{ a.u.}$ ,  $\text{H}_2$  bond length = 0.733 Å; B3LYP/6-31G\*\*:  $E_{\text{total}}(\text{H}_2) = -1.178538 \text{ a.u.}$ ,  $\text{H}_2$  bond length = 0.742 Å; UB3LYP/6-31G\*\*:  $E_{\text{total}}(\text{H}_2) = -1.178538 \text{ a.u.}$ ,  $\text{H}_2$  bond length = 0.742 Å.<sup>25</sup>

## References and notes

- (1) Gómez-Lor, B.; Koper, C.; Fokkens, R. H.; Vlietstra, E. J.; Cleij, T. J.; Jenneskens, L. W.; Nibbering, N. M. M.; Echavarren, A. M. *Chem. Commun.* **2002**, 370-371.
- (2) Koper, C.; Ruiz, M.; de Frutos, Ó.; González-Cantalapiedra, E.; Fokkens, R. H.; Nibbering, N. M. M.; Cárdenas, D. J.; Santos, A.; Gómez-Lor, B.; Jenneskens, L. W.; Echavarren, A. M. *Chem. Eur. J* **2003**, *in press*.
- (3) Marcinow, Z.; Grove, D. I.; Rabideau, P. W. *J. Org. Chem.* **2002**, *67*, 3537-3539.
- (4) Marcinow, Z.; Rabideau, P. W. *J. Org. Chem.* **2000**, *65*, 5063-5065.
- (5) Compound **1** has  $C_1$  symmetry and not five-fold symmetry (either  $C_5$  or  $C_{5v}$ ) as expected for a five-fold functionalized corannulene. This is attributed to the occurrence of steric interactions in the top part of the molecule. Notwithstanding, all non-bonded  $H_a \cdots H_a$  distances are 1.83 Å (*cf.* Chart 1).
- (6) Henderson, C. C.; Cahill, P. A. *Science* **1993**, *259*, 1885-1887.
- (7) Henderson, C. C.; McMichael Rohlfing, C.; Gillen, K. T.; Cahill, P. A. *Science* **1994**, *264*, 397-399.
- (8) Rüchardt, C.; Gerst, M.; Ebenhoch, J.; Beckhaus, H.-D.; Campbell, E. E. B.; Tellgmann, R.; Schwarz, H.; Weiske, T.; Pitter, S. *Angew. Chem. Int. Ed. Engl.* **1993**, *32*, 584-586.
- (9) Henderson, C. C.; McMichael Rohlfing, C.; Assink, R. A.; Cahill, P. A. *Angew. Chem. Int. Ed. Engl.* **1994**, *33*, 786-788.
- (10) Meier, M. S.; Weedon, B. R.; Spielmann, H. P. *J. Am. Chem. Soc.* **1996**, *118*, 11682-11683.
- (11) Spielmann, H. P.; Weedon, B. R.; Meier, M. S. *J. Org. Chem.* **2000**, *65*, 2755-2758.
- (12) Boorum, M. M.; Vasil'ev, Y. V.; Drewello, T.; Scott, L. T. *Science* **2001**, *294*, 828-831.
- (13) Henderson, C. C.; Rohlfing, C. M.; Cahill, P. A. *Chem. Phys. Lett.* **1993**, *213*, 383-388.
- (14) Chen, Z.; Thiel, W. *Chem. Phys. Lett.* **2003**, *367*, 15-25.
- (15) Möder, M.; Nüchter, M.; Ondruscka, B.; Czira, G.; Vékey, K.; Barrow, M. P.; Drewello, T. *Int. J. Mass Spectrom. Ion Proc.* **2000**, *195/196*, 599-607.
- (16) Stoddart, J. F. *Nature* **1988**, *334*, 10.



- (17) Kammermeier, S.; Jones, P. G.; Herges, R. *Angew. Chem. Int. Ed. Engl.* **1997**, *36*, 2200-2202.
- (18) Herges, R.; Deichmann, M.; Grunenberg, J.; Bucher, G. *Chem. Phys. Lett.* **2000**, *327*, 149-152.
- (19) Liu, J.; Rinzler, A. G.; Dai, H.; Hafner, J. H.; Bradley, R. K.; Boul, P. J.; Lu, A.; Iverson, T.; Shelimov, K.; Huffman, C. B.; Rodriguez-Macias, F.; Shon, Y.-S.; Lee, T. R.; Colbert, D. T.; Smalley, R. E. *Science* **1998**, *280*, 1253-1256.
- (20) Hamon, M. A.; Itkis, M. E.; Niyogi, S.; Alvarez, T.; Kuper, C.; Menon, M.; Haddon, R. C. *J. Am. Chem. Soc.* **2001**, *123*, 11292-11293.
- (21) Hamon, M. A.; Chen, J.; Hu, H.; Chen, Y.; Itkis, M. E.; Rao, A. M.; Eklund, P. C.; Haddon, R. C. *Adv. Mater.* **1999**, *11*, 834-840.
- (22) Dewar, M. J. S.; Zebisch, E. G.; Healy, E. F.; Stewart, J. J. P. *J. Am. Chem. Soc.* **1985**, *107*, 3902-3909.
- (23) Guest, M. F.; van Lenthe, J. H.; Kendrick, J.; Schöffel, K.; Sherwood, P.; Harrison, R. J. *GAMESS-UK, a package of ab initio programs*, **1998**. With contributions from: Amos, R.D., Buenker, R.J.; Dupuis, M.; Handy, N.C.; Hillier, I.; Knowles, P.J.; Bonacic-Koutecky, V.; von Niessen, W.; Saunders, V.R.; Stone, A.J. Derived from the original GAMESS code by: Dupuis, M.; Spangler, D.; Wendolowski, J.; NRCC Software Catalog, vol. 1, program no. QG01 (GAMESS), **1980**.
- (24) Cioslowski, J.; Liu, G.; Moncrieff, D. J. *Org. Chem.* **1996**, *61*, 4111-4114.
- (25) Koper, C.; van Lenthe, J. H.; Jenneskens, L. W. J. *Phys. Chem. A.* **2003**, *submitted*.



# CHAPTER 6

## Synthesis by Design of the Novel Triaza-Fullerane $C_{57}H_2N_3$ by 'Zipping up' of its Schlegel-Match Progenitor $C_{57}H_{33}N_3$

### Abstract

The first selective synthesis of the ionic triazafullerane,  $C_{57}H_2N_3$ , is reported by 'zipping up' its  $C_{57}H_{33}N_3$  (**1**) non-alternant PAH progenitor. Successive  $H_2$  losses accompanied by ring closures were induced by matrix-assisted-laser-desorption-ionization time-of-flight mass spectrometry (MALD TOF-MS) both in the positive-ion and negative-ion mode and were shown to proceed from the inside outwards. Additional proof was obtained by the behavior of a deuterated analogue ( $C_{57}H_{27}^2H_6N_3$ , **1-d<sub>6</sub>**) under similar MALDI TOF-MS conditions, as well as *semi*-empirical (AM1) and *ab initio* (RHF/6-31G\*\* and B3LYP/6-31G\*\*) calculations on the cationic and anionic species of the possible intermediates.

## 6.1 Introduction

One of the most promising approaches to modify the electronic properties of fullerenes is by substitution of carbon atoms by hetero-atoms. This will render heterofullerenes of interest for application in superconductivity, photoinduced electron transfer and organic ferromagnetism.<sup>1</sup> When one carbon atom is replaced by a nitrogen atom an open-shell (radical) system is obtained. As a consequence, azafullerenes are difficult to prepare and isolate. However, the dimers and hydroazafullerene (azafullerane) precursors *can* be prepared and isolated. Previously, besides the usual procedure of laser ablation of graphite-heteroatom composite rods,<sup>2-5</sup> defined syntheses of  $(C_{59}N)_2$ ,  $C_{59}NH$ ,  $(C_{69}N)_2$  and  $C_{59}N^+$  have been reported.<sup>6-10</sup> In these syntheses,  $C_{60}$  or  $C_{70}$  were taken as the starting compound and subsequently modified. However, no azafullerene has yet been synthesized from a non-fullerene precursor where more than one carbon atom is replaced by nitrogen atoms. Hitherto only circumstantial evidence for the preparation of  $C_{58}N_2$  from an *in-situ* generated hetero-polyene has been reported.<sup>11,12</sup>

In Chapter 4, the conversion of a unimolecular non-alternant  $C_{60}H_{30}$  polycyclic aromatic hydrocarbon (PAH) progenitor for  $C_{60}$ , which possesses the same carbon atom topology as the  $C_{60}$  Schlegel diagram, into  $C_{60}$  was reported.<sup>13-15</sup> Under proper MALDI TOF-MS conditions, the 'zipping up' of this  $C_{60}H_{30}$  PAH precursor proceeds *via* fifteen-fold consecutive  $H_2$  losses and ring closures from the inside outwards, without the occurrence of either rearrangement or degradation of the original carbon skeleton.<sup>14,16</sup> A prerequisite for the successful conversion of  $C_{60}H_{30}$  into  $C_{60}$  was shown to be the exact carbon topology as in the  $C_{60}$  Schlegel diagram, *i.e.* our Schlegel-match proposition. We have shown that if no closed carbon surface can be obtained, break down does become an important side-reaction.<sup>16,17</sup>

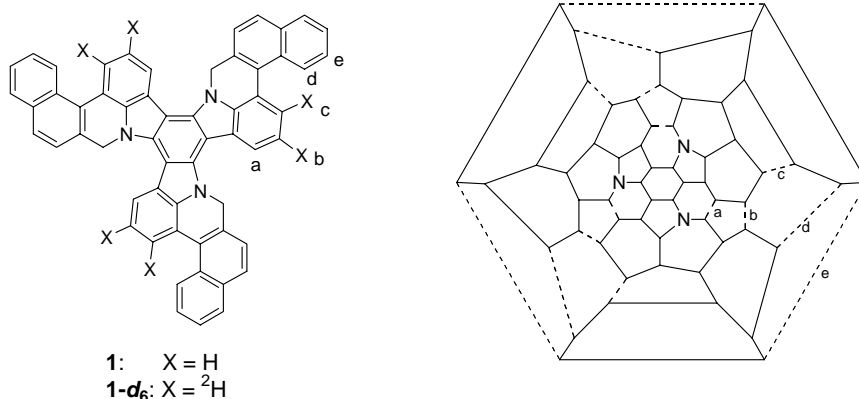


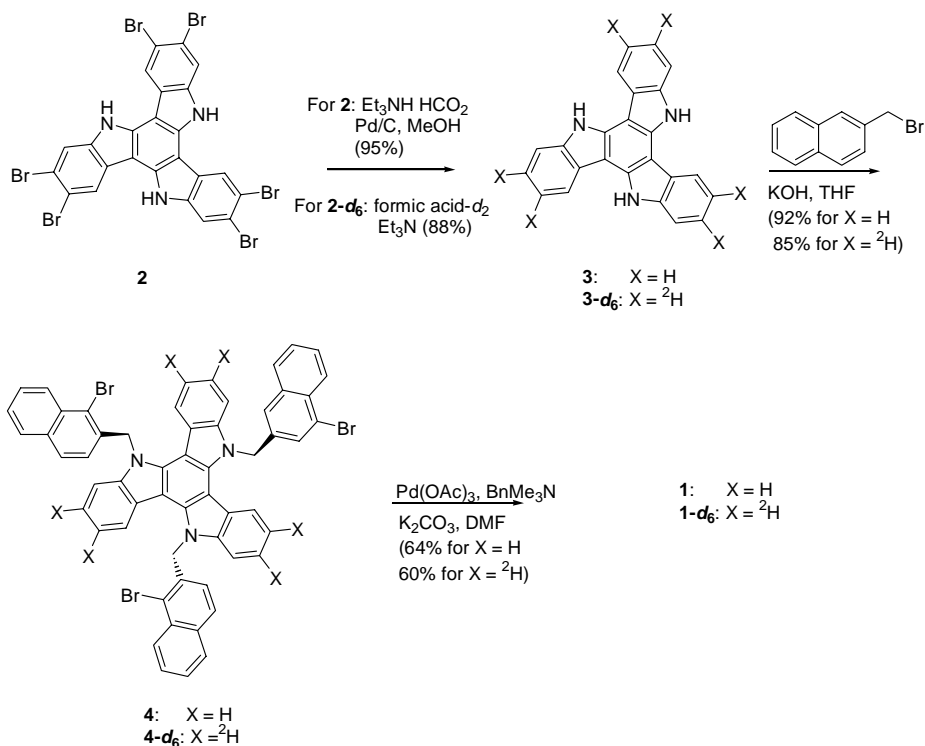
Chart 1

In this Chapter, we report the preparation of the hitherto unknown ionic triazafullerane  $C_{57}H_2N_3$ , based on our Schlegel-match proposition. In this  $C_{60}$ -related structure, three carbon atoms are replaced by three nitrogen atoms. Note that as a consequence of the presence of the three nitrogen atoms, their neighboring carbon atoms ( $sp^3$ -hybridized) possess two hydrogen atoms, *i.e.* they are  $CH_2$  moieties.

## 6.2 Results & Discussion

Both  $C_{57}H_{33}N_3$  (**1**) and a deuterated analogue  $C_{57}H_{27}^2H_6N_3$  **1-d<sub>6</sub>** were obtained in three steps from **3** (see Chart 1 and Scheme1) by the group of Echavarren (University of Madrid, Spain).

Reductive (deutero)debromination of **2** gave the triindoles **3** and **3-d<sub>6</sub>**, respectively,<sup>18,19</sup>. *N*-alkylation of **3** and **3-d<sub>6</sub>**, with 1-bromo-2-bromomethylnaphthalene gave **4** (92%) and **4-d<sub>6</sub>** (85%), which were subjected to arylation conditions [100 mol%  $Pd(OAc)_2$ ,  $K_2CO_3$ , DMF, 110°C] to give **1** (64%) and **1-d<sub>6</sub>** (60%) as yellow powders (see Experimental section).



**Scheme 1.** Synthetic route to  $C_{57}H_{33}N_3$  (**1**) and  $C_{57}H_{26}^2H_6N_3$  (**1-d<sub>6</sub>**).

### 6.2.1 Cyclodehydrogenations from $C_{57}H_{33}N_3$ (**1**) and $C_{57}H_{27}N_3$ (**1-d<sub>6</sub>**).

Compound  $C_{57}H_{33}N_3$  (**1**) is an analogue of the non-alternant PAH  $C_{60}H_{30}$  (Chapter 4)<sup>14,16</sup> in which three nitrogen atoms replace three carbon atoms. As a consequence, three  $CH_2$ -units are present in the molecule (see Chart 1). *Ab initio* (RHF/6-31G\*\* and B3LYP/6-31G\*\*) calculations show that  $C_{57}H_{33}N_3$  (**1**,  $C_3$ ) has a propeller-like structure, in which the inner core hydrogen,  $H_a$ , are positioned within the sum of their Van der Waals radius ( $H_a \cdots H$  1.82 and 2.20 Å). This renders these hydrogen atoms susceptible to undergo cyclodehydrogenation, *i.e.*  $H_2$  loss accompanied by ring closure.

To establish if cyclodehydrogenations can occur, **1** was subjected to MALDI TOF-MS conditions (see Experimental Section). At a laser fluence of 2100 (positive-ion mode), predominantly the precursor ion  $\mathbf{1}^+$  is observed [ $C_{57}H_{33}N_3^+$ ,  $m/z$  759, Figure 1A; natural isotope pattern: *calc.* 759 (100%), 760 (65%), 761 (21%), 762 (5%); *found* 759 (100%), 760 (64%), 761 (23%), 762 (6%)]. In addition, however, the closed-shell cation  $C_{57}H_{32}N_3^+$  ( $[M-1]^+$ ,  $m/z$  758, *ca.* 40%), most likely formed *via* loss of  $H\cdot$  from the precursor ion ( $\mathbf{1}^+$ ), is present. Although, the peak at  $m/z$  758 could also be attributed to the  $^{13}C$ -isotope of  $C_{57}H_{31}N_3^+$  ( $^{12}C_{56}^{13}CH_{31}N_3^+$ ), the intensity of this signal is too high since no formation of  $C_{57}H_{31}N_3$  ( $m/z$  757) *via*  $H_2$  loss and ring closure from  $\mathbf{1}^+$ , is yet observed. Upon increase of the laser fluence to 2200 *ca.* 80% of **1** is converted into  $C_{57}H_{32}N_3^+$  ( $[M-1]^+$ , not shown). This tendency to undergo facile  $H\cdot$  loss is characteristic for azafullerenes. Hitherto, all mass spectra in the reports where the syntheses of  $C_{59}NH$ ,  $C_{59}N^+$  and  $C_{69}N^+$  were described,<sup>7,8</sup> display intensive peaks corresponding to  $[M-1]^+$ . Even the 'shrink-wrap' process for (aza)fullerenes, *i.e.* subsequent loss of  $CN^-$ - and  $C_2$ -fragments, was found to take place from this  $[M-1]^+$  ion. In our case, loss of  $H\cdot$  most likely occurs from the  $CH_2$ -unit next to the nitrogen atom (see Chart 2). Hereupon, an iminium ion is formed, which will contribute to the delocalization of the positive charge into the neighboring naphthalene and benzene moieties of one of the 'propeller'-blades.

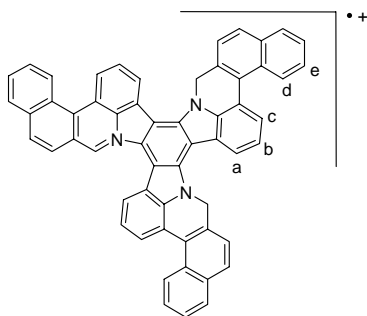
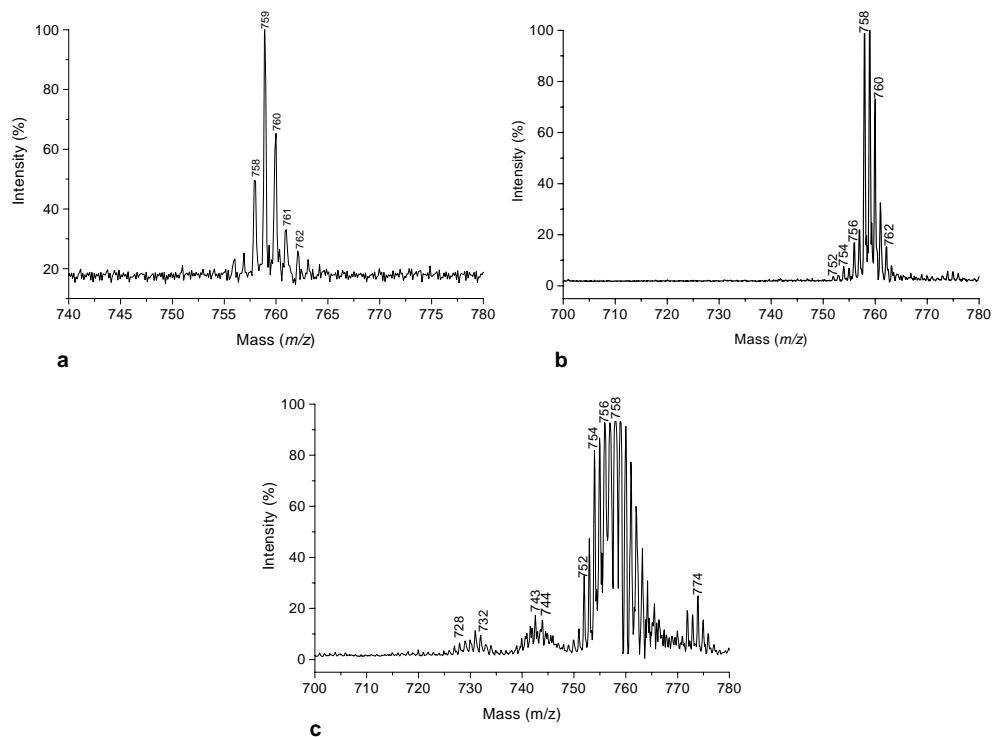


Chart 2

## Synthesis by Design of the Novel Triaza-Fullerane $C_{57}H_2N_3$



**Figure 1.** *In-source* MALDI TOF mass spectra of  $1^+$  in the positive-ion mode: **a.** laser fluence 2100, **b.** laser fluence of 2300 and **c.** laser fluence of 2400.

At a higher laser fluence of 2300, three-fold  $H_2$  losses and ring closures from  $C_{57}H_{32}N_3^+$  ( $[M-1]^+$ ), which is now predominantly formed (70%), takes place leading to the closed-shell species  $C_{57}H_{30}N_3^+$ ,  $C_{57}H_{28}N_3^+$  and  $C_{57}H_{26}N_3^+$  [ $m/z$  759 (44%), 758 (87%), 756 (13%), 754 (5%), 752 (3%), Figure 1B]. Analysis of the isotope pattern reveals that still some cyclodehydrogenations occur directly from the molecular ion ( $M^+$ )  $C_{57}H_{33}N_3^+$  (ca. 30%) *via* the open-shell radical cationic species [ $C_{57}H_{31}N_3^+$   $m/z$  757 (10%),  $C_{57}H_{29}N_3^+$   $m/z$  755 (2%),  $C_{57}H_{27}N_3^+$   $m/z$  753 (0.9%)].<sup>20</sup> It is noteworthy that cyclodehydrogenations *via* the radical cations appear to be more facile than *via* the closed-shell cationic species, which is due to their higher internal energy.<sup>21</sup> This can be deduced from the increase in the ratio between the peaks at odd and even masses upon cyclodehydrogenation with respect to the initial  $M^+/[M-1]^+$  ratio.

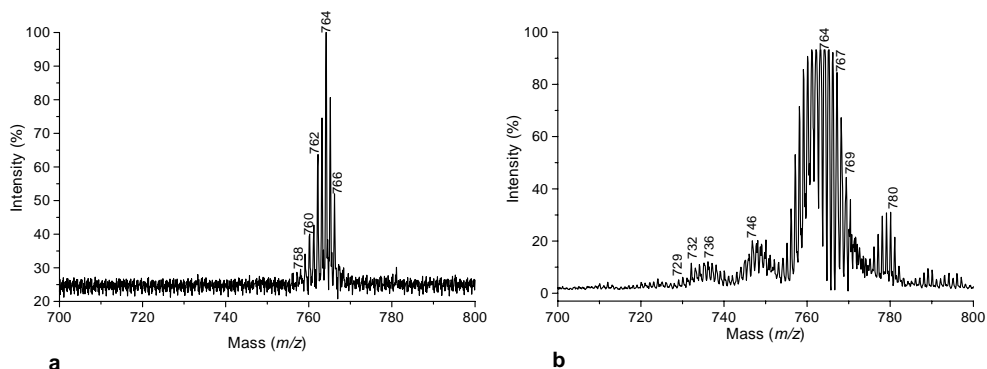


**Figure 2.** *In-source* MALDI TOF mass spectra of  $1-d_6^+$  in the positive-ion mode: **a.** laser fluence 2100 and **b.** laser fluence of 2400.

To assess whether the innermost non-bonded hydrogen indeed undergo  $H_2$  loss and ring closure first,<sup>14,16</sup> a deuterated analogue of **1**, with the deuterium atoms positioned at carbons b and c (see Chart 1) [ $C_{57}H_{27}^2H_6N_3$ ,  $1-d_6$  deuterium content *ca.* 90% according to FAB-MS] was subjected to similar MALDI TOF-MS conditions. In the positive-ion mode (laser fluence of 2100) again predominantly  $C_{57}H_{26}^2H_6N_3^+$  ( $[M-H]^+$ ,  $m/z$  764) is present, formed upon loss of  $H\cdot$  of  $1-d_6^+$  ( $m/z$  765), but in addition already three-fold  $H_2$  losses and ring closures are visible [Figure 2A;  $m/z$  764 (100%), 762 (35%), 760 (11%), 758 (2%)]. Since no loss of deuterium atoms is yet observed, this corroborates that indeed the inner core hydrogen atoms ( $H_a$ ) are eliminated first. As expected, cyclodehydrogenations *via* the radical cationic species is also favored for  $1-d_6^+$ .

Complete fifteen-fold cyclodehydrogenations of  $1^+$  *via* the two possible pathways, *i.e.* through open-shell radical cation and closed-shell cationic species starting from  $1^+$  and  $[M-H]^+$  respectively, will result in the closure of the carbon surface forming either  $C_{57}H_3N_3^+$  ( $m/z$  729) or  $C_{57}H_2N_3^+$  ( $m/z$  728). This is indeed what is observed at a laser fluence of 2400. Fifteen-fold  $H_2$  losses and ring closures giving cyclodehydrogenation products down to  $m/z$  728 are visible (Figure 1C). The isotope pattern can *only* be interpreted when both pathways, *i.e.* from  $m/z$  759 down to  $m/z$  729 *via* open-shell radical cationic species and from  $m/z$  758 down to  $m/z$  728 *via* closed-shell cationic species contribute (see Figure 1C). The presence of two regions with near zero peak intensities ( $m/z$  750 - 746 and 736 - 732) in the case of  $1^+/[M-H]^+$  is in accordance with the stepwise character of the consecutive cyclodehydrogenations (see Chapter 4).<sup>14,16</sup>



In line with this observation, the MALDI TOF-MS spectrum of **1-d<sub>6</sub><sup>+</sup>** at a laser fluence of 2400 shows cyclodehydrogenations down to  $m/z$  728 (C<sub>57</sub>H<sub>2</sub>N<sub>3</sub><sup>+</sup>, Figure 2B). This indicates that ultimately **1-d<sub>6</sub><sup>+</sup>** zippers up to the azafullerane C<sub>57</sub>H<sub>2</sub>N<sub>3</sub><sup>+</sup> ( $m/z$  728), and, hence, the deuterium loss must have occurred in one of the intermediate stages. Remarkably, the appearance of the cyclodehydrogenation pattern in Figure 2B differs from that found for the corresponding cyclodehydrogenations of **1<sup>+</sup>** (Figure 1C). The two regions with near zero peak intensities during the zipping-up of **1<sup>+</sup>** ( $m/z$  750 - 746 and  $m/z$  736 - 732, Figure 1C) do contain low intensity peaks in the case of cyclodehydrogenations from **1-d<sub>6</sub><sup>+</sup>** ( $m/z$  756 - 750 and  $m/z$  740 - 738, Figure 2B). The presence of these near zero intensity regions in the case of **1<sup>+</sup>** are rationalized by the fact that cyclodehydrogenations from C<sub>57</sub>H<sub>27</sub>N<sub>3</sub> to C<sub>57</sub>H<sub>19</sub>N<sub>3</sub> and from C<sub>57</sub>H<sub>12</sub>N<sub>3</sub> to C<sub>57</sub>H<sub>6</sub>N<sub>3</sub> occur more facile. Apparently, in the case of **1-d<sub>6</sub><sup>+</sup>** due to the deuterium-isotope effect cyclodehydrogenation of <sup>2</sup>H<sub>b</sub> and <sup>3</sup>H<sub>c</sub> are less facile.

Note that under the applied MALDI TOF-MS conditions, no 'shrink-wrap' process, *i.e.* loss of either CN- or C<sub>2</sub>- fragments, is visible at a laser fluence of 2400. This denotes that the closure of the carbon surface is achieved under very mild conditions. Notwithstanding, from laser fluences > 2300 additional mass clusters are present at  $m/z$  774 and  $m/z$  1518 in the case of **1<sup>+</sup>** and at  $m/z$  780 and  $m/z$  1524 for **1-d<sub>6</sub><sup>+</sup>**.<sup>22</sup> These clusters are not due to an impurity in the precursors; they are absent in the spectra obtained after MALDI TOF-MS at low laser fluence (1900 - 2200). However, they appear in FAB-MS spectra (matrix *o*-nitro-phenyloctylether). These extra mass clusters are attributed to the occurrence of a competitive ion-molecule side-reaction followed by a disproportionation side-reaction. This is substantiated by the following results. In MALDI TOF-MS (laser fluence > 2300) besides cyclodehydrogenations, low intensity mass clusters at  $m/z$  1518 of **1<sup>+</sup>** and  $m/z$  1524 for **1-d<sub>6</sub><sup>+</sup>** are found indicative for cluster formation due to ion-molecule reactions between C<sub>57</sub>H<sub>33</sub>N<sub>3</sub><sup>+</sup>, C<sub>57</sub>H<sub>33</sub>N<sub>3</sub><sup>+</sup> and C<sub>57</sub>H<sub>32</sub>N<sub>3</sub><sup>+</sup>.<sup>23,24</sup> Subsequent disproportionation of the ion-molecule cluster in which a fragment of *circa* 15 a.m.u. (CH<sub>3</sub> or NH) is transferred, leads to two mass clusters centered at  $m/z$  774 and  $m/z$  745 for **1<sup>+</sup>** and similarly at  $m/z$  780 and  $m/z$  750 for **1-d<sub>6</sub><sup>+</sup>**.

The clusters at  $m/z$  774 and  $m/z$  780 are clearly visible in the same MALDI TOF mass spectra (Figure 1C and 2B). The presence of the other mass cluster can be inferred from the appearance of the pattern around  $m/z$  745 in the case of **1<sup>+</sup>** and  $m/z$  750 in the case of **1-d<sub>6</sub><sup>+</sup>**; unfortunately the patterns of the cyclodehydrogenation process and the disproportionation side-reaction coincide. This is substantiated by the *post-source-decay* (PSD) spectrum of **1<sup>+</sup>**, in which the  $m/z$  759 ion is isolated prior to TOF-MS analysis (laser fluence is 2400, Figure 3). The mass cluster at  $m/z$  774 is absent and the pattern around  $m/z$  745 looks much 'cleaner'. This PSD spectrum

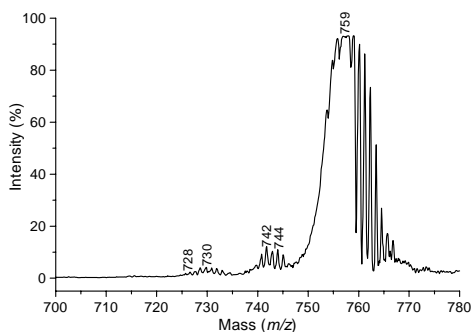


**Figure 3.** *Post-source-decay* MALDI TOF mass spectrum of  $1^+$  in the positive-ion mode at a laser fluence of 2400. Isolation of  $m/z$  759.

also shows that the ion-molecule reactions are competitive side-reactions and that all proper cyclodehydrogenations originate from the precursor ions.

In contrast to what was observed for the 'zipping-up' of the all-carbon/hydrogen  $C_{60}H_{30}$  precursor down to  $C_{60}$ ,<sup>14</sup> complete cyclodehydrogenation of  $1^-$  does *also* occur in the negative-ion mode. When the computed electron affinities (EA) of **1** and  $C_{60}H_{30}$  are compared [1.5 eV and 1.8 eV, respectively (AM1)], it is apparent that  $C_{60}H_{30}$  has the higher EA. This suggests that not the formation of the open-shell radical anion ( $1^{\cdot-}$ ), but the subsequent formation of the closed-shell anion  $C_{57}H_{32}N_3^-$  ( $[M-1]^-$ ) might facilitate cyclodehydrogenations in the negative-ion mode, probably since then delocalization of the charge is possible (Chart 3).

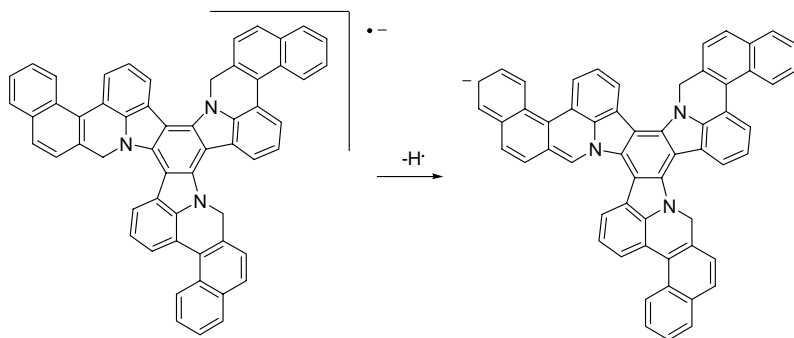


**Chart 3**

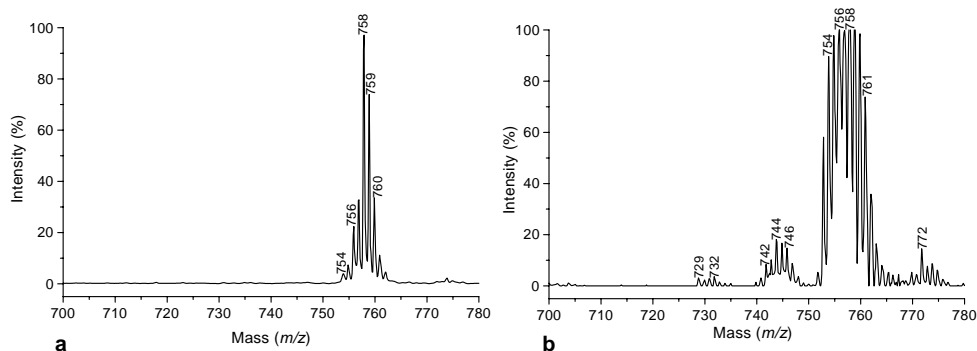


**Figure 4.** *In-source* MALDI TOF mass spectra of  $1^-$  in the negative-ion mode: **a.** laser fluence 2100, **b.** laser fluence of 2400.

The conversion of  $C_{57}H_{33}N_3^-$  ( $1^-$ ) into  $C_{57}H_{32}N_3^-$  *via* loss of  $H^-$  indeed appears to be facile in the negative-ion mode. Already at a laser fluence of 2100  $C_{57}H_{32}N_3^-$  ( $[M-H]^-$ ) is predominantly present (Figure 4A). Furthermore, two-fold  $H_2$  losses and ring closures occur, giving  $C_{57}H_{30}N_3^-$  and  $C_{57}H_{28}N_3^-$  [ $m/z$  758 (100%), 756 (28 %), 754 (8%)]. Again, cyclodehydrogenation proceed from  $1^-$  *via* radical anion intermediates and from  $C_{57}H_{32}N_3^-$  ( $[M-H]^-$ ;  $m/z$  758) *via* closed-shell anionic intermediates. The process *via* radical anionic species is again favored. Complete cyclodehydrogenation takes place at a laser fluence of 2400 giving the cyclodehydrogenation products down to  $m/z$  729 (Figure 4B). The occurrence of competitive ion-molecule and disproportionation side-reactions are also discernible in the negative-ion mode (laser fluence > 2300). This provides additional evidence that the ion-molecule reactions are indeed side-reactions. To establish that cyclodehydrogenations takes place from the precursor ions, PSD spectra in which both  $1^-$  ( $m/z$  759) or  $C_{57}H_{32}N_3^-$  ( $[M-1]^+$ ,  $m/z$  758) were isolated prior to TOF-MS analysis, were measured at different laser fluences. They are indeed nearly identical to the corresponding *in-source* spectra, with the difference that the mass cluster centered at  $m/z$  774 is absent. Hence, cyclodehydrogenations, *i.e.* intramolecular  $H_2$  loss and ring closure, originates from the precursor ions.

### 6.2.2 *Semi-empirical (AM1) and ab initio (B3LYP/6-31G\*\*) calculations*

In Chapter 4 it was shown that the driving force for the cyclodehydrogenation reactions to proceed with *regio*-chemical control is the steric congestion of the innermost hydrogen atoms.<sup>16</sup>

**Table 1.** *Semi-empirical* (AM1)  $\Delta H_f^\circ$  and  $\Delta H_r$  values (in kcalmol<sup>-1</sup>) for the conversion of C<sub>57</sub>H<sub>33</sub>N<sub>3</sub> (**1**) into C<sub>57</sub>H<sub>2</sub>N<sub>3</sub> (**11**) for both cationic and anionic species.<sup>a</sup>

Compound	Cations		Anions	
	$\Delta H_f^\circ$	$\Delta H_r$	$\Delta H_f^\circ$	$\Delta H_r$
C <sub>57</sub> H <sub>33</sub> N <sub>3</sub> ( <b>1</b> ) <sup>b</sup>	493.5		301.4	
C <sub>57</sub> H <sub>32</sub> N <sub>3</sub> ( <b>5</b> ) <sup>c</sup>	510.4	69.0	324.3	75.0
C <sub>57</sub> H <sub>26</sub> N <sub>3</sub> ( <b>6</b> )	644.5	134.1	441.2	116.9
C <sub>57</sub> H <sub>20</sub> N <sub>3</sub> ( <b>7</b> )	773.9	129.4	596.7	155.5
C <sub>57</sub> H <sub>14</sub> N <sub>3</sub> ( <b>8</b> )	934.8	160.9	705.2	108.5
C <sub>57</sub> H <sub>8</sub> N <sub>3ro</sub> ( <b>9</b> ) <sup>d</sup>	1038.8	104.0	796.4	91.2
C <sub>57</sub> H <sub>8</sub> N <sub>3rc</sub> ( <b>10</b> ) <sup>e</sup>	1029.9	95.1	789.3	84.1
C <sub>57</sub> H <sub>2</sub> N <sub>3</sub> ( <b>11</b> )	1146.8	108.0 <sup>d</sup> /116.9 <sup>e</sup>	889.4	93.0 <sup>d</sup> /100.1 <sup>e</sup>

<sup>a</sup> Only the thermodynamic most stable isomers are considered.<sup>b</sup> The radical cationic and anionic species of **1** are calculated at the UHF/AM1 level of theory, for the closedshell species of **1**:  $\Delta H_f^\circ = 357.2$  kcalmol<sup>-1</sup> (RHF/AM1). <sup>c</sup> **1**<sup>+</sup> → **6** + H;  $\Delta H_f^\circ(\text{H}) = 52.1$  kcalmol<sup>-1</sup>. <sup>d</sup> ro = ring-opened. <sup>e</sup> rc = ring-closed.

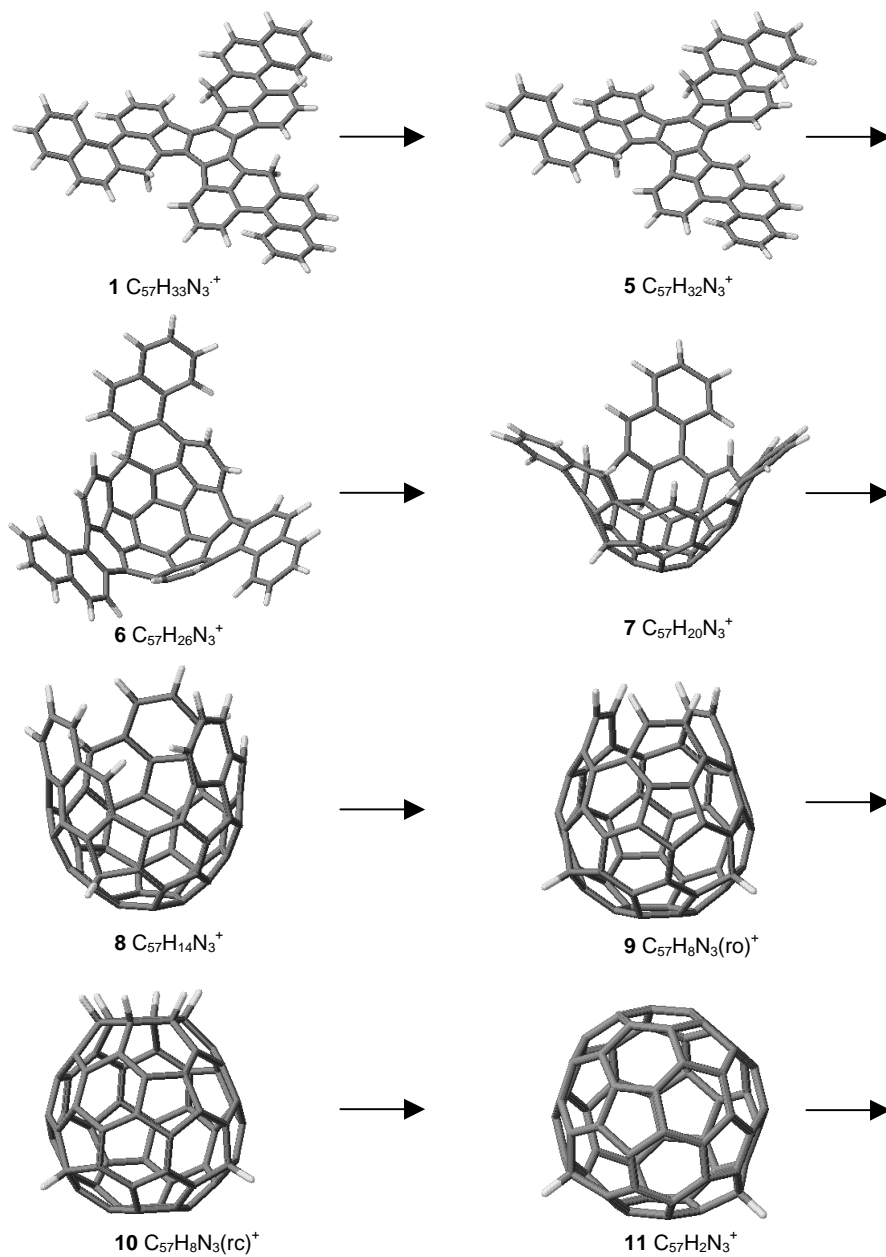
**Table 2.** *Ab initio* (B3LYP/6-31G\*\*)  $\Delta E_r$  values (in kcalmol<sup>-1</sup>) for the conversion of C<sub>57</sub>H<sub>32</sub>N<sub>3</sub> (**5**) into C<sub>57</sub>H<sub>2</sub>N<sub>3</sub> (**11**) for both cationic and anionic species.

	Cations	Anions
C <sub>57</sub> H <sub>32</sub> N <sub>3</sub> ( <b>5</b> ) → C <sub>57</sub> H <sub>26</sub> N <sub>3</sub> ( <b>6</b> )	112.2	108.6
C <sub>57</sub> H <sub>26</sub> N <sub>3</sub> ( <b>6</b> ) → C <sub>57</sub> H <sub>20</sub> N <sub>3</sub> ( <b>7</b> )	125.5	119.7
C <sub>57</sub> H <sub>20</sub> N <sub>3</sub> ( <b>7</b> ) → C <sub>57</sub> H <sub>14</sub> N <sub>3</sub> ( <b>8</b> )	115.7	102.1
C <sub>57</sub> H <sub>14</sub> N <sub>3</sub> ( <b>8</b> ) → C <sub>57</sub> H <sub>8</sub> N <sub>3ro</sub> ( <b>9</b> ) <sup>a</sup>	96.9	89.1
C <sub>57</sub> H <sub>14</sub> N <sub>3</sub> ( <b>8</b> ) → C <sub>57</sub> H <sub>8</sub> N <sub>3rc</sub> ( <b>10</b> ) <sup>b</sup>	84.3	82.3
C <sub>57</sub> H <sub>8</sub> N <sub>3ro</sub> ( <b>9</b> ) <sup>a</sup> → C <sub>57</sub> H <sub>2</sub> N <sub>3</sub> ( <b>11</b> )	64.7	39.4
C <sub>57</sub> H <sub>8</sub> N <sub>3rc</sub> ( <b>10</b> ) <sup>b</sup> → C <sub>57</sub> H <sub>2</sub> N <sub>3</sub> ( <b>11</b> )	52.0	46.2

<sup>a</sup> ro = ring-opened. <sup>b</sup> rc = ring-closed.

To validate that this is also the case here, both *semi-empirical* (RHF/AM1) and *ab initio* calculations (B3LYP/6-31G\*\*) were performed on the cations and anions of the products formed *via* the closed-shell pathway from ionic C<sub>57</sub>H<sub>32</sub>N<sub>3</sub> ( $m/\xi$  758). The main cyclodehydrogenation products, *i.e.* compounds formed after three-fold H<sub>2</sub> losses and ring closures are considered [C<sub>57</sub>H<sub>33</sub>N<sub>3</sub><sup>+</sup> (**1**), C<sub>57</sub>H<sub>32</sub>N<sub>3</sub><sup>+</sup> (**5**), C<sub>57</sub>H<sub>26</sub>N<sub>3</sub><sup>+</sup> (**6**), C<sub>57</sub>H<sub>20</sub>N<sub>3</sub><sup>+</sup> (**7**), C<sub>57</sub>H<sub>14</sub>N<sub>3</sub><sup>+</sup> (**8**), C<sub>57</sub>H<sub>8</sub>N<sub>3</sub><sup>+</sup> ring-opened (**9**), C<sub>57</sub>H<sub>8</sub>N<sub>3</sub><sup>+</sup> ring-closed (**10**) and C<sub>57</sub>H<sub>2</sub>N<sub>3</sub><sup>+</sup> (**11**)]. Similar calculations were performed for the corresponding

Synthesis by Design of the Novel Triaza-Fullerane  $C_{57}H_2N_3$



**Scheme 2.** Optimized (B3LYP/6-31G\*\*) geometries of the cationic intermediates obtained by cyclodehydrogenation of  $1^+$ .

anionic species. The B3LYP/6-31G\*\* optimized geometries of the cationic species of **1** and **5 - 11** are depicted in Scheme 2. In addition, the reaction enthalpies ( $\Delta H_r$ , *semi*-empirical methods Table 1) or the reaction energies ( $\Delta E_r$  when using *ab initio* methods, Table 2) are calculated (see Experimental Section). From the optimized geometries it can be deduced that indeed after each cyclodehydrogenation cycle the new innermost hydrogen atoms become sterically congested. Inspection of the  $\Delta H_r/\Delta E_r$  values (Table 1 and 2, respectively) shows that at both levels of theory formation of the ring-closed isomer  $C_{57}H_8N_3(rc)$  (**10**) instead of the ring-opened isomer  $C_{57}H_8N_3(ro)$  (**9**) is more favorable, and hence, 2 + 2 + 2 addition takes place.<sup>16</sup> The first three cyclodehydrogenation cycles, in which  $C_{57}H_{26}N_3$  (**6**),  $C_{57}H_{20}N_3$  (**7**) and  $C_{57}H_{14}N_3$  (**8**) are formed, are more endothermic than the following. This is in accordance with the fact that in these steps curvature is imposed.

### 6.3 Conclusions

The 'zipping up' process of the Schlegel-match triaza non-alternant PAH precursors,  $1^+/1^-$  and  $1-d_6^+/1-d_6^-$ , to closed carbon surfaces is achieved. Interestingly,  $C_{57}H_{33}N_3$  (**1**) and the ionic fullerenes  $C_{57}H_2N_3$  and  $C_{57}H_3N_3$  are more reactive than the corresponding carbon analogues ( $C_{60}H_{30}$ ,  $C_{60}$ ). This is apparent from the formation of  $[M-1]^+/[M-1]^-$  and the occurrence of competitive ion-molecule and subsequent disproportionation side-reactions. Complete cyclodehydrogenations yielding ionic  $C_{57}H_2N_3$  was possible both in the positive-ion and in the negative-ion mode. The consecutive character of the cyclodehydrogenation reactions is substantiated by PSD experiments, *semi*-empirical and *ab initio* calculations, and the cyclodehydrogenation behavior of a deuterated analogue  $1-d_6$ .

### 6.4 Experimental Section

All reactions were carried out under a  $N_2$  atmosphere. Solvents were dried and purified using standard procedures. Chemical shifts (in ppm) are given relative to TMS (0 ppm).  $J$  values are given in Hz. For the  $^1H$ -NMR spectrum multiplicity is denoted as following: s = singlet, d = doublet, t = triplet, dd = double doublet, m = multiplet.

#### Synthesis of **1**

A mixture of **4** (50 mg, 0.05 mmol),  $Pd(OAc)_2$  (11mg, 0.05 mmol),  $BnMe_3Nbr$  (23 mg, 2 mmol), and  $K_2CO_3$  (69 mg, 5 mmol) in DMA (8 ml) was stirred at 110°C for 12hr. The mixture was cooled to 23°C and the solid

was filtered off and washed with CH<sub>2</sub>Cl<sub>2</sub> and acetone. The solid was suspended in aqueous NaCN and stirred for 1 hr. The solid was filtered off and washed with water and acetone to give **1** as a yellow powder (37 mg, 61%). <sup>1</sup>H NMR (1,1,2,2-tetrachloroethane-*d*<sub>2</sub>, 26 °C, 300 MHz,  $\delta$  in ppm)  $\delta$  8.87 (d, 3 H, *J* 8.8 Hz), 8.20 (d, 3 H, *J* 8.6 Hz), 8.13 (d, 3 H, *J* 7.1 Hz), 7.92 (d, 3H, *J* 7.7 Hz), 7.86 (d, 3H, *J* 8.7 Hz), 7.43 - 7.62 (m, 12 H), 5.73 (6 H). MALDI-TOF MS:  $m/z$  758 (100%) [M<sup>+</sup>-H].

### Synthesis of **1-d**<sub>6</sub>

**1-d**<sub>6</sub> was prepared following the same procedure. <sup>1</sup>H NMR (1,1,2,2-tetrachloroethane-*d*<sub>2</sub>, 26°C, 300 MHz,  $\delta$  in ppm) 8.88 (d, 3 H, *J* 7.6 Hz), 8.20 (s, 3 H), 7.91 (d, 3 H, *J* 7.0 Hz), 7.84 (d, 3H, *J* 7.2 Hz), 7.54 - 7.62 (m, 9H), 5.71 (s, 6H). MALDI-TOF MS:  $m/z$  764 (100%) [M<sup>+</sup>-H]. Note that compounds **1** and **1-d**<sub>6</sub> readily oxidize into the corresponding amides, and must be kept under Ar. *Caution:* (CP)-PAH are potential genotoxic compounds.

### MALDI TOF-MS

Matrix-Assisted-Laser-Desorption-Ionisation (MALDI) Time-Of-Flight mass spectrometry (TOF-MS)<sup>25</sup> experiments were done using a Voyager-DE-RP MALDI-TOF mass spectrometer (Applied Biosystems/PerSeptive Biosystems, Inc., Framingham, MA, USA) equipped with delayed extraction.<sup>26</sup> A 337 nm UV N<sub>2</sub> laser producing 3ns pulses was used; the mass spectra were obtained in the linear and reflectron mode. One  $\mu$ l of a suspension of the sample in toluene was loaded on a gold-sample plate, the solvent was removed in warm air and the sample transferred to the vacuum of the mass spectrometer for analysis. *Post-source-decay* (PSD) experiments were obtained by adjusting the voltage applied to the reflector (Mirror Ratio setting). MALDI/PSD spectra record the fragment ions of spontaneously decomposing ions.

### Computational Methods

*Semi*-empirical computations (RHF/AM1 and UHF/AM1) were performed using MOPAC 7.0.<sup>27</sup> *Ab initio* calculations were performed at the B3LYP/6-31G\*\* level of theory using GAMESS-UK.<sup>28</sup> The geometries of the radical cationic species and radical anionic species of C<sub>57</sub>H<sub>33</sub>N<sub>3</sub> were optimized using the UB3LYP/6-31G\*\* methods. In the case of the *semi*-empirical AM1 method  $\Delta H_f$  is defined as  $\Delta \Delta H_f^\theta$ . Note that the experimental  $\Delta H_f^\theta$  value for H<sub>2</sub> (0.0 kcalmol<sup>-1</sup>) is used and  $\Delta H_f^\theta(\text{AM1, H}) = 52.1$  kcalmol<sup>-1</sup> (RHF/AM1: H<sub>2</sub> bond length = 0.667 Å; UHF/AM1: H<sub>2</sub><sup>+</sup> bond length = 0.979 Å). In the case of the *ab initio* calculations  $\Delta E_r = [E_{\text{total}}(\text{PAH} - 3\text{H}_2) + 3E_{\text{total}}(\text{H}_2)] - E_{\text{total}}(\text{PAH})$ .  $E_{\text{total}}(\text{H}_2)$  B3LYP/6-31G\*\* = -1.178538 a.u. with an optimized hydrogen-hydrogen bond distance of 0.742 Å. UB3LYP/6-31G\*\* = -1.178538 a.u. with an optimized hydrogen-hydrogen bond distance of 0.742 Å.

## References and notes

- (1) Hirsch, A.; Nuber, B. *Acc. Chem. Res.* **1999**, *32*, 795-804.
- (2) Guo, T.; Jin, C.; Smalley, R. E. *J. Phys. Chem.* **1991**, *95*, 4948-4950.
- (3) Pradeep, T.; Vijayakrishnan, V.; Santa, A. K.; Rao, C. N. R. *J. Phys. Chem.* **1991**, *95*, 10564-10565.
- (4) Nakamura, K.; Ishikawa, K.; Yamamoto, K.; Ohana, T.; Fujiiwara, S.; Koga, Y. *Phys. Chem. Chem. Phys.* **1999**, *1*, 2631-2633.
- (5) Hultman, L.; Stafström, S.; Czigány, Z.; Neidhardt, J.; Hellgren, N.; Brunell, I. F.; Suenaga, K.; Colliex, C. *Phys. Rev. Lett.* **2001**, *87*, 225503-1 - 2255034.
- (6) Hummelen, J. C.; Knight, B.; Pavlovich, J.; González, R.; Wudl, F. *Science* **1995**, *269*, 1554-1556.
- (7) Lamparth, I.; Nuber, B.; Schick, G.; Skiebe, A.; Grösser, T.; Hirsch, A. *Angew. Chem. Int. Ed. Engl.* **1995**, *34*, 2257-2259.
- (8) Keshavarz-K., M.; González, R.; Hicks, R. G.; Srdanov, G.; Srdanov, V. I.; Collins, T. G.; Hummelen, J. C.; Bellavia-Lund, C.; Pavlovich, J.; Wudl, F.; Holczer, K. *Nature* **1996**, *383*, 147-150.
- (9) Nuber, B.; Hirsch, A. *Chem. Commun.* **1996**, 1421-1424.
- (10) Kim, K.-C.; Hauke, F.; Hirsch, A.; Boyd, P. D. W.; Carter, E.; Armstrong, R. S.; Lay, P. A.; Reed, C. A. *J. Am. Chem. Soc.* **2003**, *25*, 4024-4025.
- (11) Tobe, Y.; Nakanishi, H.; Sonoda, M.; Wakabayashi, T.; Achiba, Y. *Chem. Commun.* **1999**, 1625-1626.
- (12) Bunz, U. H. F.; Rubin, Y.; Tobe, Y. *Chem. Soc. Rev.* **1999**, *28*, 107-119.
- (13) Boorum, M. M.; Vasil'ev, Y. V.; Drewello, T.; Scott, L. T. *Science* **2001**, *294*, 828-831.
- (14) Gómez-Lor, B.; Koper, C.; Fokkens, R. H.; Vlietstra, E. J.; Cleij, T. J.; Jenneskens, L. W.; Nibbering, N. M. M.; Echavarren, A. M. *Chem. Commun.* **2002**, 370-371.
- (15) Scott, L. T.; Boorum, M. M.; McMahon, B. J.; Hagen, S.; Mack, J.; Blank, J.; Wegner, H.; de Meijere, A. *Science* **2002**, *295*, 1500-1503.
- (16) Koper, C.; Ruiz, M.; de Frutos, Ó.; González-Cantalapiedra, E.; Fokkens, R. H.; Nibbering, N. M. M.; Cárdenas, D. J.; Santos, A.; Gómez-Lor, B.; Jenneskens, L. W.; Echavarren, A. M. *Chem. Eur. J* **2003**, *in press*.
- (17) Sarobe, M.; Fokkens, R. H.; Cleij, T. J.; Jenneskens, L. W.; Nibbering, N. M. M.; Stas, W.; Versluis, C. *Chem. Phys. Lett.* **1999**, *313*, 31-39.
- (18) Bicchi, V.; Palla, G. *Tetrahedron* **1986**, *42*, 5019-5024.
- (19) Robertson, N.; Parsons, S.; MacLean, E. J.; Coxal, R. A.; Mount, A. R. *J. Mat. Chem.* **2000**, *10*, 2043-2047.



- (20) The intensities of the peaks at odd mass are corrected for the presence of the <sup>13</sup>C- isotope of the peaks at even mass.
- (21) Kaizu, K.; Kohno, M.; Suzuki, S.; Shiromaru, H.; Moriwaki, T.; Achiba, Y. *J. Chem. Phys.* **1997**, *106*, 9954-9956.
- (22) This mass cluster is also discernible in the MALDI TOF-MS spectrum recorded at a laser fluence of 2300.
- (23) Becker, H.; Javahery, G.; Petrie, S.; Cheng, P. C.; Schwarz, H.; Bohme, D. K. *J. Am. Chem. Soc.* **1993**, *115*, 11636-11637.
- (24) Herod, A. A.; Stokes, B. J.; Hancock, P.; Kandiyoti, R.; Parker, J. E.; Johnson, C. A. F.; John, P.; Smith, G. *Journal of the Chemical Society, Perkin Transactions 2* **1994**, 499.
- (25) Karas, M.; Bahr, U.; Hillenkamp, F. *Int. J. Mass Spectrom. Ion Proc.* **1987**, *78*, 53-68.
- (26) Vestal, M. L.; Juhasz, P.; Martin, S. A. *Rapid Commun. Mass Spectrom.* **1995**, *9*, 1044-1050.
- (27) Dewar, M. J. S.; Zuebisch, E. G.; Healy, E. F.; Stewart, J. J. P. *J. Am. Chem. Soc.* **1985**, *107*, 3902-3909.
- (28) Guest, M. F.; van Lenthe, J. H.; Kendrick, J.; Schöffel, K.; Sherwood, P.; Harrison, R. J. *GAMESS-UK, a package of ab initio programs*, **1998**. With contributions from R. D. Amos, R. J. Buenker, H. J. J. van Dam, M. Dupuis, N. C. Handy, I. H. Hillier, P. J. Knowles, V. Bonacic-Koutecky, W. von Niessen, R. J. Harrison, A. P. Rendell, V. R. Saunders, A. J. Stone, D. J. Tozer, A. H. de Vries. It is derived from the original GAMESS code due to M. Dupuis, D. Spangler, J. Wendolowski, *NRCC Software Catalog, Vol. 1*, Program No. QG01 (GAMESS) **1980**.



# Part III

*Non-Alternant PAH as Sub-structures  
for Closed Carbon Surfaces*



# CHAPTER 7

## Redox Properties of Non-Alternant Cyclopenta-Fused Polycyclic Aromatic Hydrocarbons

### Abstract

The redox properties of 23 PAH, *mono*- and *bis*-CP-PAH were characterized using Cyclic Voltammetry (CV). The results show that external fusion of a cyclopenta-moiety leads to high electron affinities. A linear correlation between the LUMO energy derived from Hückel Molecular Orbital (HMO) theory and the first reduction potential is rationalized assuming that the cyclopenta-moiety acts as an electron-withdrawing *peri*-substituent with  $\sigma_m$   $0.4 \pm 0.07$ . It is proposed that upon reduction  $6\pi$  cyclopentadienide sub-structures are formed. The interpretations are validated by *ab initio* calculations [(U)B3LYP/6-31G\*\*, (U)B3LYP/DZP++ and CTOCD-DZ/6-31G\*\*].

## 7.1 Introduction

One of the most intriguing properties of the fullerenes  $C_{60}$  and  $C_{70}$  are their high and similar electron affinities (*ca.* 2.7 eV).<sup>1,2</sup> Both  $C_{60}$  and  $C_{70}$  were found to accept up to six electrons under mild conditions,<sup>3-5</sup> which renders these molecules n-type materials. The tendency to form hexa-anions was initially rationalized by recognizing that  $C_{60}$  and  $C_{70}$  consisted of several perylene units (3, Chart 1). The perylene sub-structures were considered as  $4n\pi$ -electron perimeter systems, which upon reduction with two electrons form  $6\pi$ -electron 'cyclopentadienide' sub-structures.<sup>6</sup> However, in this case a dodeca-anion is expected for  $C_{60}$  ( $C_{60}^{12-}$ ). A group theoretical analysis, however, shows that  $C_{60}$  is the first of an infinite family of fullerene isomers with six low lying acceptor orbitals, split into two sets of degenerate orbitals ( $t_{1u} + t_{1g}$ ), spanning translational and rotational symmetries and derived from bonding orbitals of the pentagons.<sup>7,8</sup>

The important role of the pentagons is also revealed by a comparison of the aromatic properties of  $C_{60}$  and  $C_{70}$ , using the magnetic criterion.  $C_{60}$  is less aromatic than  $C_{70}$ , which is rationalized by the larger fractional contribution of the paramagnetic five-membered rings, as  $C_{60}$  is composed of 12 pentagons and 20 hexagons and  $C_{70}$  of 12 pentagons and 25 hexagons.<sup>9-11</sup> On the other hand, the hexa-anion of  $C_{60}$  ( $C_{60}^{6-}$ ) shows increased aromaticity compared to the hexa-anion of  $C_{70}$  ( $C_{70}^{6-}$ ). This is attributed to the fact that the added electrons reduce the paramagnetic effect of the five-membered rings.<sup>12,13</sup> Fullerene chemistry, consequently, revived the interest in (cyclopenta-fused) polycyclic aromatic hydrocarbons [(CP)-PAH], *i.e.* CP-PAH are now regarded as key sub-structures for fullerenes and their chemistry.<sup>14-16</sup>

For their use as model compounds, it is of importance to understand the effect of peripheral cyclopenta-fusion to an alternant PAH core. Since a large set of *mono*- and *bis*-CP-PAH have been prepared in our laboratory,<sup>17-19</sup> a systematic study of the electronic properties employing cyclic voltammetry (CV) has become possible.

In this Chapter we study the redox properties of the *mono*- and *bis*-CP-PAH displayed in Chart 1. It will be shown that PAH with externally-fused cyclopenta-moieties are readily reduced and thus possess high electron affinities. In contrast to previous reports,<sup>20,21</sup> a linear correlation is found between the LUMO energies derived from HMO theory and the first reduction potential. This can be interpreted as if the cyclopenta-moiety in *mono*- and *bis*-CP-PAH acts as an electron-withdrawing substituent. This is corroborated by determination of the Hammett constant  $\sigma_m$  for the cyclopenta-moiety in structurally different CP-PAH. It is shown that upon reduction the additional electron will be mainly located in the cyclopenta-moiety leading to a  $6\pi$  cyclopentadienide sub-structure.

Redox Properties of Cyclopenta-Fused PAH

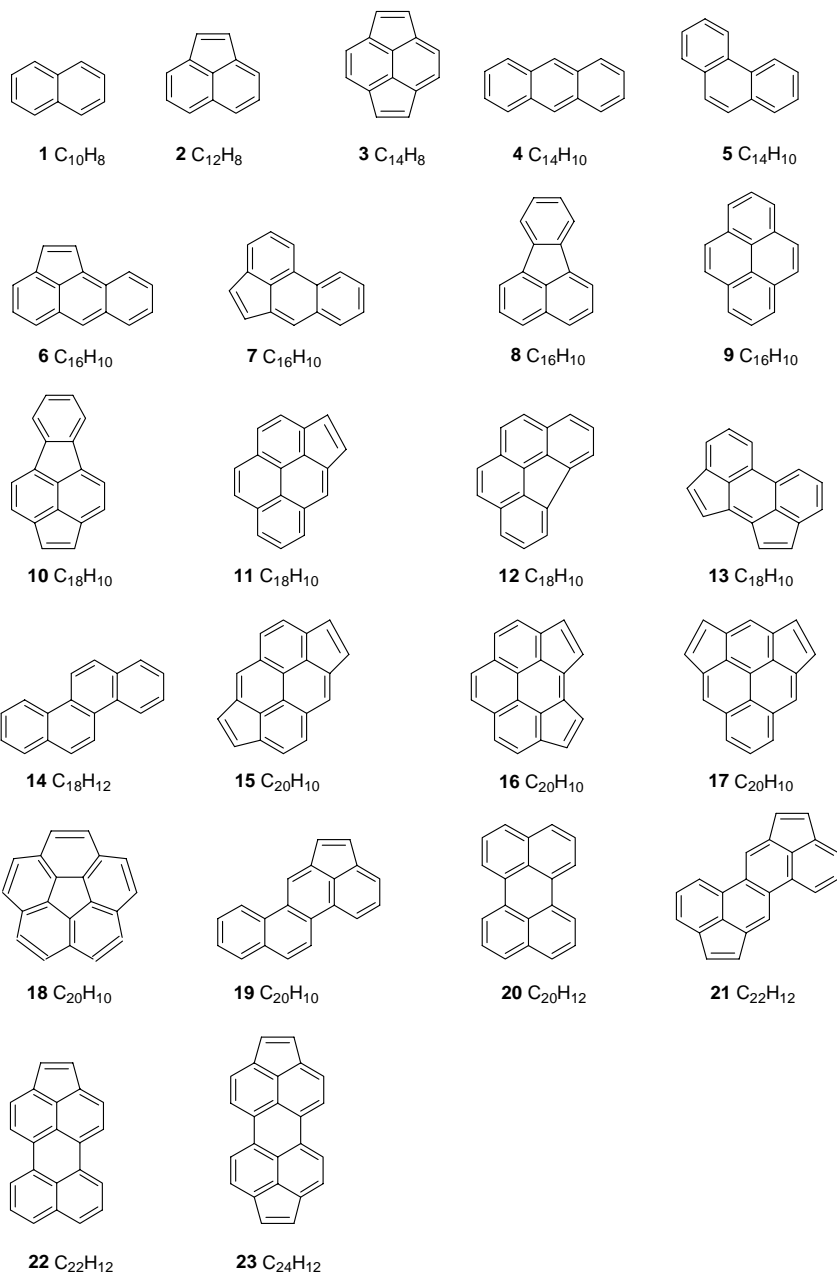
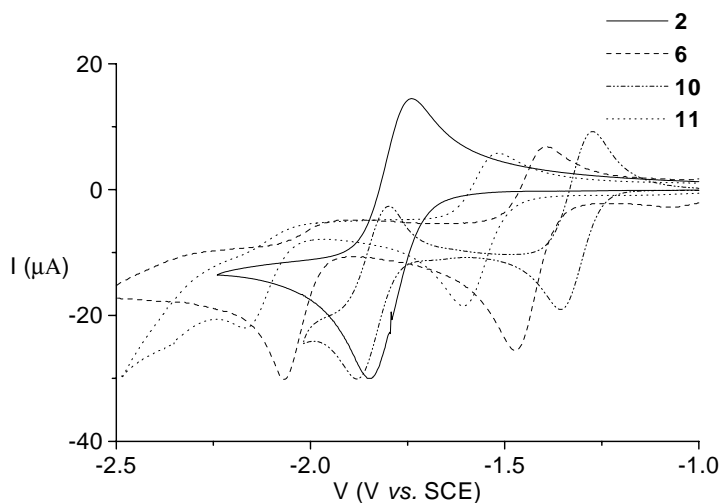


Chart 1

## 7.2 Results & Discussion

### 7.2.1 Cyclic voltammetry

Cyclic voltammograms of the alternant PAH **1**, **4**, **5**, **9**, **14** and **20**, their non-alternant *mono*- and *bis*-cyclopenta-fused congeners **2**, **3**, **6** - **8**, **10**, **11**, **13**, **15** - **17**, **19** and **21** - **23**, and the internally cyclopenta-fused PAH **12** and **18** (Chart 1) were measured in CH<sub>3</sub>CN and the results are compiled in Table 1 (see also Experimental Section). As an illustration, the cyclic voltammograms of compounds **2**, **6**, **10** and **11** are presented in Figure 1. Although the anodic behavior of the (non)-alternant PAH **1** - **23** is limited, *i.e.* all compounds possess one *irreversible* half-wave oxidation potential [ $E_{\text{onset}}(0/+1)$  in V *vs.* SCE] (Table 1 and see Experimental Section), their cathodic behavior is considerably more varied.



**Figure 1.** Reduction waves of **2**, **6**, **10** and **11** (in V *vs.* SCE, scan rate 50 mVs<sup>-1</sup>).

All available (non)-alternant PAH possess a (*pseudo*)-*reversible* first half-wave reduction potential [ $E_{1/2}(0/-1)$  in V *vs.* SCE], each with a  $\Delta E$  value ( $= E_{\text{pc}} - E_{\text{pa}}$  in V see Experimental Section) that corresponds to a one-electron process, *i.e.* the conversion of the neutral (non)-alternant PAH into its radical anion (Table 1). It is clear that reduction [ $E_{1/2}(0/-1)$ ] of non-alternant PAH containing externally-fused pentagons (*cf.* *mono*-CP-PAH **2**, **6**, **7**, **10**, **11**, **19** and **22**, and, *bis*-CP-PAH **3**, **13**, **15** -



## Redox Properties of Cyclopenta-Fused PAH

**Table 1.** Reduction and oxidation potentials for the alternant PAH and non-alternant *mono*- and *bis*-CP-PAH depicted in Chart 1 and their Hückel  $\epsilon_{\text{HOMO}}$  and  $\epsilon_{\text{LUMO}}$  energies.

Point group	$E_{1/2}(0/-1)$ (V vs. SCE)	$\Delta E$ (V)	$E_{1/2}(-1/-2)$ (V vs. SCE)	$\Delta E$ (V)	$\epsilon_{\text{LUMO}}$ HMO ( $\beta$ )	$E_{\text{onset}}(0/+1)$ (V vs. SCE)	$\epsilon_{\text{HOMO}}$ HMO ( $\beta$ )
1	$D_{2b}$	-2.66			-0.618	1.61	0.618
2	$C_{2v}$	-1.80			-0.285	1.29	0.638
3	$D_{2b}$	-1.06	-1.64	0.11	0.000	1.25	0.414
4	$D_{2b}$	-2.10			-0.414	1.23	0.414
5	$C_{2v}$	-2.62			-0.605	1.44	0.605
6	$C_s$	-1.47	-2.06 <sup>a</sup>	<i>irrev</i>	-0.187	0.83	0.517
7	$C_s$	-1.81			-0.270	1.36	0.586
8	$C_{2v}$	-1.92			-0.371	1.46	0.618
9	$D_{2b}$	-2.22	<sup>b</sup>		-0.445	1.06	0.445
10	$C_{2v}$	-1.33	-1.86	0.11	-0.099	1.20	0.494
11	$C_s$	-1.56	-2.22 <sup>a</sup>	<i>irrev</i>	-0.225	1.26	0.539
12	$C_{2v}$	-1.84			-0.378	1.44	0.618
13	$C_{2v}$	-1.33	-1.85 <sup>a</sup>	<i>irrev</i>	-0.058	1.30	0.597
14	$C_2$	-2.41			-0.520	1.33	0.520
15	$C_{2b}$	-1.15	-1.63	0.07	-0.051	0.86	0.498
16	$C_{2v}$	-1.02	-1.54	0.10	-0.040	0.86	0.454
17	$C_{2v}$	-1.32	-2.06 <sup>a</sup>	<i>irrev</i>	-0.163	1.26	0.593
18	$C_{5v}$	-1.99 <sup>c</sup>					
	$D_{5b}$				-0.477		0.738
19	$C_s$	-1.70	-2.26 <sup>a</sup>	<i>irrev</i>	-0.263	1.26	0.559
20	$D_2$	-1.81			-0.347	0.85	0.145
21	$C_{2b}$	-1.45	-1.78	0.08	-0.128	1.36	0.570
22	$C_{2v}$	-1.26	-1.78	0.07	-0.165	0.86	0.491
23	$D_{2b}$	-0.93	-1.22	0.12	-0.000	0.86	0.508

<sup>a</sup>  $E_{\text{onset}}(-1/-2)$ ; see Experimental Section. <sup>b</sup> Not detected in  $\text{CH}_3\text{CN}$ , due to available potential window. <sup>c</sup> See also <sup>23</sup>

17, 21 and 23) occurs more readily than reduction of related PAH either lacking the peripheral cyclopenta-moiety (*cf.* compounds 1, 4, 5, 8, 9, 14 and 20) or containing an internally-fused cyclopenta-moiety [*cf.* compounds 8, 12 and 18 (Table 1)]. A comparison of the  $E_{1/2}(0/-1)$  values of related *mono*- and *bis*-CP-PAH (*cf.* compounds 2 *vs.* 3, 7 *vs.* 13, 11 *vs.* 15 - 17, 19 *vs.* 21, and 22 *vs.* 23 in Table 1), furthermore shows that adding a second cyclopenta-moiety renders radical anion formation even more facile. Notice, however, that cyclopenta-fusion topology in the case of isomeric *bis*-CP-PAH does affect the reduction potentials [*cf.*  $E_{1/2}(0/-1)$  of 11 *vs.* 15 - 17 in Table 1]. Since the half-wave reduction potential  $E_{1/2}(0/-1)$  will be proportional to the gas-phase electron affinities (EA), *i.e.*  $E_{1/2}(0/-1) \propto EA$ ,<sup>2</sup> the *mono*- and *bis*-CP-PAH in Chart 1 possess electron affinities that are higher than, for example, corannulene (18) but are still significantly smaller than that of  $C_{60}$  (*cf.*  $E_{1/2}(0/-1)$  -0.26 V *vs.* SCE<sup>2</sup>).

Besides the facile first reduction [ $E_{1/2}(0/-1)$ ] of the *mono*- and *bis*-CP-PAH depicted in Chart 1, various representatives also display a second (*pseudo*)-reversible (compounds 3, 10, 15, 16 and 21 - 23) or irreversible (compounds 6, 11, 13, 17 and 19) half-wave reduction potential [ $E_{1/2}(-1/-2)$ ] that corresponds to the conversion of the radical anion into its related *bis*-anion within the accessible potential window (see Experimental Section). For the sub-series,  $E_{1/2}(-1/-2)$  in V *vs.* SCE,  $\Delta E$  ( $E_{pc} - E_{pa}$  in V) and  $E_{onset}(-1/-2)$  in V *vs.* SCE values, are reported in Table 1 (see also Experimental Section). The results show that the reduction of the radical anion to the *bis*-anion again occurs more readily for the *mono*- and *bis*-CP-PAH.

### 7.2.2 Applicability of Hückel theory

In standard Hückel theory [equal  $\alpha$  (Coulomb integral) and equal  $\beta$  (exchange integral)], the HOMO and LUMO orbitals of alternant PAH are symmetrical positioned around the  $\alpha$ -level. Hence, the first half-wave reduction potentials [ $E_{1/2}(0/-1)$  in V *vs.* SCE] show a linear correlation with the LUMO and the first half-wave oxidation potentials [ $E_{1/2}(0/+1)$  in V *vs.* SCE] give a correlation with the HOMO energy of the parent neutral PAH [applying Koopmans theorem ( $-\epsilon_{LUMO} \propto EA$  and  $-\epsilon_{HOMO} \propto IP$ )<sup>24,25</sup>].

In contrast, for non-alternant PAH containing odd-membered rings similar correlations were absent.<sup>20,21</sup> This was attributed to the fact that at the standard Hückel level of theory, non-alternant PAH have energy levels that are not symmetrically disposed about the  $\alpha$  level, and, even more importantly, atomic  $\pi$  charge densities that deviate from unity. In this case, the assumption of equal  $\alpha$  in standard Hückel theory is untenable.<sup>25</sup> Indeed, for non-alternant PAH, satisfactory linear correlations between  $E_{1/2}(0/-1)$  *vs.*  $-\epsilon_{LUMO}$  could be obtained only when a modified Hückel model was applied in which the Coulomb integrals  $\alpha$  were adjusted iteratively to self-consistency

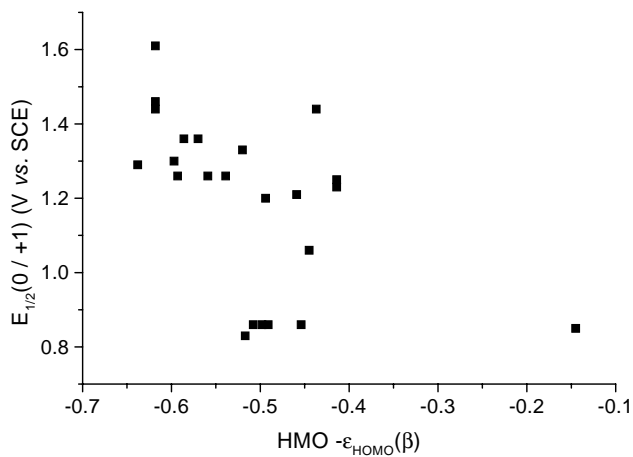


**Figure 2.** Correlation between  $E_{1/2}(0/+1)$  (V vs. SCE) of the PAH, *mono*- and *bis*-CP-PAH (Chart 1) and their Hückel  $-\epsilon_{HOMO}$  energies (Table 1).

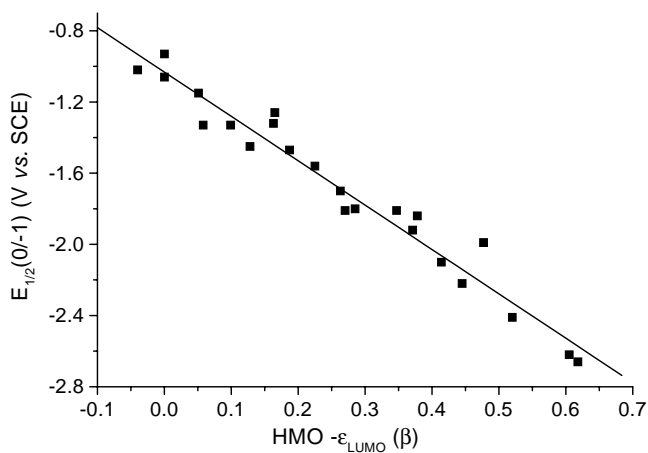


**Figure 3.** Linear correlation between  $E_{1/2}(0/-1)$  (V vs. SCE) of the PAH, *mono*- and *bis*-CP-PAH (Chart 1) and their Hückel  $\epsilon_{LUMO}$  energies (Table 1).

with  $\pi$  charge densities ( $\omega$  technique).<sup>21,26</sup> We therefore anticipated that no linear correlation in the case of *mono*- and *bis*-CP-PAH will be found between  $E_{1/2}(0/-1)$  vs.  $-\epsilon_{\text{LUMO}}$  and  $E_{\text{onset}}(0/+1)$  vs.  $-\epsilon_{\text{HOMO}}$  computed using standard Hückel theory. Indeed, no correlation is obtained between  $E_{1/2}(0/+1)$  and the standard Hückel  $-\epsilon_{\text{HOMO}}$  energy; a scatter plot is obtained (Figure 2).

Unexpectedly, however, a satisfactory linear correlation was obtained between the  $E_{1/2}(0/-1)$  values of **1** - **23** (Chart 1) and their standard Hückel  $-\epsilon_{\text{LUMO}}$  energies [cf. equation 1 in which  $\beta_0$  represents the effective resonance integral between two neighboring  $2p_\pi$  orbitals, and  $C$  a solvation term,  $r^2 = 0.958$  with  $\beta_0 = -2.49$  eV and  $C = -1.03$  (Figure 3 and Table 1)].

$$E_{1/2}(0/-1) = -\beta_0\epsilon_{\text{LUMO}} + C \quad (1)$$

Remarkably, this linear correlation clearly resembles that reported *many years ago* for *only* alternant PAH ( $\beta_0 = -2.37$  eV and  $C = -0.92$ ).<sup>25</sup> A similar, albeit less reliable, correlation is found when the alternant parent PAH species are left out ( $r^2 = 0.916$  with  $\beta_0 = -2.16$  eV and  $C = -1.07$ ). Again, the effective  $\beta_0$  value and solvation term  $C$  are in agreement with those obtained using Eqn. 1. Hence, standard Hückel theory correctly describes both qualitatively and *semi*-quantitatively the properties of *mono*- and *bis*-CP-PAH with regard to their first reduction process.

### 7.2.3 Peripheral pentagons in *mono*- and *bis*-CP-PAH act as a substituent

A rationalization for this intuitively unexpected outcome is suggested by the near constant shift of  $E_{1/2}(0/-1)$  in going from the alternant PAH to the related non-alternant CP-PAH [ $\Delta E_{\text{mono-CP-PAH}}$  ca. 0.5 - 0.7 V, Table 2 ]. Amongst the whole series, three CP-PAH display the largest  $\Delta E_{\text{mono-CP-PAH}}$  values, *viz.* acenaphthylene (**2**), acephenanthrylene (**7**) and benzo[*j*]acephenanthrylene (**19**). In analogy, the shift in  $E_{1/2}(0/-1)$  upon annelation of a second cyclopenta-moiety [ $\Delta E_{\text{bis-CP-PAH}} = E_{1/2}(0/-1)_{\text{bis-CP-PAH}} - E_{1/2}(0/-1)_{\text{mono-CP-PAH}}$ ] is tabulated (Table 2). Again, for most *bis*-CP-PAH similar values are found (ca. 0.3 - 0.5 V), with the exception of pyracylene (**3**) [ $\Delta E_{\text{bis-CP-PAH}} = 0.74$  V]. This similar positive shift suggests that annelation of the cyclopenta-moiety perturbs the core of the topologically different alternant PAHs in a systematic fashion and, hence, that the cyclopenta-moiety primarily acts as a *peri*-substituent. Notice that the  $\Delta E_{\text{bis-CP-PAH}}$  values are significantly smaller than the  $\Delta E_{\text{mono-CP-PAH}}$  values and that the CP-PAH with an internal pentagon all possess nearly similar  $E_{1/2}(0/-1)$  [**8**: -1.92 V, **12**: -1.84 V and **18**: -1.99 V].

To establish if peripherally annelated cyclopenta-moieties indeed act as *peri*-substituents we determined the Hammett substituent constant  $\sigma_m$  for this perimeter annelated CP-moiety. For

**Table 2.** Relationship between  $E_{1/2}$  (0/-1) values of PAH and the related *mono*-CP-PAH and *bis*-CP-PAH (V vs. SCE).

PAH	$E_{1/2}(0/-1)$ (V) vs. SCE	CP- PAH	$E_{1/2}(0/-1)$ (V) vs. SCE	$\Delta E_{mono-CP-}$ $E_{PAH}^a$	<i>bis</i> -CP- PAH	$E_{1/2}(0/-1)$ (V) vs. SCE	$\Delta E_{bis-CP-PAH}^b$
<b>1</b>	-2.66	<b>2</b>	-1.80	0.86	<b>3</b>	-1.06	0.74
<b>4</b>	-2.10	<b>6</b>	-1.47	0.63			
<b>5</b>	-2.62	<b>7</b>	-1.81	0.81	<b>13</b>	-1.33	0.40
<b>8</b>	-1.92	<b>10</b>	-1.33	0.59			
<b>9</b>	-2.22	<b>11</b>	-1.56	0.66	<b>15</b>	-1.15	0.41
					<b>16</b>	-1.02	0.54
					<b>17</b>	-1.32	0.24
<b>14</b>	-2.41	<b>19</b>	-1.70	0.71	<b>21</b>	-1.45	0.25
<b>20</b>	-1.81	<b>22</b>	-1.26	0.55	<b>23</b>	-0.93	0.33

<sup>a</sup>  $\Delta E_{1/2}(0/-1)_{mono-CP-PAH} - \Delta E_{1/2}(0/-1)_{PAH}$ ; <sup>b</sup>  $\Delta E_{1/2}(0/-1)_{bis-CP-PAH} - \Delta E_{1/2}(0/-1)_{mono-CP-PAH}$

**Table 3.**  $E_{onset}$  (0/-1) values (in V vs. SCE) of the *mono*-substituted derivatives for **1**(1-X), **4**(9-X), **8**(3-X) and **9**(1-X) (Chart 2).

X	$\sigma_m$	$\sigma_p$	$E_{onset}$ (0/-1)			
			<b>1</b> (1-X)	<b>4</b> (1-X)	<b>8</b> (1-X)	<b>9</b> (1-X)
H	0	0	-2.54	-2.02	-1.81	-2.13
NH <sub>2</sub>	-0.16	-0.66	<sup>a</sup>	-2.14	-1.20	-2.27
CH <sub>3</sub>	-0.06	-0.14	-2.59	-2.05	<sup>b</sup>	<sup>b</sup>
C <sub>2</sub> H <sub>5</sub>	-0.08	-0.13	-2.73	<sup>b</sup>	<sup>b</sup>	-2.18
C $\equiv$ CH	0.20	0.23	-2.20	-1.72	-1.59	-1.87
COCH <sub>3</sub>	0.36	0.47	-1.85	<sup>b</sup>	-1.41	-1.47
NO <sub>2</sub>	0.71	0.81	-1.11	-1.01	-0.89	-1.07
CP			-1.70	-1.37	-1.24	-1.49

<sup>a</sup> Not measured due to available potential window (see Experimental Section). <sup>b</sup> Not determined

the construction of the Hammett plots (Eqn. 2)<sup>27</sup> the first half-wave reduction potential of *mono*-substituted derivatives of PAH **1**(1-X), **4**(9-X), **8**(3-X) and **9**(1-X) was measured using CV (Charts 1 and 2 and Table 3).<sup>28</sup> Unfortunately, most *mono*-substituted PAH gave either a (*pseudo*)-reversible or irreversible first reduction wave. Therefore, instead of  $E_{1/2}(0/-1)$  or  $E_{pc}(0/-1)$  values,  $E_{onset}(0/-1)$  values were used, which give a reliable estimate of the substituent effect [see Experimental Section and Table 3].

$$(n/0.059) \cdot E_{\text{onset}}(X) = \rho\sigma + (n/0.059) \cdot E_{\text{onset}}(X = H) \quad (2)$$

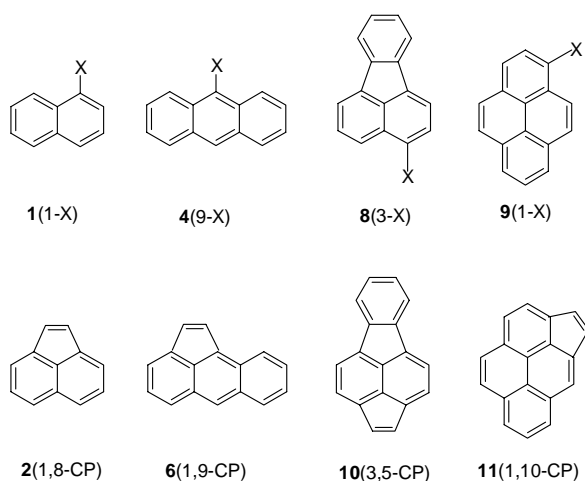


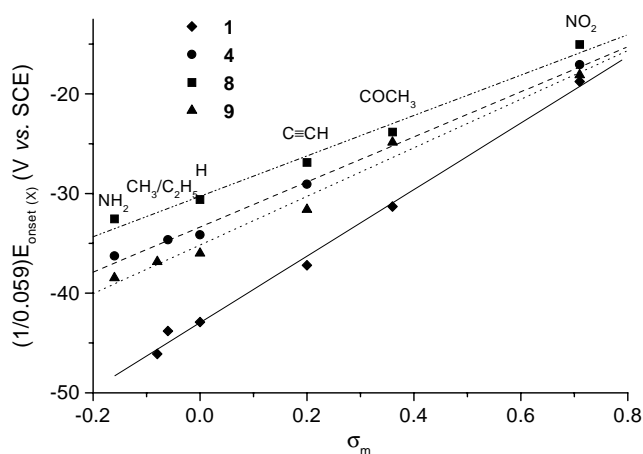
## Chart 2

For all *mono*-substituted derivatives of compounds **1(1-X)**, **4(9-X)**, **8(3-X)** and **9(1-X)** the  $E_{\text{onset}}(0/-1)$  values were plotted against the appropriate substituent constants  $\sigma_m$ , which mainly contains inductive effects.<sup>29</sup> The Hammett relationship with  $\sigma_m$  gives an excellent linear correlation over the complete  $\sigma$  – range [Figure 4, *cf.* Table 4 for correlation coefficients ( $r^2$ )]. The quality of the linear free energy relationship between  $E_{\text{onset}}(0/-1)$  and  $\sigma_m$  is substantiated by the intercepts, which correspond to the  $E_{\text{onset}}(0/-1)$  values of the parent PAH **1(1-H)**, **4(9-H)**, **8(3-H)** and **9(1-H)** (Charts 1 and 2). They are indeed in close agreement with the experimental values (Tables 3 and 4). The Hammett parameters  $\rho$ , which are positive, *i.e.* reduction will be facilitated by electron-withdrawing substituents X, reflects the sensitivity of  $E_{\text{onset}}(0/-1)$  towards substitution (Table 4). For the group of *mono*-substituted derivatives of **4(9-X)**, **8(3-X)** and **9(1-X)** similar  $\rho$  values are found, which are comparable to the  $\rho$  values reported in literature for Hammett relations between the first reduction potential of alkyl-substituted PAHs and  $\sigma^*$ .<sup>30,31</sup> For the *mono*-substituted 1-naphthalenes **1(1-X)**, however, a significantly larger  $\rho$  value (factor 1.5) is found. This

**Table 4.** Hammett parameters obtained for  $E_{\text{onset}}(0/-1)$  (in V vs. SCE) vs.  $\sigma_m$  for series **1**, **4**, **8** and **9** and  $\sigma_m$  values for **2**, **6**, **10** and **11**.

	$r^{2,a}$	$a^b$	$\rho$ (V) <sup>c</sup>	$s(\rho)^d$		$\sigma$	$s(\sigma)^d$
<b>1</b> $\sigma_m$	0.995	-2.54	2.0	0.09	<b>2</b>	0.42	0.04
<b>4</b> $\sigma_m$	0.995	-1.97	1.3	0.05	<b>6</b>	0.45	0.03
<b>8</b> $\sigma_m$	0.985	-1.79	1.2	0.09	<b>10</b>	0.46	0.05
<b>9</b> $\sigma_m$	0.983	-2.07	1.4	0.09	<b>11</b>	0.41	0.04

<sup>a</sup> Correlation coefficient. <sup>b</sup>  $a$  is  $E_{\text{onset}}(0/-1)$  for X = H (in V vs. SCE) see also Table 2. <sup>c</sup> Slope  $\times 0.059$ . <sup>d</sup> Standard deviation.

**Figure 4.** Hammett plots of **1**(1-X), **4**(9-X), **8**(3-X) and **9**(1-X) (Chart 2);  $(1/0.059) E_{\text{onset}}(0/-1)$  (V vs. SCE) vs.  $\sigma_m$  (see Table 3).

indicates that substituents in the case of **1**(1-X) exert a stronger electronic effect (enhanced interactions, *vide infra*).

From the linear free energy relationships and the  $E_{\text{onset}}(0/-1)$  of the CP-PAH **2**, **6**, **10** and **11** (Charts 1 and 2),  $\sigma_m$  values for the externally-fused cyclopenta-moiety were estimated. Interestingly, despite the substantial structural variation of **2**, **6**, **10** and **11** the  $\sigma_m$  values are 0.42, 0.45, 0.41 and 0.46, respectively; they are nearly identical! This gives compelling evidence that the externally-fused cyclopenta-moiety indeed acts as a *peri*-substituent.<sup>32</sup> The similar  $\sigma_m$  values

derived for these different CP-PAH, suggest that the cyclopenta-moiety is well described using a substituent constant that mainly consists of inductive effects.

### 7.2.4 Hückel Theory *versus* *mono*- and *bis*-CP-PAH

The satisfactory correlation between the Hückel  $-\varepsilon_{\text{LUMO}}$  and  $E_{1/2}(0/-1)$  demonstrates that standard HMO theory is capable to describe the reduction behavior of *mono*-CP-PAH and *bis*-CP-PAH. The annelation of a cyclopenta-moiety to an alternant PAH core induces a constant positive shift to  $E_{1/2}(0/-1)$ . This indicates that for different PAH, peripheral cyclopenta-fusion results in a comparable stabilization of the LUMO levels of the CP-PAH with respect to those of the alternant parent PAH cores.

For all compounds (*mono*-CP-PAH and *bis*-CP-PAH), the LUMO of CP-PAH is an *in-phase* (bonding) combination of the LUMO of ethene and the LUMO of the parent (CP)-PAH. The energy of the LUMO of the *mono*- and *bis*-CP-PAH is lower than that of its contributors. This is illustrated in Figure 5 for the series naphthalene (**1**), acenaphthylene (**2**) and pyracylene (**3**).

The stabilization of the resulting *in-phase* combination depends on the relative energies of the two parent LUMO's and the extent of their interaction. Thus, the larger  $\Delta E_{\text{mono-CP-PAH}}$  value observed for **2**, **7** and **19** and the larger  $\Delta E_{\text{bis-CP-PAH}}$  for **3** is a result of the high LUMO energies of the parent PAH, naphthalene (**1**), phenanthrene (**5**) and chrysene (**14**) ( $-0.618\beta$ ,  $-0.605\beta$  and  $-0.520\beta$ , respectively) compared to those of the other PAH presented in Chart 1 (range:  $-0.347\beta$  to  $-0.445\beta$ ). As a consequence, the smaller difference in energy from the LUMO of ethene [ $\varepsilon_{\text{LUMO}} = -1.000\beta$ ] enhances the interaction. This is in line with the larger  $\rho$  value found for the Hammett relation of the *mono*-substituted 1-naphthalenes **1**(1-X) (see section 7.2.3).<sup>33</sup> The effect of the relative energies of the parent LUMO's is also apparent from the smaller value found for  $\Delta E_{\text{bis-CP-PAH}}$  compared to  $\Delta E_{\text{mono-CP-PAH}}$  (Figures 5A *vs.* 5B and Table 2). Owing to the stabilization of the LUMO after incorporation of the first cyclopenta-moiety, the interaction between this LUMO and the LUMO of ethene will be smaller. Hence, the effect of the second cyclopenta-moiety on the reduction potential is smaller than that of the first cyclopenta-moiety.

The straightforward interaction between the LUMO levels of the alternant PAH and ethene fragments is visualized by varying the  $\beta$  value of the carbon-carbon bonds ( $0 < \beta < 1$ ) connecting the aromatic core and the etheno-bridge of acenaphthylene (**2**, Figure 6). The results unequivocally show the increase in stabilization of the LUMO level upon increase in strength of interaction. An important observation is that no significant shifting of the unoccupied orbitals, and hence, no disruption of the original orbital structure of the parent PAH occurs.



## Redox Properties of Cyclopenta-Fused PAH

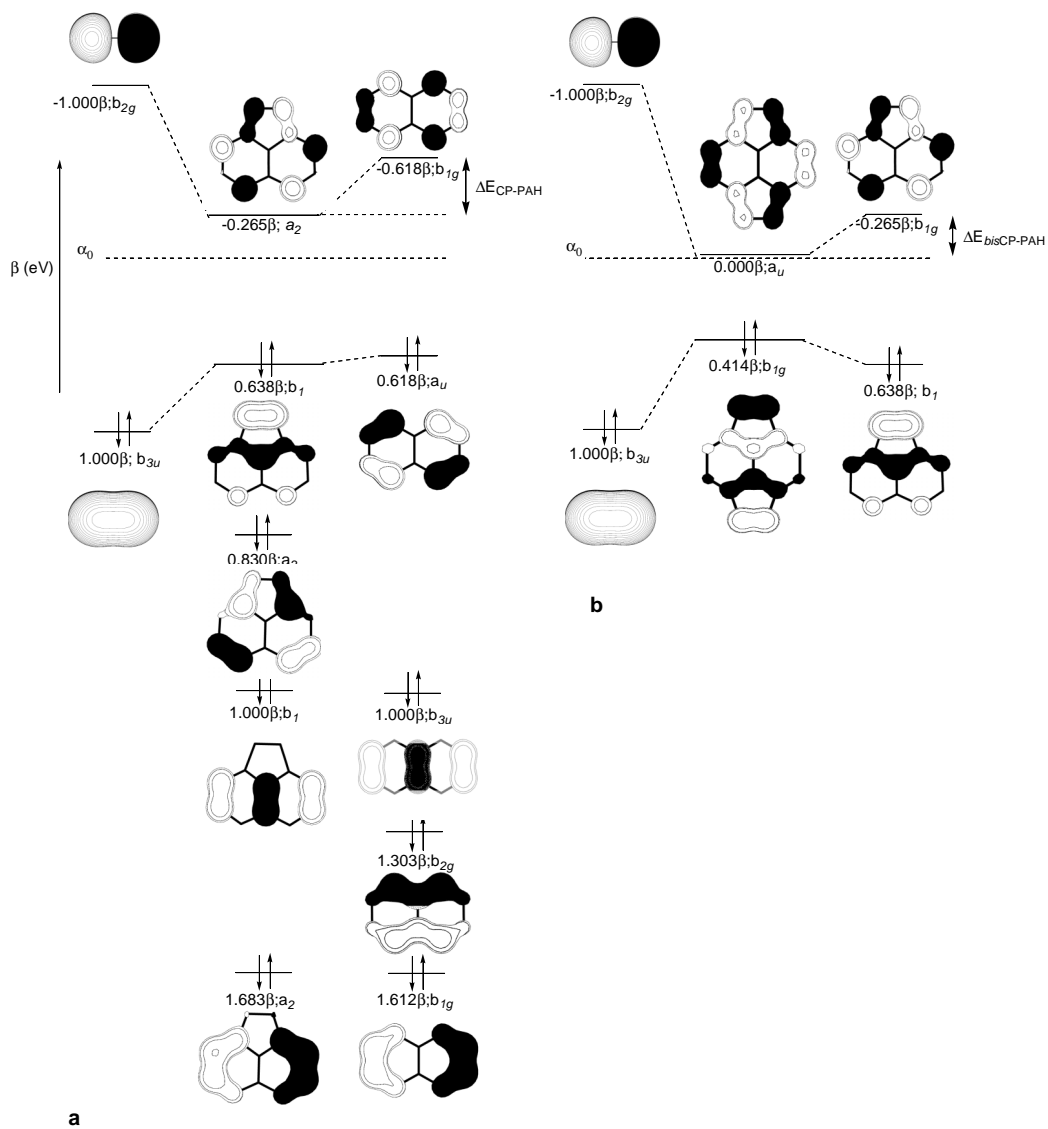


**Figure 5.** Effect of the incorporation of a cyclopenta moiety on  $\epsilon_{LUMO}$  **a.** in a PAH-core. **b.** in a CP-PAH.

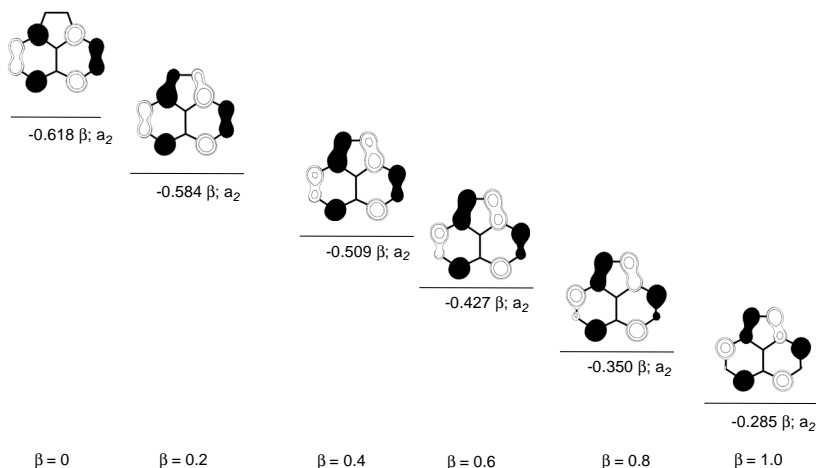


**Figure 6.** Effect of the variation of the interaction ( $\beta$ ) between the PAH core and the etheno-bridge.

A second factor that will influence the interaction between the ethene LUMO and the contributing LUMO of the (CP)-PAH are the orbital coefficients of the (CP)-PAH. This is illustrated for the three isomeric *bis*-cyclopentapyrenes **15** - **17** (Figure 7) for which also different  $E_{1/2}(0/-1)$  values are observed (Table 1). The large orbital coefficients on C5 (0.461) and C6 (0.379) in the LUMO of **11** will lead to strong interaction with the ethene fragment LUMO. Indeed isomer **16** displays the highest  $E_{1/2}(0/-1)$  (-1.02 V, Table 1). The orbital coefficients on C8 (-0.381) and C9 (0.261) in the LUMO of **11** are smaller, which is consistent with the somewhat lower  $E_{1/2}(0/-1)$  for **15** (-1.15 V). For isomer **17** the orbital coefficient on the C1 (0.185) and C10 (-0.133) in the LUMO of **11** are smallest of all. Hence, this is consistent with the observation that the smallest shift in  $E_{1/2}(0/-1)$  with respect to **11** is observed, leading to an  $E_{1/2}(0/-1)$  of -1.32 V for **17**.

In passing, scrutiny of the highest occupied MO's of **1** - **3** (see Figure 5) also clarifies the lack of correlation between the  $E_{1/2}(0/+1)$  and the  $-\epsilon_{\text{HOMO}}$  derived from standard HMO theory (Figure 2). The HOMO of ethene and the HOMO of the parent (CP)-PAH do not possess the correct phase for interaction. Thus, the HOMO of the *mono*- and *bis*-CP-PAH does not bear a clear resemblance to a non-bonding combination of the HOMO of ethene and that of the 'parent' (CP)-PAH, and consequently, the HOMO- $n$  occupied orbitals of the composite are shifted with respect to those of the parent (CP)-PAH.

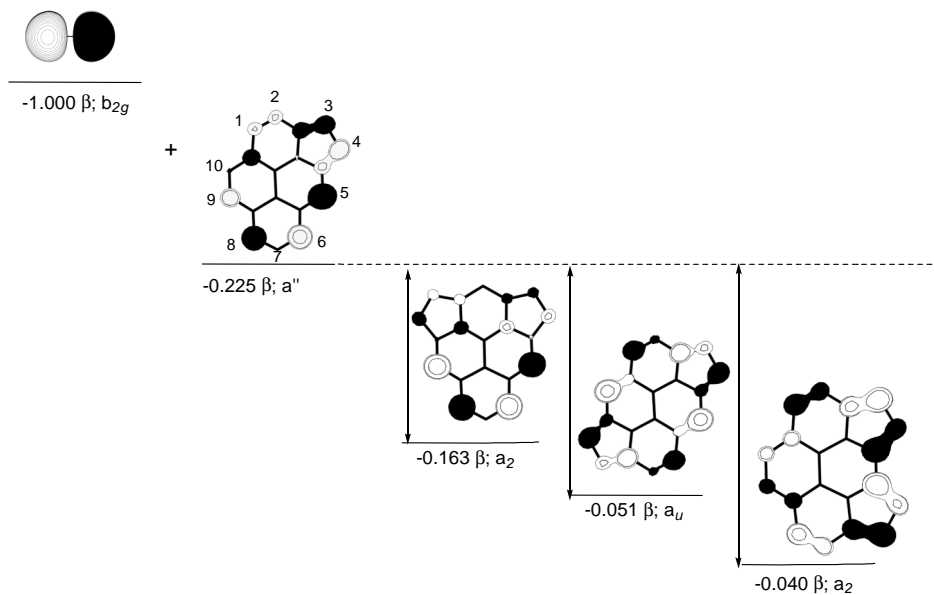


**Figure 7.** Effect of the incorporation of an additional cyclopenta moiety in **11**; the ultimate LUMO's of **15**, **16** and **17**.

### 7.2.5 The second half-wave reduction of *mono*- and *bis*-CP-PAH

Various representatives of the *mono*-CP-PAH and *bis*-CP-PAH display a second (*pseudo*)-reversible (compounds **10**, **15**, **16** and **21-23**) or *irreversible* (compounds **6**, **11**, **13**, **17** and **19**) half-wave reduction potential, *i.e.* one-electron reduction of the radical anion into the *bis*-anion takes place (Table 1 and Chart 1). A comparison of the  $E_{1/2}(-1/-2)$  [or  $E_{\text{onset}}(-1/-2)$ ] values for *mono*-CP-PAH **6**, **10**, **11** and **19** and *bis*-CP-PAH **3**, **13**, **15** - **17**, **21** and **23** with  $E_{1/2}(0/-1)$  values of (CP)-PAH with a similar PAH core but lacking one peripheral pentagon (Table 5) shows that in most cases the difference  $E_{1/2}(0/-1) - E_{1/2}(-1/-2)$  is close to zero. This suggests that, upon one-electron reduction of a *mono*- or *bis*-CP-PAH, the electronic effect of the cyclopenta-moiety on the remainder of the molecule becomes negligible. Similarly, upon two-electron reduction of a *bis*-CP-PAH the electronic effect of both cyclopenta-moieties on the remainder of the molecule is cancelled. This suggests that the added electron has to be predominantly located in the cyclopenta-moiety, which as a consequence will be converted in a  $6\pi$  cyclopentadienide sub-structure.<sup>34</sup>

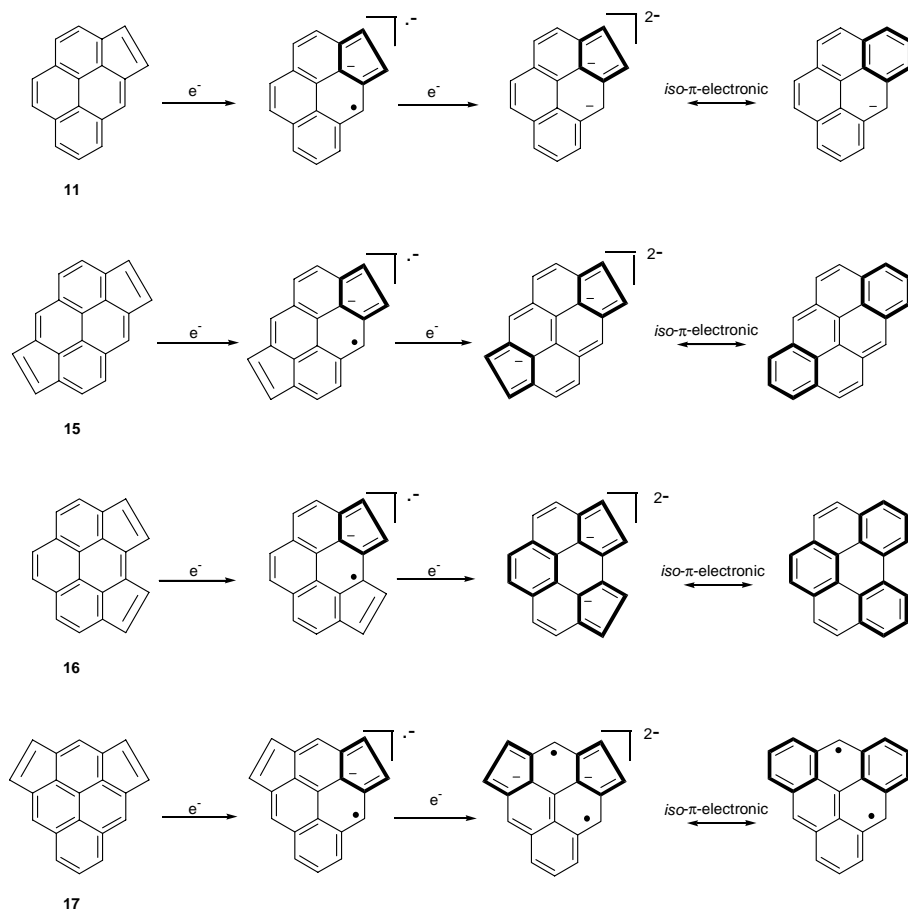
**Table 5.** Comparison of the  $E_{1/2}(0/-1)$  of parent PAH and *mono*-CP-PAH *vs.* the  $E_{1/2}(-1/-2)$  of the *mono*- and *bis*-CP-PAH, containing one additional cyclopenta-moiety (V *vs.* SCE).

PAH	$E_{1/2}$ (0/-1)	<i>mono</i> -CP- PAH	$E_{1/2}$ (-1/-2)	Difference	$E_{1/2}$ (0/-1)	<i>bis</i> -CP- PAH	$E_{1/2}$ (-1/-2)	Difference
		<b>2</b>			-1.80	<b>3</b>	-1.64	-0.16
<b>4</b>	-2.10	<b>6</b>	-2.06	-0.04				
		<b>7</b>			-1.81	<b>13</b>	-1.85	0.04
<b>8</b>	-1.92	<b>10</b>	-1.86	-0.06				
<b>9</b>	-2.22	<b>11</b>	-2.22	0.00	-1.56	<b>15</b>	-1.63	0.07
						<b>16</b>	-1.54	-0.02
						<b>17</b>	-2.06	0.50
<b>14</b>	-2.41	<b>19</b>	-2.26	-0.15	-1.70	<b>21</b>	-1.78	0.08
<b>20</b>	-1.81	<b>22</b>	-1.78	-0.03	-1.26	<b>23</b>	-1.22	-0.04

### 7.2.6 Structural features of the *mono*- and *bis*-anions of *mono*- and *bis*-CP-PAH

These surprising observations are supported by comparison of all possible Kekulé resonance structures in which  $6\pi$  cyclopentadienide sub-structures are present. In Scheme 1 the most important Kekulé resonance structures of the neutral, the radical anions and the *bis*-anions species of **11** and the isomeric dicyclopentapyrenes **15** - **17** are presented.<sup>35</sup> Notice that in the case of **11**, **15** and **16** the Kekulé resonance structure are all closed-shell, whereas it is open-shell for **17**. In the Kekulé resonance structures of the radical anion of **11** the cyclopenta-moiety is converted into a  $6\pi$  cyclopentadienide sub-structure. In the Kekulé resonance structure of the *bis*-anion of **11** this  $6\pi$  cyclopentadienide sub-structure persists, leaving a pyrene-like core with a negative charge. This rationalizes that  $E_{1/2}(-1/-2)$  of **11** is comparable to  $E_{1/2}(0/-1)$  of **9**. In the Kekulé resonance structures of the radical anions of **15**, **16** and **17** the same  $6\pi$  cyclopentadienide sub-structures as in the radical anion of **11** can be drawn. Comparable Kekulé resonance structures for the *bis*-anions of **15** and **16** show that again two  $6\pi$  cyclopentadienide sub-structures are present, thereby reducing the effect of both cyclopenta-moieties on the pyrene core. In contrast, however, such a closed-shell Kekulé resonance structure with two  $6\pi$  cyclopentadienide sub-structures cannot be drawn for the *bis*-anion of **17**, but only an open-shell structure with biradical character. In line with our contention, the second reduction potential of **17** is not similar to the first reduction potential of **11**, but 0.50 V higher (Table 5). Hence, the *bis*-anion of **17** is *destabilized* with respect to the radical anion of the parent CP-PAH (**11**).

## Redox Properties of Cyclopenta-Fused PAH



**Scheme 1.** Kekulé resonance structures of the neutral, radical anion and *bis*-anions of **11** and **15** - **17** containing 6  $\pi$ -electron cyclopentadienide sub-structures.

Note that the Kekulé resonance structures are *iso- $\pi$* -electronic with the corresponding closed-shell benzannulated pyrenes (Scheme 1).<sup>36</sup> An indication that the closed-shell Kekulé resonance structures containing 6 $\pi$  cyclopentadienide sub-structures in Scheme 1 contribute to the overall structure of the radical anions and *bis*-anions of *mono*- and *bis*-CP-PAH is suggested by the computed HMO bond orders. In the ground state *mono*- and *bis*-CP-PAH typical  $sp^2$ - $sp^2$  single (bond order 0.80) and  $sp^2$ - $sp^2$  double bonds (bond order 0.47) are found for the cyclopenta-moieties. In contrast, in the radical anion and *bis*-anions of *mono*- and *bis*-CP-PAH bond length equalization in the cyclopenta-moiety is observed. (bond order  $sp^2$ - $sp^2$  single bond 0.65;  $sp^2$ - $sp^2$

double bond 0.57). This is in line with a large contribution of Kekulé resonance structures with  $6\pi$  cyclopentadienide sub-structures. This is substantiated by available experimental results. For example, the single crystal X-ray structure of the *bis*-anion of **2** shows lengthening of the double bond and shortening of the single bond of the cyclopenta-moiety with respect to the ground state.<sup>37</sup> In agreement, also a decrease of the  $^3J_{HH}$  coupling constants for the cyclopenteno protons of the *bis*-anions of **2** (2.3 Hz), and **7** (2.8 Hz) was found with respect to the related  $^3J_{HH}$  values of the neutral systems (5.2 and 5.1 Hz, respectively).<sup>38</sup>

### 7.2.7 Corollary

The redox properties of the PAH, *mono*- and *bis*-CP-PAH in Chart 1 were assessed using CV. It is shown that peripheral fusion of a cyclopenta-moiety to a PAH core enhances the electron affinity. This is not observed for the CP-PAH with an internal cyclopenta-moiety. Unexpectedly, a linear correlation is found between  $E_{1/2}(0/-1)$  and the  $-e_{LUMO}$  energy derived from HMO theory. This is rationalized by the fact that the cyclopenta-moiety acts as an electron-withdrawing *peri*-substituent ( $\sigma_m = 0.4 \pm 0.07$ ). The observation that upon reduction the effect of the cyclopenta-moiety on the remainder of the molecule becomes negligible is rationalized by the presence of  $6\pi$  cyclopentadienide sub-structures in the radical anions and *bis*-anions of *mono*- and *bis*-CP-PAH.

## 7.3 Validation

Here we report the results of *ab initio* calculations, which validate the conclusions derived from HMO theory and Kekulé resonance structures described in the previous sections. To this end, the ground state, radical anion and *bis*-anions of selected compounds, *i.e.* the PAH **1** and **9**, the *mono*-CP-PAH **2** and **11** and the *bis*-CP-PAH **3** and **15 – 17**, were studied at various levels of theory.

### 7.3.1 Optimized geometries

The geometries of the neutral, radical anion and the *bis*-anion species of the compounds **1 - 3**, **9** and **11**, and **15 - 17** were optimized at the B3LYP/6-31G\*\* level of theory. In addition, the geometries of the neutral and radical anion species were re-optimized at the higher B3LYP/DZP++ level of theory. This basis set is particularly suited to obtain electron affinities that are in close agreement with the experimental values.<sup>39</sup> All radical anions and *bis*-anions were optimized within the point group symmetry of the ground state geometry. Unfortunately, geometry optimizations of the *bis*-anion species could not be performed with the B3LYP/DZP++

method due to linear dependencies. The B3LYP/6-31G\*\* optimized geometries of the *bis*-anion species are expected to be satisfactory, since reasonable agreement between two methods for the neutral and radical anion species was found (*vide infra*).

A comparison of the ground state geometries of naphthalene (**1**), acenaphthylene (**2**) and pyracylene (**3**) (Figure 8A), reveals that the cyclopenta-moiety indeed consists of localized sp<sup>2</sup> - sp<sup>2</sup> single [**2**: 1.477 Å, **3**: 1.496 Å, (B3LYP/DZP\*\*)] and sp<sup>2</sup> - sp<sup>2</sup> double [**2**: 1.371 Å, **3**: 1.373 Å, (B3LYP/DZP\*\*)] bonds and that the naphthalene-like core in **2** and **3** is only slightly affected. The only difference is the shortening of the central bond in between the two naphthalene rings. A comparison of the B3LYP/6-31G\*\* and B3LYP/DZP\*\* results (Figure 8), show that they are in reasonable agreement.

As shown in Figure 8, minor changes are present between the geometries of the ground state and the radical anion of naphthalene; the largest geometric change is only 0.03 Å. When the geometries of radical anions of *mono*-CP-PAH **2** and the *bis*-CP-PAH **3** are compared (Figure 8B), it is clear that these geometries change significantly from the ground state geometries. The major effect of adding electrons is found in the cyclopenta-moiety. The difference in bond length between the sp<sup>2</sup>-sp<sup>2</sup> single and sp<sup>2</sup>-sp<sup>2</sup> double bonds [**2**: 1.443 Å / 1.411 Å; **3**: 1.466 Å / 1.403 Å, (B3LYP/DZP\*\*, Figure 8B)] is clearly diminished. Besides these changes in the cyclopenta-moiety no significant structural changes are apparent in the geometries of the radical anion species; they are comparable to the changes observed for the naphthalene radical anion. A further reduction of the bond length alternation is seen for the *bis*-anions of **2** and **3** [single/double **2**: 1.414/1.442 Å, **3**: 1.433/1.430 Å, (B3LYP/6-31G\*\*, Figure 8C)].

Similar observations are made for the pyrene-series (**9**, **11** and **15** - **17**). In the neutral species of **11**, **15** - **17** clearly localized sp<sup>2</sup>-sp<sup>2</sup> double bonds are present in the cyclopenta-moiety fused to the mainly unaltered pyrene-core [sp<sup>2</sup>-sp<sup>2</sup> single/ sp<sup>2</sup>-sp<sup>2</sup> double; **11**: 1.474/1.375 Å, **15**: 1.484/1.374 Å, **16**: 1.483/1.372 Å, **17**: 1.379/1.484 Å, B3LYP/DZP\*\*]. In the corresponding radical anion species a reduction of the localization of the double bond is observed [sp<sup>2</sup>-sp<sup>2</sup> single/ sp<sup>2</sup>-sp<sup>2</sup> double; **11**: 1.447/1.408 Å, **15**: 1.456/1.391 Å, **16**: 1.455/1.400 Å, **17**: 1.46/1.39 Å, B3LYP/DZP\*\*]. In the *bis*-anions of **11**, **15** and **16** the localization of the sp<sup>2</sup>-sp<sup>2</sup> double bond in the cyclopenta-moiety has almost completely vanished [single/double; **11**: 1.425/1.430 Å, **15**: 1.437/1.417 Å, **16**: 1.424/1.423 Å, B3LYP/6-31G\*\*]. This effect is less pronounced in the *bis*-anion of **17** [sp<sup>2</sup>-sp<sup>2</sup> single/sp<sup>2</sup>-sp<sup>2</sup> double; 1.455/1.423 Å, B3LYP/6-31G\*\*].

The structural changes in going from the ground state to the radical anion and finally the *bis*-anion are in line with the changes in the bond orders derived from HMO theory. Hence,

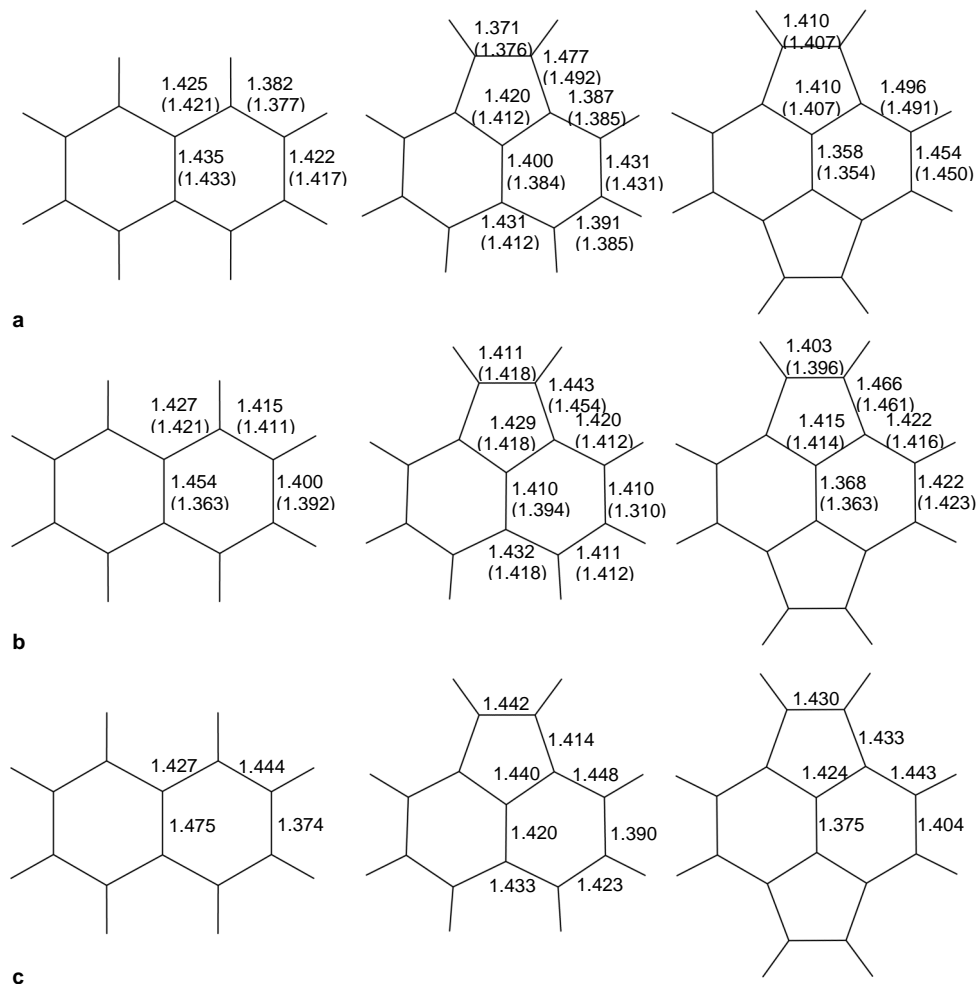


**Figure 8.** Optimized geometries at the (U)B3LYP/DZP<sup>++</sup> level of theory (Numbers in parentheses are the bond lengths at the (U)B3LYP/6-31G<sup>\*\*</sup> level of theory) for **a.** the neutral species of **1** ( $D_{2h}$ ), **2** ( $C_{2v}$ ) and **3** ( $D_{2h}$ ), **b.** the radical anions of **1** ( $D_{2h}$ ), **2** ( $C_{2v}$ ) and **3** ( $D_{2h}$ ) and **c.** the *bis*-anions of **1** ( $D_{2h}$ ), **2** ( $C_{2v}$ ) and **3** ( $D_{2h}$ ) at the (U)B3LYP/6-31G<sup>\*\*</sup> level of theory.

evidence is found for the presence of  $6\pi$  cyclopentadienide sub-structures in the radical anions and *bis*-anions. To gain more clear support for our contentions, the magnetic properties of selected closed-shell neutral and *bis*-anions species were evaluated.



### 7.3.2 Visualization of the $6\pi$ cyclopentadienide sub-structures

According to Hückel-London theory,<sup>40</sup> a monocycle containing  $4n+2$   $\pi$ -electrons will sustain a diatropic (aromatic) ring current, whereas a monocycle with  $4n$   $\pi$ -electrons will display a paratropic (*anti*-aromatic) ring current when exposed to a perpendicular magnetic field. If upon reduction of the *mono*-CP-PAH **11** and the *bis*-CP-PAH **15** – **17**  $6\pi$  cyclopentadienide sub-structures ( $4n + 2$   $\pi$ -electron ring) are formed, this should exhibit a considerable effect on the magnetic properties of the systems.

Recently, the reliable *ab initio* all-electron distributed-origin method (CTOCD-DZ/6-31G\*\*//RHF/6-31G\*\*) has been used to study the magnetic effect of cyclopenta-fusion to a pyrene core by direct computation of the ring currents.<sup>41</sup> These  $\pi$ - and total ( $\sigma + \pi$ ) current density maps of **9**, **11** and **15** – **17** revealed that the number and distribution of the cyclopenta-moieties indeed affect the local pattern of induced current. Whereas in the case of **11** and **17** the cyclopenta-moieties exert a minor effect on the pyrene core, for **15** and **16** strong paratropic ring currents (*anti*-aromatic) are present in the cyclopenta-moieties.

Upon addition of two extra electrons, the LUMO of the neutral species will become the HOMO of the *bis*-anion. The resulting HOMO will be stabilized and thereby isolated between the other occupied and unoccupied orbitals. The magnetic effect of the two added electrons that occupy the HOMO in the *bis*-anions can now be probed. To this end, the current density maps of the *bis*-anions were calculated at CTOCD-DZ/6-31G\*\*//RHF/6-31G\*\* level of theory (see Computational Methods).

In Figure 9, the current density maps are shown for all  $\pi$ - and HOMO-electron distributions computed for the *bis*-anions of **11**, **15** and **16**. Anticlockwise circulation of electrons is diamagnetic, whilst paramagnetic circulation is clockwise. In the  $\pi$ -plot of the *bis*-anion of **11** (Figure 9a) a strong diatropic, *i.e.* aromatic, circulation is visible in the cyclopenta-moiety. This is in agreement with the presence of a  $6\pi$  cyclopentadienide sub-structure (Scheme 1). In addition, a weaker diatropic current along part of the perimeter is present. According to the isopocentric feature of CTOCD-DZ, the diatropic circulation, which is present in the cyclopenta-moiety of the *bis*-anion has its origin in transitions from the HOMO ( $10a''$ ). This is discernible from the current density map where only contributions from the HOMO are considered (Figure 9b). Evidence that no other orbitals significantly contribute to the diatropic current in the cyclopenta-moiety of the *bis*-anion is obtained from the current density map where contributions from all  $\pi$ -orbitals minus the HOMO are plotted (not shown). In this case, only a diatropic ring current along the perimeter is present.

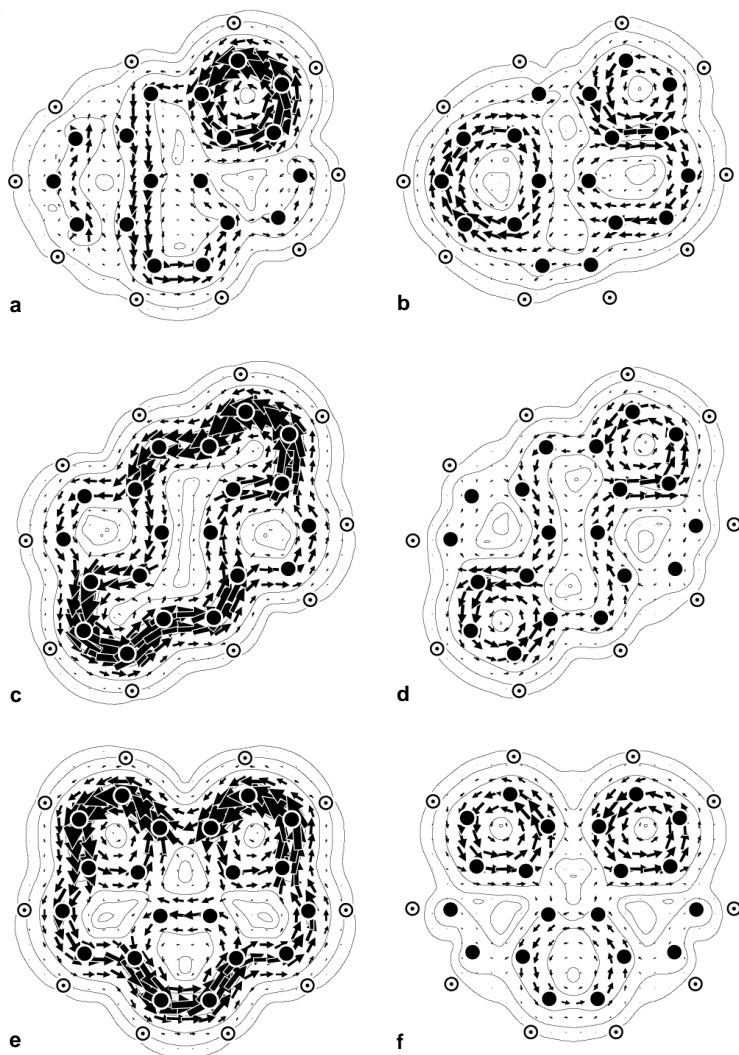


**Figure 9.** Orbital contributions to the current density in the *bis*-anions (CTOCD-DZ//6-31G\*\*//6-31G\*\*) **a.** cyclopenta[*g,d*]pyrene ( $C_3$ ) (**11**): a complete  $\pi$  map, **b.** cyclopenta[*g,d*]pyrene ( $C_3$ ) (**11**): contributions from the two electrons in the HOMO ( $10a''$ ), **c.** dicyclopenta[*ad,jk*]pyrene ( $C_{2h}$ ) (**15**): a complete  $\pi$  map, **d.** dicyclopenta[*ad,jk*]pyrene ( $C_{2h}$ ) (**15**): contributions from the two electrons in the HOMO ( $6a_0$ ), **e.** dicyclopenta[*ad,jl*]pyrene ( $C_{2v}$ ) (**16**): a complete  $\pi$  map and **f.** dicyclopenta[*ad,jl*]pyrene ( $C_{2v}$ ) (**16**): contributions from the two electrons in the HOMO ( $5a_2$ ).

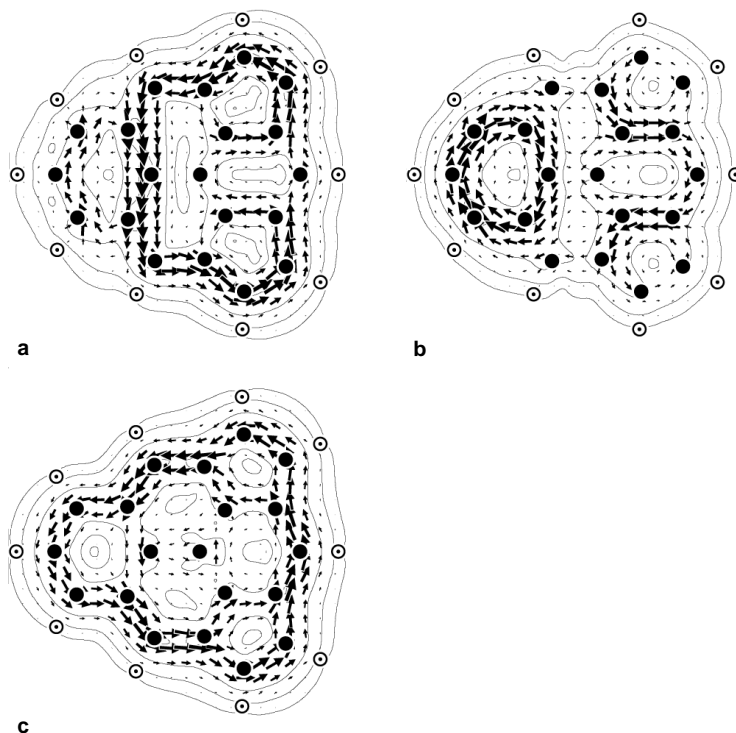


**Figure 10.** Orbital contributions to the current density of the *bis*-anion in dicyclopenta[*ad,mm*]pyrene ( $C_{2v}$ ) (CTOCD-DZ/6-31G\*\*//6-31G\*\*) (**16**). **a.** a complete  $\pi$  map, **b.** contributions from the two electrons in the HOMO ( $5a_2$ ) and **c.** the current arising from all  $\pi$ -orbitals but the HOMO ( $5a_2$ ).

Similar features are present in the  $\pi$ -current density maps for the *bis*-anions of **15** and **16** (Figure 9c,d and 9e,f). Strong diamagnetic circulations are present in the cyclopenta-moieties, which have their origin in transition from the HOMO level ( $6a_u$  for **15** and  $5a_2$  for **16**, see Figure 9d and 9f). Again, a weak diatropic pyrene perimeter current is present which is a result of the other  $\pi$ -orbitals. Note that the total  $\pi$ - and HOMO-current density maps of **11**, **15** and **16** display delocalization patterns that are in excellent agreement with those suggested in the proposed Kekulé resonance structures (Scheme 1). In **15** this pattern corresponds to that of the *iso*- $\pi$ -electronic chrysene, while the delocalization pattern in **16** matches that of *iso*- $\pi$ -electronic triphenylene.

The *bis*-anion of **17**, however, displays different features (Figure 10). Although, in the  $\pi$ -map (Figure 10a) diatropic features in the cyclopenta-moieties are present, the HOMO electrons

( $5a_2$ , see Figure 10b) are not solely responsible for this current. As illustrated by the remainder plot [all  $\pi$ -contributions – HOMO ( $5a_2$ ), Figure 10c], other  $\pi$  orbitals also contribute. Note that a special feature is further discernible in the remainder plot, *i.e.* bifurcation in the two cyclopentamoiety, which points to the presence of *both* diatropic and paratropic ring current contributions. This shows that the *bis*-anion of **17** possesses a more complex behavior and is in line with the fact that not one closed-shell Kekulé resonance structure containing two  $6\pi$  cyclopentadienide sub-structures can be drawn for **17**.

Notwithstanding, the CTOCD-DZ results show that for **11**, **15** and **16** upon addition of two electrons to the LUMO of the neutral species, the paratropic, *i.e.* *anti*-aromatic, character of the cyclopenta-moiety is quenched and replaced by strong diamagnetic, *i.e.* aromatic, circulations on these rings. These results are in good agreement with the Kekulé resonance structures with  $6\pi$  cyclopentadienide sub-structures in the pentagons (Scheme 1). Apparently, the Kekulé resonance structures that are *iso*- $\pi$ -electronic with closed-shell benzannulated PAH, are the structures that will predominantly contribute in the Valence Bond description of the *bis*-anions of compounds **11**, **15** and **16**. For **17** it is expected that not one structure will dominate since not one closed-shell Kekulé resonance structure can be drawn.

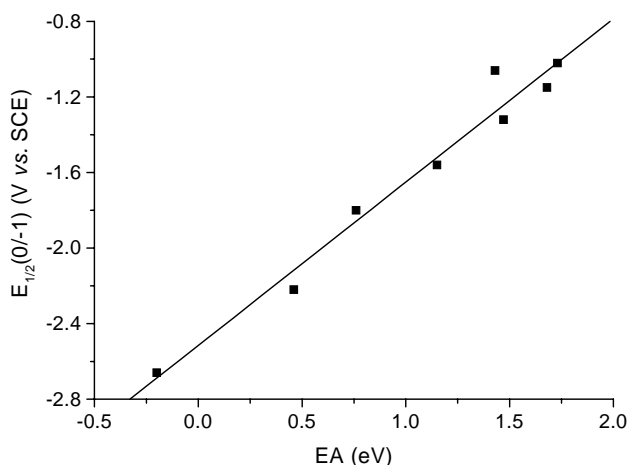
### 7.3.3 High electron affinities of *mono*- and *bis*-CP-PAH

The CV results have unequivocally shown that annelation of a cyclopenta-moiety to an alternant PAH core renders reduction of these compounds considerably more facile. Since the  $E_{1/2}(0/-1)$  values after correction for solvation are proportional to the gas-phase electron affinity, *mono*- and *bis*-CP-PAH are expected to have high electron affinities. To verify this supposition the electron affinities (EA) of the compounds **1** - **3**, **11** and **15** - **17** were calculated at the B3LYP/DZP<sup>++</sup> level of theory (Table 6). This huge basis set, which contains both polarization and diffuse functions, has been recommended since it gives EA's that are in close agreement with experimental results.<sup>39,42,43</sup> Hitherto, the only experimentally determined EA's for the compounds studied here are for **1** ( $-0.19 \pm 0.03$  eV) and **9** ( $0.56 \pm 0.06$  eV). The results in Table 6 show that indeed a remarkably good agreement is present between the calculated EA values at B3LYP/DZP<sup>++</sup> level of theory and these experimental values. As shown by a comparison of the computed EA values for the alternant PAH **1** and **9** with the corresponding CP-PAH **2** and **11**, the presence of a cyclopenta-moiety leads to a substantial increase of the EA [ $\Delta E_{A_{CP-PAH-PAH}} = 0.96$  eV (**2** to **1**) and  $\Delta E_{A_{CP-PAH-PAH}} = 0.69$  eV (**9** to **11**)]. The larger effect of the CP-moiety in the case of **2** compared

**Table 6.** Calculated Electron Affinities (EA) for PAH **1** and **9**, *mono*-CP-PAH **2** and **11**, and *bis*-CP-PAH **3** and **15 - 17** displayed in Chart 1 at the (U)B3LYP/DZP<sup>++</sup> level of theory.

	EA (eV)	$\Delta EA_{bis\text{-}CP\text{-}PAH}/\Delta EA_{mono\text{-}CP\text{-}PAH}^a$
<b>1</b>	-0.20	
<b>2</b>	0.76	0.96
<b>3</b>	1.43	0.67
<b>9</b>	0.46	
<b>11</b>	1.15	0.69
<b>15</b>	1.68	0.53
<b>16</b>	1.73	0.58
<b>17</b>	1.47	0.32

<sup>a</sup>  $\Delta EA_{bis\text{-}CP\text{-}PAH} = EA_{bis\text{-}CP\text{-}PAH} - EA_{mono\text{-}CP\text{-}PAH}$ ,  $\Delta EA_{mono\text{-}CP\text{-}PAH} = EA_{mono\text{-}CP\text{-}PAH} - EA_{PAH}$

**Figure 11.** Linear correlation between the calculated electron affinities (EA, Table 6) and the experimental reduction potentials ( $E_{1/2}(0/-1)$ , Table 1) for compounds **1 - 3**, **9**, **11**, **15 - 17**.

to **11**, is a consequence of the enhanced interaction between the CP-moiety and the naphthalene core (*vide supra*).

In line with the CV results for the *bis*-CP-PAH **3** and **15 - 17** even higher EA values are computed. The highest values are found for **15** and **16** (1.68 and 1.73 eV), which are in the range

of EA values calculated for *perfluorinated* PAH, of which perfluorinated anthracene displayed the highest EA of 1.84 eV.<sup>43</sup> Notice that these EA values are considerably higher than the estimated EA of corannulene (0.50 eV).<sup>44</sup> Hence, CP-PAH are expected to be very good electron acceptors.

In accordance with what was previously found, on the basis of the CV results [ $\Delta E_{\text{mono-CP-PAH}}$  is between 0.55 - 0.86 V and  $\Delta E_{\text{bis-CP-PAH}}$  is between 0.33- 0.74 (Table 2)] the effect of annelation of a second CP-moiety on the EA is smaller than that of the first [0.69 - 0.96 eV computed for the first CP-moiety vs. 0.32 - 0.67 eV computed for second the CP-moiety (Table 6)]. Furthermore, the effect of the topology of CP-fusion is clearly discernible in the computed EA's for **15** - **17** (1.68, 1.73 and 1.47 eV, respectively). The same trend as was found in the experimental  $E_{1/2(0/-1)}$  [ $E_{1/2(0/-1)}$  of **16** >  $E_{1/2(0/-1)}$  of **15** >  $E_{1/2(0/-1)}$  of **17**] is neatly reproduced by the calculated EA values.

A good linear correlation is obtained when the experimentally determined  $E_{1/2(0/-1)}$  values (Table 1) are plotted against the EA values calculated at the B3LYP/DZP<sup>++</sup> level of theory (Figure 11,  $r^2 = 0.968$ , slope = 0.86, intercept = -2.515 V). The intercept of this line corresponds to  $-\Delta\Delta G_{\text{solv}} + E_{\text{ref}}$ ,<sup>2</sup> where  $E_{\text{ref}}$  is -4.71 V since the potentials are referenced to SCE.<sup>45</sup> This leads to a value of 2.20 eV for  $-\Delta\Delta G_{\text{solv}}$ , which is moderately higher than the  $-\Delta\Delta G_{\text{solv}}$  values reported for alternant PAH (1.99 eV).<sup>2</sup> The value of  $-\Delta\Delta G_{\text{solv}}$  primarily depends on the degree of charge delocalisation.<sup>46</sup> Therefore, the higher value for  $-\Delta\Delta G_{\text{solv}}$  found for CP-PAH compared to that for alternant PAH, indicates that in CP-PAH the charge is more localized.

## 7.4 Conclusions

The evaluation of the redox properties of a large series of PAH, *mono*- and *bis*-CP-PAH has led to unexpected results. The externally-fused cyclopenta-moiety acts as a *peri*-substituent and its presence leads to high electron affinities. Upon reduction the effect of this substituent is quenched by the formation of  $6\pi$  cyclopentadienide sub-structures. In first instance, these results were rationalized on the basis of simple models as Hückel and the use of Kekulé resonance structures. The usefulness of these models is proven by validation using *ab initio* calculations.

These results corroborate the findings that upon reduction of the fullerenes  $C_{60}$  and  $C_{70}$  the electrons predominantly occupy the cyclopenta-moieties and thereby significantly alter the magnetic properties.<sup>12,13</sup> Hence, the presence of the cyclopenta-moieties in  $C_{60}$  and  $C_{70}$  renders these molecules good electron acceptors and therefore good n-type materials.

## 7.5 Experimental section

### Cyclic Voltammetry

Cyclic Voltammetry (CV) was performed using an EG&G Potentiostat/Galvanostat Model 263A in CH<sub>3</sub>CN (freshly distilled from CaH<sub>2</sub>) containing 0.1 M Bu<sub>4</sub>NPF<sub>6</sub> as supporting electrolyte at a scanning rate of 50 and 100 mVs<sup>-1</sup> (potential window -2.5 to +3 V). Redox potentials were determined relative to an Ag/AgNO<sub>3</sub> reference electrode (0.1 M in CH<sub>3</sub>CN) and were referenced to SCE by measuring the oxidation potential of the FeCp<sub>2</sub>/FeCp<sub>2</sub><sup>+</sup> couple (0.31 V *vs.* SCE). For irreversible electrochemical processes E<sub>onset</sub> values instead of peak potentials (E<sub>pc/pa</sub>) are reported. The use of peak potentials (E<sub>pc/pa</sub>) can give unreliable information, owing to the dependence of E<sub>pc/pa</sub> on factors such as solvent, electrolyte, scan rate and the concentration of the analyte.<sup>28</sup>

### Synthesis

The *mono*-substituted derivatives of the PAH **1**, **4**, **8** and **9** with X = C≡CH, COCH<sub>3</sub>, CP were synthesized according to literature procedures.<sup>17,18,47,48</sup> The *mono*-substituted derivatives of the PAH **1**, **4**, **8** and **9** with X = NH<sub>2</sub> were obtained by catalytic reduction of the corresponding compound with X = NO<sub>2</sub> (pH<sub>2</sub>/1atm, Pd/C). All other compounds were purchased commercially. *Caution:* (CP)-PAHs are potential genotoxic compounds.

### Computational Methods

Hückel calculations were run on a PC with a QCPE program, Computer Utilities Package (QCMP021) in the standard Hückel approximation (with all  $\alpha$ 's equal and  $\beta$ 's equal).

The neutral, radical anions and the *bis*-anions of the compounds **1** - **3**, **9**, **11** and **15** - **17** were studied with the (U)B3LYP method using GAMESS-UK;<sup>49</sup> the 6-31G\*\* as well as a double- $\zeta$  basis set with polarization and diffuse functions (denoted DZP<sup>++</sup>) were used.<sup>39</sup> For the neutral and the radical anions optimizations were performed at both levels of theory, the geometry of the *bis*-anions were only optimized at the B3LYP/6-31G\*\* level of theory. When using UB3LYP no spin contamination was observed for the open-shell radical cations. All optimizations of the radical anions and *bis*-anions were performed in the symmetry point group of the ground state to avoid linear dependencies. The adiabatic electron affinities (AEA) for the molecules were computed as the difference between the total energy of the geometry-optimized neutral and the total energy of the corresponding geometry-optimized radical anion, within the symmetry point group of the ground state, at the B3LYP/DZP<sup>++</sup> level of theory.<sup>39</sup>

The current density maps of the neutral and *bis*-anion species of compounds **11** and **15** - **17** were computed using the CTOCD-DZ distributed-origin method at the *ab initio* Hartree Fock level of theory in the

6-31G\*\* basis.<sup>50</sup> Herefore, the geometries were optimized at the RHF/6-31G\*\* level of theory using the GAMESS-UK program.<sup>49</sup> All geometries were planar and characterized as stationary points by Hessian calculations. The maps were computed by using the CTOCD-DZ (diamagnetic zero) program as implemented in the Exeter version of SYSMO.<sup>51</sup>

## References and notes

- (1) Curl, R. F.; Smalley, R. E. *Science* **1988**, *242*, 1017.
- (2) Ruoff, R. S.; Kadish, K. M.; Boulas, P.; Chen, E. C. M. *J. Phys. Chem.* **1995**, *99*, 8843-8850.
- (3) Haufler, R. E.; Conceicao, J.; Chibante, L. P. F.; Chai, Y.; Byrne, N. E.; Flanagan, S.; Haley, M. M.; O'Brien, S. C.; Pan, C.; Xiao, Z.; Billups, W. E.; Ciufolini, M. A.; Hauge, R. H.; Magrave, J. L.; Wilson, L. J.; Curl, R. F.; Smalley, R. E. *J. Phys. Chem.* **1990**, *94*, 8634-8636.
- (4) Dubois, D.; Kadish, K. M. *J. Am. Chem. Soc.* **1991**, *113*, 7773-7774.
- (5) Allemand, P.-M.; Koch, A.; Wudl, F.; Rubin, Y.; Diederich, F.; Alvarez, M. M.; Anz, S. J.; Whetten, R. L. *J. Am. Chem. Soc.* **1991**, *113*, 1050-1051.
- (6) Wudl, F. *Acc. Chem. Res.* **1992**, *25*, 157-161.
- (7) Fowler, P. W.; Ceulemans, A. *J. Phys. Chem.* **1995**, *99*, 508-510.
- (8) Hirsch, A.; Chen, Z.; Jiao, H. *Angew. Chem. Int. Ed. Engl.* **2000**, *39*, 3915-3917.
- (9) Pasquarello, A.; Schlüter, M.; Haddon, R. C. *Phys. Rev. A* **1993**, *47*, 1783-1789.
- (10) Saunders, M.; Cross, R. J.; Jiménez-Vázquez, H. A.; Shimshi, R.; Khong, A. *Science* **1996**, *271*, 1693-1697.
- (11) Haddon, R. C. *Science* **1993**, *261*, 1545-1550.
- (12) Sternfeld, T.; Hoffman, R. E.; Aprahamian, I.; Rabinovitz, M. *Angew. Chem. Int. Ed. Engl.* **2001**, *40*, 455-457.
- (13) Sternfeld, T.; Thilgen, C.; Hoffman, R. E.; Rosario Colorado Heras, M. d.; Diederich, F.; Wudl, F.; Scott, L. T.; Mack, J.; Rabinovitz, M. *J. Am. Chem. Soc.* **2002**, *124*, 5734-5738.
- (14) Homann, K.-H. *Angew. Chem. Int. Ed. Engl.* **1998**, *37*, 2434-2451.
- (15) Rabideau, P. W.; Sygula, A. *Acc. Chem. Res.* **1996**, *29*, 235-242.
- (16) Preda, D. V.; Scott, L. T. *Tetrahedron Lett.* **2000**, *41*, 9633-9637.
- (17) Sarobe, M.; Zwikker, J. W.; Snoeijer, J. D.; Wiersum, U. E.; Jenneskens, L. W. *J. Chem. Soc., Chem. Commun.* **1994**, 89-90.
- (18) Sarobe, M.; Snoeijer, J. D.; Jenneskens, L. W.; Slagt, M. Q.; Zwikker, J. W. *Tetrahedron Lett.* **1995**, *36*, 8489-8492.



- (19) Sarobe, M.; Flink, S.; Jenneskens, L. W.; Zwikker, J. W.; Wesseling, J. *J. Chem. Soc., Perkin Trans. 2* **1996**, 2125-2131.
- (20) Haddon, R. C. *Phil. Trans. R. Soc. Lond. A* **1993**, *343*, 53-62.
- (21) Fry, A. J.; Foc, P. C. *Tetrahedron* **1986**, *42*, 5255-5266.
- (22) Meerholz, K.; Heinze, J. *J. Am. Chem. Soc.* **1989**, *111*, 2325-2326.
- (23) Seiders, T. J.; K., B. K.; Siegel, J. S.; Gleiter, R. *Tetrahedron Lett.* **2000**, *41*, 4519-4522.
- (24) Koopmans, T. *Physica* **1934**, *1*, 104.
- (25) Streitwieser, A. *Molecular Orbital Theory for Organic Chemists*; Wiley: New York, 1961.
- (26) Note that the correlations could be further improved by adjustment of the exchange integral ( $\beta$ ) with  $\pi$ -bond orders.
- (27) In equation 2,  $n$  stands for the number of electrons involved in the redox process.
- (28) Bard, A. J.; Faulkner, L. R. *Electrochemical methods*; John Wiley & Sons: New York, 1980.
- (29) Exner, O. *Correlation Analysis of Chemical Data*; Plenum Press: New York, 1988.
- (30) Klemm, L. H.; Koilik, A. J.; Desai, K. B. *J. Org. Chem.* **1963**, *28*, 625-630.
- (31) Klemm, L. H.; Koilik, A. J. *J. Org. Chem.* **1963**, *28*, 2044-2049.
- (32) In contrast to the excellent Hammett relations found between  $E_{\text{onset}}(0/-1)$  and  $\sigma_m$  for the series **1**, **4**, **8** and **9**, no single correlation spanning the whole  $\sigma$ -range was found if  $\sigma_p$ , which contains both inductive and mesomeric effects, was used. The  $\text{NH}_2$  derivatives deviate markedly, presumably due to a dominating resonance effect. This resonance effect will influence the mode of charge distribution and thereby  $\rho$ . As a consequence, the Hammett relation between the reduction potential and  $\sigma_p$  yields two lines, one for  $\sigma_p < 0$  and one for  $\sigma_p > 0$ , of which the first has a smaller  $\rho$  value. Since the reduction potential  $E_{\text{onset}}(0/-1)$  of the cyclopenta-fused PAHs falls in the same range as the acetyl-substituted PAHs, the line for  $\sigma_p > 0$  will be of interest. We noted that the linear relationship for  $\sigma_p > 0$  is comparable to the one obtained for the relation between the  $E_{\text{onset}}(0/-1)$  and  $\sigma_m$ .
- (33) Koper, C.; Jenneskens, L. W.; Sarobe, M. *Tetrahedron Lett.* **2002**, *43*, 3833-3836.
- (34) Dang, H.; Levitus, M.; Garcia-Garibay, M. A. *J. Am. Chem. Soc.* **2002**, *124*, 136-143.
- (35) Havenith, R. W. A.; Lenthe, J. H.; Dijkstra, F.; Jenneskens, L. W. *J. Phys. Chem. A* **2001**, *105*, 3838-3845.
- (36) Aihara, J. *J. Chem. Soc., Perkin Trans. 2* **1996**, 2185-2195.
- (37) Rhine, W.; Davis, J. H.; Stucky, G. *J. Organomet. Chem.* **1977**, *134*, 139-149.
- (38) Cohen, Y.; Roelofs, N. H.; Reinhardt, G.; Scott, L. T.; Rabinovitz, M. *J. Org. Chem.* **1987**, *52*, 4207-4214.

## Chapter 7

- (39) Rienstra-Kiracofe, J. C.; Barden, C. J.; Brown, S. T.; Schaefer, H. F. *J. Phys. Chem. A* **2001**, *105*, 524-528.
- (40) Coulson, C. A.; Mallion, R. B. *J. Am. Chem. Soc.* **1976**, *98*, 592-598.
- (41) Steiner, E.; Fowler, P. W.; Jenneskens, L. W.; Havenith, R. W. A. *Eur. J. Org. Chem.* **2002**, 163-169.
- (42) Gonzales, J. M.; Barden, C. J.; Brown, S. T.; Schleyer, P. v. R.; Schaefer, H. F.; Li, Q.-S. *J. Am. Chem. Soc.* **2003**, *125*, 1065-1071.
- (43) Xie, Y.; Schaefer, H. F.; Cotton, F. A. *Chem. Commun.* **2003**, 102-103.
- (44) Chen, G.; Cooks, R. G.; Corpuz, E.; Scott, L. T. *J. Am. Soc. Mass. Spectrom.* **1996**, *7*, 619-627.
- (45) Shalev, H.; Evans, D. H. *J. Am. Chem. Soc.* **1989**, *111*, 2667-2674.
- (46) Chen, E. C. M.; Wenthworth, W. E. *Mol. Cryst. Liq. Cryst* **1989**, *171*, 271.
- (47) Sarobe, M. *Polycyclic Aromatic Hydrocarbons under High Temperature Conditions. Consequences for Carbon Build up during Combustion and Fullerene Formation Processes*; Utrecht University: Utrecht, The Netherlands, **1998**.
- (48) Sarobe, M.; Jenneskens, L. W.; Wesseling, J.; Snoeijer, J. D.; Zwikker, J. W.; Wiersum, U. E. *Liebigs. Ann./Recueil* **1997**, 1207-1213.
- (49) Guest, M. F.; van Lenthe, J. H.; Kendrick, J.; Schöffel, K.; Sherwood, P.; Harrison, R. J. *GAMESS-UK, a package of ab initio programs*, **1998**. With contributions from: Amos, R.D., Buenker, R.J.; Dupuis, M.; Handy, N.C.; Hillier, I.; Knowles, P.J.; Bonacic-Koutecky, V.; von Niessen, W.; Saunders, V.R.; Stone, A.J. Derived from the original GAMESS code by: Dupuis, M.; Spangler, D.; Wendolowski, J.; NRCC Software Catalog, vol. 1, program no. QG01 (GAMESS), **1980**.
- (50) Steiner, E.; Fowler, P. W. *Int. J. Quant. Chem.* **1996**, *60*, 609-616.
- (51) Lazeretti, P.; Zanasi, R. *JYSMO package*; University of Modena, 1980.

# CHAPTER 8

## Novel Cyclohepta-Fused Non-Alternant Polycyclic Aromatic Hydrocarbons: Syntheses and Redox Properties

### Abstract

The novel cyclohepta[*c,d*]pyrene (**1**) and cyclohepta[*c,d*]fluoranthene (**2**) are obtained by Flash Vacuum Thermolysis (FVT) of the *bis*-acetylated precursors **20** and **25** at 500°C and 300°C, respectively. FVT at higher temperatures (900°C) leads in both cases to the formation of the thermodynamically more stable cyclopenta[*c,d*]pyrene (**6**) and cyclopenta[*c,d*]fluoranthene (**7**), respectively. In addition, the synthesis of another cyclohepta-fused PAH (CH-PAH), cyclohepta[*ℓ,ℓ'*]anthracene (**5**) was attempted; only circumstantial evidence for its formation could be obtained.

A survey on the redox properties of the CH-PAH **1**, **2**, pleiadiene (**3**), cyclohepta[*j,k*]phenanthrene (**4**) and 4,5-benzocyclohepta[1,2,3-*de*]naphthalene (**16**) shows that CH-PAH are more readily oxidized than the corresponding PAH and cyclopenta-fused PAH. A linear correlation is found between the first oxidation potential [ $E_{\text{onset}}(0/+1)$ ] and the HOMO energy derived from Hückel theory ( $-\epsilon_{\text{HOMO}}$ ).

## 8.1 Introduction

(Non)-alternant polycyclic aromatic hydrocarbons (PAH) are of interest since they constitute sub-structures of fullerenes and carbon nanotubes. In this context, hitherto especially the non-alternant cyclopenta-fused (CP)-PAH have been studied since they represent the key sub-structures of classical fullerenes, *i.e.* those fullerenes composed of pentagons and hexagons.<sup>1-3</sup> The pentagons are responsible for imposing positive curvature as well as the high electronegativity in C<sub>60</sub> and C<sub>70</sub>.<sup>4,5</sup> Furthermore, CP-PAH are widespread in our environment since they are invariably generated during (incomplete) combustion processes.<sup>6</sup> This is of relevance while many representatives possess genotoxic properties.<sup>7,8</sup>

Recently, cyclohepta-fused (CH) non-alternant PAH have been identified as interesting synthetic targets since the cyclohepta-moiety is also an important fragment to impose negative curvature in, for example, bended carbon nanotubes.<sup>9-12</sup> Unfortunately, however, not many PAH containing perimeter annelated cyclohepta-moieties are known and available in sufficient amount to investigate their properties. In contrast to their CP-PAH counterparts, CH-PAH have also not been detected as constituents in combustion effluents.<sup>6</sup>

Notwithstanding, CH-PAH are expected to have interesting properties since a butadiene-moiety (containing  $4\pi$  electrons) instead of an ethene-moiety (containing  $2\pi$  electrons) is fused to an alternant PAH core. This will affect the curvature in especially circumscribed systems,<sup>13</sup> but in addition also influence the electronic and magnetic properties of the molecule. Whereas the CP-moiety is responsible for the extraordinary electronegativity of C<sub>60</sub> and C<sub>70</sub>, *i.e.* renders these molecules n-type materials,<sup>4,14</sup> CH-PAH are expected to induce electropositive properties to carbon nanotubes, and thus may induce p-type character. An indication for such behavior was found previously looking at the redox properties of [7]circulene. Despite the fact that this molecule has an internal cyclohepta-moiety, it possesses a fairly low irreversible first oxidation wave positioned at *ca.* 0.9 V *vs.* SCE.<sup>15</sup> This is of importance since one of the major challenges in carbon nanotube chemistry has become the selective preparation of tubes containing tailor-made defects such as pentagons and heptagons to induce either n- or p-type character.<sup>16</sup> Furthermore, CH-PAH are non-alternant PAH and therefore expected to also possess worthwhile magnetic properties.

Unfortunately, however, the known representatives of the CH-PAH series, such as pleiadiene (**3**), dipleiadiene and cyclohepta[*j,k*]phenanthrene (**4**) are only accessible *via* lengthy syntheses and in most cases a mixture of constitutional isomers is formed.<sup>17-19</sup>

In this Chapter the syntheses of the novel CH-PAH, cyclohepta[*c,d*]pyrene (**1**) and cyclohepta[*c,d*]fluoranthene (**2**) as well as an attempted synthesis of cyclohepta[*k,l*]anthracene (**5**)

are reported. Assignment of the  $^1\text{H}$ - and  $^{13}\text{C}$ -NMR chemical shifts of **1** and **2** already indicates that the CH-moiety exerts a considerable effect on the magnetic properties. The magnetic properties of CH-PAH will be discussed in detail in the following Chapter (Chapter 9). Furthermore, the redox properties of these molecules, together with those of pleiadiene (**3**), cyclohepta[*j,k*]phenanthrene (**4**) and 4,5-benzocyclohepta[1,2,3-*de*]naphthalene (**16**) (Chart 1) are studied using Cyclic Voltammetry (CV). The influence of the CH-moiety on the redox properties is evaluated by comparison with the redox properties of the corresponding PAH and CP-PAH (Chart 1).

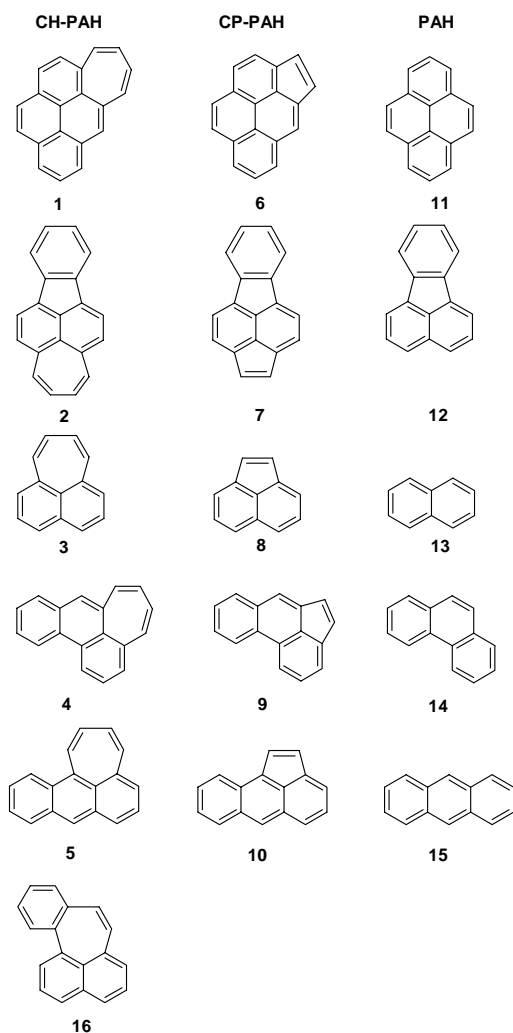
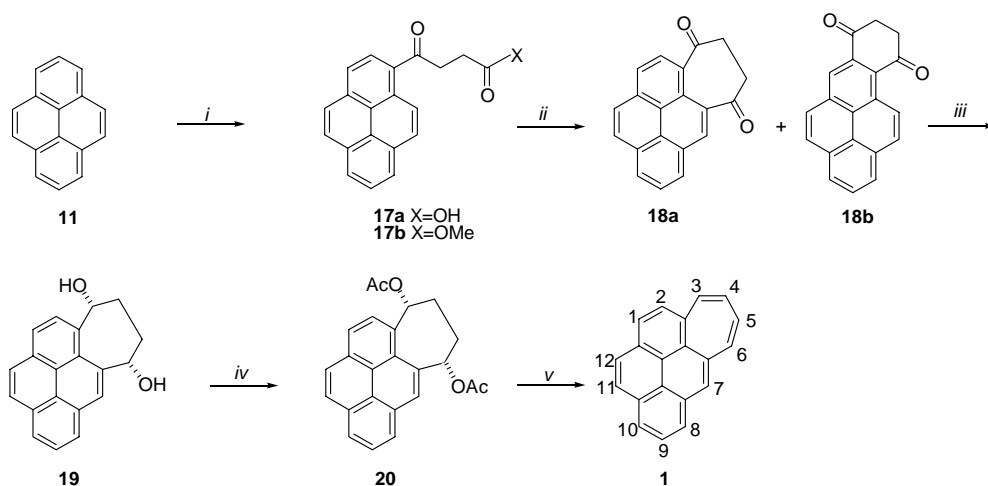


Chart 1

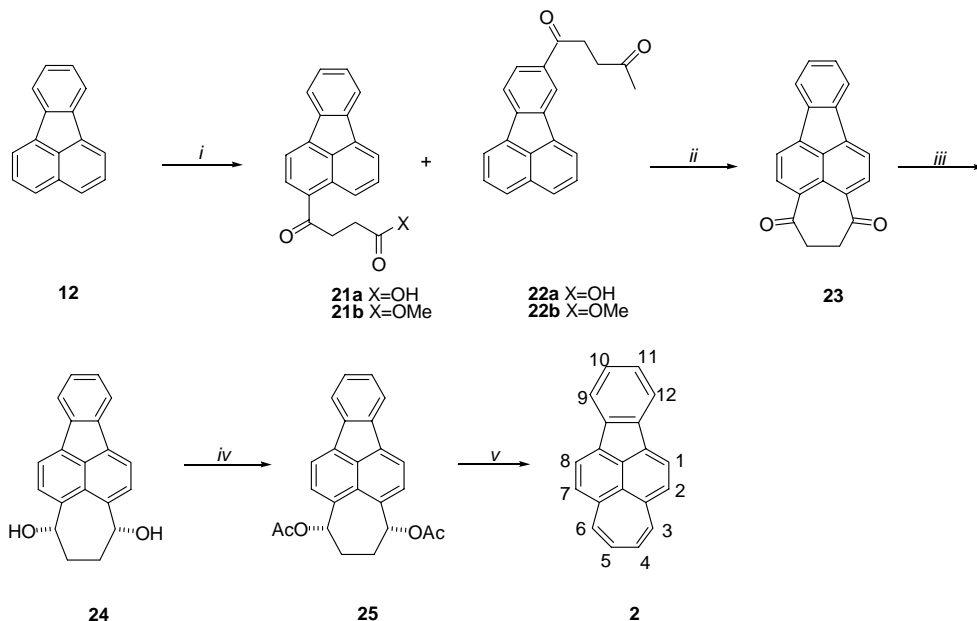
## 8.2 Results &amp; discussion

8.2.1 Syntheses of cyclohepta[*c,d*]pyrene (**1**) and cyclohepta[*c,d*]fluoranthene (**2**)

Cyclohepta[*c,d*]pyrene (**1**) and cyclohepta[*c,d*]fluoranthene (**2**) were prepared using a similar synthetic approach (see Schemes 1 and 2). The first step involves Friedel-Crafts acylation of succinic anhydride to either pyrene (**11**) or fluoranthene (**12**). Whereas, acylation of pyrene gives the correct isomer (**17a**, Scheme 1), acylation of **12** yielded besides the desired isomer **21a** (30 %), compound **22a** as an undesired side product (50 %, Scheme 2). To purify **17a** and **21a/22a**, they were converted into the corresponding methylesters (**17b** and **21b/22b**) and subjected to flash chromatography followed by recrystallization from toluene (see Experimental Section). Ring closure of the esters **17b** and **21b** by an internal Friedel Crafts acylation in a melt of AlCl<sub>3</sub>/NaCl gave the *bis*-ketones **18a/18b** (combined yield 56 %) and **23** (yield 50%), respectively. Notice that 1,2,3,4-tetrahydro-dioxo-cyclohexa[*a*]pyrene (**18b**) (10%) is a precursor for benzo[*a*]pyrene. Both **18a/18b** and **23** were purified by flash chromatography followed by recrystallization from toluene. Reduction of the *bis*-ketones **18a** and **23** with NaBH<sub>4</sub> proceeded quantitatively and afforded mixtures of the different possible stereoisomers of **19** and **24**, respectively, which were directly converted to the compounds **20** and **25** by acylation.



**Scheme 1.** Synthesis of cyclohepta[*c,d*]pyrene (**1**). *i* AlCl<sub>3</sub>/ succinic anhydride, *ii* AlCl<sub>3</sub>/NaCl (T = 150°C), *iii* NaBH<sub>4</sub> in benzene, *iv* CH<sub>3</sub>COCl and pyridine in CH<sub>2</sub>Cl<sub>2</sub>, and, *v* FVT at 500°C.



**Scheme 2.** Synthesis of cyclohepta[*6,4*]fluoranthene (**2**). *i* AlCl<sub>3</sub>/ succinic anhydride, *ii* AlCl<sub>3</sub>/NaCl (T = 150°C), *iii* NaBH<sub>4</sub> in benzene, *iv* CH<sub>3</sub>COCl and pyridine in CH<sub>2</sub>Cl<sub>2</sub>, and, *v* FVT at 300°C.

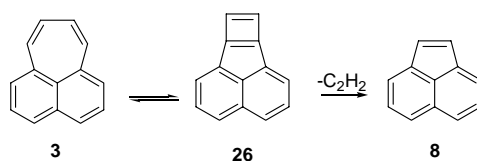
For the conversion of **20** and **25** into **1** and **2**, respectively, Flash Vacuum Thermolysis (FVT) was applied. Elimination of acetic acid is known to occur at relatively low temperatures under FVT conditions.<sup>20</sup> FVT of **20** at 500°C afforded the desired cyclohepta[*6,4*]pyrene (**1**) in quantitative yield [mass recovery 80%, sublimation (subl.) rate 10 mg h<sup>-1</sup>, subl. temperature 150°C]. As expected, elimination of the two molecules of acetic acid was shown to be a consecutive (two-step) process. At lower temperatures (FVT at 200°C) in addition the two possible *mono*-acetylated compounds were identified in the pyrolysate (<sup>1</sup>H-NMR, overall yield 30% at 200°C). FVT of **25** gave cyclohepta[*6,4*]fluoranthene (**2**) also in quantitative yield already at 300°C [mass recovery 90%, subl. rate 15 mg h<sup>-1</sup>, subl. temperature 150°C]. The difference in temperature for the complete conversion of **20** and **25** into **1** and **2**, respectively, is currently attributed to the stereochemistry of the *bis*-acetylated precursors **20** and **25**. The novel CH-PAH **1** and **2** were purified by flash chromatography followed by recrystallization from *n*-pentane (see Experimental Section). Their structures were assigned on the basis of <sup>1</sup>H-, <sup>13</sup>C-NMR, 2D-NMR, GC-MS and elemental analysis (see Experimental Section).<sup>21</sup> It is noteworthy that the <sup>1</sup>H-NMR chemical shifts of **1** and **2** display an interesting feature. The <sup>1</sup>H-NMR chemical shifts of both the cyclohepta-moiety and the aromatic core of **1** are considerably shifted up-field with respect to those of **2** (average up-field

shift *ca.* 0.4 ppm). This indicates that in **1** additional shielding effects are present, whilst they are not in **2**. The magnetic properties of CH-PAH are subject of a detailed investigation in Chapter 9.

FVT of **20** and **25** at temperatures above 900°C showed that both cyclopenta[*c,d*]pyrene (**6**) and cyclopenta[*c,d*]fluoranthene (**7**), respectively were formed. Independent FVT of pleiadiene (**3**, Chart 1), which was obtained *via* a literature procedure,<sup>22</sup> corroborated that under these conditions the CH-PAH behave like transient intermediates that are directly converted to the cyclopenta-fused derivatives; at 900°C pleiadiene (**3**) gave acenaphthylene (**8**) quantitatively.

A rationalization for these observations is given in Scheme 3. Here, the intermediacy of the cyclobuta-derivative **26** is proposed from which extrusion of a C<sub>2</sub>H<sub>2</sub>-fragment can take place. This will give the thermodynamically more stable cyclopenta-fused PAH (**6**). This is further substantiated by independent FVT at 900°C of 6b,8a-dihydrocyclobuta[*d*]acenaphthylene (**26**), which was prepared independently by the photochemical cycloaddition of maleic anhydride to acenaphthylene.<sup>22</sup> Upon FVT at 900°C of **26** acenaphthylene (**8**) was obtained as the sole product.

These observations provide an explanation for the fact that up till now CH-PAH have not been identified as constituents of combustion exhausts. Although accretion of C<sub>4</sub>H<sub>4</sub> units to alternant PAH might occur,<sup>23</sup> CH-PAH will probably not be stable enough to survive the high temperature conditions. Rearrangement to the thermodynamic more stable CP-PAH is likely to occur.



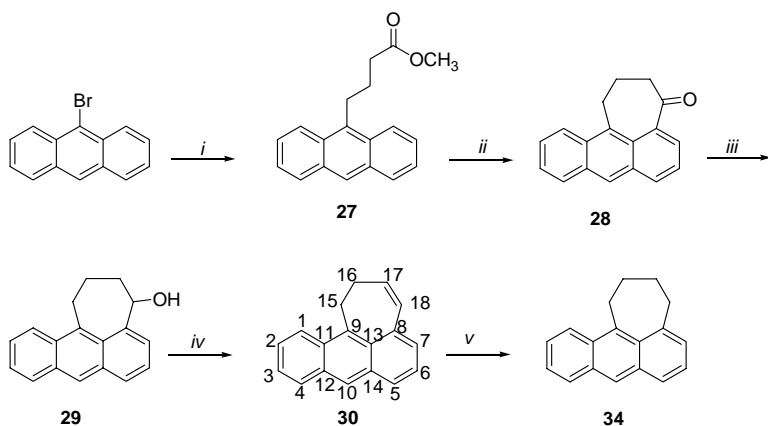
**Scheme 3.** Formation of **1** upon FVT of **20** and subsequent rearrangement to cyclopenta[*c,d*]pyrene (**6**).

### 8.2.2 Attempted synthesis of cyclohepta[*k,l*]anthracene (**5**)

Another synthetic objective was the CH-PAH cyclohepta[*k,l*]anthracene (**5**). However, a similar synthetic approach as was followed for **1** and **2**, was found to be unsuitable for **5**. Although, Friedel-Crafts acylation of succinic anhydride to anthracene gave minor amounts of 4-(9-anthracenyl)-4-oxobutanoate, the subsequent internal Friedel-Crafts in an AlCl<sub>3</sub>/NaCl melt was unsuccessful. Besides traces of the ring-closed product, the major product was anthracene, *i.e.* decomposition of **27** occurs. This is attributed to the special reactivity of the 9 and 10 positions of anthracene.<sup>24,25</sup>



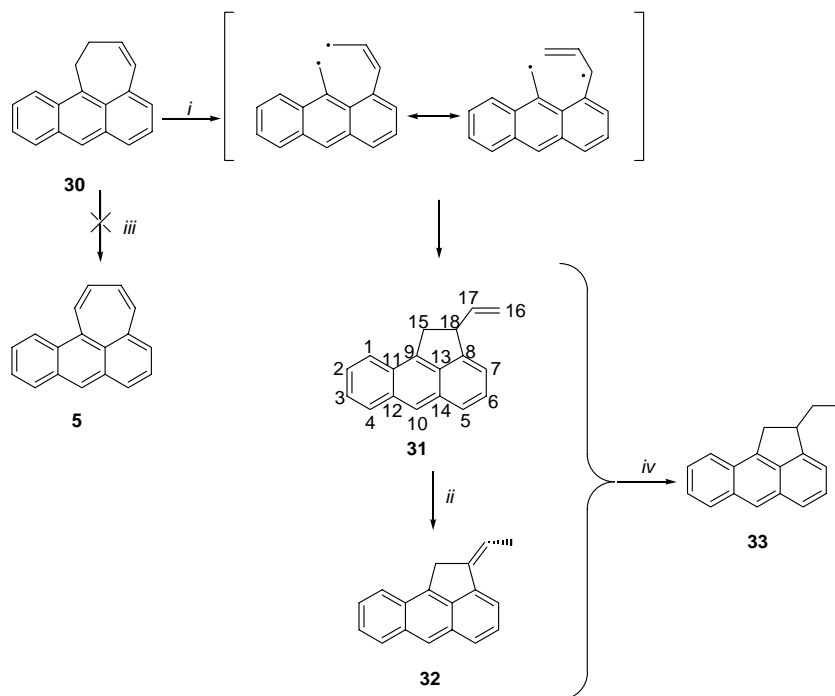
Therefore, a different approach was followed (Scheme 4). Suzuki-coupling of methyl-but-3-enoate to 9-bromoanthracene afforded **27**.<sup>26</sup> Ring closure of **27** was achieved in a melt of P<sub>2</sub>O<sub>5</sub> (yield 75 %) and followed by quantitative reduction of ketone **28** with NaBH<sub>4</sub>. The alcohol **29** was converted to the alkene **30** by treatment with PBr<sub>3</sub> and elimination of the dibromophosphate intermediate. The structure of **30** was assigned on the basis of its analytical data (<sup>1</sup>H-, <sup>13</sup>C-, 2D-NMR, GC-MS and elemental analysis). The formation of **30** was further corroborated by its conversion into compound **34** by catalytic hydrogenation (see Scheme 4 and Experimental Section)



**Scheme 4.** Synthesis of cyclohepta[*k,l*]anthracene (**5**). *i* Suzuki-coupling, *ii* P<sub>2</sub>O<sub>5</sub>, *iii* NaBH<sub>4</sub> in benzene, *iv* PBr<sub>3</sub>, and, *v* pH<sub>2</sub>/1atm, Pd/C.

The conversion of **30** into the desired **5** was initially attempted by FVT. However, pyrolysate analysis [T = 700°C, mass recovery 70%, subl. rate 5 mg h<sup>-1</sup>, subl. temperature 80°C] revealed that instead of **5** a mixture of compounds was present all with *m/z* 230 (GC-MS). The main product (*ca.* 80%) that was formed after FVT at 700°C was isolated from the pyrolysate by recrystallization from *n*-pentane and identified as **31** on the basis of spectroscopic analysis as well as its conversion into **33** by catalytic hydrogenation (Pd/C, pH<sub>2</sub> 1atm, see Experimental Section and Scheme 5). The <sup>1</sup>H-NMR spectrum of the hydrogenated compound **33** displays a characteristic triplet ( $\delta = 1.11$ , *J* 7.2 Hz). This indicates that a CH<sub>3</sub>-group is present in the **33**, and that consequently, a terminal alkene (**31**) was formed upon FVT of **30** at 700°C. Hence, the seven-membered ring is converted into a five-membered ring containing a terminal alkene. 2D-NMR-

analysis confirmed that the proposed structure of the rearranged product **31** is indeed correct (Scheme 5 and see also Experimental Section).



**Scheme 5.** Rearrangement of **30** under FVT conditions to **31** and **32**. *i* FVT at 700°C, *ii* 1,3H-shift, *iii* DDQ, and, *iv*  $\text{PH}_2/1\text{atm}$ , Pd/C.

The formation of **31** from **30** is rationalized by invoking the homolytic scission of the benzylic and allylic  $\text{sp}^3\text{-sp}^3$  carbon bond. The biradical intermediate will be stabilized by conjugation (Scheme 5). At 700°C besides **31** another PAH with  $m/z$  230 was formed (*ca.* 4%). The 700°C pyrolysate could be enriched in this compound (*ca.* 15%) by recrystallization from *n*-pentane (see Experimental section). The  $^1\text{H-NMR}$  spectrum of this enriched pyrolysate contained two doublets at 2.24 and 2.05 ppm ( $J$  7.2 Hz) and two quartets of triplets at 6.54 ppm ( $^3J_{\text{HH}}$  6.9 Hz and  $^3J_{\text{HH}}$  2.4 Hz), which indicate that these compounds are the *cis*- and *trans*- isomers of **32**, formed from **31** *via* 1,3H-shifts under FVT-conditions (Scheme 5). The structural assignment of **32**

is further corroborated by catalytic hydrogenation of the enriched 700°C pyrolysate, which contained both **31** and **32**. This yielded *only* 2-ethyl-1,2-dihydro-cyclopenta[*k,l*]anthracene (**33**).

Since FVT of **30** did not afford the desired **5**, a different approach to introduce full  $\pi$ -conjugation in the CH-moiety was attempted. To this end, **30** was treated with 2,3-dichloro-5,6-dicyano-1,4-benzoquinone (DDQ),<sup>27</sup> which gave a complicated mixture of compounds with  $m/z$  228. Analysis of this mixture by <sup>1</sup>H-NMR displayed a set of signals at 6.84 (d,  $J$  12.0 Hz), 6.40 (d,  $J$  10.8 Hz), 6.01 (m) and 5.80 (m) ppm, which are in line with the coupling patterns expected for the cyclohepta-protons of **5** (Figure 1A). This was substantiated by a COSY-experiment, which displayed the correct coupling constants, and simulation of the <sup>1</sup>H-NMR-spectrum using Mestrec (Figure 1B).

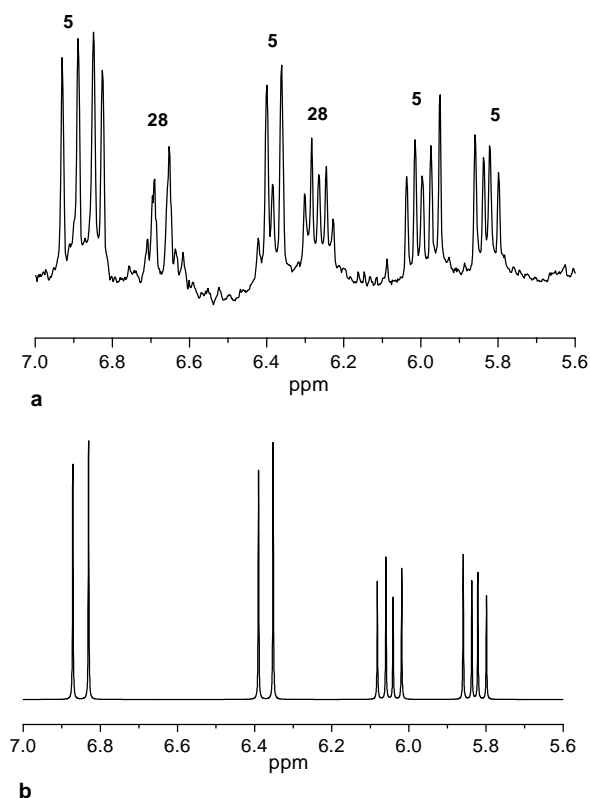
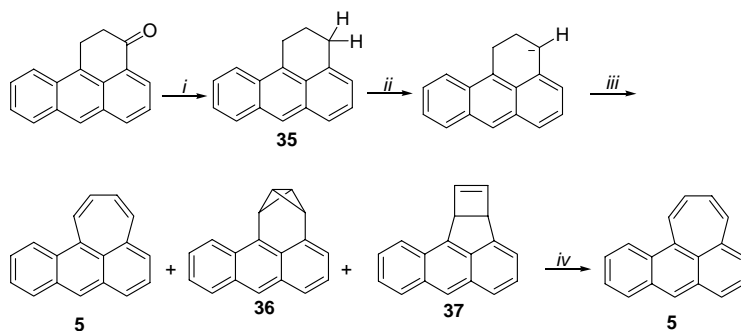


**Figure 1.** a. <sup>1</sup>H-NMR signals assigned to the cyclohepta-moiety of cyclohepta[*k,l*]anthracene (**5**). b. Simulated <sup>1</sup>H-NMR signals assigned to the cyclohepta-moiety of cyclohepta[*k,l*]anthracene (**5**).

Unfortunately, **5** could not be isolated since it decomposed during work-up.<sup>28</sup> Possibly, since CH-PAH are particularly sensitive towards oxidation. This was also reported for cyclohepta[*f,g*]acanthrylene.<sup>28</sup> Hence, FVT of *bis*-acetylated precursors is the method of choice, *i.e.* the protecting group can be eliminated under mild conditions. Unfortunately, the *bis*-acetylated precursor for **5** is not readily accessible. Another approach to **5** is carbene addition to dihydrobenz[*k,l*]anthracene (**35**, Scheme 6). Although, this is likely to yield a mixture of isomers (**5**, **36** and **37**, Scheme 6), FVT of the complete mixture at low temperature should predominantly give **5**. Note that the reaction mixture of cyclohepta[*j,k*]phenanthrene (**4**), prepared via a similar route,<sup>18</sup> gives the desired **4** in 80% yield upon FVT at 300°C.



**Scheme 6.** Proposed alternative route toward cyclohepta[*k,l*]anthracene (**5**). *i* reduction with  $\text{LiAlH}_4/\text{AlCl}_3$ , *ii*  $n\text{-BuLi}$ , *iii*  $\text{CH}_2\text{Cl}_2/n\text{-BuLi}$ , and, *iv* FVT at 700°C.

### 8.2.3 Redox properties of cyclohepta-fused PAH

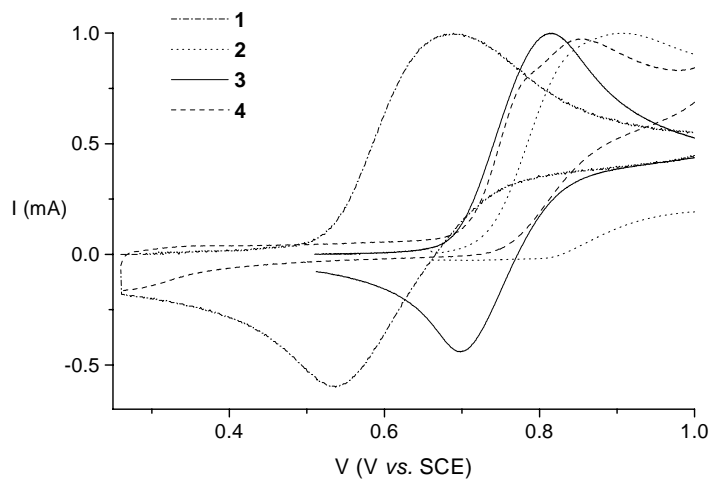
The redox properties of the externally-fused novel CH-PAH **1** and **2** and of **3** and **4** were determined using Cyclic Voltammetry in  $\text{CH}_3\text{CN}$ .<sup>18</sup> In Table 1 the results are summarized.

Compounds **1** and **3** display a (*pseudo*)-reversible oxidation wave [ $E_{1/2}(0/+1)$ ], as can be seen from the listed  $\Delta E$  ( $= E_{\text{pc}} - E_{\text{pa}}$ ), which corresponds to the formation of the radical cation from the neutral species (see Figure 2). An *irreversible* oxidation [ $E_{\text{onset}}(0/+1)$ , see Experimental Section] is found for **2**, **4** and **16** (see Figure 2). All compounds show a second *irreversible* oxidation wave that corresponds to formation of the *bis*-cation from the radical cation [ $E_{\text{onset}}(+1/+2)$ ]. A (*pseudo*)-reversible first reduction potential [ $E_{1/2}(0/-1)$ ], which corresponds to the formation of the radical anion of the neutral species, was found for all CH-PAH. In addition, all compounds display a

**Table 1.** Oxidation and reduction potentials (V *vs.* SCE) of **1** - **4** and **16** measured in acetonitrile and the HOMO and LUMO energies (in  $\beta$ ) derived from HMO theory.

	$E_{1/2}(0/+1)$ (V)	$\Delta E$ (V)	$E_{1/2}(+1/+2)$ (V)	$\Delta E$	$E_{1/2}(0/-1)$ (V)	$\Delta E$ (V)	$E_{\text{onset}}(-1/-2)$ (V)	$\Delta E$	$\epsilon_{\text{HOMO}}$ ( $\beta$ )	$\epsilon_{\text{LUMO}}$ ( $\beta$ )
<b>1</b>	0.62	0.12	1.09	<i>irrev.</i>	-1.86	0.10	-2.11	<i>irrev.</i>	0.198	-0.432
<b>2</b>	0.75	<i>irrev.</i>	1.40	<i>irrev.</i>	-1.81	<i>irrev.</i>	-2.53	<i>irrev.</i>	0.325	-0.469
<b>3</b>	0.76	0.10	1.30	<i>irrev.</i>	-2.04	0.11	-2.42	<i>irrev.</i>	0.241	-0.457
<b>4</b>	0.66	<i>irrev.</i>	1.63	<i>irrev.</i>	-2.01	0.08	<sup>a</sup>	<i>irrev.</i>	0.246	-0.442
<b>16</b>	0.96	<i>irrev.</i>	1.40	<i>irrev.</i>	-2.14	0.12	-2.45	<i>irrev.</i>	0.314	-0.496

<sup>a</sup>not detected in CH<sub>3</sub>CN, outside the potential window (see Experimental Section).


**Figure 2.** First oxidation waves [ $E_{1/2}(0/+1)$ ] for **1**, **2**, **3** and **4** (in V *vs.* SCE, scan rate 50 mVs<sup>-1</sup>).

second *irreversible* reduction potential that corresponds to the conversion of the radical anion in the *bis*-anion [ $E_{\text{onset}}(-1/-2)$ ].

**Anodic behavior**

At first sight, the redox behaviour of CH-PAH is markedly different from that of the corresponding CP-PAH. Oxidation of the non-alternant PAH containing CH-moieties (**1** - **4** and **16**) is considerably more facile than that of the corresponding PAH or CP-PAH (Table 2 and see Chapter 7). Oxidation of a CH-PAH containing an internal CH-moiety, viz. **16** [ $E_{\text{onset}}(0/+1)$  0.96 V *vs.* SCE], is somewhat more difficult than oxidation of the CH-PAH with externally-fused CH-moieties (**1** - **4**). The  $E_{\text{onset}}(0/+1)$  value of **16** is in good agreement with that reported for the internal CH-PAH [7]circulene (0.73 V *vs.* Ag/Ag<sup>+</sup>, *ca.* 0.99 V *vs.* SCE).<sup>15</sup>

**Table 2.** Relationship between the  $E_{\text{onset}}(0/+1)$  values of PAH and the  $E_{\text{onset}}(0/+1)$  values of the related CH-PAH.

PAH	$E_{1/2}(0/+1)$	CH-PAH	$E_{1/2}(0/+1)$	$\Delta E_{\text{CH-PAH}}(0/+1)^a$
<b>11</b>	1.06	<b>1</b>	0.62	-0.44
<b>12</b>	1.46	<b>2</b>	0.75	-0.76
<b>13</b>	1.61	<b>3</b>	0.76	-0.85
<b>14</b>	1.44	<b>4</b>	0.66	-0.78

$$^a \Delta E_{\text{CH-PAH}}(0/+1) = E_{1/2}(0/+1)_{\text{CH-PAH}} - E_{1/2}(0/+1)_{\text{PAH}}$$

For alternant PAH it is well documented that the first reduction wave [ $E_{1/2}(0/+1)$ ] gives a linear correlation with the HOMO energy ( $\epsilon_{\text{HOMO}}$ ) of the neutral molecule derived using Hückel theory.<sup>29</sup> For non-alternant PAH comparable correlations were considered to be less reliable or even absent.<sup>30,31</sup> However, whilst no correlation was found for the non-alternant CP-PAH between  $E_{1/2}(0/+1)$  and the standard Hückel  $-\epsilon_{\text{HOMO}}$  (Chapter 7), a satisfactory linear correlation is obtained here between the  $E_{\text{onset}}(0/+1)$ , derived for the 5 CH-PAH together with the  $E_{\text{onset}}(0/+1)$  of their 4 parent PAH, and the corresponding  $-\epsilon_{\text{HOMO}}$  energies [for  $E_{\text{onset}}(0/+1)$  see Experimental Section,  $r^2 = 0.962$  with  $\beta_0 = -2.15$  eV and  $C = 1.81$ , according to *Eqn 1*, (Figure 3)].

$$E_{\text{onset}}(0/+1) = -\beta_0 \epsilon_{\text{HOMO}} + C \quad \text{Eqn. 1}$$

In *Eqn. 1*  $\beta_0$  represents the effective resonance integral between two neighboring  $2p_\pi$  orbitals and  $C$  a solvation term. The value found for  $\beta_0$  (-2.15 eV) is in good agreement with the value found for the corresponding correlation in which only alternant PAH were used ( $\beta_0 = -2.05$  eV).<sup>29</sup>

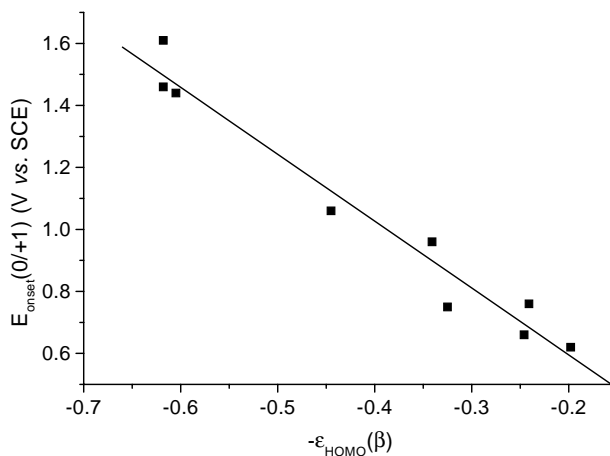


**Figure 3.** Linear correlation between  $E_{\text{onset}}(0/+1)$  (V vs. SCE) of the PAH and CH-PAH (Chart 1) and their Hückel  $-\epsilon_{\text{HOMO}}$  energies (Table 2).

This indicates that annelation of a cyclohepta-moiety exerts a (near) constant effect on the HOMO. The Hückel model proposed in Chapter 7 to describe the *cathodic* behavior of CP-PAH is applied here to describe the *anodic* behavior of CH-PAH. For the latter, the HOMO of the parent PAH and the HOMO of butadiene possess the correct phase to interact, leading to a HOMO that corresponds to the *out-of-phase* combination of the participants (Figure 4).<sup>4</sup> As a consequence, the HOMO of the CH-PAH will be positioned higher in energy, *i.e.* destabilized, with respect to its contributors (see Figure 4). Since the orbitals possess the correct phase to interact, no significant shifting of the occupied HOMO-*n* orbitals will occur, and therefore no disruption of the alternant PAH structure takes place. Hence, annelation of a CH-moiety leads to a similar negative shift of  $E_{1/2}(0+1)$  of the CH-PAH with respect to the  $E_{1/2}(0+1)$  of the parent PAH (Table 3). Note that for the corresponding CP-PAH no correlation between the first oxidation wave and the  $-\epsilon_{\text{HOMO}}$  energy derived from HMO theory was obtained. In this case the HOMO of ethene and the HOMO of the alternant PAH do not have the correct phase to interact. Therefore, shifting of the HOMO-*n* occupied orbitals does occur, and hence no straightforward correlation can be derived (see also Chapter 7).

The magnitude of the negative shift of  $E_{1/2}(0+1)$  is dependent on the interaction between the  $\epsilon_{\text{HOMO}}$  of the parent PAH (**11**:  $0.445\beta$ , **12**:  $0.618\beta$ , **13**:  $0.618\beta$ , **14**:  $0.605\beta$ ) and that of butadiene

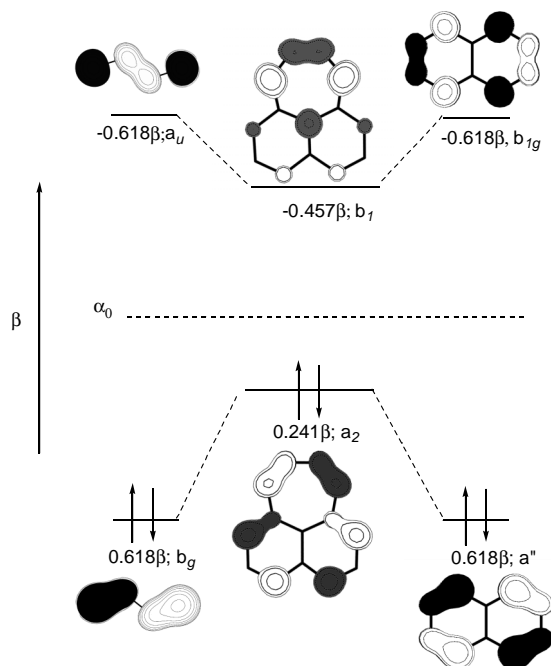


**Figure 4.** Effect of the incorporation of a cyclohepta-moiety in an alternant PAH core on  $\epsilon_{\text{HOMO}}$ .

( $0.618\beta$ ) (see Chapter 7). The  $\epsilon_{\text{HOMO}}$  of **11** is significantly higher in energy ( $0.445\beta$ ) and therefore a significantly smaller shift in  $E_{1/2}(0/+1)$  is observed for **1** (Table 2).

All CH-PAH **1** - **4** and **16** display a second oxidation potential, which is not observed for the PAH and CP-PAH studied in Chapter 7. Remarkably, this second oxidation potential [ $E_{\text{onset}}(+1/+2)$ ] is close to the first oxidation potential [ $E_{\text{onset}}(0/+1)$ ] of the corresponding PAH lacking the CH-moiety (Table 3). This indicates that after oxidation, the effect of the fused CH-moiety on the remainder of the molecule is reduced. This can be explained if the positive charge, formed upon the first oxidation, predominantly resides in the CH-moiety, giving a tropylium cation containing six  $\pi$ -electrons (Scheme 7). Note that the radical cation is *iso*- $\pi$ -electronic with the phenalyl radical.<sup>32</sup>

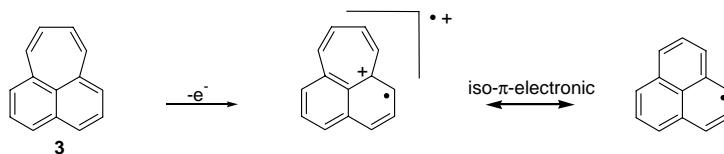
It is noteworthy that the  $E_{\text{onset}}(+1/+2)$  of **2** and **16** are identical (1.40 V *vs.* SCE). This corroborates the interpretation of the presence of a tropylium sub-structure. After oxidation the effect of the CH-moiety in **2** and **16** is reduced; the second oxidation takes place at the naphthalene core [ $E_{\text{onset}}(0/+1)$  of **13** is 1.45 V *vs.* SCE]



**Table 3.** Relationship between the  $E_{1/2}(0/+1)$  values of PAH and the  $E_{1/2}(0/+1)$  values of the related CH-PAH (V vs. SCE).

PAH	$E_{\text{onset}}(0/+1)$	CH-PAH	$E_{\text{onset}}(+1/+2)$	Difference
<b>11</b>	1.06	<b>1</b>	1.09	0.03
<b>12</b>	1.46	<b>2</b>	1.40	0.06
<b>13</b>	1.45	<b>3</b>	1.30	0.15
<b>14</b>	1.44	<b>4</b>	1.63	0.19

$$^a \Delta E_{\text{CH-PAH}}(0/+1) = E_{1/2}(0/+1)_{\text{CH-PAH}} - E_{1/2}(0/+1)_{\text{PAH}}$$


**Scheme 7.** Formation of a tropylium sub-structure upon oxidation of a CH-PAH.

### Cathodic behavior

Comparison of the first reduction potentials [ $E_{1/2}(0/-1)$ ] of the CH-PAH **1** - **4** to the first reduction potential of the corresponding PAH **11** - **13** (Table 4), shows that in the case of **1**, **3** and **4** reduction occurs more readily for the CH-PAH. However, the  $E_{1/2}(0/-1)$  of **2** is identical to that of the corresponding PAH **12**.

**Table 4.** Relationship between the  $E_{1/2}(0/-1)$  values of PAH and the  $E_{1/2}(0/-1)$  values of the related CH-PAH (V vs. SCE).

PAH	$E_{1/2}(0/-1)$	CH-PAH	$E_{1/2}(0/-1)$	$\Delta E_{\text{CH-PAH}}(0/-1)^a$
<b>11</b>	-2.22	<b>1</b>	-1.86	0.37
<b>12</b>	-1.81	<b>2</b>	-1.81	0.00
<b>13</b>	-2.66	<b>3</b>	-2.04	0.62
<b>14</b>	-2.62	<b>4</b>	-2.01	0.61

$$^a \Delta E_{\text{CH-PAH}}(0/-1) = E_{1/2}(0/+1)_{\text{CH-PAH}} - E_{1/2}(0/+1)_{\text{PAH}}$$

Furthermore, no correlation is obtained when the  $E_{1/2}(0/-1)$  of the CH-PAH together with the parent PAH are plotted against the  $-\epsilon_{\text{LUMO}}$  energies. Figure 4 show that in this case the

LUMO of the parent PAH does not have the correct phase to interact with that of butadiene. Hence, shifting of the occupied orbitals does occur and Hückel theory cannot be straightforwardly applied to describe the cathodic behavior of CH-PAH.

### 8.3 CH-PAH and CP-PAH are *anti*-symmetric

Previously, it was noted by Michl that the behavior of acenaphthylene (**8**) and pleiadene (**3**) displayed an *anti*-symmetric relationship.<sup>33</sup> In this Chapter it is shown that in general, the electronic behavior of CP-PAH is *anti*-symmetric with that of CH-PAH. From Table 5 this effect is apparent when the differences between the HOMO energies of the parent PAH and CH-PAH [ $\Delta\epsilon_{\text{HOMO PAH - CH-PAH}}$ ] are compared with the differences between the LUMO energies of CP-PAH with their parent PAH [ $\Delta\epsilon_{\text{LUMO CP-PAH - PAH}}$ ]. These values are similar. The minor differences are a consequence of the fact that the LUMO of ethene ( $-1.000 \beta$ ) is further positioned from the  $\alpha$ -level than the HOMO of butadiene ( $0.618 \beta$ ). Hence, the destabilisation of the HOMO of CH-PAH is somewhat enhanced. This *anti*-symmetric behavior is also displayed in the following. CP-PAH can stabilize negative charge while a  $6\pi$  cyclopentadienide sub-structure can be formed and therefore have high electron affinities, whereas CH-PAH can stabilize positive charge upon formation of a  $6\pi$  tropylium sub-structure and are thus expected to have low ionisation potentials.

**Table 5.** Relation between the HOMO of CH-PAH and the LUMO of CP-PAH

CH-PAH	$\Delta\epsilon_{\text{HOMO}} (\text{CH-PAH} - \text{PAH})$ ( $\beta$ )	CP-PAH	$\Delta\epsilon_{\text{LUMO}} (\text{PAH} - \text{CP-PAH})$ ( $\beta$ )
<b>1</b>	0.247	<b>6</b>	-0.220
<b>2</b>	0.293	<b>7</b>	-0.272
<b>3</b>	0.377	<b>8</b>	-0.333
<b>4</b>	0.359	<b>9</b>	-0.314

### 8.4 Conclusions

The novel CH-PAH **1** and **2** have been synthesized in good yield *via* a route in which the ultimate step consists of FVT of the *bis*-acetylated precursors **20** and **25**. These CH-PAH are shown to decompose to the thermodynamic more stable CP-derivatives under FVT conditions at high temperatures (900°C). A mechanism involving cyclobuta-substituted PAH, from which  $\text{C}_2\text{H}_2$

extrusion takes place, is proposed to account for this observation. The conversion of CH-PAH in CP-PAH explains why CH-PAH have not been identified in combustion exhausts. The attempted synthesis of **5**, which was hampered by the fact that the penultimate *bis*-acetylated precursor is not readily accessible, shows that FVT of *bis*-acetylated precursors is the method of choice to obtain CH-PAH.

CH-PAH display interesting anodic behaviour. They are more readily oxidized than the corresponding alternant PAH and non-alternant CP-PAH. Since a linear correlation is obtained between the  $E_{\text{onset}}(0/+1)$  and the  $-\epsilon_{\text{HOMO}}$  energy derived from HMO theory, the CH-moiety is anticipated to act as a substituent. The *anti*-symmetric behaviour of CH-PAH and CP-PAH renders these molecules interesting candidates for the preparation of all carbon/hydrogen CP-CH-PAH donor-acceptor compounds.

## 8.5 Experimental section

All reactions were carried out under a  $\text{N}_2$  atmosphere. Solvents were dried and purified using standard procedures. Commercially available reagents were used without further purification. Column chromatography was performed on Merck kieselgel 60 silica (230-400 ASTM). Melting points are uncorrected.  $^1\text{H}$  (300.13 MHz) and  $^{13}\text{C}$  (75.47 MHz) NMR spectra were recorded on a Bruker AC 300 spectrometer and a Varian 300 NMR using  $\text{CDCl}_3$  as the solvent unless stated otherwise. Chemical shifts (in ppm) are given relative to TMS (0 ppm) in the case of  $^1\text{H}$ -NMR and relative to  $\text{CDCl}_3$  (77.00 ppm) in the case of  $^{13}\text{C}$ -NMR.  $J$  values are given in Hz. For the  $^1\text{H}$ -NMR spectrum multiplicity is denoted as following: s = singlet, d = doublet, t = triplet, dd = double doublet, m = multiplet. In  $^{13}\text{C}$ -NMR the signals are indicated with q = quaternary carbon, t = tertiary carbons and s = secondary carbon. Infrared spectra were recorded with a FTIR Mattson Galaxy FTIR 5000 in optically pure KBr. GC-MS spectra were measured on a ATI Unicam Automass System 2 quadrupole mass spectrometer (column: J&W Scientific DB-15ms, length 30m, ID 0.25 mm and film thickness 0.25mm; injector temperature: 300°C, temperature program: 2 min 200°C – (10°Cmin<sup>-1</sup>) - 280°C; carrier gas He). Elemental analysis was carried out by H. Kolbe Mikroanalytisches Laboratorium Mülheim a.d. Ruhr, Germany. UV/Vis spectra were obtained with a Varian Cary 1 UV/Vis spectrophotometer. The assignment of the  $^1\text{H}$ -NMR signals of **1**, **2** and **32** - **36** was achieved by COSY and NOESY experiments [NMR-samples were degassed, 90°-pulse and  $t_1$  were determined for every compound.],  $^{13}\text{C}$ -NMR signals were assigned by HETCOR [ $J_{1\text{kh}} = 160\text{Hz}$ ] and long-range HETCOR-experiments [ $J_{\text{nh}} = 4, 6$  or  $8$  Hz]. Not all quaternary carbons are assigned.

*Caution:* non-alternant PAH are potential genotoxic compounds.

### Cyclic Voltammetry

## Chapter 8

Cyclic voltammetry (CV) was performed using an EG&G Potentiostat/Galvanostat Model 263A in CH<sub>3</sub>CN (freshly distilled from CaH<sub>2</sub>) containing 0.1 M Bu<sub>4</sub>NPF<sub>6</sub> as supporting electrolyte at scanning rates of 50 and 100 mV s<sup>-1</sup> (potential window -2.5 to +3 V) and were referenced to SCE by measuring the oxidation potential of the FeCP<sub>2</sub>/FeCP<sub>2</sub><sup>+</sup> couple (0.31V *vs.* SCE).

For *irreversible* electrochemical processes  $E_{\text{onset}}$  values instead of peak potentials ( $E_{\text{pc/pa}}$ ) are reported. The use of peak potentials can give unreliable information due to the dependence of  $E_{\text{pc/pa}}$  on factors such as solvent, electrolyte, scan rate and the concentration of the analyte.<sup>34</sup>

First oxidation potentials [ $E_{\text{onset}}(0/+1)$  in V *vs.* SCE] of the alternant PAH **11** – **14**, and the  $\epsilon_{\text{HOMO}}$  energy derived using HMO theory.

Alternant PAH	$E_{\text{onset}}(0/+1)$ (V <i>vs.</i> SCE)	$\epsilon_{\text{HOMO}}$ ( $\beta$ )
<b>11</b>	1.06 (irrev.)	0.886
<b>12</b>	1.46 (irrev.)	0.618
<b>13</b>	1.61 (irrev.)	0.618
<b>14</b>	1.44 (irrev.)	0.605

### Hückel calculations

Hückel Molecular Orbital (HMO) Calculations were run on a PC with a QCPE program, Computational Utilities Package (QCMP021) in the standard Hückel approximation (with all  $\alpha$ 's and  $\beta$ 's equal).

### General Flash Vacuum Thermolysis Procedure<sup>35</sup>

A commercial Thermolyne 21100 tube furnace containing an unpacked quartz tube (length 40 cm and diameter 2.5 cm) was used in all FVT experiments. The pressure during all FVT-experiment was 0.001 mmHg. The products were rinsed from the tube or the cold-trap with distilled CH<sub>2</sub>Cl<sub>2</sub>, after which the pyrolysate composition was determined by GC and <sup>1</sup>H-NMR.

### Methyl-4-(1-pyrenyl)-4-oxo-butanoate (17b)

To an ice-cooled suspension of 10.0 g (50.0 mmol) pyrene (**11**) and 5.8 g succinic anhydride (58.0 mmol) in 250 ml CH<sub>2</sub>Cl<sub>2</sub>, 13.0g (97.5 mmol) AlCl<sub>3</sub> was added. After stirring at room temperature for 24 hr, the reaction mixture was hydrolyzed by adding it to ice-water (200 g) and 1M HCl and extracted with CH<sub>2</sub>Cl<sub>2</sub> (3 x 200 ml). After concentration of the combined organic layers an orange solid was obtained. Yield 13.0 g (43.0 mmol, 86 %) of **17a**.

<sup>1</sup>H-NMR: (δ, ppm) 8.95 (1H, d, *J* 9.44), 8.35 (1H, d, *J* 8.30), 8.21 (2H, m), 8.15 (2H, m), 8.03 (3H, AB, J), 3.54 (2H, t, *J* 6.65/6.25), 2.94 (2H, t, *J* 6.50/6.28).

The reaction mixture was directly converted to the methyl ester (**17b**) by dissolving 13.0 g of **17a** MeOH (300 ml) and addition of a catalytic amount of 37% HCl (1 ml). After heating at reflux temperature overnight, the reaction mixture was cooled to room temperature upon which orange crystals precipitated. Analytically pure **17b** (6.5 g, 20.6 mmol, 41%) was obtained after recrystallization from MeOH (0.03 gml<sup>-1</sup>, m.p. 103 - 105 °C)

<sup>1</sup>H-NMR: (δ, ppm) 8.94 (1H, d, *J* 9.42), 8.39 (1H, d, *J* 8.06), 8.23 (2H, m), 8.17 (2H, m), 8.05 (3H, AB, J), 3.75 (3H, s), 3.56 (2H, t, *J* 6.65), 2.94 (2H, t, *J* 6.55)

<sup>13</sup>C-NMR: (δ, ppm) 202.3 (q), 173.4 (q), 133.8 (q), 131.8 (q), 131.0 (q), 130.5 (q), 129.6 (t), 129.5 (t), 129.4 (q), 127.3 (q), 127.0 (t), 126.4 (t), 126.2 (t), 126.2 (t), 126.0 (t), 124.9 (t), 124.3 (q), 124.0 (t), 51.9 (s), 37.0 (s), 28.7 (s).

ν 1739 (s), 1672 (s), 1166 (m), 1120 (m) cm<sup>-1</sup>. GC-MS *m/z* 316 (M<sup>+</sup>, 20%), 229 (M<sup>+</sup>- C<sub>4</sub>H<sub>7</sub>O<sub>2</sub>, 100%), 201 (M<sup>+</sup>- C<sub>5</sub>H<sub>7</sub>O<sub>3</sub>, 80%).

### 1,2,3,4-Tetrahydro-dioxo-cyclohepta[*c,d*]pyrene (**18a**)

To a melt (150°C) of 25 g AlCl<sub>3</sub> (18.8 mmol) and 5 g NaCl 2.0 g (6.3 mmol) of **17b** was added in small portions. The melt was stirred under N<sub>2</sub> for 30 min., after which the reaction mixture was hydrolyzed with ice-water/1 M HCl. Standard work up yielded a red oil (1.34 g). The crude product was purified using flash chromatography (silica, eluent CHCl<sub>3</sub>) and subsequent recrystallization from toluene (5 mgml<sup>-1</sup>), which gave 1.0 g **18a** (3.5 mmol, 56%) as an orange solid (m.p. 116 - 118°C).

<sup>1</sup>H-NMR: (δ, ppm) 8.81 (1H, s), 8.56 (1H, d, *J* 8.13), 8.37 (2H, AB, *J* 8.54/8.27), 8.25 (1H, d, *J* 8.16), 8.17 (1H, d, *J* 8.86), 8.10 (2H, m), 3.33 (4H, s)

<sup>13</sup>C-NMR: (δ, ppm) 202.5 (q), 201.5 (q), 135.0 (q), 134.9 (q), 134.4 (t), 132.9 (q), 131.1 (q), 129.6 (t), 129.0 (t), 129.0 (t), 128.9 (q), 128.7 (t), 127.8 (t), 126.9 (q), 126.9 (t), 126.0 (t), 125.6 (q), 124.9 (q), 38.6 (s), 37.8 (s). ν 1738 (s), 1730 (s) cm<sup>-1</sup>. GC-MS *m/z* 284 (M<sup>+</sup>).

### 1,2,3,4-Tetrahydro-dihydroxy-cyclohepta[*c,d*]pyrene (**19**)

To a solution of 1.0 g (3.5 mmol) of **18a** in 50 ml benzene, 0.4 g (10.0 mmol) NaBH<sub>4</sub> in MeOH (5 ml) was added. After stirring at room temperature for 3 hr., water (25 ml) was added, the organic fraction separated, dried (MgSO<sub>4</sub>), filtered, and concentrated *in vacuo*. The resulting white solid (0.91 g, 3.2 mmol, 91%, m.p. 122 - 124 °C) was used without further purification.

<sup>1</sup>H-NMR: (δ, ppm) 8.11 (3H, m), 7.99 (2H, s), 7.98 (1H, ab), 7.73 (1H, d, *J* 7.7), 7.72 (1H, s), 5.64 (2H, m), 2.61, 2H, m), 2.08 (2H, m)

$^{13}\text{C}$ -NMR: ( $\delta$ , ppm) 131.7 (q), 130.8 (q), 124.5 (q), 124.4 (q), 123.5 (q), 120.5 (t), 120.4 (t), 119.6 (t), 118.3 (t), 117.9 (t), 117.9 (t), 117.5 (q), 116.7 (q), 114.1 (t), 112.5 (t), 71.9 (t), 71.8 (t), 28.6 (s), 26.9 (s) GC-MS  $m/z$  270 ( $\text{M}^+ - \text{H}_2\text{O}$ ), 252 ( $\text{M}^+ - 2\text{H}_2\text{O}$ ).

### 1,2,3,4-Tetrahydro-diacetyl-cyclohepta[*c,d*]pyrene (20)

To an ice-cooled solution of 0.5 g (1.1 mmol) of **19** in  $\text{CH}_2\text{Cl}_2$  (30 ml) and pyridine (0.2 ml) a solution of acetylchloride (0.2 g, 2.6 mmol) in  $\text{CH}_2\text{Cl}_2$  (10 ml) was slowly added. After stirring the reaction mixture for 3 hr. at room temperature, 20 ml of water was added. The organic layer was separated, dried with  $\text{CaCl}_2$  and evaporated, which yielded an orange oil. Flash chromatography (silica, eluent *n*-hexane) yielded a colorless oil (0.190 g, 0.66 mmol, 60%).

$^1\text{H}$ -NMR: ( $\delta$ , ppm) 8.24 (1H, s), 8.20 (3H, m), 8.05 (2H, s), 8.04 (2H, m), 6.70 (2H, m), 2.50 - 2.35 (4H, m), 2.27 (3H, s), 2.24 (3H, s).

$^{13}\text{C}$ -NMR: ( $\delta$ , ppm) 170.3 (q), 170.0 (q), 135.9 (q), 135.3 (q), 135.2 (q), 134.1 (q), 131.4 (q), 131.1 (q), 130.1 (q), 130.1 (q), 127.5 (t), 127.4 (t), 127.3 (t), 127.3 (t), 126.1 (t), 125.7 (t), 125.4 (t), 125.1 (t), 74.6 (t), 74.1 (t), 31.8 (s), 30.9 (s), 29.0 (s), 28.7 (s). GC-MS  $m/z$  252 (Two-fold elimination of acetic acid occurs in the injector). The mass spectrum is similar to that measured for **1**.

### Cyclohepta[*c,d*]pyrene (1)

FVT of **20** (20.0 mg, 0.079 mmol, subl. temperature  $150^\circ\text{C}$ , subl. rate  $10 \text{ mg h}^{-1}$ ) at  $500^\circ\text{C}$  yielded 90 % of **1**. Crude **1** was purified by flash chromatography (silica, eluent *n*-hexane) and subsequent recrystallization from *n*-hexane ( $2 \text{ mg ml}^{-1}$ ), which yielded dark brown crystals [15 mg, 0.06 mmol, m.p.  $128^\circ\text{C}$  (dec.)]

$^1\text{H}$ -NMR: ( $\delta$ , ppm) 7.73 (1H, d,  $J$  7.4), 7.71 (2H, m), 7.67 (2H, m), 7.61 (1H, m), 7.21 (1H, d,  $J$  8.0, H2), 7.08 (1H, s, H7), 6.22 (1H, m, H3), 6.19 (1H, m, H6), 5.54 (2H, m, H4/H5).

$^{13}\text{C}$ -NMR: ( $\delta$ , ppm) 142.3 (t, C3), 140.9 (q), 140.6 (t, C6), 138.7 (q), 137.6 (q), 134.9 (q), 134.8 (q), 133.5 (q), 132.3 (t, C2), 130.5 (t, C4 or C5), 130.1 (t, C7), 130.1 (q), 129.8 (t, C4 or C5), 129.5 (t), 129.5 (t), 129.0 (t), 128.7 (t), 128.6 (q), 125.4 (t), 124.7 (t).

GC-MS  $m/z$  252 ( $\text{M}^+$ , 100%), 226 ( $\text{M}^+ - \text{C}_2\text{H}_2$ , 70%), 113 (33%) E.A. calc. for  $\text{C}_{20}\text{H}_{12}$ ; C 95.21%, H 4.79%. Found: C 95.08%; H 4.83%. UV/Vis (cyclohexane)  $\lambda_{\text{max}}$ . (log  $\epsilon$ ): 411.8 (0.74), 400.0 (0.91), 390.5 (0.87), 381.2 (1.01), 293.6 (1.17), 242.0 (3.57), 193.4 (1.78).

### Methyl-4-(8-fluoranthyl)-4-oxo-butanoate (21) and Methyl-4-(3-fluoranthyl)-4-oxo-butanoate (22)

To an ice-cooled suspension of 10.0 g (50.0 mmol) fluoranthene (**12**) and 5.8 g succinic anhydride (58.0 mmol) in  $\text{CH}_2\text{Cl}_2$  (250 ml), 13.0 g (97.5 mmol)  $\text{AlCl}_3$  was added. After stirring at room temperature for 24 hr., the reaction mixture was hydrolyzed by adding it to ice-water (200 ml) and 1M HCl and extracted with  $\text{CH}_2\text{Cl}_2$  (3 x 200 ml). After concentration of the combined organic layers an orange solid was obtained. Yield 7.2 g (25 mmol, 50 %). This mixture contained 50 % **21a**, 30% of **22a** and 20 % **12**.

From the reaction mixture the methyl ester was prepared by dissolving 10 g in MeOH (300 ml) and 37% HCl (1 ml). After heating at reflux temperature overnight, the reaction mixture was cooled to room temperature. **21b** (5.5 g, 17.5 mmol, 35 %) and **22b** (2.4 g, 7.5 mmol, 15%) could be isolated by repeated recrystallization from MeOH (0.03  $\text{gml}^{-1}$ , m.p. 131 - 133°C)

$^1\text{H-NMR}$  **21b**: ( $\delta$ , ppm) 8.70 (1H, d,  $J$  8.3 ), 8.23 (1H, d,  $J$  7.4), 7.80 (4H, m), 7.44 (2H, m), 7.67 (1H, dd,  $J$  7.3/8.3), 3.46 (2H, t,  $J$  6.6), 2.88 (2H, t,  $J$  6.6).

$^1\text{H-NMR}$  **22b**: ( $\delta$ , ppm) 8.51 (1H, s), 8.08 (6H, m), 7.69 (2H, AB,  $J$  7.4), 3.43 (2H, t,  $J$  6.6), 2.86 (2H, t,  $J$  6.6)

$^{13}\text{C-NMR}$  **21b**: ( $\delta$ , ppm) 200.3 (q), 197.9 (q), 142.0 (q), 140.7 (q), 138.3 (q), 137.1 (q), 133.1 (q), 131.3 (q), 130.3 (q), 129.0 (t), 127.8 (t), 127.6 (t), 127.0 (t), 122.4 (t), 121.6 (t), 121.0 (t), 120.7 (t), 118.7 (t), 51.9 (s), 35.6 (s), 28.3 (s).

$^{13}\text{C-NMR}$  **22b**: ( $\delta$ , ppm) 200.5 (q), 197.9 (q), 143.9 (q), 139.8 (q), 136.2 (q), 135.9 (q), 135.8 (q), 133.3 (q), 130.2 (q), 128.3 (s), 128.2 (s), 128.1 (s), 128.0 (s), 127.3 (s), 121.5 (s), 121.4 (s), 121.3 (s), 120.9 (s), 52.0 (s), 33.7 (t), 28.6 (t). GC-MS  $m/z$  316 ( $\text{M}^+$ ).

### 1,2,3,4-Tetrahydro-dioxo-cyclohepta[*c,d*]fluoranthene (**23**)

To a melt (150°C) of 25 g  $\text{AlCl}_3$  (18.8 mmol) and 5 g NaCl 2.0 g (6.3 mmol) of **21b** was added in small portions. The melt was stirred under  $\text{N}_2$  for 30 min., after which it was hydrolyzed with ice-water and 1M HCl. Standard extraction procedures yielded a red oil. The crude product was purified using flash chromatography (silica, eluent  $\text{CHCl}_3$ ) and subsequent recrystallization from toluene (3  $\text{mgml}^{-1}$ ), which yielded 1.0 g **23** (3.5 mmol, 56%) as an orange solid.

$^1\text{H-NMR}$ : ( $\delta$ , ppm) 8.57 (2H, d,  $J$  7.4), 7.96 (2H, d,  $J$  7.4), 7.85 (2H, m), 7.39 (2H, m), 3.15 (4H, s)

$^{13}\text{C-NMR}$ : ( $\delta$ , ppm) 197.8 (q), 142.4 (q), 138.6 (q), 134.3 (t), 132.4 (q), 132.3 (q), 128.8 (t), 125.6 (q), 121.9 (t), 119.3 (t), 37.0 (s). GC-MS  $m/z$  284 ( $\text{M}^+$ ).

### 1,2,3,4-Tetrahydro-dihydroxy-cyclohepta[*c,d*]fluoranthene (**14**)

To a solution of 1.0 g (3.5 mmol) of **13** in 50 ml benzene, 0.4 g (10.0 mmol)  $\text{NaBH}_4$  in 5 ml MeOH was added. After stirring at room temperature for 3 hr., water (25 ml) was added, the organic fraction separated, dried ( $\text{MgSO}_4$ ), filtered, and concentrated *in vacuo*. The resulting orange solid was purified by flash

## Chapter 8

chromatography (silica, eluent acetone: *n*-hexane 3:7), which yielded a white solid (0.91 g, 3.2 mmol, 91%, m.p. 153 - 155°C)

<sup>1</sup>H-NMR: (δ, ppm) <sup>1</sup>H-NMR: 7.87 (4H, m), 7.62 (2H, d, *J* 6.9), 7.38 (2H, m), 5.30 (2H, broad s), 1.98 (4H, s).  
<sup>13</sup>C-NMR (in DMSO-*d*<sub>6</sub>): (δ, ppm) 144.0 (q), 138.3 (q), 138.1 (q), 135.1 (q), 127.2 (t), 127.1 (q), 126.3 (t), 121.2 (t), 120.0 (t), 70.4 (t), 31.9 (s). GC-MS *m/z* 270 (M<sup>+</sup> - H<sub>2</sub>O), 252 (M<sup>+</sup> - 2H<sub>2</sub>O).

### 1,2,3,4-Tetrahydro-diacetyl-cyclohepta[*c,d*]fluoranthene (15)

To an ice-cooled solution of 0.5 g (1.1 mmol) of **24** in 30 ml CH<sub>2</sub>Cl<sub>2</sub> and 0.2 ml pyridine a solution of acetylchloride (0.2 g, 2.6 mmol) in 10 ml CH<sub>2</sub>Cl<sub>2</sub> was slowly added. After stirring the reaction mixture for three hr. at room temperature, 20 ml of water was added. The organic layer was separated, dried with CaCl<sub>2</sub> and evaporated, which yielded an orange oil (0.190 g, 0.66 mmol, 60%).

<sup>1</sup>H-NMR: (δ, ppm) 7.86 (4H, m), 7.64 (2H, d, *J* 7.1), 7.34 (2H, m), 6.64 (2H, m), 2.4-2.3 (4H, m), 2.14 (6H, s)  
<sup>13</sup>C-NMR: (δ, ppm) 170.2 (q), 143.6 (q), 142.5 (q), 139.0 (q), 137.0 (q), 128.4 (q), 128.0 (t), 127.8 (t), 121.4 (t), 119.8 (t), 74.0 (t), 29.2 (s), 21.4 (s). GC-MS *m/z* 252 (Two-fold elimination of acetic acid occurs in the injector). The mass spectrum is similar to that measured for **2**.

### Cyclohepta[*c,d*]fluoranthene (2)

FVT of **25** (20.0 mg, 0.079 mmol, sublimation temperature 120°C, sublimation rate mg·h<sup>-1</sup>) at 500°C yielded 90% of **2**. Crude **2** was purified by flash chromatography (silica, eluent *n*-pentane) and subsequent recrystallization from pentane (2 mg·ml<sup>-1</sup>), which yielded red crystals (10 mg, 0.04 mmol, m.p. 190 - 192 °C)

<sup>1</sup>H-NMR: (δ, ppm) 8.30 (2H, m, H10/H11), 8.26 (2H, d, *J* 7.4 H1/H8), 7.65(2H, m, H9/H12), 7.59 (2H, d, *J* 7.4 H2/H7), 7.18 (2H, m, H3/H6), 6.37 (2H, m, H4/H5).

<sup>13</sup>C-NMR: (δ, ppm) 138.4 (q, C12a), 137.6 (t, C3/C6), 136.5 (q, C12b), 133.1 (q, C2a), 132.7 (q, C2c), 131.6 (q, C2b), 127.8 (t, C2/C12), 126.9 (t, C4/C5), 126.6 (t, C9/C12), 121.7 (t, C1/C8), 121.1 (t, C10/11).

GC-MS *m/z* 252 (M<sup>+</sup>, 100%), 226 (M<sup>+</sup>-C<sub>2</sub>H<sub>2</sub>, 70%), 113 (33%) UV/Vis (cyclohexane) λ<sub>max</sub>. (log ε): 474.5 (0.06), 460.8 (0.06), 443.7 (0.06), 330.8 (0.40), 319.4 (0.57), 256.5 (0.36), 235.6 (0.21), 219.8 (0.40), 216.1 (0.41), 195.4 (0.69).

### Methyl-but-3-enoate

To a solution of vinylacetic acid ( 10.13 g, 117 mmol) in 90 ml MeOH 1.5 ml 37% HCl was added. The mixture was refluxed for 1 hr. The MeOH was removed *in vacuo*. Subsequently, the product was dissolved in CH<sub>2</sub>Cl<sub>2</sub>, washed with brine and water, dried (MgSO<sub>4</sub>) and filtered. After concentrating the filtrate *in vacuo* a colorless oil was obtained (7.73 g, 77 mmol, 66 %).



$^1\text{H-NMR}$ : ( $\delta$ , ppm): 5.89 (2H, m), 5.15 (2H, d,  $J$  7.2), 3.70 (3H, s), 3.11 (2H, d,  $J$  7.2)

### Methyl 4-(9-anthracenyl)butanoate (27)

All solvents and solutions used in this reaction were vigorously degassed by three freeze-thaw cycles under Ar. 9-BBN (105 ml of a 0.5 M solution in THF) was added to methyl but-3-enoate (3.93 g, 39.3 mmol) under Ar. The solution was stirred at room temperature for 2 hr., after which complete addition was observed in  $^1\text{H-NMR}$ . This solution was then added to a solution of 9-bromoanthracene (9.13 g, 35.7 mmol) and dichloro[1,1'-*bis*(diphenylphosphino)ferrocene]palladium(II) (0.70 g, 0.76 mmol) in DMF (80 ml), followed by addition of a solution of  $\text{K}_3\text{PO}_4$  (24.9 mg, 107 mmol) in  $\text{H}_2\text{O}$  (35 ml). The resulting mixture was heated under reflux for 15 hr., after which the starting material had completely disappeared (GC). The mixture was cooled to room temperature, water was added and extracted with  $\text{CH}_2\text{Cl}_2$ . The combined organic layers were washed with brine and water, dried ( $\text{MgSO}_4$ ) and concentrated *in vacuo*. The product was purified by flash column chromatography (silica, eluent *n*-hexane to remove anthracene,  $\text{CH}_2\text{Cl}_2$  to yield **27**). Recrystallization from *n*-hexane yielded **27** yellow/white needles [30% - 50%, m.p. 69 – 71°C (lit<sup>26</sup> 73 – 75°C)]

$^1\text{H-NMR}$ : ( $\delta$ , ppm) 8.30 (1H, s), 8.28 (2H, d,  $J$  9.0), 7.98 (2H, d,  $J$  8.4), 7.49 (4H, m), 3.73 (3H, s), 3.67 (2H,  $J$  8.2), 2.50 (2H, t,  $J$  7.2), 2.13 (2H, tt,  $J$  7.6,  $J$  7.6)

$^{13}\text{C-NMR}$ : ( $\delta$ , ppm) 174.2 (t), 134.1 (q), 131.8 (q), 129.9 (q),  $\delta$  129.5 (t), 126.2 (q), 126.2 (t), 125.9 (t), 125.1 (t), 124.5 (t), 51.8 (t), 34.2 (s), 27.4 (s), 26.3 (s),

$\nu$  1728 (s), 1205 (m)  $\text{cm}^{-1}$ .

### 1,2,3,4-Tetrahydro-4-oxo-cyclohepta[*k,l*]anthracene (28)

To a melt (85°C) of 55 g polyphosphoric acid (38.8 mmol) 2.98 g of (**27**) (10.7 mmol) was added in small portions. After stirring for 90 min. the melt was hydrolyzed by adding ice water. The aqueous layer was extracted with  $\text{CH}_2\text{Cl}_2$  and the combined organic layers were washed with brine and water, dried ( $\text{MgSO}_4$ ) and concentrated *in vacuo*. The resulting crude product was purified using column chromatography (silica, eluent  $\text{CH}_2\text{Cl}_2$ : *n*-hexane, 7:3), which yielded **28** as a pale yellow solid [1.85 g, 8.0 mmol, 75%, m.p. 82 - 84°C (lit<sup>26</sup> 84 - 85°C)]

$^1\text{H-NMR}$ : ( $\delta$ , ppm) 8.37 (1H, s), 8.29 (1H, d,  $J$  8.7), 8.04 (1H, d,  $J$  8.1), 8.03 (1H, d,  $J$  8.1), 7.82 (1H, d,  $J$  6.9), 7.50 (3H, m), 3.57 (2H, t,  $J$  6.9), 2.77 (2H, t,  $J$  7.5), 2.52 (2H, tt,  $J$  7.2).

$^{13}\text{C-NMR}$ : ( $\delta$ , ppm) 205.5 (q), 139.8 (q), 134.1 (q), 132.9 (t), 132.3 (q), 131.4 (q), 129.6 (q), 129.4 (t), 127.4 (t), 126.8 (t), 126.7 (t), 125.8 (t), 124.4 (t), 124.2 (t), 42.1 (s), 29.0 (s), 27.7 (s).  $\nu$  1700  $\text{cm}^{-1}$ .

GC-MS  $m/z$  246 ( $\text{M}^+$ , 100%), 230 (10%), 218 (60%), 202 (30%), 189 (60%).

### 1,2,3,4-Tetrahydro-4-hydroxy-cyclohepta[*k,l*]anthracene (29)

To a solution of **28** (1.0 g, 4.06 mmol) in 40 ml ether, a suspension of NaBH<sub>4</sub> (0.17 g, 4.47 mmol) in 10 ml ethanol was added drop-wise. The reaction mixture was stirred for 18 hr. at room temperature and subsequently poured into an aqueous solution of HCl (pH = 2). The aqueous layer was extracted with CH<sub>2</sub>Cl<sub>2</sub>, the combined organic layers washed with water, dried (MgSO<sub>4</sub>) and the solvents were removed *in vacuo*. After removal of the solvent and addition of CH<sub>2</sub>Cl<sub>2</sub>, the mixture was washed with water, dried (MgSO<sub>4</sub>) and concentrated *in vacuo*. The product **29** was obtained in pure form as a yellow solid (0.98 g, 4.0 mmol, 98%, m.p. 99 - 101°C).

<sup>1</sup>H-NMR: (δ, ppm) 8.24 (1H, s), 8.23 (1H, d, *J* 7.8), 7.95 (1H, d, *J* 9.0), 7.83 (1H, d, *J* 8.4), 7.61 (1H, d, *J* 6.6), 7.46 (1H, m), 7.44 (1H, m), 7.37 (1H, m), 5.47 (1H, m), 3.86 (1H, m), 3.56 (1H, m), 2.38 (1H, m), 2.22 (1H, m), 2.10 (1H, m), 1.95 (1H, m).

<sup>13</sup>C-NMR: (δ, ppm) 142.2 (q), 136.8 (q), 132.6 (q), 131.2 (q), 131.0 (q), 130.1 (q), 129.0 (t), 126.0 (t), 125.8 (t), 125.1 (t), 124.6 (t), 124.4 (t), 123.0 (t), 73.4 (s), 35.3 (s), 29.1 (s), 24.7 (s). ν 3282 (s), 1064 (m) cm<sup>-1</sup>. GC-MS: *m/z* 248 (M<sup>+</sup>, 100%), 230 (M<sup>+</sup>-H<sub>2</sub>O, 100%), 202 (95%), 189 (10%), 114 (15%), 101 (15%).

### 1,2-Dihydro-cyclohepta[*k,l*]anthracene (**30**)

To a solution of **29** (0.84 g, 3.38 mmol) in CHCl<sub>3</sub> (45 ml) a solution of PBr<sub>3</sub> (0.35 g, 0.37 mmol) in CHCl<sub>3</sub> was added. The resulting reaction mixture was stirred for 2 hr. and hydrolyzed. The aqueous layer was extracted with CHCl<sub>3</sub>, and the combined organic layers washed with water. The organic layers were consequently dried (MgSO<sub>4</sub>), filtered and concentrated *in vacuo*. The crude product was purified by flash-chromatography (silica, eluent *n*-hexane) and recrystallization from *n*-hexane (10 mgml<sup>-1</sup>). Yield 0.70 g [3.0 mmol, 90% of a yellow solid, m.p. 61 - 63°C].

<sup>1</sup>H-NMR (for numbering see Scheme 4): (δ, ppm) 8.29 (1H, d, *J* 9.0), 8.25 (1H, s), 7.93 (2H, dd, *J* 2.1/7.5), 7.77 (2H, dd, *J* 3.0/6.3), 7.44 (2H, m), 7.43 (2H, m), 7.34 (2H, m), 6.64 (2H, td, *J* 11.7/1.5), 6.23 (1H, td, *J* 11.7/5.4), 3.72 (2H, t, *J* 5.2), 2.75 (2H, m).

<sup>13</sup>C-NMR: (δ, ppm) 136.8 (q), 135.8 (q), 133.9 (t), 133.3 (t), 132.8 (q), 131.8 (q), 131.5 (t), 130.3 (q), 130.0 (q), 129.1 (t), 129.0 (t), 126.7 (t), 125.8 (t), 125.2 (t), 125.0 (t), 124.4 (t), 30.2 (s, two isochronous carbon atoms).

GC-MS: *m/z* 230 (M<sup>+</sup>, 100%), 215 (80%), 202 (80%), 113 (30%), 101 (30%). E.A. calc. for C<sub>18</sub>H<sub>14</sub>: C 93.87 %, H 6.13%. Found C 94.01 %, H 6.21%. UV/Vis (cyclohexane) λ<sub>max</sub>. (log ε): 410.0 (0.31), 387.5 (0.32), 368.3 (0.19), 296.0 (0.37), 283.4 (0.42), 263.0 (2.59), 212.0 (1.03), 192.0 (1.21).

**2-Ethenyl-1,2-dihydro-cyclopenta[*k,l*]anthracene (31)**

FVT of **30** (30 mg, 0.13 mmol, subl. temperature 80°C, subl. rate 5 mg·h<sup>-1</sup>) at 700°C (mass recovery 70%) afforded a mixture that contained 80% of **31**. Analytically pure **31** was obtained after recrystallization of the pyrolysate from *n*-pentane (30 mg·ml<sup>-1</sup>) as dark red crystals (m.p. 75 - 76°C).

<sup>1</sup>H-NMR (acetone-*d*<sub>6</sub>, for numbering see Scheme 5): (δ, ppm) 8.29(1H, s, H10), 8.12 (1H, m, H4), 8.03 (1H, m, H1), 7.79, 1H, d, *J* 8.4, H5), 7.51 (3H, m, H2/H3/H6), 7.19 (1H, d, *J* 6.6, H7), 6.10 (1H, ddd, *J* 17.1/8.7/8.1, H17), 5.35 (1H, d, *J* 17.1, H16), 5.15 (1H, d, *J* 9.9, H16), 4.51 (1H, broad t, *J* 7.8, H18), 4.09 (1H, dd, *J* 17.7/8.1, H15), 3.56 (1H, dd, *J* 18.0/3.3, H15).

<sup>13</sup>C-NMR: (δ, ppm): 148.8 (q), 141.0 (t, C17), 140.4 (q), 136.7 (q), 134.2 (q), 130.1 (q), 129.6 (t, C4), 128.0 (t), 127.3(q) 125.5 (t), 125.0 (t, C2, C3, C6), 124.8 (t, C1), 123.0 (t, C5), 121.7 (t, C10), 118.1 (t, C7), 114.3 (t, C16), 48.2 (s, C18), 37.1 (s, C15). GC-MS: *m/z* 230 (M<sup>+</sup>, 100%), 215 (75%), 202 (50%), 113 (25%), 101 (25%).

**Selected analytical data for compound 32**

Compound **32** was usually formed upon FVT at 700°C of **30** in *ca.* 4% yield (<sup>1</sup>H-NMR) as a side product. Other products are **31** (80%) and **30** (16%). A sample enriched in **32** (up to 15%) was obtained by recrystallization from *n*-pentane (30 mg·ml<sup>-1</sup>). Selected NMR data for **32** were taken from the <sup>1</sup>H and <sup>13</sup>C NMR spectra of this enriched fraction.

<sup>1</sup>H NMR (C<sub>6</sub>D<sub>6</sub>): (δ, ppm) stereoisomer A. 2.05 (3H, d, *J* 7.2, H16), 4.29 (2H, s, H15), 6.54 (1H, qt, *J* 6.9/2.4, H17); stereoisomer B. 2.24 (3H, d, *J* 7.2, H16), 4.36 (2H, s, H15). <sup>13</sup>C NMR (C<sub>6</sub>D<sub>6</sub>): (δ, ppm) 113.3 (t, C17), 34.0 (s, C15), 30.2 (s, C16). GC-MS: *m/z* 230 (M<sup>+</sup>, 50%), 215 ([M<sup>+</sup>-CH<sub>3</sub>], 100%).

**2-Ethyl-1,2-dihydro-cyclopenta[*k,l*]anthracene (33)**

Compound **33** was obtained by catalytic hydrogenation of **31** (8 mg, 0.035 mmol) with H<sub>2</sub> (p<sub>H2</sub>/1atm) and Pd on activated carbon (1 mg, 10%) in THF (10 ml). After 15 min. the catalyst was filtered off and the filtrate concentrated *in vacuo* yielding **33** (7 mg, 90%) as a colorless oil.

<sup>1</sup>H-NMR (similar numbering as for **31**, Scheme 5): (δ, ppm): 8.21 (1H, s, H10), 8.06 (1H, m, H4), 8.00 (1H, m, H1), 7.74 (1H, d, *J* 8.1, H5), 7.47 (3H, m, H2/H3/H6), 7.22 (1H, d, *J* 6.6, H7), 3.94 (1H, dd, *J* 17.7/7.8, H15), 3.80 (1H, m, H18), 3.43 (1H, d, *J* 17.4, H15), 2.06 (1H, m, H17), 1.80 (1H, m, H17), 1.11 (3H, t, *J* 7.2, H16).

<sup>13</sup>C-NMR (C<sub>6</sub>D<sub>6</sub>): (δ, ppm) 150.7 (q), 141.4 (q), 137.4 (q), 134.2 (q), 130.2 (q), 129.8 (q), 127.1 (q), 130.2 (t, C4), 127.1 (t, C2, C3 or C6), 127.2 (q), 125.2 (t, C2, C3 or C6), 125.0 (t, C1), 124.5 (t, C2, C3 or C6), 122.9 (t, C5), 121.8 (t, C10), 117.1 (t, C7), 45.2 (t, C18), 36.1 (s, C15), 30.1 (s, C17), 11.6 (p, C16). GC-MS: *m/z* 232 (M<sup>+</sup>, 100%), 215 (15%), 203 (100%), 101 (10%).

**1,2,3,4-Tetrahydro-cyclohepta[*k,l*]anthracene (34)**

Compound **34** was obtained by catalytic hydrogenation of **30** (20 mg, 0.087 mmol) with H<sub>2</sub> (p<sub>H2</sub>/1atm) and Pd on activated carbon (2 mg, 10%) in THF (20 ml). After 15 min. the catalyst was filtered off and the filtrate concentrated *in vacuo* yielding **34** (18 mg, 90%) as a light yellow oil.

<sup>1</sup>H-NMR (similar numbering as for **30**, Scheme 4): (δ, ppm): 8.26 (1H, d, *J* 8.4, H1), 8.23 (1H, s, H10), 7.90 (1H, d, *J* 8.4, H4), 7.67 (1H, d, *J* 8.4, H5), 7.42 (2H, m, H2/H3), 7.22 (2H, m, H6/H7), 3.72 (2H, t, *J* 5.6, H15 or H18), 3.30 (2H, t, *J* 5.6, H15 or H18), 2.20-2.00 (4H, m, H16/H17).

<sup>13</sup>C-NMR: (δ, ppm) 141.3 (q), 137.3 (q), 133.1 (q), 131.4 (q), 130.6 (q), 129.0 (q), 127.6 (t), 126.5 (t), 126.3 (t), 125.9 (t), 125.5 (t), 125.0 (t), 124.8 (t), 124.5 (t), 35.3 (s), 27.7 (s), 27.1 (s), 26.7 (s). GC-MS *m/z* 232 M<sup>+</sup>, 100%), 217 (60%), 202 (50%), 191 (20%), 101 (30%).

**References and notes**

- (1) Jenneskens, L. W.; Sarobe, M.; Zwikker, J. W. *Pure & Appl. Chem.* **1996**, *68*, 219-224.
- (2) Scott, L. T. *Pure & Appl. Chem.* **1996**, *68*, 291-300.
- (3) Preda, D. V.; Scott, L. T. *Tetrahedron Lett.* **2000**, *41*, 9633-9637.
- (4) Koper, C.; Jenneskens, L. W.; Sarobe, M. *Tetrahedron Lett.* **2002**, *43*, 3833-3836.
- (5) Fowler, P. W.; Ceulemans, A. *J. Phys. Chem. A.* **1995**, *99*, 508-510.
- (6) Lafleur, A. L.; Howard, J. B.; Taghizadeh, K.; Plummer, E. F.; Scott, L. T.; Necula, A.; Swallow, K. C. *J. Phys. Chem.* **1996**, *100*, 17421-17428.
- (7) Jacob, J. *Pure & Appl. Chem.* **1996**, *68*, 301-308.
- (8) Howard, J. B.; Longwell, J. P.; Marr, J. A.; Pope, C. J.; Busby, W. F., Jr.; Lafleur, A. L.; Taghizadeh, K. *Combust. Flame* **1995**, *101*, 262-270.
- (9) Mackay, A. L.; Terrones, H. *Nature* **1991**, *352*, 762.
- (10) Iijima, S.; Ichihashi, T.; Ando, Y. *Nature* **1992**, *356*, 776-778.
- (11) Yao, Z.; Postma, H. W. C.; Balents, L.; Dekker, C. *Nature* **1999**, *402*, 273-276.
- (12) Iijima, S. *J. Chem. Phys.* **1996**, *104*, 2089-2092.
- (13) Acocella, A.; Havenith, R. W. A.; Steiner, E.; Fowler, P. W.; Jenneskens, L. W. *Chem. Phys. Lett.* **2002**, *363*, 64-72.
- (14) Fowler, P. W.; Ceulemans, A. *J. Phys. Chem.* **1995**, *99*, 508-510.
- (15) Matsuda, M.; Matsubara, H.; Sato, M.; Okamoto, S.; Yamamoto, K. *Chemistry Letters* **1996**, 157-158.
- (16) Avouris, P. *Acc. Chem. Res.* **2002**, *35*, 1026-1034.
- (17) Pagni, R. M.; Watson, C. R. *Tetrahedron Lett.* **1973**, *1*, 59-60.
- (18) Pagni, R. M.; Burnett, M.; Hazell, A. C. *J. Org. Chem.* **1978**, *43*, 2750-2752.

- (19) Vogel, E.; Neumann, B.; Klug, W.; Schmickler, H.; Lex, J. *Angew. Chem.* **1985**, *97*, 1044-1045.
- (20) Jenneskens, L. W.; Hoefs, C. A. M.; Wiersum, U. E. *J. Org. Chem.* **1989**, *54*, 5811-5814.
- (21) Besides FVT of the *bis*-acetylated precursors **20** and **25** also the two related dihydroxy-compounds **19** and **24** were subjected to FVT. However, this gave the CH-PAH **1** and **2** only in very small amounts from T > 900°C. Instead the cyclopenta-fused analogues, cyclopenta[*c,d*]pyrene (**6**) and cyclopenta[*c,d*]fluoranthene (**7**) were predominantly formed. Apparently, the activation barrier for elimination of H<sub>2</sub>O is too high for the preparation of **1** and **2**. This suggests that both **1** and **2** are only stable in a distinct temperature range under FVT conditions.
- (22) Shields, J. E.; Gavrilovic, D.; Kopecky, J.; Hartmann, W.; Heine, H.-G. *J. Org. Chem.* **1974**, *39*, 515-520.
- (23) Kroto, H. W. *J. Chem. Soc., Faraday Trans.* **1990**, *86*, 2465-2468.
- (24) Sarobe, M. *Polycyclic Aromatic Hydrocarbons under High Temperature Conditions. Consequences for Carbon Build up during Combustion and Fullerene Formation Processes.*; Utrecht University: Utrecht, The Netherlands, **1998**.
- (25) Schleyer, P. v. R.; Manoharan, M.; Jiao, H.; Stahl, F. *Org. Lett.* **2001**, *3*, 3643-3646.
- (26) Esteban, G.; Lopez-Sanchez, A.; Martinez, E.; Plumet, J. *Tetrahedron Lett.* **1998**, *54*, 197-212.
- (27) Tintel, C.; Cornelisse, J.; Lugtenburg, J. *Recl. Trav. Chim. Pays-Bas* **1983**, *102*, 14-20.
- (28) Morita, K.; Aida, T.; Morinaga, K.; Tsunetsugu, J. *J. Chem. Soc., Perkin Trans. 2* **1994**, 1215-1220.
- (29) Streitwieser, A. *Molecular Orbital Theory for Organic Chemists*; Wiley: New York, 1961.
- (30) Haddon, R. C. *Phil. Trans. R. Soc. Lond. A* **1993**, *343*, 53-62.
- (31) Fry, A. J.; Foc, P. C. *Tetrahedron* **1986**, *42*, 5255-5266.
- (32) Aihara, J. *J. Chem. Soc., Perkin Trans. 2* **1996**, 2185-2195.
- (33) Michl, J. *J. Am. Chem. Soc.* **1976**, 4546-4549.
- (34) Bard, A. J.; Faulkner, L. R. *Electrochemical methods*; John Wiley & Sons: New York, **1980**.
- (35) Brown, R. F. C. *Pyrolytic Methods in Organic Chemistry*; Academic Press: New York, **1980**; Vol. 41.



# CHAPTER 9

## Magnetic Properties of Cyclohepta-Fused Non-Alternant Polycyclic Aromatic Hydrocarbons

### Abstract

The magnetic properties of the non-alternant cyclohepta-fused polycyclic aromatic hydrocarbons (CH-PAH) cyclohepta[*c,d*]pyrene (**1**), cyclohepta[*c,d*]fluoranthene (**2**), pleiadiene (**3**) and cyclohepta[*j,k*]phenanthrene (**4**), have been studied by comparing their <sup>1</sup>H-NMR chemical shifts with those of the corresponding alternant PAH and related non-alternant cyclopenta-fused PAH (CP-PAH). Although a significant up-field shift of the protons attached to the aromatic core of **1**, **3** and **4** is observed, it is absent for **2**. Insight in the origin of this difference is obtained using *ab initio* calculations. The  $\pi$ -current density maps of **1** – **4** and cyclohepta[*j,k*]anthracene (**5**) are visualized by direct computation using the reliable CTOCD-DZ *ab initio* distributed-origin coupled Hartree-Fock method. In addition, the integrated properties [the <sup>1</sup>H-NMR chemical shifts and the nucleus independent chemical shift (NICS)] were calculated using the CTOCD-PZ2 method. This substantiated that in **1**, **3** - **5** paratropic ring currents are present in the CH-moiety, whilst the two double bonds in the CH-moiety of **2** are localized.

## 9.1 Introduction

Despite its importance no clear definition of the concept of aromaticity is yet available. This is predominantly caused by the fact that suitable reference systems are required that often are (experimentally) inaccessible. As a consequence, several criteria for aromaticity exist, both experimental as well as theoretical, but there is still no agreement about *the* criterion for aromaticity.<sup>1</sup>

In this context, non-alternant polycyclic aromatic hydrocarbons (PAH) are interesting systems due to the fact that they contain multiple-fused  $\pi$ -conjugated rings of which at least one is odd-membered.<sup>2</sup> The distinct rings may have different degrees of (local) aromaticity, which contribute to the total (global) aromaticity of the compound.

One of the most frequently used criterion for aromaticity is the magnetic criterion, *i.e.* the presence of cyclic electron delocalization. According to Hückel-London theory, a  $\pi$ -conjugated monocycle containing  $4n + 2$   $\pi$ -electrons will sustain a diatropic ring (aromatic) ring current, whereas a monocycle containing  $4n$   $\pi$ -electrons will sustain a paratropic (*anti*-aromatic) ring current when a magnetic field is applied.<sup>3</sup> Although, these ring currents are not directly observable, they can be inferred from for example <sup>1</sup>H-NMR chemical shifts, the magnetic anisotropy ( $\Delta\zeta$ ), exaltation of isotropic magnetic susceptibility ( $\Lambda$ ) or the nucleus independent chemical shift (NICS). Fortunately, they can also be visualized directly by computation of the all-electron current density maps (CTOCD-DZ).<sup>4-7</sup> <sup>1</sup>H-NMR is a useful technique to get an impression of the global aromaticity of the compound.<sup>8</sup> For example, for cyclopenta-fused PAH (CP-PAH) up-field shifts for the <sup>1</sup>H-NMR chemical shifts of the aromatic core protons, compared to those of the corresponding alternant PAH are in certain cases observed.<sup>9</sup> In Chapter 8 it was noted that the experimental <sup>1</sup>H-NMR data of the cyclohepta-fused PAH (CH-PAH) cyclohepta[*c,d*]pyrene (**1**), cyclohepta[*c,d*]fluoranthene (**2**), pleiadene (**3**) and cyclohepta[*j,k*]phenanthrene (**4**) indicate that CH-annulation does affect the global aromaticity of CH-PAH.

In this Chapter we study the magnetic properties of the novel CH-PAH cyclohepta[*c,d*]pyrene (**1**) and cyclohepta[*c,d*]fluoranthene (**2**) and compare them with the magnetic properties of the reported pleiadene (**3**) and cyclohepta[*j,k*]phenanthrene (**4**) (Chart 1). Insight in the global aromatic properties is obtained by comparing the <sup>1</sup>H-NMR chemical shifts of the CH-PAH with those of the corresponding PAH and related CP-PAH (Chart 1). The data are analyzed and interpreted using the results of *ab initio* calculations, *i.e.* computed current density maps and integrated magnetic properties (<sup>1</sup>H-NMR chemical shifts and NICS values). In addition, predictions are made for the hitherto unknown compounds cyclohepta[*f,g*]aceanthrylene (**19**) and



## Magnetic Properties of Cyclohepta-Fused Non-Alternant PAH

cyclohepta[*b*,*l*]acanthrylene (**20**) (Chart 2), which consist of an anthracene core with both an annelated cyclopenta- and a cyclohepta-moiety.

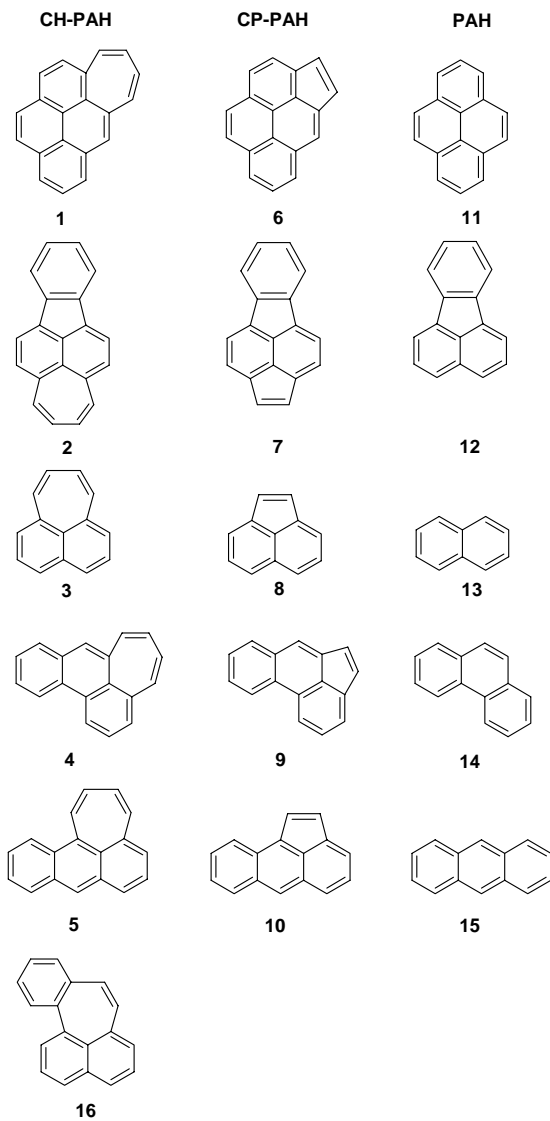


Chart 1

## 9.2 Aromaticity: the magnetic criterion

### 9.2.1 <sup>1</sup>H-NMR spectroscopy of CH-PAH

The assignment of the <sup>1</sup>H-NMR chemical shifts of the CH-PAH cyclohepta[*c,d*]pyrene (**1**) and cyclohepta[*c,d*]fluoranthene (**2**) has been described in Chapter 8 (see Experimental Section). The <sup>1</sup>H-NMR assignments of the CH-PAH pleiadene (**3**)<sup>10</sup> and cyclohepta[*j,k*]phenanthrene (**4**)<sup>11</sup>, and the corresponding PAH and related CP-PAH were taken from literature.<sup>12,13</sup>

In Figure 1 the <sup>1</sup>H-NMR spectra of cyclohepta[*c,d*]pyrene (**1**) and cyclohepta[*c,d*]fluoranthene (**2**) are shown. The cyclohepta protons of **1** are positioned at 6.22 ppm (H3 and H6) and 5.54 ppm (H4 and H5, see Figure 1). For comparison, the vinylic-protons in 4,5-benzocyclohepta[1,2,3-*de*]naphthalene (**16**) resonate at 6.45 ppm.<sup>11</sup> Hence, this suggests that the <sup>1</sup>H-NMR chemical shifts for the CH-moiety of **1** are positioned at higher field. The <sup>1</sup>H-NMR resonances of the aromatic protons are all < 7.8 ppm. In Table 1 the average <sup>1</sup>H-NMR chemical shifts of the CH-moiety [ $\delta_{av}(7)$ ] and of the pyrene core [ $\delta_{av}(6)$ ] of **1** are compared with the corresponding  $\delta_{av}(6)$  values found for cyclopenta[*c,d*]pyrene (**6**) and pyrene (**11**). Whereas the average <sup>1</sup>H-NMR chemical shift of the pyrene core [ $\delta_{av}(6) = 8.18$  ppm] in **6** is not significantly altered to that in **11** [ $\delta_{av}(6) = 8.14$  ppm], it is shifted up-field in **1** [ $\delta_{av}(6) = 7.55$  ppm]. The largest effect is visible for the aromatic protons next to the CH-moiety (H2 and H7), which resonate at 7.08 ppm (H7) and 7.21 ppm (H2). However, if the  $\delta_{av}(6)$  is calculated without these two resonances, there is still an effect of the CH-moiety on the aromatic core [**1**:  $\delta_{av}(6)_{corr.} = 7.71$  ppm, **11**:  $\delta_{av}(6) = 8.14$  ppm].

In contrast to what is found for **1**, the <sup>1</sup>H-NMR spectrum of **2** does not display the overall up-field shift of its <sup>1</sup>H-NMR signals (Figure 1). It is neither observed for the cyclohepta protons [7.18 ppm (H3, H6) and 6.37 ppm (H4, H5)] nor for the protons attached to the PAH core [ $\delta_{av}(6) = 7.95$  ppm, compare **12**:  $\delta_{av}(6) = 7.72$  ppm, **7**:  $\delta_{av}(6) = 7.17$  ppm, (Table 1)]. An effect on the <sup>1</sup>H-NMR chemical shift of the peripheral cyclopenta-moiety hydrogen atoms in the case of cyclopenta[*c,d*]fluoranthene (**7**) was observed, but attributed to the interaction between the external and peripheral cyclopenta-moieties.<sup>14</sup>

For pleiadene (**3**)<sup>15</sup> [ $\delta_{av}(6) = 6.93$  ppm and  $\delta_{av}(7) = 5.70$  ppm] and cyclohepta[*j,k*]phenanthrene (**4**)<sup>11</sup> [ $\delta_{av}(6) = 7.51$  ppm and  $\delta_{av}(7) = 5.89$  ppm] comparable up-field <sup>1</sup>H-NMR chemical shifts for both the protons attached to the CH-moiety and the aromatic protons were found as for **1** (Table 1). In the case of **4** again the largest effect of the CH-moiety is present for the neighboring protons [H3 (6.95 ppm) and H8 (7.00 ppm), see for numbering Figure 7]. The  $\delta_{av}(6)$  without these two protons is, however, still shifted up-field with respect to that of **14** [**4**:  $\delta_{av}(6)_{corr} = 7.67$  ppm and **14**:  $\delta_{av}(6) = 7.92$  ppm].

Magnetic Properties of Cyclohepta-Fused Non-Alternant PAH

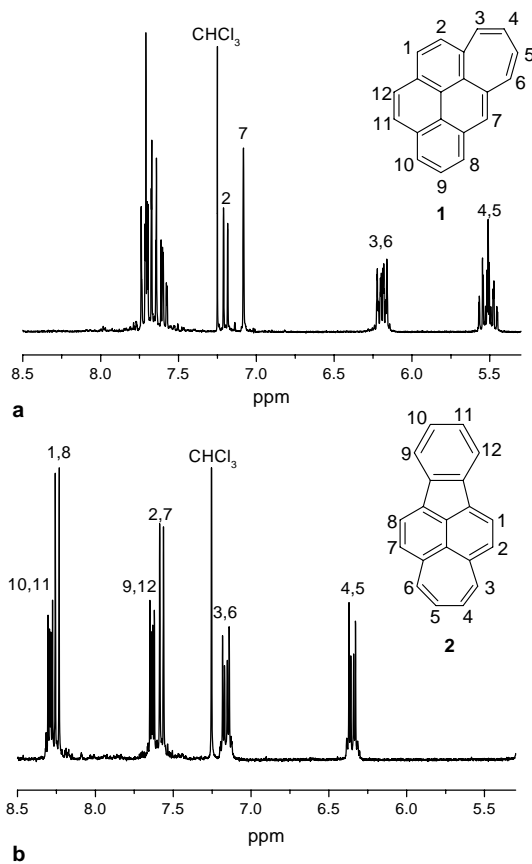


**Figure 1.** Expansion of the <sup>1</sup>H-NMR spectrum (solvent CDCl<sub>3</sub>, range 8.5 - 5.5 ppm) of **a.** cyclohepta[6,d]pyrene (**1**) **b.** cyclohepta[6,d]fluoranthene (**2**).

**Table 1.** Comparison of the average <sup>1</sup>H NMR chemical shift of the accessible CH-PAH **1,2,3** and **4** with their CP-PAH congeners **5, 6, 7** and **8** and the corresponding PAH **9, 10, 11** and **12**.

	CH-PAH				CP-PAH				PAH			
	1	2	3	4	6	7	8	9	11	12	13	14
$\delta_{av}(6)$	7.55	7.95	6.93	7.51	8.18	7.17	7.68	7.96	8.14	7.72	7.65	7.92
$\delta_{av}(5/7)$	5.88	6.77	5.70	5.89	7.32	6.52	7.07	7.17				

These results indicate that in the case of compounds **1**, **3** and **4** fusion of the CH-moiety to the alternant PAH core affects the magnetic properties of the whole molecule, whereas this is not the case for **2**. Since, for **1**, **3** and **4** *up-field* shifts are observed, it can be concluded that the global aromaticity of these CH-PAH is reduced compared to the corresponding alternant PAH cores. To gain more detailed insight in the magnetic properties of the CH-PAH **1** – **4**, *i.e.* especially the paratropic and diatropic contributions of the distinct rings (local aromaticity) to the  $\pi$  and total ( $\sigma + \pi$ ) current density maps of the molecule (global aromaticity), current density maps were calculated using the reliable CTOCD-DZ *ab initio* method. Subsequently, integrated magnetic properties (<sup>1</sup>H-NMR chemical shifts and NICS values) were calculated from the current density maps using the CTOCD-PZ2 method (see Experimental Section).

### 9.2.2 Current density maps of CH-PAH

In non-alternant PAH, such as CH-PAH that contain annulated odd- and even-membered rings, different local paratropic and diatropic contributions determine the overall (global) aromaticity of the compounds. These contributions can be visualized by calculation of the all-electron current density maps, using the *ab initio* all electron distributed origin method [continuous transformation of origin of current density (CTOCD-DZ)].<sup>16</sup> Since the current density at each point is computed with that point as the origin of gauge, *i.e.* CTOCD-DZ is *ipsocentric*, a physically realistic analysis of the different orbital contributions to the computed current density can be made.<sup>7</sup> It has been shown that in many  $\pi$ -conjugated polycyclic systems the currents densities maps are predominantly determined by occupied to un-occupied transitions around the HOMO – LUMO gap.<sup>7,17</sup> A rotational transition will lead to a paratropic ring current, while a translational transition will lead to a diatropic ring current.<sup>7,18</sup>

Firstly, we turn to compounds **1** and **3** – **5** since the CTOCD-DZ results reveal that these CH-PAH show a similar behavior. The current density maps of **1**, **3** – **5** induced by a magnetic field perpendicular to molecular plane were calculated (see Experimental Section). In Figures 2 - 4 these current-density maps are shown (anticlockwise circulation is diamagnetic, whilst paramagnetic circulation is clockwise). For compound **1** a diatropic ('aromatic') circulation is observed around the  $14\pi$ -electron pyrene-perimeter in the total  $\pi$ -only map (Figure 2A). This diatropic current is typical for the parent PAH pyrene (**9**).<sup>19</sup> In addition, a relatively strong paratropic ('*anti*-aromatic') current is present in the CH-moiety. When the different orbital contributions to these currents are evaluated, it is shown that the paratropic current in the CH-moiety is a result of transitions from the two electrons of the HOMO (10a", -6.34 eV). The pyrene-like diatropic current has its origin in transitions from the HOMO-1 (9a", -7.95 eV).

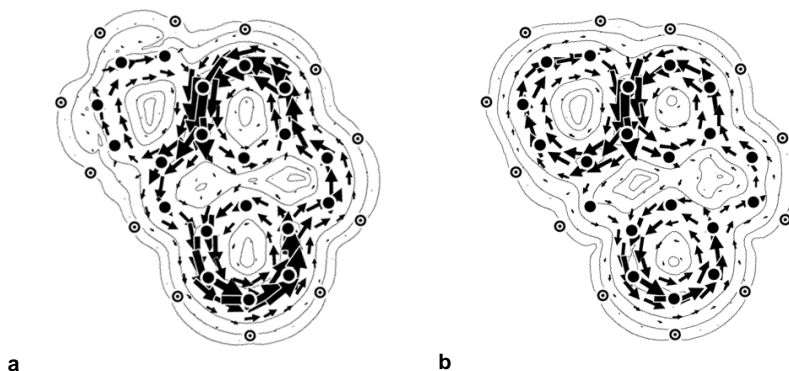


**Figure 2.** Computed CTOCD-DZ current density maps for cyclohepta[*c,d*]pyrene (**1**,  $C_2$ ) **a.**  $\pi$ -only map and **b.** sum of HOMO and HOMO-1 ( $10a''$  en  $9a''$ ).

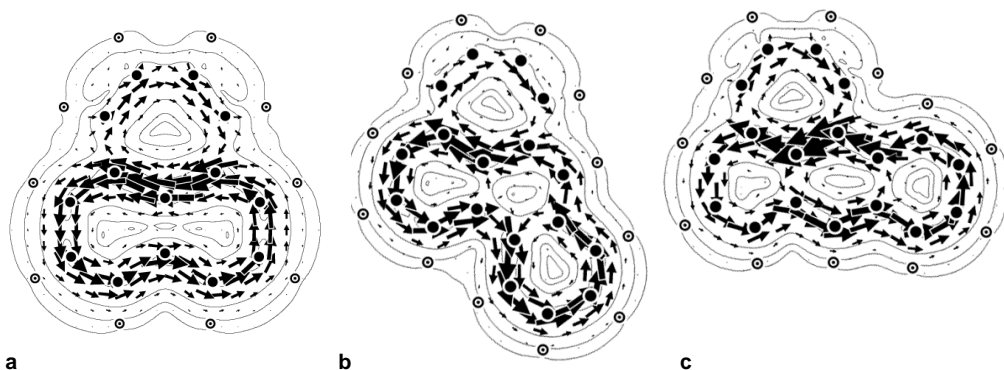


**Figure 3.** Computed CTOCD-DZ  $\pi$ -only maps **a.** for pleiadiene (**3**,  $C_{2v}$ ) **b.** for cyclohepta[*j,k*]phenanthrene (**4**,  $C_s$ ) and **c.** for cyclohepta[*l,m*]anthracene (**5**,  $C_s$ ).

In fact, these two orbitals determine the main features of the total  $\pi$ -only map. Calculation of the sum plot, *i.e.* the current density map of the [HOMO + HOMO-1 ( $10a''$  +  $9a''$ )]-electron distribution (Figure 2B), corroborates this analysis; it is nearly identical to the  $\pi$ -only map (Figure 2A).

In the CTOCD-DZ  $\pi$ -only current density maps of compounds **3** – **5** (Figure 3) similar phenomena are apparent. Besides diatropic circulations that are typical for the parent PAH **13** – **15**,<sup>20,21</sup> paratropic ring currents are present in the CH-moiety. Also in the case of the compounds **3** – **5**, two  $\pi$ -orbitals primarily determine the  $\pi$ -only current density map. Whereas, the paratropic current has its origin in transitions from the HOMO [**3**:  $3a_2$ , -6.67 eV; **4**:  $9a''$ , -6.67 eV; **5**:  $9a''$ , -6.25 eV], the HOMO-1 [**3**:  $4b_1$ , -8.70 eV; **4**:  $8a''$ , -8.00 eV; **5**:  $8a''$ , -8.42 eV] transitions give rise to the typical alternant PAH diatropic features.

In contrast to what was found for **1**, **3** - **5**, no paratropic ring current in the CH-moiety is discernible in the  $\pi$ -only current density map calculated for **2** (Figure 4A)! It contains merely two localized double bonds. In addition, the typical 'disjoint' structure of fluoranthene is visible, *i.e.* a diatropic benzene-like current and a diatropic naphthalene-like current.<sup>14</sup> Analysis of the different orbital contributions to the  $\pi$ -only current density map shows that in the case of **2** instead of two, three  $\pi$ -orbitals contribute, *viz.* the HOMO ( $4a_2$ , -6.64 eV), the HOMO-1 ( $6b_1$ , -7.87 eV) and the HOMO-2 ( $5b_1$ , -8.82 eV). The HOMO-current density map displays only a weak paratropic current along the CH-moiety (Figure 4B), the HOMO-1 a diatropic current in the benzene-moiety of **2** (Figure 4C) and the HOMO-2 a diatropic current in the naphthalene moiety of **2** (Figure 4D).

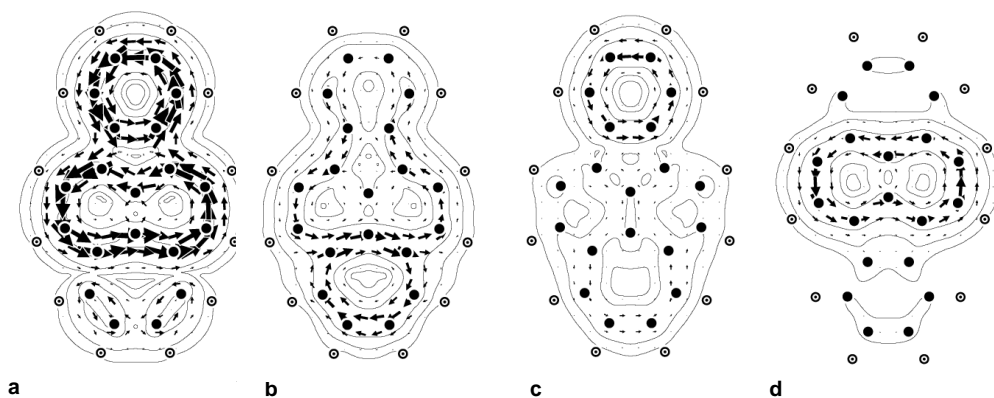


**Figure 4.** Orbital contributions to the ring currents in cyclohepta[6,7]fluoranthene (**2**,  $C_{2v}$ ) computed by the CTOCD-DZ method **a.**  $\pi$ -only map and **b.**  $4a_2$  (HOMO), **c.**  $6b_1$  (HOMO-1) and **d.**  $5b_1$  (HOMO-2) molecular orbitals.

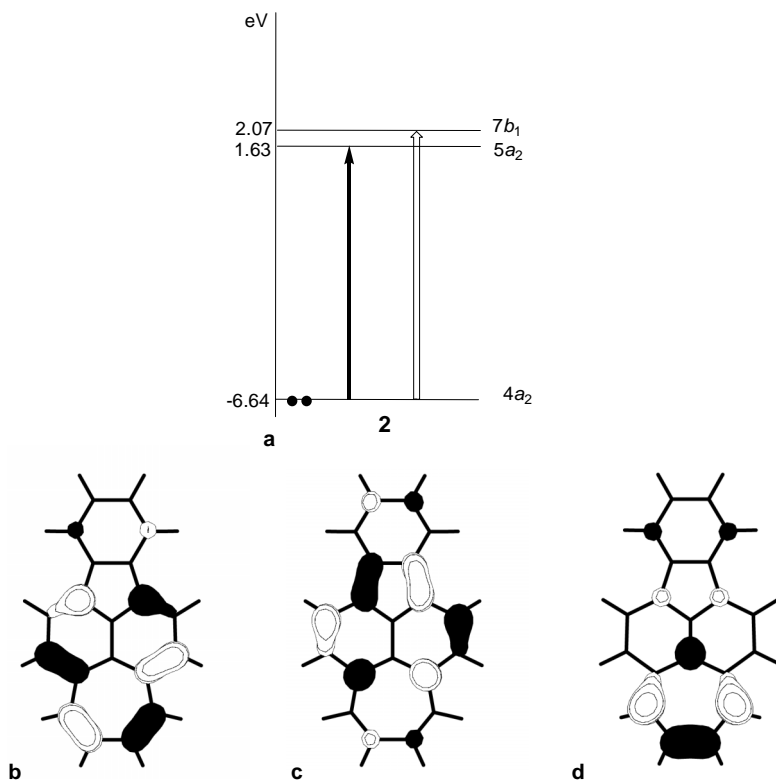


**Figure 5.** a. Orbital energy level diagram showing the transitions responsible for the orbital currents in **2**. Filled arrows represent translational transitions and open arrows rotational transitions from occupied levels. b. Molecular orbital plot of the HOMO of **2** ( $4a_2$ ). c. Molecular orbital plot of the LUMO of **2** ( $5a_2$ ). d. Molecular orbital plot of the LUMO+1 of **2** ( $7b_1$ ).

Comparison of the orbital structures of cyclohepta[*c,d*]fluoranthene (**2**) and pleiadene (**3**) rationalizes the presence of localized double bonds in the  $\pi$ -only current density map of **2** (Figures 5 and 6). The ring currents in the CH-moiety have its origin in transitions from the HOMO. When the HOMO, LUMO and LUMO+1 of **2** and **3** are compared, it is evident that both compounds possess similar HOMO's (**2**:  $4a_2$  -6.64 eV, **3**:  $3a_2$  -6.67 eV). The LUMO and LUMO+1, however, are inverted in **2** compared to **3** (**2**: LUMO  $5a_2$ , 1.63 eV; LUMO+1  $7b_1$ , 2.07 eV, **3**: LUMO  $5b_1$ , 2.33 eV; LUMO+1  $4a_2$ , 2.62 eV). This results in a rotationally allowed (open arrow) HOMO - LUMO transition for **3** ( $3a_2$  to  $5b_1$ ), but a translationally allowed (filled arrow) transition for **2** ( $4a_2$  to  $5a_2$ ). Furthermore, Figure 5 shows a translationally allowed HOMO - LUMO+1 transitions for

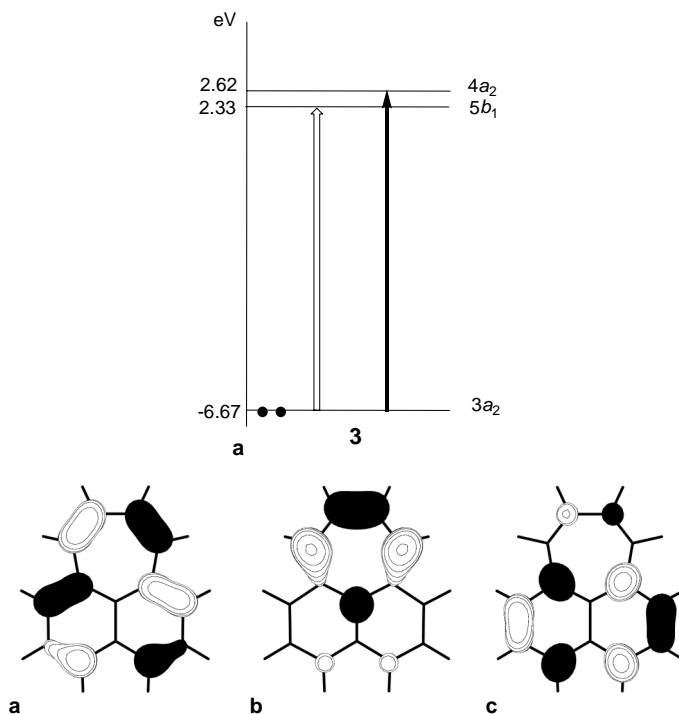


**Figure 6. a.** Orbital energy level diagram showing the transitions responsible for the orbital currents in **3**.

Filled arrows represent translational transitions and open arrows rotational transitions from occupied levels. **b.** Molecular orbital plot of the HOMO of **3** ( $3a_2$ ). **c.** Molecular orbital plot of the LUMO of **3** ( $5b_1$ ). **d.** Molecular orbital plot of the LUMO+1 of **3** ( $4a_2$ ).

**3** ( $3a_2$  to  $4a_2$ ), and Figure 4 a rotationally allowed HOMO – LUMO+1 for **2** ( $4a_2$  to  $7b_1$ ). The relative intensities of these transition are now of relevance. Whereas, the rotational transitions have comparable intensity, the translational transition in **2** is enhanced. This results in a larger diatropic current in **2** that reduces the paratropic current in the CH-moiety and consequently leads to localization of the two double bonds.

### 9.2.3 NICS values and <sup>1</sup>H-chemical shifts of CH-PAH

In 1996 the Nucleus Independent Chemical Shift (NICS) criterion was introduced as a probe for local ring current contributions.<sup>6</sup> The mean absolute nuclear shielding ( $\sigma_{av}$ ) in the geometric center of a ring is computed and converted into a shift by reversing its sign. A negative sign reflects a



local diatropic (aromatic) ring current, whereas a positive sign indicates local paratropic (*anti*-aromatic) ring current contributions. The  $\sigma_{av}$  values can also be obtained by appropriate integration of the CTOCD-PZ2 current densities (see Experimental Section).<sup>19</sup> In Figure 7 the computed NICS values are presented for compounds **1** – **5**. For all compounds, negative NICS values are found for the rings in the PAH core and positive values for the CH-moieties. This is in line with the CTOCD-DZ current density maps (section 9.2.2), which gave diatropic ring currents in the core and paratropic currents in the CH-moiety. Notice, however, that the NICS value of the CH-moiety of **2** is considerably smaller (2.3 ppm) compared to the values of the CH-moieties in **1** and **3** – **5** (7.0, 6.7, 6.0 and 6.0 ppm, respectively).

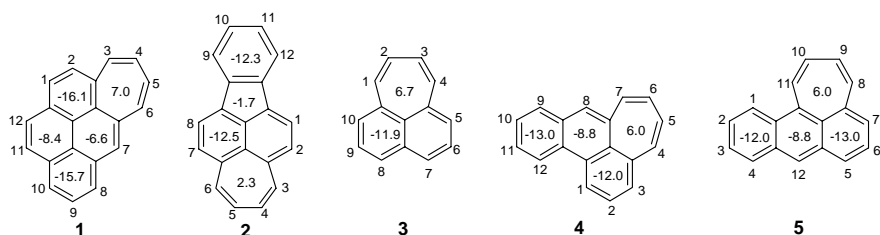


**Figure 7.** Computed nuclear shielding constants (NICS) at the ring centers of **1** – **5** (in ppm).

In addition, the <sup>1</sup>H-NMR chemical shifts were computed with the CTOCD-PZ2 method. Selected resonances for compounds **1** – **5** are compiled in Table 2. The calculated chemical shifts are generally shifted up-field by up to 0.6 ppm from the corresponding experimental values. Notwithstanding, the general trends and features found experimentally are reproduced. The protons attached to the aromatic cores of **1**, and **3** – **5** are shifted up-field as is illustrated by the calculated average shift [ $\delta_{av}(6)_{calc.}$ ]. In addition, all core protons neighboring the CH-moiety possess the largest up-field shifts [**1**: H2, H7; **3**: H(5, 10); **4**: H3, H8, **5**: H1, H7)].

#### 9.2.4 Magnetic properties of CP-PAH and CH-PAH versus CP-CH-PAH: a prediction

For the CH-PAH **1**, **3**, **4** and **5** and the CP-PAH **6**<sup>14</sup> and **8**<sup>19</sup> current density maps show similar features. The original PAH structure is conserved but in addition a paratropic current is present in the CP- or CH-moiety. The magnitude of this paratropic current influences the global aromaticity of the compound. When the CH-PAH (**1**, **3** and **4**) and the CP-PAH (**6** and **8**) are compared, it can be stated that the paratropic currents are more pronounced in the CH-moieties. The effect of the paratropic current in the CH-moiety is only comparable to the effect of the fusion of *two*

**Table 2.** Comparison of the selected experimental  $^1\text{H}$ -NMR chemical shifts (ppm) and the computed hydrogen nuclear magnetic shieldings (CTOCD-PZ2) for compounds **1** – **4**.

Compound	Nucleus <sup>a</sup>	$\delta_{\text{calc}}$	$\delta_{\text{exp}}$	$\delta_{\text{av}}(6)_{\text{calc}}^b/\delta_{\text{av}}(6)_{\text{exp}}$	$\delta_{\text{av}}(7)_{\text{calc}}/\delta_{\text{av}}(7)_{\text{exp}}$
<b>1</b>	H(1)	7.47	7.74	7.31/7.55	5.49/5.88
	H(2)	7.00	7.21		
	H(3)	5.84	6.23		
	H(4)	5.11	5.54		
	H(5)	5.21	5.54		
	H(6)	5.80	6.22		
	H(7)	6.60	7.08		
<b>2</b>	H(1, 8)	7.52	8.26	7.43/7.95	6.07/6.77
	H(2, 7)	7.07	7.59		
	H(3,6)	6.38	7.18		
	H(4,5)	5.76	6.37		
	H(9,12)	7.67	7.65		
	H(10,11)	7.49	8.30		
<b>3</b>	H(1,4)	5.55	6.01	6.70/6.93	5.25/5.70
	H(2,3)	4.95	5.37		
	H(5,10)	6.30	6.63		
	H(6,9)	6.85	6.99		
	H(7,8)	6.94	7.21		
<b>4</b>	H(3)	6.61	6.95	7.27/7.51	5.58/5.89
	H(4)	5.62	6.26		
	H(5)	5.04	5.57		
	H(6)	4.98	5.57		
	H(7)	5.67	6.15		
	H(8)	6.32	7.00		
<b>5</b>	H(8)	5.68	6.40	7.03	5.50/6.26
	H(9)	4.93	5.80		
	H(10)	5.05	6.01		
	H(11)	6.30	6.84		

<sup>a</sup> See Figure 7. <sup>b</sup> For  $\delta_{\text{av}}(6)_{\text{calc}}$  all computed  $^1\text{H}$ -NMR chemical shifts of the hexagons are used.

cyclopenta-moieties. This is evident when the  $\delta_{\text{av}}(6)$  and  $\delta_{\text{av}}(5)$  of **1** and **6** are compared to those of dicyclopenta[*cd,jk*]- (**17**) and dicyclopenta[*cd,jg*]pyrene (**18**).<sup>9</sup> These *bis*-cyclopenta-fused pyrenes

display larger up-field  $^1\text{H-NMR}$  chemical shifts than **6** but smaller shifts than **1** [ $\delta_{\text{av}}(6)/\delta_{\text{av}}(5/7)$ : **17** 7.55/6.66 ppm, **18** 7.58/6.90 ppm, **6** 8.18/7.32 ppm, **1** 7.65/5.97 ppm].<sup>9,19</sup>

The dissimilar magnetic properties of **2**, compared to **1**, **3** - **5** suggest that also other non-alternant PAH with both a CP-moiety and a CH-moiety integrated in the alternant core, may display special features. To evaluate the interaction between CP- and CH-moieties, two hitherto elusive isomers of anthracene with both a CP- and a CH-moiety fused to the alternant anthracene core (**19** and **20**, Chart 2) were studied using the CTOCD-DZ method.

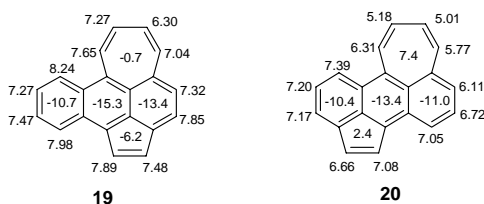
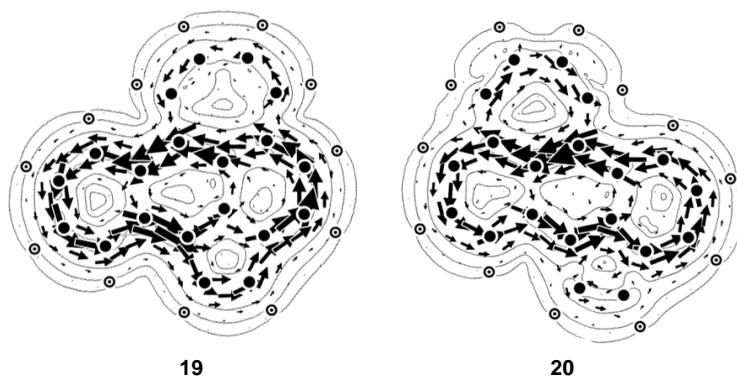


Chart 2

Although the synthesis of **19** has been attempted, this compound has never been isolated.<sup>22</sup> Compounds **19** and **20** have similar total energies [**19** is 6.3 kcalmol<sup>-1</sup> more stable (RHF/6-31G\*\*), see Experimental section]. In Figure 8 the  $\pi$ -only current density maps of **19** and **20** are shown. For both compounds a diatropic current around the anthracene core is visible. For **20**, in addition two paratropic currents are present; one in the CP-moiety and one in the CH-moiety. Surprisingly, no paratropic current, but a diatropic current is observed in the CH-moiety of **19**. Furthermore, the CP-moiety displays a special feature. Both a paratropic and a diatropic ring current are visible in this CP-moiety, *i.e.* the ring current is bifurcated. Scrutiny of the different orbital contributions for **20** indicates that it is a disjoint structure where three different orbitals contribute to the three different ring currents in the molecule. The current density map of the HOMO (10a", -6.30 eV) displays the paratropic current in the CH-moiety, the HOMO-1 (9a", -8.12 eV) the paratropic current in the CP-moiety and the HOMO-2 (8a", -8.47 eV) the diatropic current in the anthracene core. For **19** the same three orbitals (HOMO: 10a" -6.40 eV; HOMO-1: 9a" -7.71 eV and HOMO-2: 8a" -8.50 eV) contribute to the total  $\pi$ -only current density map, but now the different orbital contributions are not clearly localized in distinct rings of the molecule. It is remarkable, that although both a CH-moiety and CP-moiety are present in this molecule that normally give rise to paratropic ring currents, such ring current contributions are not discernible in the total  $\pi$ -only map of **19** and point to the importance of odd-membered ring topology. This effect is also apparent from the calculated NICS values and  $^1\text{H-NMR}$  chemical shifts for **19** and **20**

(Chart 2). All NICS values for **19** are negative, albeit weak in the CH-moiety of **19**, which implies that only local aromatic contributions are present. The CH-moiety in **20** has a comparable NICS value (7.4 ppm) as computed for **1**, **3** – **5**. Furthermore, the calculated average  $^1\text{H-NMR}$  chemical shifts are shifted up-field in the case of **20**, but not for **19** [**19**:  $\delta_{\text{av}}(6)$  7.69 ppm,  $\delta_{\text{av}}(7)$  7.16 ppm; **20**:  $\delta_{\text{av}}(6)$  6.94 ppm,  $\delta_{\text{av}}(7)$  5.57 ppm].



**Figure 8.** Computed CTOCD-DZ  $\pi$ -only current density maps for **19** and **20**.

### 9.3 Conclusions

The CH-PAH **1** and **3** – **5** display strong paratropic ring currents in the CH-moiety that decrease the global aromaticity of the compounds. This is observed experimentally from the up-field shift of the aromatic protons in the  $^1\text{H-NMR}$  spectra of **1**, **3** and **4**. For **2** that contains both an externally-fused CH-moiety and an internally CP-moiety in its structure, no up-field shifts in the  $^1\text{H-NMR}$  spectrum were observed. Theoretical evaluation of the magnetic properties with CTOCD-DZ, NICS and calculated  $^1\text{H-NMR}$  chemical shifts corroborated that paratropic currents are present in the CH-moieties of **1**, **3** and **4**, but that the double bonds in the CH-moiety of **2** are localized.

For the anthracene derivatives **19** and **20** that have both an externally-fused CH-moiety and a externally-fused CP-moiety annelated to the anthracene core, remarkably different features are observed depending on the topology of CH/CP-fusion. In **20** no interaction between the CH- and CP-moiety is present, which results in two paratropic ring currents in the CH- and CP-moiety.

Interaction in **19** is possible, which results in diatropic ring current in the CH-moiety and bifurcation in the CP-moiety. Hence, although two 'anti-aromatic' moieties are fused to the anthracene core, no large reduction of the global aromaticity is expected.

## 9.4 Experimental section

### Computational Methods

The magnetic properties of compounds **1 - 5** and **19 - 20** were computed using the CTOCD distributed-origin method at the *ab initio* Hartree-Fock level of theory. The maps were computed using the DZ (diamagnetic zero) formulation and the integrated properties using the PZ2 (paramagnetic zero) variant all with the 6-31G\*\* basis using the Exeter version of SYSMO.<sup>23</sup> For consistency, the molecular geometries were optimized at the RHF/6-31G\*\* using the GAMESS-UK program.<sup>24</sup> All stationary points were characterized by Hessian calculations. Hessian calculations for **1**, **2** and **4** have shown that the planar geometries are genuine minima since no imaginary vibrations were found. For compound **3**, weak imaginary vibrations are found, which indicates that the planar geometry is a shallow minimum. Compound **5** does not have planar geometry as a minimum, but the deviation of planarity in the ground state geometry is 16 degrees. This is not expected to influence the calculated current density maps.

The total energies of the compounds **1 - 5** and **19 - 20** are listed in the following Table.

Total energies ( $E_{\text{tot}}$  in hartree) of the compounds **1 - 5** and **19 - 20** calculated at the RHF/6-31G\*\* level of theory.

Compound	$E_{\text{tot}}$ (hartree)	Symmetry	HOMO (in eV) (symmetry)	LUMO (in eV) (symmetry)
1	-764.397903	$C_s$	-6.34 (10a'')	1.81 (11a'')
2	-764.385296	$C_{2v}$	-6.64 (4a <sub>2</sub> )	1.63 (5a <sub>2</sub> )
3	-535.981597	$C_{2v}$	-6.67 (3a <sub>2</sub> )	2.33 (5b <sub>1</sub> )
4	-688.637156	$C_s$	-6.67 (9a'')	2.20 (10a'')
5	-688.616971	$C_s$	-6.25 (8a'')	1.74 (10a'')
19	-764.350188	$C_s$	-6.40 (10a'')	1.02 (11a'')
20	-764.340077	$C_s$	-6.30 (10a'')	1.01 (11a'')

## References and notes

- (1) See the complete issue *Chem. Rev.* **2001**, *101*, 1115-1566.
- (2) Streitwieser, A. *Molecular Orbital Theory for Organic Chemists*; Wiley: New York, 1961.
- (3) Mallion, R. B. *Pure & Appl. Chem.* **1980**, *52*, 1541-1548.
- (4) Fleischer, U.; Kutzelnigg, W.; Lazaretti, P.; Muhlenkamp, V. *J. Am. Chem. Soc.* **1994**, *116*, 5298-5306.
- (5) Schleyer, P. v. R.; Jiao, H. *Pure & Appl. Chem.* **1996**, *68*, 209-218.
- (6) Schleyer, P. v. R.; Maerker, C.; Darnsfeld, A.; Jiao, H.; van Eikema Hommes, N. J. R. *J. Am. Chem. Soc.* **1996**, *118*, 6317-6318.
- (7) Steiner, E.; Fowler, P. W. *J. Phys. Chem. A.* **2001**, *105*, 9553-9562.
- (8) Mitchell, R. H. *Chem. Rev.* **2001**, *101*, 1301-1316.
- (9) Sarobe, M.; Flink, S.; Jenneskens, L. W.; van Poecke, B. L. A.; Zwikker, J. W. *J. Chem. Soc., Chem. Commun.* **1995**, 2415-2416.
- (10) Vogel, E.; Neumann, B.; Klug, W.; Schmickler, H.; Lex, J. *Angew. Chem.* **1985**, *97*, 1044-1045.
- (11) Pagni, R. M.; Burnett, M.; Hazell, A. C. *J. Org. Chem.* **1978**, *43*, 2750-2752.
- (12) Jans, A. W. H.; Tintel, C.; Cornelisse, J.; Lugtenburg, J. *Magn. Res. Chem.* **1986**, *24*, 101-104.
- (13) Dosa, P. I.; Schleifenbaum, A.; Vollhardt, K. P. C. *Org. Lett.* **2001**, *3*, 1017-1020.
- (14) Fowler, P. W.; Steiner, E.; Acocella, A.; Jenneskens, L. W.; Havenith, R. W. A. *J. Chem. Soc., Perkin Trans. 2* **2001**, 1058-1065.
- (15) Shields, J. E.; Gavrilovic, D.; Kopecky, J.; Hartmann, W.; Heine, H.-G. *J. Org. Chem.* **1974**, *39*, 515-520.
- (16) Zanasi, R.; Lazzeretti, P.; Malagoli, M.; Piccinini, F. *J. Chem. Phys.* **1995**, *18*, 7150-7157.
- (17) Fowler, P. W.; Steiner, E.; Jenneskens, L. W. *Angew. Chem. Int. Ed. Engl.* **2001**, *40*, 362.
- (18) Steiner, E.; Fowler, P. W. *J. Chem. Soc., Chem. Commun.* **2001**, 2220-2221.
- (19) Steiner, E.; Fowler, P. W.; Jenneskens, L. W.; Havenith, R. W. A. *Eur. J. Org. Chem.* **2002**, 163-169.
- (20) Steiner, E.; Fowler, P. W. *Int. J. Quant. Chem.* **1996**, *60*, 609-616.
- (21) Ligabue, A.; Pincelli, U.; Lazzeretti, P.; Zanasi, R. *J. Am. Chem. Soc.* **1999**, *121*, 5513-5518.
- (22) Morita, K.; Aida, T.; Morinaga, K.; Tsunetsugu, J. *J. Chem. Soc., Perkin Trans. 2* **1994**, 1215-1220.
- (23) Lazzeretti, P.; Zanasi, R. *SYSMO package*; University of Modena, 1980.

- (24) Guest, M. F.; van Lenthe, J. H.; Kendrick, J.; Schöffel, K.; Sherwood, P.; Harrison, R. J. *GAMESS-UK, a package of ab initio programs*, **1998**. With contributions from: Amos, R.D., Buenker, R.J.; Dupuis, M.; Handy, N.C.; Hillier, I; Knowles, P.J.; Bonacic-Koutecky, V.; von Niessen, W.; Saunders, V.R.; Stone, A.J. Derived from the original GAMESS code by: Dupuis, M.; Spangler, D.; Wendolowski, J.; NRCC Software Catalog, vol. 1, program no. QG01 (GAMESS), **1980**.





## Summary and outlook

The investigations described in this thesis were initiated to study aspects of the chemistry of non-alternant PAH that are connected to the formation, the selective synthesis and the properties of closed carbon surfaces. Especially, the combination of synthesis, involving Flash Vacuum Thermolysis (FVT), advanced spectroscopic techniques and state-of-the-art *ab initio* quantum chemical calculations has resulted in insights on very different areas of non-alternant PAH chemistry. The electronic and magnetic properties of key sub-structures of classical fullerenes, *i.e.* cyclopenta-fused PAH, have been described and new sub-structures of bended carbon nanotubes, cyclohepta-fused PAH, have been identified, synthesized and their properties studied. Finally, non-alternant PAH are shown to be unimolecular progenitors for previously known and unknown closed carbon surfaces.

**Chapter 1** provides an introduction to the research described in this thesis. The connection between the chemistry of (2D) non-alternant PAH and (3D) closed carbon surfaces, such as fullerenes and carbon nanotubes, is exemplified.

Fundamental processes responsible for the build up and rearrangement of non-alternant PAH in the gas-phase using Flash Vacuum Thermolysis (FVT) are the subject of **Part I** of this thesis (**Chapters 2** and **3**). Convincing evidence is given on the basis of FVT of selectively deuterated ethynyl-substituted (E-PAH) for the formation of cyclopenta-fused PAH (CP-PAH) from E-PAH *via* the proposed Brown mechanism, *i.e.* ethynyl-ethylidene carbene equilibration followed by insertion of the ethylidene carbene into a PAH C-H bond. However, this mechanism was recently refuted on the basis of *ab initio* calculations. Unexpectedly, but rewardingly, a hitherto unknown hydrogen migration process was identified. It is shown that the hydrogen atoms of alternant PAH and CP-PAH are mobile; they migrate under high temperature conditions along the perimeter of the molecule. A mechanism involving carbene intermediates is proposed to rationalize these observations. The facile deuterium migration has important consequences for the interpretation of (previous) mechanistic studies on the high temperature chemistry of (CP)-PAH.

In **Part II** of this thesis (**Chapters 4 – 7**) the use of unimolecular non-alternant PAH progenitors for the synthesis of C<sub>60</sub>, C<sub>70</sub> and heterofullerenes is explored. The synthesis by design of C<sub>60</sub> starting from the C<sub>60</sub>H<sub>30</sub> PAH benzo[1,2-*e*:3,4-*e'*:5,6-*e''*]tribenzo[*g*]acephenanthrylene is

achieved *via* fifteen-fold consecutive H<sub>2</sub> losses and ring closures induced by matrix-assisted-laser-desorption-ionization time-of-flight mass spectrometry (MALDI TOF-MS). In C<sub>60</sub>H<sub>30</sub> the innermost non-bonding hydrogen atoms are sterically congested and therefore susceptible to undergo cyclodehydrogenation, *i.e.* H<sub>2</sub> loss followed by ring closure. This leads to curling up of the carbon skeleton, whereupon the next set of inner-core, non-bonded hydrogen atoms becomes sterically congested and, thus, prone to undergo the next set of cyclodehydrogenations. Hence, the process of imposing curvature and finally closure of the carbon surface resembles a zipper behavior. Both *semi*-empirical and *ab initio* calculations support this ‘zipping up process’. The results unequivocally show that the carbon topology of the C<sub>60</sub>H<sub>30</sub> precursor, which exactly matches the carbon topology of C<sub>60</sub>, is a prerequisite. This has led to the Schlegel-match proposition as a design criterion for the identification and preparation of (novel) unimolecular precursors for closed carbon surfaces.

Based on these results two different unimolecular precursors for C<sub>70</sub> are proposed (**Chapter 5**). One is a Schlegel-match precursor, *viz.* a corannulene derivative. The other C<sub>70</sub> progenitor is a derivative of a fullerene pipe. The latter is proposed as a viable precursor since *ab initio* calculations have shown that in the ‘zipping up’ process intermediates that contain a closed carbon surface are more stable than constitutional isomers where the surface is not yet closed. The results of the calculations indicate that both progenitors can be converted into C<sub>70</sub> by cyclodehydrogenations under similar conditions as applied to C<sub>60</sub>H<sub>30</sub> rendering their syntheses worthwhile.

An ultimate objective of designing selective synthesis for closed carbon surfaces is to be able to modify their properties by for example the incorporation of hetero-atoms or by the preparation of endohedral fullerenes. A particular ensuing goal is the preparation of azafullerenes; incorporation of nitrogen atoms is expected to add electropositive character to the 3D molecule. Hence, based on the Schlegel-match proposition a C<sub>57</sub>H<sub>33</sub>N<sub>3</sub> non-alternant PAH was identified as a precursor for a C<sub>60</sub>-derivative in which three carbon atoms are replaced by nitrogen atoms, *i.e.* the novel triazafullerane C<sub>57</sub>H<sub>3</sub>N<sub>3</sub> and its ionic analogues C<sub>57</sub>H<sub>2</sub>N<sub>3</sub><sup>+</sup>/C<sub>57</sub>H<sub>2</sub>N<sub>3</sub><sup>-</sup>. It is shown that the non-alternant C<sub>57</sub>H<sub>33</sub>N<sub>3</sub> hetero-PAH indeed converts into an (ionic) azafullerane *via* successive H<sub>2</sub> losses and ring closures under MALDI TOF-MS conditions. Again, imposing curvature and finally closure of the surface proceeds from the inside outwards (‘zipping up’ process). This is substantiated by *ab initio* calculations on the neutral, cationic and anionic species of the proposed intermediates as well as ‘zipping up’ of a deuterated analogue (C<sub>57</sub>H<sub>27</sub><sup>2</sup>H<sub>6</sub>N<sub>3</sub>) under similar MALDI TOF-MS conditions. Interestingly, the conversion to a 3D closed surface can be achieved both in the positive-ion mode and the negative-ion mode. The success of the Schlegel-match proposition also renders the selective preparation of endohedral fullerenes viable. It is envisaged that trapping

of one of the intermediate ions formed during the 'zipping up' process in the mass spectrometer followed by addition of an ion or gas and subsequent further closure of the surface may give access to endohedral fullerenes by design.

In **Part III** of this thesis (**Chapter 7 – 9**) the electronic and magnetic properties of fullerene and carbon nanotube sub-structures are explored. At first instance, the properties of the key sub-structures of classical fullerenes, *viz.* those entirely composed of hexagons and pentagons, *i.e.* cyclopenta-fused PAH were considered. The electronic effect of the externally-fused cyclopenta-moiety on a PAH perimeter in CP-PAH was studied by Cyclic Voltammetry (CV). A series of 23 PAH, *mono*- and *bis*-CP-PAH were examined. *Mono*- and *bis*-CP-PAH with externally-fused cyclopenta-moieties were shown to undergo facile reduction and, hence, are expected to have high electron affinities (EA). In contrast to previous reports, a linear correlation between the LUMO energy ( $\epsilon_{\text{LUMO}}$ ) derived from Hückel Molecular Orbital (HMO) theory and the first reduction potential is obtained. This is shown to be the consequence of the fact that the cyclopenta-moiety acts as an electron-withdrawing *peri*-substituent. This contention is supported by the nearly identical Hammett constants ( $\sigma_{\text{m}}$ ) for the cyclopenta-moiety in four structurally different CP-PAH. It is proposed that upon reduction (addition of electrons)  $6\pi$  cyclopentadienide sub-structures are present. Both the calculated geometries of the radical-anions and *bis*-anions of selected (*bis*)-CP-PAH as well as the calculated magnetic properties of the *bis*-anions support this view.

To compare the electronic behavior of cyclopenta-fused PAH with that of their cyclohepta-fused counterparts, efficient syntheses of CH-PAH had to be developed since only a few representatives were known and only available lengthy syntheses (**Chapter 8**). Cyclohepta-fused PAH are also interesting synthetic targets from another perspective. Whereas the cyclopenta-moiety (pentagon) leads to positive curvature, a cyclohepta-moiety (heptagon) can induce negative curvature in a graphitic sheet. The syntheses of the novel cyclohepta-fused PAH, cyclohepta[*c,d*]pyrene and cyclohepta[*c,d*]fluoranthene is achieved by FVT of *bis*-acetylated precursors at remarkably low temperatures. It is shown that CH-PAH are only stable in a limited temperature range ( $T < 900^{\circ}\text{C}$ ). At higher temperatures conversion to their cyclopenta-fused counterparts takes place, *i.e.*  $\text{C}_2\text{H}_2$  extrusion occurs from the CH-moiety. This observation explains that up till now no CH-PAH have been identified in combustion mixtures.

The electronic behavior of CH-PAH is *anti*-symmetric with that of the corresponding CP-PAH. Whereas CP-PAH have high electron affinities, CH-PAH have low first oxidation potentials. This can be rationalized on the basis of their molecular orbital properties, *i.e.* whereas the presence of a pentagon renders a compound n-type, the heptagon leads to p-type character. A particular interesting future goal will be the synthesis of structures with both pentagons and

heptagons integrated in the structure, resembling all carbon/hydrogen donor-acceptor compounds. Finally, the magnetic properties of a series of CH-PAH are discussed in **Chapter 9**. The presence of a heptagon leads in most cases to a strong paratropic current in this ring when a magnetic field is applied. This is inferred from up-field shifted  $^1\text{H}$ -NMR chemical resonances. When both a pentagon and a heptagon are present in the structure in some cases an interesting interaction occurs, which leads to new and unexpected properties. This renders such molecules interesting synthetic targets.

## Samenvatting

Het in dit proefschrift beschreven onderzoek heeft tot doel verschillende aspecten van de chemie van tweedimensionale (2D) niet-alternerende polycyclische aromatische koolwaterstoffen (PAKs) te onderzoeken, die gerelateerd zijn aan de chemie van driedimensionale (3D) gesloten koolstofoppervlakken. Een relatie tussen deze twee klassen van verbindingen is op verschillende gebieden aanwezig. In de gasfase worden bijvoorbeeld onder vergelijkbare condities zowel niet-alternerende PAKs als gesloten koolstofoppervlakken gevormd. Gesloten koolstofoppervlakken kunnen verder op selectieve wijze gesynthetiseerd worden uit niet-alternerende PAKs. Als laatste, vormen niet-alternerende PAKs sleutel substructuren van gesloten koolstofoppervlakken. De combinatie van synthese, waarbij gebruik werd gemaakt van Flits Vacuum Thermolyse (FVT), geavanceerde spectroscopische technieken en *ab initio* berekeningen, heeft geleid tot nieuwe inzichten. De elektronische en magnetische eigenschappen van de substructuren van klassieke fullerenen, d.w.z. cyclopenta-gefuseerde PAKs worden beschreven. Verder zijn nieuwe sleutel substructuren van gebogen koolstofbuizen, cyclohepta-gefuseerde PAKs, gemaakt en hun eigenschappen bestudeerd. Tot slot, zijn niet-alternerende PAKs gebruikt als uitgangsstoffen in de selectieve synthese van bekende en tot nu toe onbekende gesloten koolstofoppervlakken.

**Hoofdstuk 1** geeft een introductie voor het in dit proefschrift beschreven onderzoek. De relatie tussen de chemie van (2D) niet-alternerende PAKs en (3D) gesloten koolstofoppervlakken, zoals fullerenen en koolstof nanobuizen, wordt duidelijk gemaakt.

Een aantal fundamentele processen van belang voor de opbouw en omleggingen van niet-alternerende PAKs onder hoge temperatuurcondities in de gasfase worden in **Deel I** van dit proefschrift (**Hoofdstukken 1 en 2**) bestudeerd met behulp van Flits Vacuum Thermolyse (FVT). Met FVT van selectief gedeuteerde ethynyl-gesubstitueerde PAKs (E-PAKs) is vastgesteld dat cyclopenta-gefuseerde PAKs (CP-PAK) gevormd worden *via* het Brown mechanisme vanuit E-PAK. Dit mechanisme (ethynyl-ethylideen equilibratie gevolgd door C-H insertie van het gevormde ethylideen carbeen) is recent ter discussie gesteld op basis van *ab initio* berekeningen. Naast experimenteel bewijs voor dit mechanisme werd onverwacht ontdekt dat de waterstof atomen van zowel alternerende als niet-alternerende PAKs mobiel zijn onder discrete FVT condities en kunnen migreren langs de perimeter van het molecuul. Een mechanisme, waarin

carbeen intermediairen een rol spelen, wordt voorgesteld om de migraties te verklaren. Het feit dat de migratie van waterstof atomen zo makkelijk plaatsvindt, heeft belangrijke consequenties voor de interpretatie van (eerder gepubliceerde) mechanistische studies naar het hoge temperatuur gedrag van (niet-)alternerende PAKs.

In **Deel II** van dit proefschrift (**Hoofdstukken 4 – 7**) wordt de reikwijdte bestudeerd van het door ons voorgestelde Schlegel-match principe. Dit principe stelt het gebruik voor van unimoleculaire niet-alternerende PAKs met de juiste koolstoftopologie als uitgangsmateriaal voor 3D gesloten koolstofoppervlakken. Op basis van dit principe is  $C_{60}$  verkregen vanuit de niet-alternerende  $C_{60}H_{30}$  PAK benzo[1,2-*e*:3,4-*e'*:5,6-*e''*]tribenzo[*f*]acephenanthryleen d.m.v. vijftienvoudig  $H_2$  verlies en ringsluiting, zgn. cyclodehydrogenaties, onder MALDI TOF-MS condities. De binnenste niet-gebonden waterstof atomen in  $C_{60}H_{30}$  zijn sterisch gehinderd en daardoor gevoelig voor cyclodehydrogenatie. De opeenvolgende cyclodehydrogenaties zorgen voor het opkrullen van het koolstofskelet, de volgende set van niet-bindende waterstof atomen komen daarbij binnen de som van de Van der Waals radius. Dit is van belang voor de volgende serie van cyclodehydrogenaties. Dus, de kromming van het koolstofskelet en de uiteindelijke sluiting, vinden plaats volgens een ritsproces. Zowel *semi*-empirische als *ab initio* berekeningen bevestigen deze experimentele resultaten. Het blijkt hierbij essentieel te zijn dat de uitgangsstof voldoet aan het Schlegel-match principe, aangezien anders ook degradatiereacties optreden van het PAK skelet.

Naar aanleiding van deze resultaten worden twee unimoleculaire uitgangsstoffen voor  $C_{70}$  voorgesteld (**Hoofdstuk 5**). Terwijl één voldoet aan het Schlegel-match principe, heeft de ander al een gesloten koolstofskelet lijkend op een fullereenpijp. Deze laatste structuur is voorgesteld omdat uit berekeningen blijkt dat gesloten koolstofoppervlakken tijdens het ritsproces stabiel zijn dan niet-gesloten oppervlakken. Op grond van berekeningen wordt verwacht dat beide uitgangsstoffen d.m.v. cyclodehydrogenaties kunnen worden omgezet in  $C_{70}$  onder soortgelijke condities als gebruikt werden voor het 'ritsen' van  $C_{60}H_{30}$  tot  $C_{60}$ . Dit maakt de synthese van deze structuren interessante doelen.

Het uiteindelijke doel van het ontwerpen van selectieve syntheses voor fullerenen is de mogelijkheid om de fullereenstructuur en dus de fullereeneigenschappen te kunnen modificeren. Dit kan door de introductie van hetero-atomen in het skelet of de synthese van endohedrale fullerenen. Een bijzonder interessante mogelijkheid is de introductie van stikstof atomen aangezien deze elektropositieve eigenschappen in het uiteindelijke molecuul kunnen introduceren. Daarom werd op basis van het Schlegel-match principe, de niet-alternerende  $C_{57}H_{33}N_3$  PAK ontworpen en gesynthetiseerd (**Hoofdstuk 6**). Deze verbinding is een precursor voor de triazafulleraan  $C_{57}H_3N_3$  en zijn ionogene analoge  $C_{57}H_2N_3^+$  /  $C_{57}H_2N_3^-$ , d.w.z.  $C_{60}$  derivaten waarin drie koolstof atomen

zijn vervangen door stikstof atomen onder MALDI TOF-MS condities. Door middel van cyclodehydrogenaties werd  $C_{57}H_{33}N_3$  omgezet in de tot nu toe onbekende azafulleraan  $C_{57}H_2N_3$ . De cyclodehydrogenaties vinden plaats op een stapsgewijze manier, van binnen naar buiten. Dit wordt ondersteund door zowel *ab initio* berekeningen als experimenteel door 'het ritsen' van een gedeutereerd analoog,  $C_{57}H_{27}N_3$  onder vergelijkbare MALDI TOF-MS condities. Opmerkelijk, kon in het geval van de stikstofhoudende  $C_{57}H_{33}N_3$  PAK ook cyclodehydrogenaties worden geïnduceerd in de negatieve-ion modus.

Het succes van het Schlegel-match principe maakt het mogelijk om ook selectief endohedrale fullerenen te maken. Tijdens het ritsproces kan bijvoorbeeld een intermediair ion in de massaspectrometer 'getrapt' worden. Vervolgens kan dan een gas of ion ingelekt worden, waarna de structuur verder gesloten wordt.

In het laatste deel van dit proefschrift (**Hoofdstukken 7 – 9**) worden de elektronische en magnetische eigenschappen van sleutel substructuren van fullerenen en koolstofbuizen bestudeerd. In eerste instantie worden de eigenschappen van cyclopenta-ge-substitueerde PAKs (CP-PAK) bestudeerd. Dit zijn sleutel substructuren van klassieke fullerenen, d.w.z fullerenen opgebouwd uit vijf- en zesringen. Het elektronische effect van de extern geannuleerde vijftring op de eigenschappen van CP-PAKs werd bestudeerd met behulp van Cyclische Voltammetry (CV) aan 23 PAKs, *mono*-CP-PAKs en *bis*-CP-PAKs. *Mono*-CP-PAKs en *bis*-CP-PAKs met extern geannuleerde vijftringen bleken makkelijk te reduceren en hebben daarom een hoge elektronenaffiniteit (EA). In tegenstelling tot wat eerder in de literatuur beschreven is, bestaat er een lineaire correlatie tussen de energie van de LUMO, bepaald met behulp van Hückel Moleculaire Orbital theorie, en de eerste reductie potentiaal. Dit blijkt een gevolg te zijn van het feit dat de extern geannuleerde vijftring kan worden beschreven als een elektronenzuigende *peri*-substituent. Identieke Hammett constanten ( $\sigma_m$ ) werden gevonden voor de vijftringen in vier verschillende CP-PAKs. De resultaten suggereren dat na reductie,  $6\pi$  cyclopentadienide substructuren aanwezig zijn in CP-PAKs. Dit is in overeenstemming met zowel de berekende geometrie van de radicaal anionen en *bis*-anionen als de berekende magnetische eigenschappen van de *bis*-anionen.

Om het elektronische gedrag van CP-PAKs te kunnen vergelijken met dat van cyclohepta-geannuleerde PAKs (CH-PAKs), moesten voor de laatste klasse van verbindingen eerst efficiënte syntheses ontworpen worden. De synthese van CH-PAKs is ook interessant vanuit een geheel ander perspectief. Terwijl de aanwezigheid van pentagons leidt tot positieve kromming, kunnen heptagons negatieve kromming in een grafietvlak introduceren. Tot nu toe waren alleen een paar van deze verbindingen toegankelijk via lastige syntheseroutes. De nieuwe CH-PAKs, cyclohepta[*c,d*]pyreen en cyclohepta[*c,d*]fluorantheen, werden verkregen met behulp van FVT van

*bis*-geacetylerde PAKs bij lage temperaturen. CH-PAKs blijken in een beperkt temperatuurgebied stabiel te zijn, aangezien FVT bij hogere temperaturen leidt tot de vorming van de corresponderende CP-PAKs. Dit verschijnsel geeft een mogelijke verklaring voor het feit dat tot nog toe geen CH-PAKs zijn geïdentificeerd in verbrandingsmengsels. Waarschijnlijk zijn ze niet stabiel genoeg tijdens hoge temperatuur condities.

De elektronische eigenschappen van CH-PAKs zijn *anti*-symmetrisch met die van de corresponderende CP-PAKs. Terwijl CP-PAKs hoge elektronen affiniteiten hebben, hebben CH-PAKs lage ionisatie potentialen. Deze relatie kan worden gerationaliseerd op grond van hun moleculaire orbital eigenschappen. Dus, terwijl de aanwezigheid van een pentagon leidt tot verbindingen met n-type karakter, induceren heptagons p-type karakter. Een interessante andere toepassing kan daarom de synthese van donor-acceptor verbindingen zijn, die alleen uit koolstof en waterstof bestaan, maar zowel een pentagon als een heptagon bevatten.

Als laatste worden de magnetische eigenschappen van een serie CH-PAH bestudeerd (**Hoofdstuk 9**). De aanwezigheid van een heptagon leidt tot sterke paratropie ringstromen in deze ring in de aanwezigheid van een magnetisch veld. Dit is afgeleid van de up-field verschoven <sup>1</sup>H-NMR resonanties. Wanneer zowel een pentagon als een heptagon geïntegreerd zijn in dezelfde PAK structuur kan dit leiden tot interessante nieuwe eigenschappen.



## Dankwoord

Een proefschrift schrijven is een enorm karwei en daaraan hebben dan ook veel mensen op zeer diverse wijze een bijdrage geleverd. Deze laatste bladzijden wil ik graag gebruiken om een aantal van hen in het bijzonder te bedanken.

Allereerst mijn promotor, Prof. Dr. L. W. Jenneskens. Beste Leo, de gedrevenheid waarmee je mijn promotieonderzoek begeleidde was een grote stimulans. Ik blijf me verbazen over de oneindige energie die je hebt om alle manuscripten tot in de kleinste details te corrigeren.

Dr. Joop van Lenthe en Dr. Remco Havenith wil ik bedanken voor hun hulp bij alle berekeningen. Beste Remco, toen ik zelf ging rekenen was je altijd bereid mijn vragen te beantwoorden en eventuele ‘bugs’ te verhelpen. Dit heeft ertoe geleid dat ik mijn (super-)computervrees heb overwonnen.

De massaspectrometristen Prof. Dr. Nico Nibbering en Dr. Roel Fokkens hebben een grote bijdrage geleverd aan hoofdstuk vier en zes. De bijzonder prettige meetsessies in Enschede waren een welkome afleiding op het werk in Utrecht.

Without compounds no measurements and therefore I want to thank Dr. Berta Gómez-Lor and Prof. Dr. Antonio Echavarren for the fruitful collaboration on the ‘zipping up’ of the large PAH.

I am very grateful for the collaboration with Prof. Dr. Patrick W. Fowler and Dr. Erich Steiner on the subject of the magnetic properties of non-alternant PAH. In addition, I would like to thank Professor Fowler for his useful comments on Chapter 7.

Dr. Tom Visser van de vakgroep infrarood spectroscopie wil ik bedanken voor de bijdrage aan hoofdstuk twee en drie. Ik vind het een mooie toepassing van IR!

De beide doctoren van de FOC, Jan Zwikker en Kees van Walree, zijn tijdens het onderzoek een grote hulp geweest bij het oplossen van velerlei praktische problemen. Veel dank hiervoor.

Een deel van het synthese werk was niet tot stand gekomen zonder hulp van keuze- of hoofdvak studenten. Bart Suijkerbuijck, Pieter Bruijnicx, Erik Laureijs, Jan van Geldrop, Sipke Wadman en Tjeerd Raijmakers, bedankt voor jullie inzet!

De FOC was niet hetzelfde geweest zonder alle Aio's, ex-Aio's, medewerkers en studenten. Hen wil ik bedanken voor de nodige afleiding bij het werk. Een speciaal woord van dank is bestemd voor Ed Vlietstra en Vera Kaats-Richter. Het werk dat jullie op de vakgroep doen is soms niet direct zichtbaar, maar ik ben jullie zeer erkentelijk voor alle hulp met onder andere het scannen van platen, opnemen van HPLC's en GC-MS-en.

Gelukkig was er buiten het werk geen gebrek aan mogelijkheden om te ontspannen. Dit was onder andere te danken aan de dames van het USC-bestuur Reinie, Dorien, Femke, Brita en Astrid. De etentjes, wandelingen en kwintet/kwartet weekenden waren altijd gezellig.

Er is geen betere manier om te ontspannen dan muziek te maken (of een muziek project te organiseren). Daarom wil ik alle leden van Arezzo bedanken voor de heerlijke repetities, concerten en natuurlijk de uurtjes in 'het Pandje'. De mede-bestuursleden van Marzimino, Frank, Freek, Femke en uiteraard ook Chris, zorgden voor de nodige afleiding. Dat het een mooie opera mag worden!

Beste Herman, heel veel dank voor de supersnelle lay-out actie. Ik vind de omslag erg geslaagd. Natuurlijk zal ik de interesse en steun van Sarah, Wibren, Wilma, Taco en Elles, Karin en Ronald, Alie, Hans en Anja, Ralph en Michele en Oma ook niet vergeten.

Marijo, als collega wil ik je bedanken voor de interesse in mijn werk en het lezen van alle manuscripten. Ik ben bijzonder blij met je vriendschap en wens je alle succes met de laatste paar maanden op de FOC. Monique en Liesbeth, wat is het toch heerlijk om af en toe je frustraties kwijt te kunnen bij iemand die in het zelfde schuitje zit. Monique, nog even doorbijten en dan gaan we de afronding van onze promoties eens heel goed vieren!

Lieve Wim en Marjan, ik mag inderdaad van geluk spreken met zulke schoonouders. Het is werkelijk onmogelijk om na een weekendje Rustenburg niet ontspannen naar huis te gaan! Lieve Papa en Mama, dit proefschrift is opgedragen aan jullie. Ik ben bijzonder gelukkig met jullie liefde en steun. Mede dankzij jullie voorbeeld had ik het doorzettingsvermogen om dit proefschrift af te ronden.

En dan Guido, mijn lief, jou kan ik niet genoeg bedanken. Je ontzettende optimisme is voor mij van onschatbare waarde geweest bij het schrijven van dit proefschrift.

Carola

April 2003

## Curriculum Vitae

De schrijfster van dit proefschrift werd op 17 juni 1975 geboren te Soest. In 1993 haalde zij het gymnasium diploma aan het Baarnsch Luceum te Baarn. In september van datzelfde jaar begon zij met de studie Scheikunde aan de Universiteit Utrecht en het propedeutisch examen werd afgelegd in augustus 1994. Zij volgde twee bijvakken bij de vakgroep Fysisch-Organische Chemie (Prof Dr. L. W. Jenneskens) en de vakgroep Organische Synthese (Prof. Dr. G. van Koten) en in het kader van een bijvak deed zij gedurende 5 maanden onderzoek aan polyurethaan harsen bij AKZO Nobel Central Research te Arnhem (Arnhem, Dr. J. A. J. Schutyser en Utrecht Dr. J. Boersma). Na een hoofdvak onderzoek bij de vakgroep Fysisch-Organische chemie, werd in januari 1999 het doctoraal examen gehaald. Van maart 1999 tot juni 2003 was zij als AIO verbonden aan de sectie Fysisch-Organische Chemie van de Universiteit Utrecht, alwaar zij onder leiding van Prof. Dr. L. W. Jenneskens het in dit proefschrift beschreven onderzoek verrichtte.



## List of Publications

Publications on which this Thesis is based:

1. C. Koper, L.W. Jenneskens and M. Sarobe, Externally-Fused Cyclopenta-moieties in Non-alternant CP-PAHs act as *Peri*-substituents, *Tetrahedron Lett.*, **2002**, *43*, 3833-3836.
2. B. Gómez-Lor, C. Koper, R. H. Fokkens, E. J. Vlietstra, T. J. Cleij, L.W. Jenneskens, N. M. M. Nibbering and A. M. Echavarren, Zipping up 'the Crushed Fullerene' C<sub>60</sub>H<sub>30</sub>: C<sub>60</sub> by Fifteen-fold Consecutive Intramolecular H<sub>2</sub> losses, *Chem. Comm.*, **2002**, 370-371.
3. C. Koper, M. Ruiz, O. de Frutos, E. González-Cantalapiedra, R. H. Fokkens, N. M. M. Nibbering, D. J. Cárdenas, A. Santos, B. Gómez-Lor, L.W. Jenneskens, A. M. Echavarren, Benzo[1,2-*e*:3,4-*e'*:5,6-*e''*]tribenzo[*l*]acephenanthrylene (C<sub>60</sub>H<sub>30</sub>): a Progenitor of C<sub>60</sub>. Its Synthesis by Palladium-Catalyzed Arylation and Stepwise Conversion into C<sub>60</sub>, *Chem. Eur. J.*, **2003**, *in press*.
4. C. Koper, J. H. van Lenthe and L.W. Jenneskens, Identification of Progenitors for C<sub>70</sub>, *J. Phys. Chem. A.*, **2003**, *submitted*.
5. C. Koper, R. W. A. Havenith, T. Visser, C. A. van Walree, L. W. Jenneskens, Unexpectedly Facile Hydrogen Migrations in Cyclopenta-Fused Polycyclic Aromatic Hydrocarbons under High Temperature Conditions, *J. Am. Chem. Soc.*, **2003**, *submitted*.
6. C. Koper, M. Sarobe and L. W. Jenneskens, Redox Properties of Non-alternant Cyclopenta-Fused Polycyclic Aromatic Hydrocarbons, *Chem. Eur. J.*, **2003**, *submitted*.
7. C. Koper, B. Gómez-Lor, R. H. Fokkens, N. M. M. Nibbering, L.W. Jenneskens and A. M. Echavarren, Synthesis by Design of the Novel Triazafullerene C<sub>57</sub>H<sub>2</sub>N<sub>3</sub>, *to be submitted*.

8. C. Koper, S. H. Wadman, T. M. Raaymakers, V. M. Kaats-Richters, J. W. Zwikker, C. A. van Walree, L. W. Jenneskens, Synthesis and Electronic Properties of Cyclohepta-Fused Polycyclic Aromatic Hydrocarbons, *to be submitted*.
9. C. Koper, R. W. A. Havenith, E. Steiner, P. W. Fowler, L. W. Jenneskens, Magnetic Properties of Cyclohepta-Fused Polycyclic Aromatic Hydrocarbons, *to be submitted*.
10. C. Koper, P. Todorov, J. H. van Lenthe, L. W. Jenneskens, Electron Affinities of Cyclopenta-Fused Polycyclic Aromatic Hydrocarbons, *to be submitted*.
11. C. Koper, R. W. A. Havenith, L. W. Jenneskens, E. Steiner, P.W. Fowler, Magnetic Properties of the *Bis*-anions of Cyclopenta-Fused Polycyclic Aromatic Hydrocarbons, *to be submitted*.

Other Publications:

12. D. Heymann, L. W. Jenneskens, J. Jehlicka, C. Koper, E. J. Vlietstra, Biogenic Fullerenes?, *Int. J. Astrobiol.* **2003**, *in press*.
13. D. Heymann, L. W. Jenneskens, J. Jehlicka, C. Koper, E. J. Vlietstra, Terrestrial and Extraterrestrial Fullerenes, *Fullerenes, Nanotubes and Carbon Nanostructures* **2003**, *submitted*.
14. W. D. Oosterbaan, C. Koper T. W. Braam, F. J. Hoogesteger, J. J. Piet, B. A. J. Jansen, C. A. van Walree, H. J. van Ramesdonk, M. Goes, J. W. Verhoeven, W. Schuddeboom, J. M. Warman and L. W. Jenneskens, Oligo(cyclohexylidene)s and Oligo(cyclohexyl)s as Bridges for Photoinduced Intramolecular Charge Separation and Recombination, *J. Phys. Chem. A.*, **2003**, *in press*.



